Chapter - M

MODELLING, SIMULATION, OPTIMIZATION

MODELLEME, SİMÜLASYON, OPTİMİZASYON

Assessment of Grinding Flowsheet Designs of Aghdarreh Gold Ore Processing Plant Based on Circuit Simulation Approach

A. Farzanegan
School of Mining, University College of Engineering, University of Tehran, Tehran, Iran

A. Ebtedaei Ghalaei
Faculty of Mining Engineering, University of Kashan

ABSTRACT The run of mine ore from Aghdarreh gold mine must be comminuted to achieve the desired degree of liberation of gold particles. Currently, comminution circuits include a single-stage crushing using a jaw crusher and a single-stage grinding using a Semi-Autogenous Grinding (SAG) mill in closed circuit with a hydrocyclone package. The gold extraction is done by leaching process using cyanidation method through a series of stirred tanks. In this research, an optimization study of Aghdarreh plant grinding circuit performance was done to lower the product particle size (P_{80}) from 70 μm to approximately 40 μm by maintaining current throughput using modeling and simulation approach. After two sampling campaigns from grinding circuit, particle size distribution data were balanced using NorBal software. The first and second data sets obtained from the two sampling campaigns were used to calibrate necessary models and validate them prior to performing simulation trials using MODSIM software.

Computer simulations were performed to assess performance of two proposed new circuit flowsheets. The first proposed flowsheet consists of existing SAG mill circuit and a new proposed ball mill in closed circuit with a new second hydrocyclone package. The second proposed flowsheet consists of existing SAG mill circuit followed by a new proposed ball mill in closed circuit with the existing hydrocyclone package. In all simulations, SAGT, CYCL and MILL models were selected to simulate SAG mill, Hydrocyclone packages and ball mill units. SAGT and MILL models both are based on the population balance model of grinding process. CYCL model is based on Plitt's empirical model of classification process in hydrocyclone units. It was shown that P_{80} can be reduced to about 40 μm and 42 μm for the first and second proposed circuits, respectively. Based on capital and operational costs, it can be concluded that the second proposed circuit is a more suitable option for plant grinding flowsheet modification.

1 INTRODUCTION

There are some benefits for Grinding operation optimization including decreased unit operation costs, increased capacity and production of more valuable metals and improved performance of downstream processes due to improved feed size distribution. In most plants, optimization criteria are defined based on the following purposes, a) Capacity maximizing while maintaining current final product specification, b) Finer final product size while maintaining current capacity and c) Minimizing operation costs while maintaining both current capacity and product size (Napier-Munn et al. 1996).

Nowadays, process modeling and simulation is one of the main optimization tools used in industry. The optimization using simulation consists of several stages, a) characterize operation parameters of feed in laboratory tests, b) estimate machine

parameters, using plant survey (model calibration), c) performing simulations to explore possible optimization solutions by changing circuit flowsheet or process equipment or operating conditions, and d) evaluation of solutions found through simulation studies by running plant tests under proposed flowsheet modifications or operating conditions(Napier-Munn et al. 1996).

Aghdarreh gold processing plant is located near Takab at north-west of Iran. Run-of-Mine (ROM) ore is processed through several stages including crushing, grinding and cyanidation leaching. In this research, grinding optimization studies were done with the objective of decreasing particle size of grinding circuit product under the same current capacity. Process modeling and simulation approach was used to find optimization solutions considering the requirements of downstream leaching process.

1.1 Grinding circuit sampling

A sampling campaign from grinding circuit was planned to assess its performance under the current operating conditions. Presently, particles with a size greater than90 μm enter to underflow stream and are recirculated to Semi-Autogenous Grinding (SAG) mill. The hydrocyclone overflow first passes through a trash screen to remove any oversize pieces of material and then enters to the leaching circuit (Figure 1).

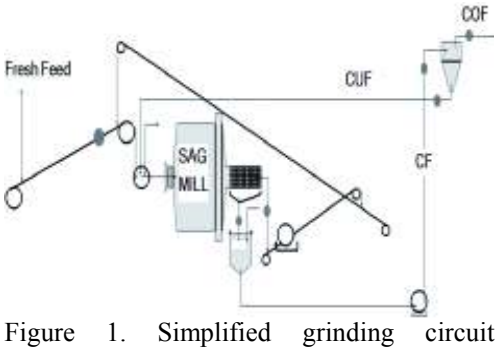

Figure 1. Simplified grinding circuit flowsheet of Aghdarreh gold processing plant and sampling locations.

In order to evaluate processing units and circuit performance, sampling from fresh feed, mill product and scats reject returning to the SAG mill, streams around hydrocyclone including feed, overflow and underflow was necessary. Two sampling campaign were scheduled so that the first sampling campaign data can be used to calibrate models and the second sampling campaign data can be used to validate simulation models.

The samples was collected from various locations including trammel screen undersize, scats reject and streams around hydrocyclone, simultaneously. A composite sample for each location was then obtained by combining partial samples collected every 10 minutes and for a period of 2 hours to reduce possible sampling errors due to operation fluctuations. To sample SAG mill fresh feed, belt conveyor was stopped and a sample was taken by removing material over a two-meter length. Operating condition during sampling was recorded.

Particle Size distribution of all samples except mill fresh feed and scats reject was determined using 6730 to 38 μm screens. Solids content of all samples was also determined. Mill fresh feed particle size distribution was also determined using rod screens and laboratory screens. Weight of these samples after drying was 75 and 105 kg. Fresh feed flow rates for first and second stage sampling were 142 and 141 t/h that is almost two times of designed capacity. For mass balance of hydrocyclone streams flow rates and size distribution of hydrocyclone streams NorBal software (Spring 1996) was used. Specify gravity (SG) of fresh feed solid particles is 2.9. The circulating load ratio obtained for first sampling campaign using two methods, i. e., based on streams solids content and particle size distributions were equal to 2.68 and 2.69, respectively. For second sampling campaign, the circulating load ratio obtained using both methods were equal to 2.59 and 2.66, respectively. Then specification of hydrocyclone feed, hydrocyclone overflow and hydrocyclone underflow streams

calculated for two-stage sampling. Then for to specify hydrocyclone current efficiency and perform necessary changes for its improvement, basis measured data, hydrocyclone tromp curve for two stage sampling provide before modification and after modification, in Excel software. Fluid (water) recovery to underflow (R_f) obtained for two sampling campaign was equal to 0.44 and 0.43 that implies a weak performance of hydrocyclone.

1.2 MODSIM software

MODSIM is a steady-state simulator that calculates the detailed mass balances for any ore dressing plant. The simulation results reported by MODSIM includes total flow rates of water and solids, the particle size distribution of the solid phase, the distribution of particle composition and the average assay of the solid phase. MODSIM is based on a modular structure which permits new models to be added for simulation of various unit operations (King 2001).

2 THEORY

2.1 SAG mill modeling

In MODSIM, one of the simulation models used for a SAG mill unit is SAGT (Semi-Autogenous Grinding with Trommel) model. In this model, a SAG mill with a trommel screen at mill discharge is modeled using the full population balance including particle attrition and wear (King 2001b). In this model, three distinct breakage mechanisms have been considered, namely surface attrition, impact breakage and self-breakage splitting. The mill is assumed to be perfectly mixed with post classification at discharge grate. The load in the mill is calculated from the mill dimensions and the average residence time is calculated as the ratio of the load to the throughput. Water can be added directly to the mill feed at a pre-specified rate or the simulator will calculate the water addition rate that is required to achieve a specified solid content in the mill discharge (King 2001).

2.2 Breakage process modeling

Impact breakage is modeled using the standard Austin breakage and selection functions. The specific rate of breakage due to self-breakage mechanism for particles smaller than 12.5 mm is significantly low and can be ignored confidently. The dominant breakage mechanism in this particle size range is impact breakage. A standard laboratory ball mill was used to determine breakage and selection functions parameters in Austin model (Hasani et al. 2009).

2.2.1 Selection function

The variation of specific rate of breakage with particle size can be fitted by the following model (Austin et al. 1984):

$$S_i = \frac{S_1\left(\frac{x_i}{1000}\right)^{\alpha}}{1+\left(\frac{x_i}{\mu}\right)^{\Lambda}} \quad (1)$$

Where S_1 is selection function value at 1 mm and its value is changing with of grinding properties variation, x_i is particle size (μm) and α is positive value that commonly is between 0.5-1.5 depended on mineral material properties, μ is particle size at which correction coefficient $Q_i=1+(x_i/\mu)^{\Lambda}$ is equal with 0.5 and Λ is positive number ($\Lambda \geq 1$) which indicates how fast breakage rate will be decreased with increasing size particle depending on mineral properties but μ changes with mill condition. To characterize impact breakage by grinding balls, laboratory standard tumbling ball mill tests were performed.

The optimal values of parameters of Austin model in Equation (1) were estimated for laboratory measured selection function vs. particle size by applying least-square method and using SOLVER non-linear optimization tool of Excel (Figure 2). The selection function model obtained is given in Equation (2).

$$S_i = \frac{0.1\left(\frac{x_i}{1000}\right)^{1.33}}{1+\left(\frac{x_i}{150}\right)^{3.16}} \quad (2)$$

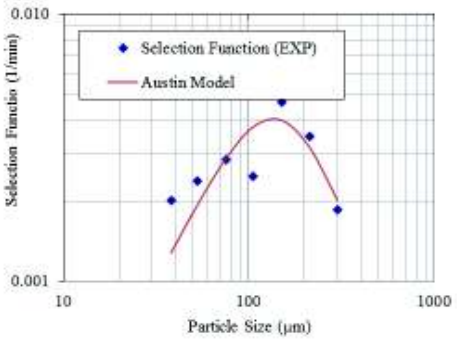

Figure 2. Estimated selection function data points fitted with Austin model

2.2.2 Impact breakage function

In AG/SAG mills, there are two main breakage mechanisms: impact (high energy) and abrasion (low energy). For impact breakage mechanism, JKMRC institute is using the model of the percentage of broken product passing 1/10 the original particle size, t_{10}. Equation (3) relates t_{10} to E_{CS} which is specific energy of comminution (Napier-Munn et al. 1991):

$$t_{10} = A\left(1-e^{-bE_{cs}}\right) \quad (3)$$

The impact breakage parameters, namely A and b, are determined using a high energy impact breakage device called JK Drop Weight Tester. Specific energy of comminution, E_{cs}, in Equation 3 can be calculated according to experimental setup data, as follows (Napier-Munn et al. 1991):

$$\frac{0.0272\,M_d\left(h_i - h_f\right)}{m} \quad (4)$$

Where, M_d is drop weight mass (kg), m is the medium mass of per particle size class (g), h_i is initial height of drop weight above the anvil (cm), h_f is final height of drop weight above the anvil (cm).

It is noted that A is the maximum t_{10} value achieved. This is significant for higher energy breakage. The parameter b is related to the overall slope of t_{10} versus E_{cs} curve at the lower energies. A and b are interdependent, since the value of one will directly affect the other. Parameters A and b are related and usually are reported by $A.b$ as a single value to indicate the ore hardness in terms of impact breakage. The $A.b$ parameter is the slope of the t_{10} vs. E_{cs} curve at its origin and it is a measure of breakage of the ore at lower energy levels.

2.2.3 Abrasion breakage modeling

To characterize abrasion breakage mechanism, the parameter t_a is defined as one tenth of t_{10} as follows (Napier-Munn et al. 1991):

$$t_a = \frac{t_{10}}{10} \quad (5)$$

The abrasion breakage parameter, t_a, is determined by performing a tumbling test. A lower value of t_{10} (hence a lower t_a value) indicates that there is a lower percentage of material passing 1/10th the original particle size, or greater resistance to abrasion breakage. Napier-Munn et al. indicate a possible correlation between the impact ($A.b$) and abrasion (t_a) parameters and the Bond ball mill work index given by the equations (Hasani et al. 2009):

$$A \times b = -3.5 W_i + 117 \quad (6)$$

$$t_a = 19.7 W_i^{-1.34} \quad (7)$$

These relations using test on 47 type different ore by JKMRC institute is given. Table 1 shows work index and parameters of abrasion and impact breakage mechanisms of Aghdarreh mixed ore.

Accordingly, the impact breakage mechanism model for Aghdarreh mixed ore can be written as:

$$t_{10} = 67.51\left(1 - e^{-1 \times E_{CS}}\right) \quad (8)$$

Table 1. Parameters of abrasion and impact breakage mechanisms of Aghdarreh mixed ore

Ore type	W_i (kWh/t)	$A \times b$	t_a
Mixed	14.14	67.51	0.57

2.3 Classification process modeling

One of the best empirical models of hydrocyclone units is Plitt's model that was originally introduced in 1976. In MODSIM software, Plitt's model can be selected by user to simulate hydrocyclone units. The set of four equations which are collectivity referred as Plitt's model are as follows (Plitt 1976):

$$d_{50c} = CF_1 \frac{39.7 D_c^{0.46} D_i^{0.6} D_o^{1.21} \eta^{0.5} \exp 0.063\phi}{D_u^{0.71} h^{0.38} Q^{0.45} (\rho_s - \rho)^{0.5}} \quad (9)$$

$$S = CF_2 \frac{1.9\left(D_u / D_o\right)^{3.31} h^{0.54} \left(D_u^2 + D_o^2\right)^{0.36} \exp 0.0054\phi}{D_c^{1.11} H^{0.24}} \quad (10)$$

$$m = CF_3 \times 1.94 \left(\frac{D_c^2}{Q}\right)^{0.15} \exp\left(-1.58 \frac{S}{1+S}\right) \quad (11)$$

$$p = CF_4 \frac{1.88 Q^{1.78} e^{0.0055}}{D_c^{0.37} D_i^{0.94} h^{0.28} \left(D_u^2 + D_o^2\right)^{0.87}} \quad (12)$$

The Plitt's model includes two sets of variables; dependent variables are as follows: corrected cut point (d_{50c}), pressure (P), stream volume splitting ratio (S) and separation sharpness (m). Independent variables are hydrocyclone diameter (D_o), vortex diameter (D_o), spigot diameter (D_u), inlet diameter (D_i), composition of those ($D_u / D_o, D_o^2 + D_u^2$) and also vortex free height (h). η is slurry viscosity, ϕ is volume solid percentage of hydrocyclone feed, Q is volume flow rate of hydrocyclone feed, ρ_s is solid density and CF_1 to CF_4 are Plitt's model calibration coefficients. The Influence of feed size particle on Plitt's model is not obvious from main specification of Plitt's model. Solids content, solids flow rate, solids density and slurry density are feed parameters that are used in model structure. The recovery of feed solids to underflow in ith size class (R_i) is calculated using the following equation:

$$R_i = R_f + (1 - R_f) \times \left(1 - e^{-0.693\left(\frac{d_i}{d_{50c}}\right)^m}\right) \quad (13)$$

Where d_i is the particle size of ith size class and R_f is the recovery of feed water to underflow. Plitt's model has various applications such as process analysis and diagnosis by looking at the values of d_{50c}, m and R_f parameters estimated based on plant data. Plitt's model also can be used in circuit design to find the appropriate hydrocyclone geometry and the required number of the hydrocyclones (Plitt 1976).

3 RESULTS AND DISCUSSION

3.1 Aghdarreh SAG mill

The specification of Aghdarreh SAG mill unit and operating condition recorded at sampling times are shown in Table 2.

Starkey (2007) have considered that Aghdarreh mill ($D/L < 1$) can be operated at mill loads equal to 20%, 26% and 30%. Mill load (volume) parameter for the Aghdarreh mill can be increased to 35%. The maximum suitable ball charge is 12%. The weight of mill load for 12% ball charge with 26% mill load is 105 t. Starkey used SAGDesign (Standard Autogenous Grinding Design) method to estimate grinding power required to achieve a final product with a d_{80} equal to 35 µm. The proposed flowsheet by Starkey includes the existing SAG mill circuit followed by installing a new ball mill in closed circuit with either the existing hydrocyclone package or a new one.

Table 2. Dimensions and operating parameters of Aghdarreh SAG mill

Parameters	Value
Diameter (m)	5
Center line length (m)	8.27
Belly length (m)	6.36
Trunnion diameter (m)	1.2
Load volume (%)	21
Ball volume (%)	10
Ball size (mm)	90
Mill speed (%)	75
Grate aperture (mm)	23
Trommel mesh size (mm)	16

3.2 Aghdarreh hydrocyclone modeling

The goal of Aghdarreh hydrocyclone performance optimization was to achieve a product with a d_{80} size smaller than 50 μm through changing hydrocyclone parameters. Simulation was used for testing possible solutions for hydrocyclone optimization. The CYCL model available in MODSIM, based on Plitt's model, was selected as hydrocyclone classifier model (King 2001). Table 3 shows design variables of Aghdarreh plant.

For both sampling campaigns, d_{50c} was obtained by plotting hydrocyclone classification curve based on measured flow rates and particle size distributions. The hydrocyclone pressure, P, measured value was equal to 175 kPa is corrected. The values of R_f and S are obtained using the adjusted flow rates of hydrocyclone streams. However, parameters d_{50c} and R_f as well as m can be calculated more accurately by fitting Equation (13) to measured R_f values in Excel spreadsheet software with least squared method and SOLVER non-linear optimization tool.

Table 3. Aghdarreh hydrocyclone geometry

Parameter	Value
Inlet Diameter (cm)	6
Hydrocyclone Diameter (cm)	25
Free height of hydrocyclone (cm)	105
Vortex Diameter (cm)	8.7
Spigot Diameter (cm)	7

3.3 MODSIM predictions

After the breakage different mechanisms of semi-autogenous mill and selection of Plitt's model for hydrocyclone, the performance of Aghdarreh grinding circuit is predicted for the two sampling campaign using MODSIM software. The predicted and measured values of streams specification of mill and hydrocyclone are shown in Tables 4 and 5. Also particle size distributions of various streams can be seen in Figures 3 to 6.

The mill power draws were 1754 and 1814 kW for two sampling campaigns, respectively. The average residence time of solid particles inside the mill during both sampling campaigns was estimated to be around 5.9 min. Also mill load weight excluding grinding balls was estimated to be equal to 46.1 and 42.6 t, respectively.

Table 4. The predicted and measured values of streams specification around SAG mill using MODSIM

Stream		First sampling campaign				Second sampling campaign			
		Solids (t/h)	d_{80} (μm)	Solids content (%)	Water (m^3/h)	Solids (t/h)	d_{80} (μm)	Solids content (%)	Water (m^3/h)
Trommel undersize	Measured	462.5	702.5	68	363.4	433.7	338.1	68	204.1
	Predicted	465.1	188	66.2	237.2	432	187	65.8	225
Fresh feed	Measured	125.5	104000	88.4	16.5	120.8	112000	85.7	20.2
Scats reject	Measured	6	20000	95	0.32	6	21000	95	0.32
	Predicted	0.01	20900	95	0.0005	0.01	20300	95	0.0003

Table 5. The predicted and measured values of streams specification around hydrocyclone package using MODSIM

Stream		First sampling campaign				Second sampling campaign			
		Solids (t/h)	d_{80} (µm)	Solids content (%)	Water (m^3/h)	Solids (t/h)	d_{80} (µm)	Solids content (%)	Water (m^3/h)
CF	Measured	462.5	306	56	363.4	433.7	320.9	58	314.1
	Predicted	465.1	188	56.6	357.2	432	187	56.7	330
COF	Measured	125.5	69.4	38	205	120.8	72.7	40.2	180
	Predicted	125.5	69.1	39.6	191.5	120.8	72.3	40.8	175.2
CUF	Measured	336.9	444.9	68	158.6	312.9	508.8	70	134.1
	Predicted	339.5	226	67.2	165.7	311.1	225	66.8	154.8

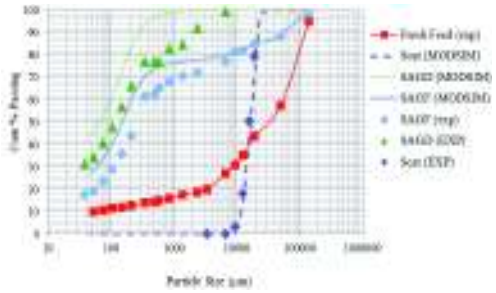

Figure 3. PSD of various streams around SAG mill unit in first sampling campaign

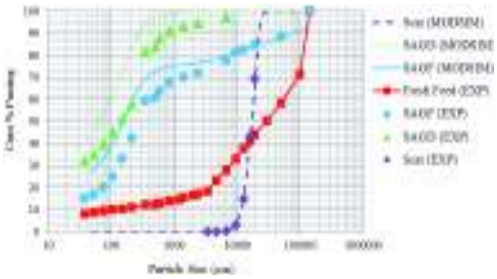

Figure 5. PSD of various streams around SAG mill unit in second sampling campaign

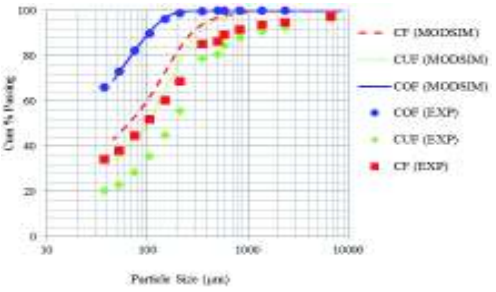

Figure 4. PSD of streams around hydrocyclone unit in first sampling campaign

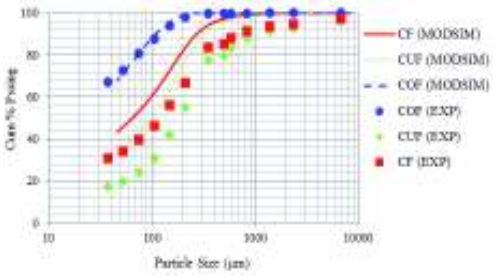

Figure 6. PSD of various streams around hydrocyclone unit in second sampling campaign (MODSIM predictions are based on non-calibrated Plitt's model)

3.4 Plitt's model calibration

The Plitt's model parameters determined based on the model predictions and measured data are usually different due to inherent empirical nature of the Plitt's model. Therefore, Plitt's model must be adjusted to measured hydrocyclone device condition using a set of calibration coefficients. Given a set of measured efficiency curve parameters based on several sampling from streams around the hydrocyclone and corresponding parameter values obtained from Plitt's model, it is possible to determine calibration factors using the linear regression curve fitting procedure. In this research, to calculate these

coefficients measured and predicted values of d_{50c}, m and R_f parameters given in Table 6 were used in Equation (14).

Table 7 is showing the calibration coefficients of Aghdarreh hydrocyclone Plitt's model. In MODSIM, hydrocyclone pressure, P, must be given as a known parameter data, thus a calibration coefficient for this parameter was not calculated.

Table 6. The parameters of Plitt's model in the first sampling campaign

Parameter	Measured	Predicted
d_{50c} (μm)	89.1	85.53
S	1.11	1.201
m	1.10	0.348

$$Calibration\ Factor(CF) = \frac{measured\ values}{predicted\ values} \quad (14)$$

Table 7. Calibration coefficients of Plitt's model adjusted to Aghdarreh hydrocyclone

CF_i	Parameter	Value
CF_1	d_{50c} (μm)	1.04
CF_2	S	0.92
CF_3	m	3.1

3.5 Models validation and simulations

In order to validate Plitt's model, data set obtained from second sampling campaign was used as an independent data set from the data set used to build the model. The particle size distribution of various circuit streams are predicted using MODSIM software by application CF_i obtained based on the second sampling campaign (Table 8).

Table 8. Post-calibration predicted specification of grinding circuit streams by MODSIM

Stream	Solid (t/h)	d_{80} (μm)	Solids content %	Water (m^3/h)
Trommel undersize	456.5	225	69.6	199.5
Scats reject	0.0022	19900	95.0	0.00012
CF	456.5	225	60.0	304.5
COF	120.8	73	40.8	175.2
CUF	335.6	255	72.2	129.3

For the second sampling campaign after calibration, mill power, mean residence time of solid particles in mill and weight of mill load without ball charge were equal to 1830 kW, 5.8 min and 44.3 t, respectively. The particle size distributions of circuit streams predicted after calibration are shown in Figure7.

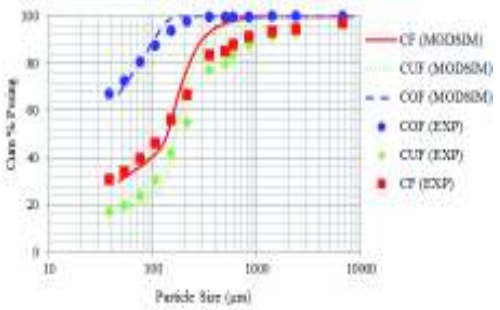

Figure 7. PSD of various streams around hydrocyclone unit in second sampling campaign (MODSIM predictions are based on calibrated Plitt's model)

As a rough observation if one compare predicted and measured PSDs in Figures. 7 and 8, obviously, predicted PSDs of streams around hydrocyclone are closer to measured PSDs after calibration of Plitt's model. The product size, P_{80}, was obtained 73 μm which is very closed to measured value. To compare, the pre-calibration and post-calibration values of Plitt's model parameters have been shown in Table 9.

It is noted that circulating load, hydrocyclone feed solids content, mill load and F_{80} are the four most important

parameters that affect P_{80} of product particle size distribution.

Table 9. Plitt's model parameters for second sampling campaign

Parameter	Measured	Pre-calibration	Post-calibration
d_{50c}, (μm)	88	91.65	116.9
S	1.09	1.21	1.13
m	1.18	0.35	0.72

It was very difficult to study the effect of F_{80} on P_{80} because fresh feed had relatively large variations and also was not under control. Also, the effect of circulating load on P_{80} could not be studied as circulating load is not an independent variable that can be changed directly. Therefore, only the effects of mill load (volumetric) and solids content of hydrocyclone feed of P_{80} were studied and necessary data was collected for a period of 8 weeks. The results are shown in Figures 8 and 9 (data are the average of per week and is collected in 8 week).

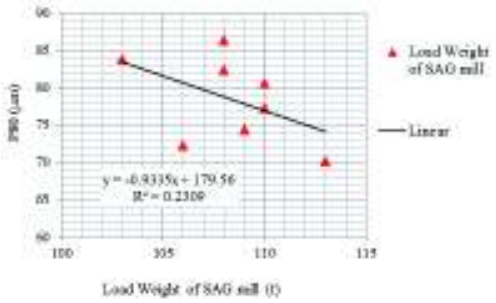

Figure 8. The effect of mill load on P_{80}

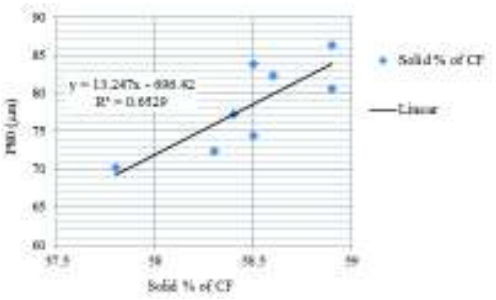

Figure 9. The effect of solids content of hydrocyclone feed on P_{80}

As Figures 8 and 9 show, P_{80} is decreased by an increase in mill load and is increased with an increase in solids content of hydrocyclone feed. Simulation trials of grinding circuit performance to achieve a P_{80} less than 70 μm have shown that volumetric mill load (26%, 30% and 35%) has the maximum impact on P_{80}. In addition, hydrocyclone geometrical variables in Plitt's model, number of operating hydrocyclone and solids content of hydrocyclone feed affect product size significantly. Table 10 is showing simulated grinding circuit performance with 6 hydrocyclone in operation, vortex diameter equal to 82 mm and spigot diameter equal to 70 mm.

Table 10. Results of grinding circuit performance simulation for various mill loads

Parameter	Mill load (volumetric)		
	26%	30%	35%
d_{50c} (μm)	94.2	87.2	81.35
S	1.34	1.33	1.32
Mill load without ball (t)	61.1	74.3	91
Mill power, (kW)	1944.3	2011	2067.1
Solids residence time, (min)	7.4	9.4	12
m	0.7	0.7	0.7
R_f	0.48	0.49	0.49
P_{80}, (μm)	61.7	56.1	50.9

Simulations showed that mill load and solids content of hydrocyclone feed have the greatest impact on P_{80} of grinding circuit product. By decreasing solids content from 58.3% to 57.2% (by increasing water addition rate to hydrocyclone sump from 105 m^3/h to 130m^3/h), P_{80} was reduced around 2 μm (from 72.4 to 70.4 μm). The flow rate of water addition to hydrocyclone sump could not be increased over 130 m^3/h, as solids content of hydrocyclone overflow which feeds leaching process had to be within a limited range of 37-38 %.

3.6 Proposed grinding circuit flowsheets

The simulation of current grinding circuit flowsheet under the best operating condition showed that product size, P_{80}, can be

reduced maximum to 51 μm. However, based on mineralogical studies (AMTEL 2008) finer grinding (less than 51 μm) is needed in order to increase plant current recovery from 90% to 95%. For this reason, simulations were performed assuming two proposed grinding circuit flowsheet by adding a ball mill unit after SAG circuit. The proposed ball mill was designed to process 130 t/h of feed produced by SAG circuit. The specification of proposed ball mill is shown in Table 11 (Starkey 2007).

Table 11. Proposed ball mill specification (Starkey 2007)

Mill type	Diameter (m)	Length (m)	Rotational speed (rpm)	Critical speed (%)	P_{80} (μm)	Calculated power (kW)	Installed power (kW)	Load volume (%)
Overflow	3.66	5.24	16.9	75	30 - 40	939	950	40

The "MILL" model of MODSIM was selected for the ball mill simulation. In this model, the mill is assumed to be a single perfectly mixed region (King 2001b). A standard Austin model was considered as selection function which includes a maximum that defines the onset of abnormal breakage as size gets larger. For Austin model parameters, values provided by the MODSIM software were used to define selection function of the proposed ball mill as follows:

$$S_i = \frac{0.4\left(\frac{x_i}{1000}\right)^{0.5}}{1+\left(\frac{x_i}{10}\right)^{2.513}} \quad (15)$$

The ore breakage distribution function in MILL model is defined by Broadbent and Callcott (1956) as given in Equation (16):

$$B_{i1} = \Phi\left(\frac{d_i}{d_1}\right)^{\gamma} + (1-\Phi)\left(\frac{d_i}{d_1}\right)^{\beta} \quad (16)$$

Where d_i and d_1 are the *i*th screen size and the first screen size (300 micron), respectively. Φ, γ and β are model parameters that γ and β are as impact breakage mechanism and cleave mechanism, respectively. The breakage distribution function of Aghdarreh gold ore was determined by performing laboratory grinding tests and using BFDS software to process test data based on Herbst and Fuerstenau method (Hoseinzadeh Gharehgheshlagh 2007):

$$B_{i1} = 0.673\left(\frac{d_i}{d_1}\right)^{1.043} + (1-0.673)\left(\frac{d_i}{d_1}\right)^{6} \quad (17)$$

The mean residence time of the solids must be given (5 min). The model does not need any details of the mill geometry. Water can be added directly to the mill feed at a pre-specified rate or the simulator will calculate the water addition rate that is required to achieve a given solids content in the mill discharge (King 2001).

3.7 First grinding flowsheet design

In this flowsheet, the overflow of first hydrocyclone package enters the proposed ball mill which is in closed circuit with a second hydrocyclone package (Figure 10). The CYCL model with similar parameters was selected to simulate the second hydrocyclone package.

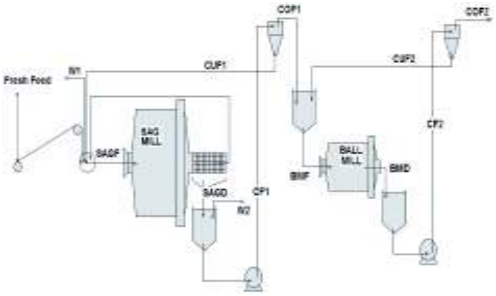

Figure 10. First grinding circuit flowsheet proposed for Aghdarreh which includes installing a ball mill in closed circuit with a second hydrocyclone package following existing SAG mill circuit

The simulation results of first proposed circuit showed that for load volumes equal 21% and 35%, P_{80} is reducing to 42.6 and 40.4 μm, respectively, that is showing the adding influence of the ball mill. Figure 11 is showing the particle size distribution of different streams.

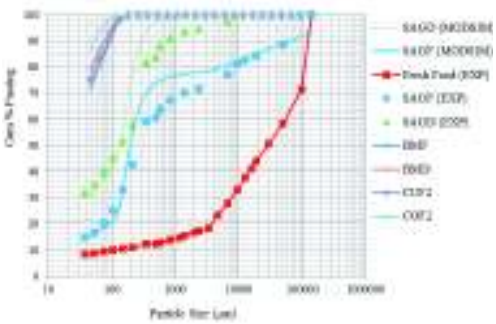

Figure 11. PSD of various streams of first proposed grinding circuit for a load volume equal to 21%

In MILL model, the inquired power of ball mill is estimated using the equation include Bond Work Index (W_i) as allow as:

$$P = 65.4 \times W_i \tag{18}$$

The measured work index (W_i) for Aghdarreh mixed ore is 14.14 kWh/t , thus the required ball mill power calculated based on Equation (18) is equal to 925 kW which is less than 950 kW (the power of proposed ball mill). Therefore the proposed ball mill is also suitable for development of grinding circuit in this situation.

3.8 Second grinding flowsheet design

In this flowsheet, the underflow of first hydrocyclone package enters the ball mill which its discharge is returned to hydrocyclone sump (Figure 12). The simulation results of second proposed circuit showed that for load volumes equal to 21% and 35%, P_{80} will be reduced to 46 and 42 μm, respectively. Figure 15 is showing the particle size distribution of different streams.

For this flowsheet, in MILL model, ball mill power is estimated using the equation that includes Bond Work Index (W_i) as follows:

$$P = 32 \times W_i \tag{19}$$

The required ball mill power in this case using Equation (19) is equal to 453 kW which indicates the proposed ball mill is suitable for development of grinding circuit in this situation.

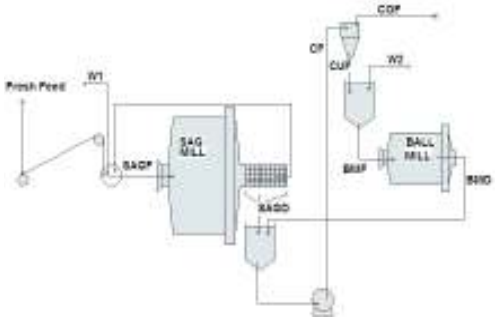

Figure12. Second grinding circuit flowsheet proposed for Aghdarreh which includes installing a ball mill in closed circuit with the existing hydrocyclone package after SAG mill circuit

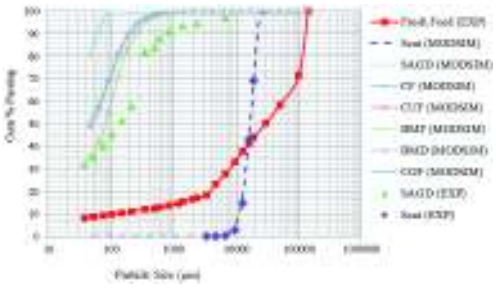

Figure13. PSD of various streams of second proposed grinding circuit for a load volume equal to 21%.

4 CONCLUSIONS

Simulations carried out based on the current grinding circuit flowsheet with vortex and spigot diameters equal to 82 and 70 mm, respectively, 6 hydrocyclones in operation and volumetric mill load equal to 35 % showed that P_{80} can be reduced to 51 μm. These results indicate that volumetric mill load has the maximum influence on P_{80} reduction because of increased residence time to 12 min and further chance of particles to be broken due to increased contact frequency. Mill power drawn can be increased to 2067 kW. Also, separation sharpness (m) can be increased to 0.7 that shows improvement of hydrocyclone performance relative to current practice.

The simulations results for the two proposed new circuits showed that P_{80} can be reduced further to 40 μm and 42 μm for the first and second proposed circuits, respectively. Based on capital and operational costs, it can be concluded that the second proposed circuit is a suitable option for plant grinding flowsheet modification.

ACKNOWLEDGMENTS

The authors would like to thank Aghdarreh gold processing plant administration for supporting this research and sincere cooperation of plant personnel.

REFERENCES

AMTEL Report (2), 2008. Distribution of gold and mercury in feed hydrocyclone products of Aghdarreh, AMTEL Institute, pp. 1-2.

Austin, L. G., Klimple, R. P., Luckie, P.T., 1984. Process Engineering of Size Reduction: Ball Milling, SME/AIME, New York.

Broadbent, S. R., and T.G. Callcott, T.G., 1956. Philosophical Transactions of the Royal Society of London, A249, 99.

Hasani, S., Dehghani, A., Khosravi, M, 2009. Determination of Work Index by abrasion mill and drop weight apparatus, 3rd Conference of Iran Mining Engineering, pp. 1786.

Hasani, S., Dehghani, A., Khosravi, M., 2009, "Breakage experiments for modeling of the AG and SAG mills", 3rd Conference of Iran Mining Engineering, pp. 1778.

Hoseinzadeh Gharehgheshlagh, H., 2007, "Comminution Optimization of semi autogenous mill of Aghdarreh processing plant", M. Sc. Thesis, Faculty of Mining and Metallurgical Engineering, University of Yazd, pp. 114.

King, R. P, 2001, "Modeling and Simulation of Mineral Processing Systems"; Department of Metallurgical Engineering, University of Utah, USA, pp. 201-202.

King, R. P., 2001b, "The User Manual of MODSIM", Department of Metallurgical Engineering, University of Utah, USA, pp. 1-2, 37, 55.

Napier–Munn, T. J., Morrell, S., Morrison, R. D. and Kojovic, T., 1996, "Mineral Comminution Circuits", JKMRC, Australia, pp. 318-320, 332.

Plitt, L. R., 1976, "A Mathematical Model of the Hydrocyclone Classifier", CIM Bulletin, Vol. 69, No. 776, pp. 114-123.

Spring, R, 1992, "NORBAL3 Software for Material Balance Reconciliation", NORANDA Technology Center.

Starkey, J., 2007, "The Optimization Report of Aghdarreh Comminution Circuit", Report to Aghdarreh Gold Company.

Developing the Software Programme to Evaluate the Potentiality of Open Pit Mining Method of Ore Deposit

A.Abbasi, M.Osanloo
Department of Mining and Metallurgical Engineering, Amirkabir University of Technology, Tehran, Iran

R.Khalokakaie
Department of Mining, Geophysics and petroleum Engineering, Shahrood University of Technology, Shahrood, Iran

ABSTRACT Development and extraction of minerals by open pit mining method is a complex operation that may extend over several decades and requires very large investments. Any mistake in evaluating the potentiality of this method will lead to irretrievable losses. So far, an integrated software package for this purpose has been not provided. The use of most commercial software packages in open pit optimization is restricted to input a geological block model. Available packages in mineral deposit evaluation are depended to user judgment in determining the limits of mineral deposit. This increases the error when there is insufficient exploration data. To overcome these shortcomings, a software program called OPME was developed. The software receives exploratory and economic data, and determines ore reserves, geological and economic block model, and ultimate pit limits. High speed, acceptable accuracy, user-independence nature and graphical and numerical displays are some of software capabilities. To verify the software, its result was compared with the result of Datamine and NPVScheduler softwares in Bagq iron ore of Iran. Comparison showed that error percent in both ore estimation and ultimate pit limit design is negligible.

KEYWORD Ore reserves estimation, Block model, Ultimate pit limit, OPME software

1 INTRODUCTION

Many technical reasons such as: the possibility of using huge machines, mining the large-scale with low-grade reserves, high capacity, low mining costs, rapid return on investment, safety and etc., has led to comprehensiveness of open pit mining method. Significantly, more than 70% of the world mineral production is now obtained from surface mines (Balamadeswaran 2011). Development and extraction of minerals by this method is a complex operation that may extend over several decades and require very large investments.

The use of computers in planning and design of an open pit mine is inevitable, in order to reduce calculation time and increase accuracy. There are currently many professional software packages, which include economic evaluation of open pit mine, the geology of the ore body, transport communications and other technological processes (Milena, et al. 2011). The most commonly software packages include: Gemcom, Surpac, Minex, Whittle 4D and

4X, Mintec, Datamine, Micromine and NPVScheduler.

Application base of computer techniques for open pits planning and design is block model. Blocks are used to discrete the deposit into mineable volumes. The planning of mine starts by geological block model, formed based on exploratory data. Geological block model must be identify by its grade, tonnage, joint, presence of water ant its density. Each properties of block (such as grade, tonnage and rock characteristics), is estimated based on exploratory data. The most used ore deposit estimation methods are kriging and inverse distance weighting techniques (Brooker 1977, David 1979, Diehl & David 1982, Modis et al. 2008). In the next step, economic block model is developed based on economic parameters. Almost all the existing pit design methods receive this block model as input. Some attempts in determining ultimate pit limits include: graph theory (Lerchs & Grossmann, 1965 and Zhao & Kim 1992), network or maximal flow techniques (Johnson 1968, Picard 1976, Johnson & Barnes 1988, Giannini 1991, Yegulalp & Arias 1992, Hochbaum & Chen 2000 and Osanloo et al. 2010), various versions of the floating or moving cone (Lemieux 1979, Kakaie et al. 2011), the Korobov algorithm (Korobov 1974) and the corrected form of the Korobov algorithm (Dowd & Onur 1993), dynamic programming (Lerchs & Grossmann, 1965, Koenigsberg 1982, Wilke & Wright 1984 and Yamatomi et al. 1995), mathematical programming (Underwood & Tolwinski 1998), integer programming (Meyer 1969), transportation problem (Huttagosol & Cameron 1992), genetic algorithm (Denby & Schofield 1994 and Saavedra-Rosas 2010), parameterisation techniques (Bongarcon & Marechal, 1976) and Pit-blend optimization (Rahmanpour & Osanloo 2012).

Uncertain conditions of mining project in the early stages of exploration, high cost of purchasing and employing the commercial software packages, high error in the presence of low exploratory data due to user-depended nature of these packages and the need for quick and acceptable accuracy of result motivated us to develop the Open Pit Mine Evaluator (OPME) software.

2 THE OPME SOFTWARE

The OPEM software was developed to evaluate the open pit mining potentiality during exploration stage. The software was written entirely in Visual C++ 6.0 using the Microsoft Visual Studio 2000 framework and can be implemented under various versions of Windows. The main window of software is displayed in Figure 1.

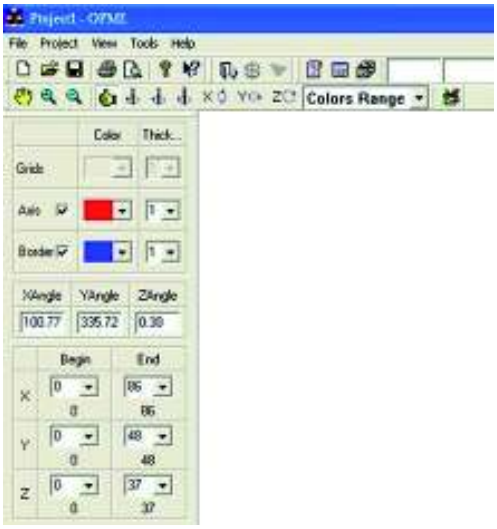

Figure 1. Main window of software

When the program is initiated, some commands are not immediately available, since are related to other options. These commands are only available after related commands have been executed. Figure 2 shows the procedure of evaluating the open pit mining potentiality using the software.

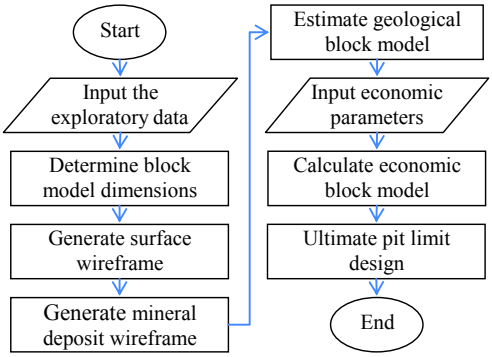

Figure 2. The procedure of evaluating the potentiality of open pit mining method

It must be noted that all the evaluation process, except data entry and exchange information is done automatically without user intervention.

3 MINERAL DEPOSIT EVALUATION

3.1 Import Exploratory Data

Prerequisite of open pit mining method evaluation is to load input data to the software. Command *File | Import Files* or button ( ) are embedded for this purpose. Input data, shown in Figure 3, include: pit slope, bench height and collars, survey, assay, geology and topography files. Table 1 display acceptable format of input text files.

3.2 Create Block Model

According to input exploratory data, a large rectangular block is defined, sufficient to encompass all the mineralization. Also effective radius and size of small blocks is estimated. These parameters are displayed in a dialogue box (Figures 4), to confirm or modify by the user.

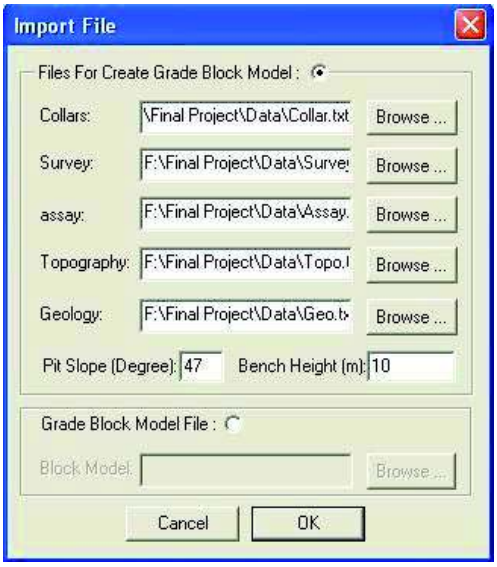

Figure 3. Input data dialogue box

3.3 Generate Topography Model

Based on topography data, the relative height of the surface is estimated for each column of block model. Figure 5 shows 3D view of boreholes among topography model. By click on the button ( ) or command *View|3DView*, a dialogue box is showed for selecting the objects for 3D viewing.

Table 1. Acceptable format of input files

	Format					
Collars	BHID DH2675	XCollar 8075.296	YCollar 6634.682	ZCollar 387.0823		
Survey	BHID DH2675	Az 180.29	Dip 29.95			
Assay	BHID DH2675	From 0	To 69.75	Grade 0		
Geology	BHID DH2675	From 82	To 100	Rock 6		
Topography	XTopo 8209.604	YTopo 6200	ZTopo 500			
Grade Block Model	nX 20 XBlock 7880.00	nY 21 YBlock 6280.00	nZ 13 Zblock 340.00	dX 40 Grade 0.08	dY 40 Rock 6	dZ 20

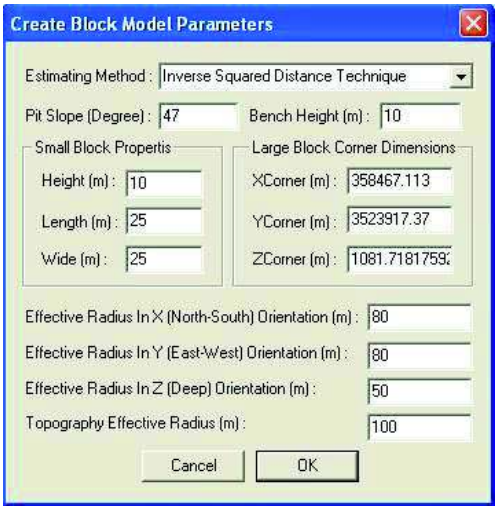

Figure 4. Block model dialogue box

3.4 Ore Reserve Estimation

3.4.1 Specify deposit boundaries

Before calculating grade, tonnage and rock characteristics of blocks, it is needed to specify the resource boundaries. This is done automatically by the software and based on exploratory data and block model parameters.

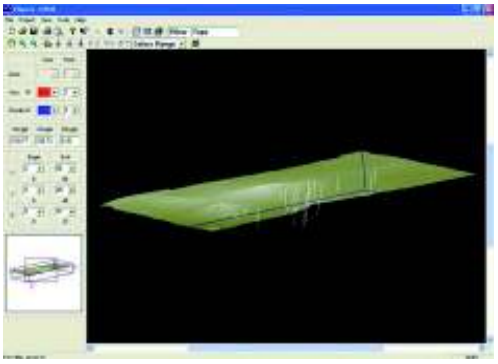

Figure 5. 3D view of topography model

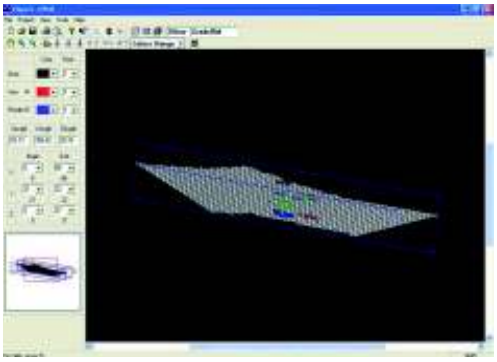

Figure 6. A section of grade block model

3.4.2 Estimate properties of blocks

Rock characteristics of blocks are determined from geology data. The blocks inside resource boundaries are named ore blocks and the other ones are waste block. The grade of resource blocks is estimated using nearest distance, inverse distance, inverse squared distance and Kriging techniques. A cross-section of grade block model is demonstrated in Figure 6. The software also has the capability of displaying numerical data. This is done by clicking on the button ( ) or command *View*| *Report*. Figure 7 shows grade block model data.

4 OPEN PIT OPTIMIZATION

4.1 Calculate Economic Block Model

To determine economic value of blocks, economic data for each rock types is imported to the software, through a dialogue box (Figure 8). To do so, one must click on the button ( ) or command *Project* | *Create Economic Block Model*.

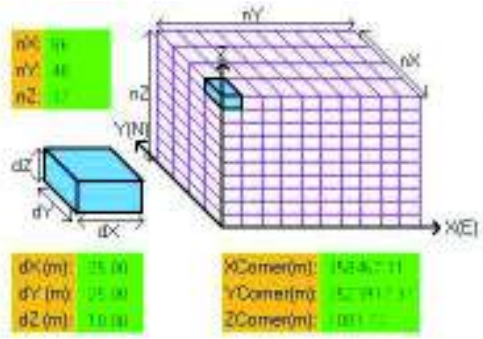

Parameter			
Air Blocks	0	45625	45625
Waste Blocks	45241	60611	105852
Ore Blocks	1256	3	1259
Unknown Blocks	0	0	0
Total	46497	106239	152736

Average Grade(%)	42.75	53.97	42.77

Parameter			
Waste Blocks	788827062.50	1024146875.00	1812973937.50
Ore Blocks	11284776.46	37947.33	11322723.79

Figure 7. Geological block model data

Figure 8. Grade block model parameters

4.2 Ultimate Pit Limit Design

Pit design relies on preliminary analysis consisting of (1) an ore body block model consists of a volume of material and the corresponding mineral properties; (2) the value of each block, which is determined by comparing market prices for commodity or final product with mining and processing costs; and (3) a geometric model of the deposit. Blocks are used as spatial reference points. Geometric constraints ensure that the pit walls are stable and that the equipment can access the areas to be mined (Newman et al. 2010).

Four methods are used by software to calculate ultimate pit limit: floating cone I & II, Korobov and Lerchs & Grossmann algorithms. Command *Project | Ultimate Pit Limit Design* or button ( ) are embedded for the selection of pit design method. Figure 9 displays a 3D view of ultimate pit limit.

5 SOFTWARE VALIDATION

A case study was used to test the application of the software. The study is taken from anomaly No.11 of Bafq iron ore mine located in Yazd province of Iran. To comparison, the mine was also assessed via Datamine and NPVScheduler softwares. The overall results of ore deposit evaluation by OPME and Datamine softwares are given in Table 2. Economic block model parameters and the overall results of open pit optimization by both the OPME and

NPVScheduler softwares are summarized in Table 3.

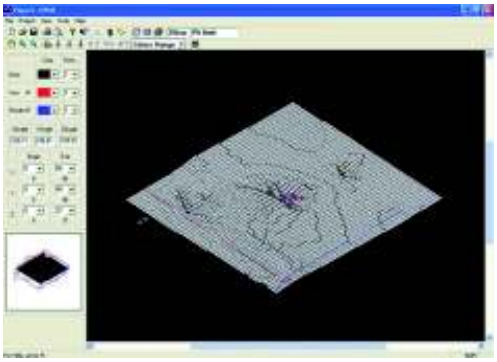

Figure 9. A 3D view of ultimate pit limit

Table 2. Results of ore deposit evaluation

	Parameter	OPME software	Datamine software
Ore Deposit	Ore deposit (Ton)	11322724	11754000
	Average grade (%)	42.77	49.34
Grade block model	Ore blocks(No.)	1148	1259
	Waste blocks(Ton)	53489	45241
	Ore blocks (Ton)	11752749	11322724
	Waste blocks (Ton)	869109423	788827063

Table 3. Results open pit optimization

	Parameter	OPME software	NPV Scheduler
Economic block model	Positive blocks(No.)	1161	1148
	Negative blocks(No.)	45342	53489
Ultimate pit limit	Ore blocks(Ton)	5545764	9026110
	Waste blocks(Ton)	9881125	23046020
	Number of blocks	1254	1972
	Value (M$)	1000	886

6 DISCUSSION AND CONCLUSION

predicting the potentiality of open pit mining method of mineral deposits in the early stage of exploration can be effective on the manner of budget provisioning for commissioning, equipping, developing, producing, and estimating the total income and cost of mining project. Uncertain conditions of mining project in the early stages of exploration, high cost of purchasing and employing the commercial software packages, high error in the presence of insufficient exploratory data due to user-depended nature of these packages and the need to quick and acceptable accuracy of result, motivated us to develop the OPME software. The software receives exploratory and economic data; estimate mineral resource tonnage and grade, define economic block model, and ultimate pit limits; displays the outputs results in the form of graphical and numerical displays; and records the results in several data files for further uses. To verify the software, the anomaly No.11 of Bafq iron ore mine of Iran was assessed with OPME, Datamine and NPVScheduler softwares. The overall results are summarized in Tables 2 & 3. Comparison shows that there is a small difference between the results of this software and the results of Datamine and NPVScheduler. This difference is acceptable, since the software is used for evaluating the potentiality of open pit mining method during early stage of exploration.

REFERENCES

Balamadeswaran, P., Natarajan, S., 2011, Explore the future of mineral deposits, *Mine Planning & Equipment Selection (MPES)*, pp. 97-115.

Bongarcon, D.F., Marechal, A., 1976, A new method for open pit design: Parameterization of the final pit contour, *In Proceedings 14th Int. APCOM 1976*, pp. 573-583.

Brooker, PI, 1977, Block estimation at various stages of deposit development, Proc. *14th Symposium Application of computer methods in mineral industry,* New York, pp. 995–1003.

Complete Mining Software Solutions, http://www.minesight.com/

David, M., 1979, Grade and tonnage problems, *Computers method for the 80s in the mineral industry*, New York, pp. 170–189.

Denby, B., Schofield, D., 1994, Open pit design and scheduling by use of genetic algorithm, *Transactions of the Ins. of Mining and Metallurgy*, vol. 103, pp. A21- A26.

Diehl, P., David, M., 1982, Geostatistical concepts and algorithms for ore reserve classification, *The 17th International Symposium on the Application and Operation Research in the Mineral Industry (APCOM17),* pp. 413–424.

Dowd, P.A., Onur, A.H., 1993, Open pit optimization – part 1: optimal open pit design, *Trans. Instn Min. Metall,102,* pp. A95-A104.

Elahi zeyni, E., Kakaie, R., Yousefi, A., 2011, A new algorithm for optimum open pit design Floating cone method III, *Journal of Mining & Environment,* Vol.2, No.2, pp. 118-125.

Giannini, L M., Caccetta, L., Kelsey, P., and Carras, S., 1991, PITOPTIM: A new high speed network flow technique for optimum pit design facilitating rapid sensitivity analysis, *AusIMM* Proc. No. 2,

algorithms for the open pit mining problem, *Operation Research*, 48(6), pp. 894-914.

InfoMine - Mining Intelligence and Technology, http://www.infomine.com/

Johnson, T B., 1968, pp. 57-62.

Hochbaum, D S., and Chen, A., (2000), Performance analysis and best implementation of old and new Optimum open pit mine production scheduling, PhD thesis*, Operations research department, Uni. of California, Berkeley, C.A.*

Johnson, T.B., Barnes, R.J., 1988, Application of maximal flow algorithms to ultimate pit design, Engineering design: Better results through operations research methods, Levary, R.R. (ed.), (Amsterdam: North Holland Publ. Co.), pp. 518-531.

Koenigsberg, E., 1982, The optimum contours of an open pit mine: an application of dynamic programming, *Proc. 17th Int. APCOM*, pp. 274-287.

Lemieux, M., 1979, Moving cone optimizing algorithm, *Computer methods for the 80s in the mineral industry,* pp. 329-345.

Lerchs, H., Grossmann, I., 1965, Optimum design of open-pit mines, *CIM Bulletin*, pp. 58 17–24.

Meyer, M., 1969, Applying linear programming to the design of ultimate pit limits, *Management Science*, vol. 16, pp. B121- B135.

Micromine, innovative software solutions and services to the mining, http://www.micromine.com/

Milena, M., Vladimir, C., Nebojša, G., 2011, Computer programs for design and modelling in mining, *Underground mining engineering,* volume 19., pp.109-124.

Mining Software Solutions, http://www.gemcomsoftware.com/

Modis, K., Stavrou, S., Terezopoulos, N., Vattis, D., 2008, Geostatistics versus inverse distance squares in ore reserves estimation: comparative case study in copper ore body in Cyprus. *Mining Technol*gy, 117 (1), pp. 48–52.

Newman, A. M., Rubio, E., Caro, R., Weintraub, A., Eurek, K., 2010, A review of operations research in mine planning, *Interfaces*, 40(3), pp. 222-245.

Osanloo, M., Rahmanpour, M., & Sadri, A. 2010, Ultimate pit limit of iron ore mines using maximum network flow, *MPES 2010*, pp. 81-87.

Picard, J C., 1976, Maximal closure of a graph and application to combinatorial problems, *Management Science*, 22, pp. 1268-1272.

Rahmanpour, M., Osanloo, M., Pit limit determination considering blending requirements, *MINE PLANNING AND EQUIPMENT SELECTION (MPES), pp. 564-572.*

Saavedra-Rosas, J., 2010, A New Genetic Algorithm for Open Pit Design – The Two-Dimensional Case, *MINE PLANNING AND EQUIPMENT SELECTION (MPES)*, pp. 95-103.

Underwood, R., Tolwinski, B., 1998, A mathematical programming viewpoint for solving the ultimate pit problem, *European J. of Operational Research*, 107, pp. 96-107.

Wilke, F.L., Wright, E.A., 1984, Determining the optimal ultimate pit design for hard rock open pit mines using dynamic programming, *Erzmetall*, 37, pp.139-144.

Yamatomi, J., Mogi, G., Akaike, A., Yamaguchi, U. 1995, Selective extraction dynamic cone algorithm for three-dimensional open pit designs, *25th Int. APCOM,* Brisbane, pp. 267-274.

Yegulalp, T M., and Arias, A J., 1992, A fast algorithm to solve the ultimate pit limit problem, *Proc. 23th Int. APCOM*, pp. 391-397.

Zhao, Y., and Kim, Y C., 1992, A new optimum pit limit design algorithm, *Proc. 23th Int. APCOM*, pp. 423-434.

Effect of Gas Velocity and Temperature on Drying of an Individual Iron Ore Pellet – CFD Simulation

A. Gitiara, A. Namehi, H. Vali, H. Shahrokhshahi, H. Soltani, S. Razavi, E. K. Alamdari

Department of Mining and Metallurgical Engineering, Amirkabir University of Technology, Tehran, IRAN

ABSTRACT The objective of the study is to model convective drying of an individual iron ore pellet to reduce energy consumption by means of optimization the operating conditions of iron ore pellet industries. To achieve this purpose, a numerical modeling is implemented taking into account flow of gas and heat transfer within and around the pellet in commercial available software for Computational Fluid Dynamics based on finite element method. A real pellet is optically scanned for its geometry and simulations of the drying are validated by comparing to actual measurements in an industrial scale plant with very good agreement. The effect of gas velocity, gas temperature and the drying air composition ($\%CO_2$) on the drying rate of pellet is investigated. The results show that the front will have a non-symmetrical form arising from the surrounding fluid flow and increasing of gas temperature is more effective than gas velocity.

Keywords: Drying; Iron oxide pellets; CFD

1 INTRODUCTION

Iron oxide pellets are one of the main feed s ources for blast furnaces or direct reduction processes of the iron and steel making industry (Tsukerman et al., 2007). A pelletizing plant generally consists of four stages: drying zone, pre-heat zone, firing zone and a cooling zone (Ljung et al., 2011). The first stage of drying is updraft to prevent condensation of water and consequential pellet deformation in the bottom layers of the pellet bed .Drying is continued in a subsequent downdraft stage by relatively hot gases coming from the firing zone of the furnace. Figure 1 depicts schematic of a typical straight-grate induration system (Barati, 2008).

In the preheating phase, pellets are heated to about 1000°C by downdraft gas flowing through the bed. Hot gas is typically recycled from the cooling zone and augmented with auxiliary heat from hood burners, if required. During this phase, pellets are completely dried and reactions such as decomposition of carbonates (e.g. lime, dolomite), magnetite oxidation and coke combustion take place. The reactions continue in the firing stage, where the gas temperature is raised to ~1350°C. The strength of the pellets increases at this stage because of recrystallization, sintering and formation of partially liquid phases (Barati, 2008). The dominating heat transfer mechanism is thus forced convection; over 90 per cent of the heat is transferred this way (Meyer, 1980) (Ljung et al., 2011).

Induration of pellets is generally performed by straight grate or grate-kiln processes. Typical for both types of processes is that balled pellets made from a mixture of iron ore, additives, and water (so-called green pellets) through all four mentioned zones (Ljung et al., 2011). For the pellets to be dried as efficiently as possible, it is of highest importance that this process is known in detail. The One important reason to keep the temperature fairly low is the risk for early oxidation of the magnetite. In this work, the influence of temperature and gas velocity was taken into account by the use of computational fluid dynamics (CFD).

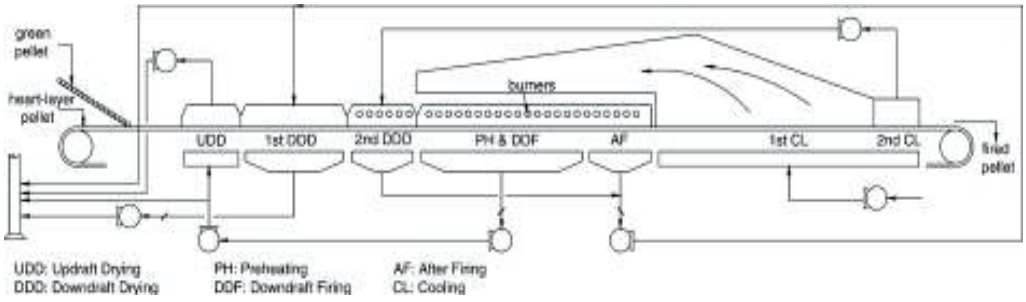

Figure 1.Schematic diagram of the straight-grate pellet induration system

The induration zone of the furnace is generally divided into several sections and the gas flow rate through each section is controlled by a separate fan. This is intended to provide the operator with the flexibility of controlling the heating profile for better pellet quality and grate bar protection. After firing, burnt pellets undergo cooling where ambient air is drawn upward through the bed. The hearth layer prevents a severe thermal shock to the pellets by preheating the air. The off-gas leaving the early stage of cooling has a temperature around 1000 °C. The gas is directed to the firing and preheating zones where is it further heated by the burners. The gases from the later stages of cooling have lower temperature; hence they are used for drying of pellets (Barati, 2008).

It is clear from the description of the process that considerable attention has been paid to enhancing the energy efficiency of the overall process.

A review of applications of CFD in drying processes in general was provided by Jamaleddine and Ray (Jamaladdine and Ray, 2010), Zili (Zili, 1999). Two-dimensional simulations were performed by Carmo and Lima (Ljung et al., 2011), who investigated drying of an oblate spherical solid.

2 MODELING

2.1 Transport Equations

The dominant heat transfer mechanisms are radiation and convection between gas and pellet. Thurlby et al. (Thurlby et al., 1979) have comparatively examined the effect of radiation and found that its effect is negligible. Mitterlehner et al. (Mitterlehner et al., 2004), Pomerleau et al. (Pomerlau et al., 2003) and other investigators have, therefore, ignored the radiation in their plant simulation.

The governing equations for the surrounding fluid flow around the pellet as well as for the heat transfer within the pellet are here outlined.

2.1.1 Surrounding fluid flow

The following continuity (eq. 1), momentum (eq. 2) and energy (eq. 3) equations govern the surrounding fluid flow:

$$\frac{\partial \rho}{\partial t} + \nabla.(\rho u) = 0 \quad (1)$$

$$\rho \frac{Du}{Dt} = -\nabla p + \mu \nabla^2 u \quad (2)$$

$$\rho C_p \frac{\partial T}{\partial t} + \rho C_p \, u.\nabla T = \nabla.(k \nabla T) + Q \quad (3)$$

where ρ, u, T, Cp and k are the density (kg/m^3), the velocity (m/s), the temperature (K), the specific heat at constant pressure (J/kg K) and the thermal conductivity (W/m K) of the surrounding fluid. Furthermore, Q is the energy source term (W/m^2) and μ is the dynamic viscosity (kg/m s).

2.1.2 Heat transfer within the pellet

Heat transfer within the solid pellet is given by equation 4.

$$\rho \, C_p \frac{\partial T}{\partial t} - \nabla.(k \nabla T) = Q \quad (4)$$

Following this discussion, the total loss of heat from the surrounding air at the interface is given by equation 5.

$$Q = h(T_s - T_\infty) \quad (5)$$

where h is convection heat transfer coefficient (W/m^2 K) and T_s and T_∞ are solid surface and gas temperature (K).

2.2 Model Geometry:

The shape of pellet is approximated to the sphere in order to simplify the calculation. The diameter of this square is measured 6mm according to real pellet. For simulating the surrounding fluid flow, the pellet geometry is placed in a cylinder with the height of 60mm and diameter of 36 mm width and the pellet is placed at the distance of 12mm from the inlet. The model simplified because of its symmetry and 2 dimensional simulation implemented in the study, see Figure 2.

2.3 Meshing

This mesh is used in all further simulations. The mesh resolution at the interface is displayed in Figure 3.

2.4 Initial and Boundary Conditions

The convective heat transfer coefficient at the interface between the pellet and the fluid region is estimated to be the same as that of a solid due to the small size of the particles building the pellet as compared to the pellet itself. These data was tabulated at tables 1, 2, and 3.

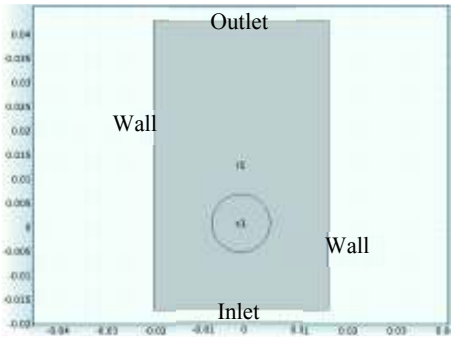

Figure 2. Model geometry with boundary conditions.

2.5 Gas Composition Effect

As a substantial proportion of inlet gas at the drying zone retrieved from firing and

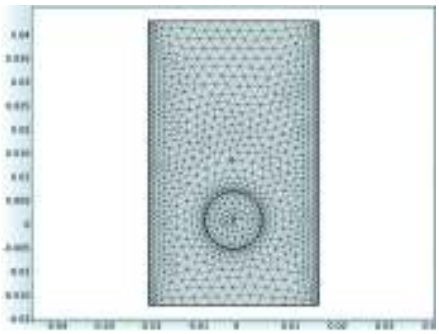

Figure 3. Mesh resolution

Table 1. Boundary conditions in constant pressure

Grid no.	$T_{in}(^{\circ}C)$	$\Delta P(pa)$
1	100	15
2	150	15
3	200	15
4	250	15
5	300	15

Table 2. Boundary conditions in constant Temperature

Grid no.	$\Delta P(pa)$	$T_{in}(^{\circ}C)$
1	5	200
2	10	200
3	15	200
4	20	200
5	30	200
6	40	200
7	50	200
8	60	200
9	70	200
10	80	200
11	90	200

Table 3. Values of pellet parameters used as the base case of simulation.

Parameter	Value	Reference
Density	5262(Kg/m^3)	(Ljung et al., 2010)
Thermal conductivity	5.27(W/m K)	(Clark, 1996)
Specific heat capacity	586 (J/Kg K)	(Waples, 2004)

cooling zone, gas composition includes CO_2 which is produced by burners, so the CO_2 existence effects are simulated in this study. To achieve this purpose a, b, and c coefficients in heat capacity in constant pressure, Cp (Eq. 6), modified with respect to CO2 and air volume percentages.

$$C_p = a + bT + cT^{-2} \quad (6)$$

2.6 Simulation Technique

The simulations were carried out with the commercial software COMSOL v4.3a, which is based on finite element method (FEM), on a desktop personal computer.

3 RESULTS AND DISCUSSION

The flow around the pellet is calculated by time dependent laminar simulations. The velocity and temperature fields are displayed in Figures 4 to 5 and 6to 8 respectively. Drying simulations are performed with boundary conditions representing the experiment described in the 2.4section.

Since the gas volumetric flow rate is constant, in a cross section that includes pellet, the gas flow area decreases thus gas velocity will increase markedly around the pellet thus an individual pellet can affect the gas velocity in the whole pallet. As the Figures 4 and 5 illustrate, wake area diminished by increase the gas velocity and therefore heat transfer can be improved at the upstream side of the pellet. Additionally, it can be obtained from these figures that the gas velocity near the surface was not

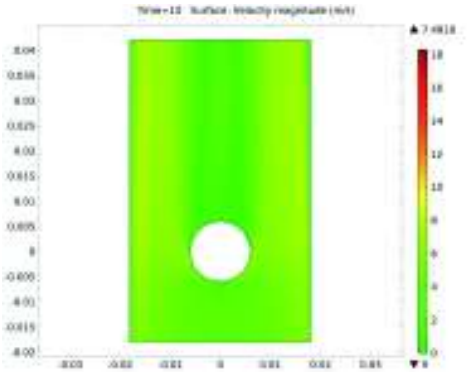

Figure 4. Velocity magnitude for flow at $\Delta P = 10$

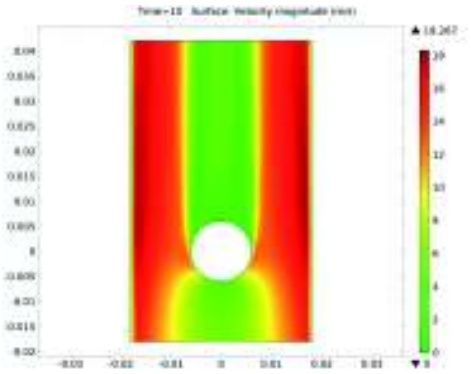

Figure 5. Velocity magnitude for flow at $\Delta P = 60$

changed considerably and the relation between pressure difference and the pellet temperature is lower than linear.

As the figures 6 and 7 show, gas temperature falls at the upstream side of the pellet and this decreases the drying rate of the upper pellets in the pallet. Furthermore, during the time, temperature of pellet will increase gradually. It is clear from the figure 10 that the difference between the highest and the lowest temperature on a selected cut-line (see fig. 9) will be decrease within the pellet as the time passes; therefore, to avoid excessive thermal stresses and cracking in the pellets more attention should be paid at

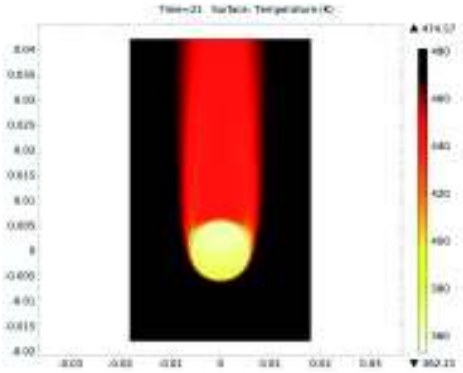

Figure 6. Temperature of surrounding air flow with corresponding solid temperature at$\Delta \mathbf{P} = \mathbf{15}$, t =21s.

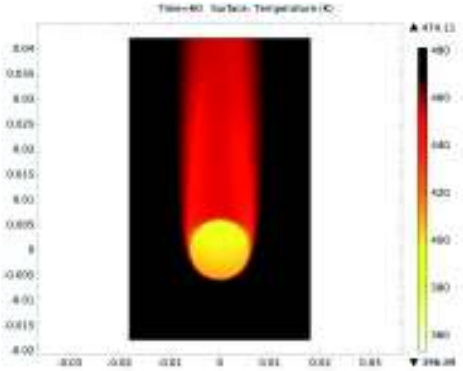

Figure 7. Temperature of surrounding air flow with corresponding solid temperature at $\Delta \mathbf{P} = \mathbf{15}$, t=60s.

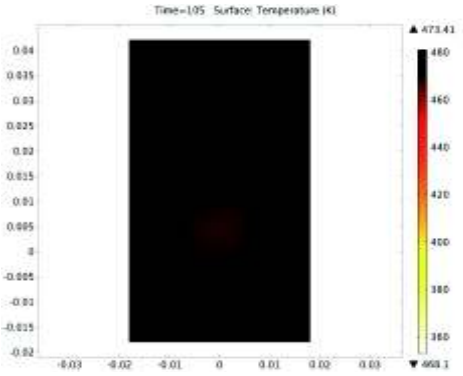

Figure 8. Temperature of surrounding air flow with corresponding solid temperature at$\Delta \mathbf{P} = \mathbf{15}$, t =steady state.

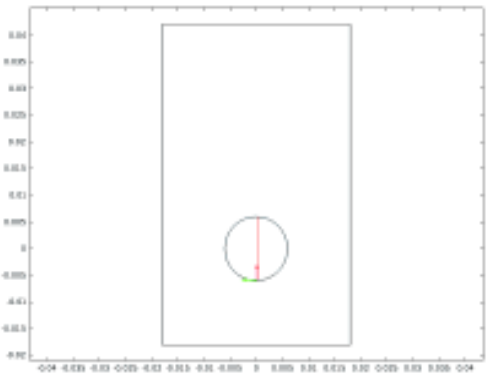

Figure 9. Model geometry also indicating the evaluation cut-line.

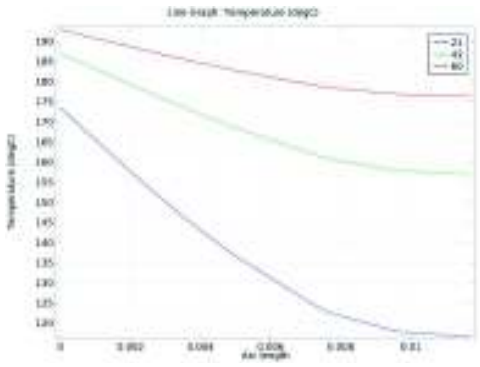

Figure 10. Temperature profile at the evaluation cut-line.

the beginning of drying process. Figure 12 depicts the temperature variations in 5 selected dots that are shown in figure 11 and it is clear that temperature increasing rate is higher at the downstream side of the pellet in comparison to the upstream side. Temperature profiles is calculated in various boundary conditions in order to determine the gas temperature and inlet-outlet pressure difference (gas velocity) impact on minimum temperature of an individual pellet that can be seen in figure 13 and 14 respectively. As is illustrated by the figure 14 relationship between minimum temperature within the pellet and diverse inlet gas temperature is

linear and its impact is more considerable than inlet gas velocity.

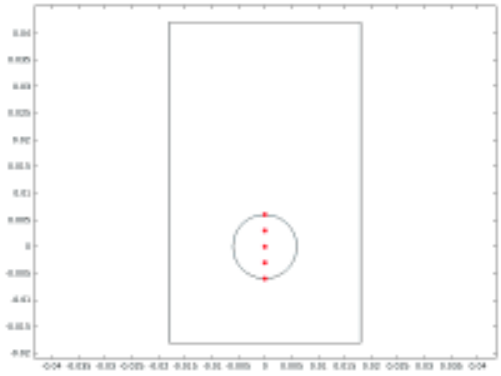

Figure 11. Model geometry also indicating the five evaluation points.

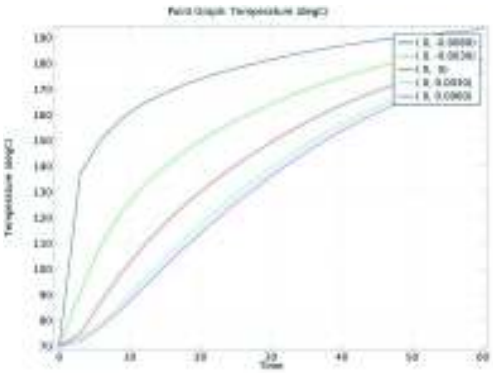

Figure 12. Temperature profile at the evaluation points.

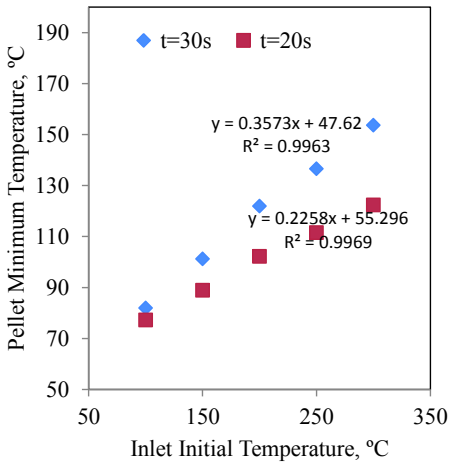

Figure 13. Pressure difference and the pellet temperature

Finally the CO_2 existence effects are simulated in this study with two different compositions, %10 and %35 CO_2 in volume ratio, and the final results show that existence of CO_2 affects pellet minimum temperature directly at the drying zone. Calculated data at t=60 seconds are 411K (%35 CO2), 404K (%10 CO2) and 396K (%0 CO2). As the figue.15 shows the relation between K and %CO_2 for three different temperatures, by increasing the percentage of CO_2, the heat transfer coefficient is linearly descending so the pre-produced heat is trapped inside the box and increasing of pellet minimum temperature during this study is logical and reasonable relationship.

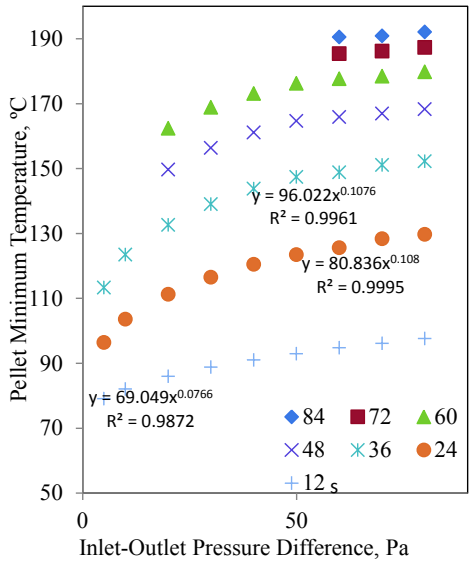

Figure 14. Inlet-outlet pressure difference impact on pellet temperature

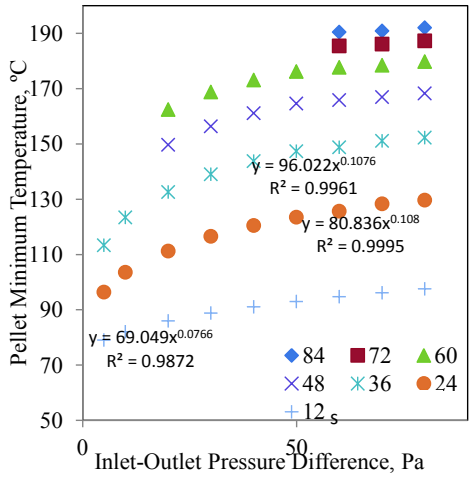

Figure 15. Inlet-outlet pressure difference impact on pellet temperature

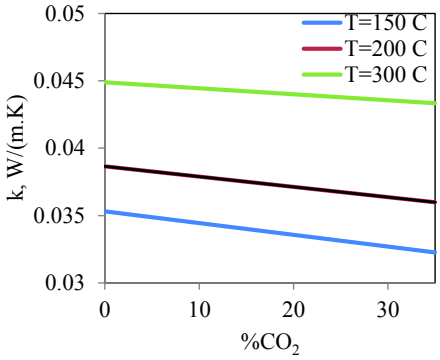

Figure 16. Gas composition (%CO_2) and thermal conductivity coefficient

4 CONCLUSION

In this work, drying of an individual iron ore pellet is simulated at various inlet air and temperatures. The results indicate that:

- The effect of gas temperature on the heat transfer is more considerable than that of gas velocity.
- Consistence of CO_2 in the inlet gas composition can enhanced the heat transfer between gas and solid pellet.
- Required time to reach the steady state fell as the gas temperature or velocity increased as well as both.
- Drying rate is decreased by an exponentially function related to time.

ACKNOWLEDGEMENT

The authors would like to acknowledge the R&D center of GolGohar Iron Ore Co. for contribution of the plant data for assessment of the model.

REFERENCES

T. Tsukerman , C. Duchesne , D. Hodouin, On the drying rates of individual iron oxide pellets, *Int. J. Miner. Process.* 83 (2007) 99–115

Anna-Lena Ljung, T. StaffanLundström, Kent Tano, (2011),"Simulation of convective drying of a cylindrical

MansoorBarati,Dynamic simulation of pellet induration process in straight-grate system, *Int. J. Miner. Process.* 89 (2008) 30–39

Anna-Lena Ljung, T. Staffan Lundström, B. Daniel Marjavaara& Kent Tano (2011): Influence of Air Humidity on Drying of Individual Iron Ore Pellets, *Drying Technology*, 29:9, 1101-1111

T.J. Jamaleddine, M.B. Ray, Application of computational fluid dynamics for simulation of drying processes: a review, *Drying Technol*. 28 (2010) 120–154.

L. Zili, Heat and mass transfer during drying in cylindrical packed beds, Numer. *Heat Tranfer A-Appl*. 36 (1999) 201–228.

J.A. Thurlby, R.J. Batterham, R.E. Turner, *International Journal of Mineral Processing* 6 (6) (1979) 43–64.

J. Mitterlehner, G. Loeffler, F. Winter, H. Hofbauer, H. Schmid, E. Zwittag, H. Buergler, O. Pammer, H. Stiasny;, *ISIJ International* 44 (1) (2004) 11–20.

D. Pomerleau, A. Desbiens, D. Hodouin, Optimization of a simulated iron-oxide pellets induration furnace, in: *11th Mediterranean Conference on control and Automation*, 2003.

Ljung, A.-L.; Lundstrom, T.S.; Sjo¨strom, U.; Marjavaara, B.D.;Lindblom, B.; Tano, K. Drying of an iron ore pellet: Investigationof the influence of surface irregularities and overall geometry. *Proceedings(CD) of the Third International Conference on Porous Mediaand its Applications in Science and Engineering, Montecatini, Italy,* June 20–25, 2010

Clark, S.P. Handbook of Physical Constants; Geological Society of America: New York, 1966

Waples, D.W. A review and evaluation of specific heat capacities ofrocks, minerals, and subsurface fluids. Part 1: Minerals and nonporous rocks. *Natural Resources Research* 2004, 13, 97

Single-Objective Optimization of Closed Ball-Milling Circuit of Esfordi Phosphate Plant

Z. S. Mirzaei
Faculty of Mining Engineering, University of Kashan, Kashan, Iran

A. Farzanegan
School of Mining, University College of Engineering, University of Tehran, Tehran, Iran,

ABSTRACT The subject of this project is optimization of closed ball-milling circuit at Esfordi phosphate plant, based on integration of process simulation and genetic algorithm (GA) concepts. At Esfordi plant, the fine particles (-20 μm) in cyclone underflow contain a high grade of Iron which are subjected to over grinding which consequently cause some problems in the downstream process, i.e., flotation. Hence, the first optimization goal was set to adjust the d_{80} of overflow at 100 μm that is 94 μm presently. The second goal was set to increase the d_{80} of underflow to 500 μm from the current value of 205 μm. If the second optimization goal is satisfied, it can reduce fine particles in underflow stream. In order to evaluate circuit performance, samples were collected from various points of circuit every 10 minute during 3 hours. The samples were analyzed to obtain size distributions, weight and percent solids. The obtained data set was then mass balanced and was used to calculate efficiency curve, circulating load and other properties for various streams. The BMCS® (BMCS-based Modular Comminution Simulator) under MATLAB software was used in this investigation to search for the optimal operating condition of the comminution circuit so that a pre-defined process goal can be achieved. The search process is done using genetic algorithm. The goal of the current project was set to improve ore grinding in ball mill unit and increase the efficiency of particle size classification by hydrocyclone unit. The GA optimization was done in single objective form so that the optimization goal was to achieve a pre-defined particle size for overflow or underflow streams separately. The circuit simulations optimized by GA produced various results and conditions that each of them can be recommended for plant testing and performance improvements.

1 INTRODUCTION

Optimization techniques target improving plant performance through better utilization of energy and equipment. In plant operation, optimization leads to better yields of valuable products (or reduced yields of contaminants), reduced energy and reagent consumption, higher production rates, and fewer shutdowns. Optimization can be effected by applying off-line (circuit analysis and simulations) or on-line (manual or automatic control strategies) techniques. Optimization can be limited to a particular segment of a plant for local optimization, or it can be at plant scale for a global optimization (Farzanegan, 1998).

In mineral processing plants, generally the optimization is done on comminution circuits containing crushers and mills and classification systems. These circuits which are the most important part in mineral processing plants, the energy consumption is very high. None-optimized performance of these circuits effects on performance of down streams circuits. Optimization in these circuits increases the quality of production and leads to optimized usage of energy.

Whereas the comminution circuits are utilized in many industries, decreasing the energy consumption will affect the production costs. Combining process simulation and numerical optimization algorithms provides a more powerful tool for mineral processors to find the best circuit design and operation parameters.

The fine particles (-20 μm) in cyclone underflow contain a high grade of Iron which subject to over grinding and cause some problems in the downstream process, i.e., flotation stage. So, the first purpose of optimization was set to adjust the d_{80} of overflow at 100 μm that is 94.2 μm presently. The second purpose was set to increase the d_{80} of underflow to 500 μm from the current value of 205 μm. Reach to the second purpose of optimization cause to decrease of fine particles in underflow stream.

This project aimed to optimize of ball mill circuit of Esfordi Phosphate plant by combination of simulator algorithm with Genetic Algorithm (GA). Esfordi Phosphate plant is located in Yazd province, Bafgh. In past decade, GA approach has been successfully applied to design and optimize comminution circuits (While et al., 2004, Becker et al., 2004; Mitra and Gopinath, 2004)

2 MATERIALS AND METHODS

2.1 Sampling and Data Collection

As it is shown in Figure 1, the comminution circuit in Esfordi phosphate plant is consisted of a rod mill in open circuit which its discharge goes to a collection sump. In this circuit, a ball mill is closed with a hydrocyclone. The discharge of the ball mill together with discharge of rod mill forms the final feed to the hydrocyclone. The classified coarse particles report to the cyclone underflow which is called the circulating load and is fed to ball mill for more size reduction. The classified fine particles report to cyclone overflow which is the feed to the desliming hydrocyclone package.

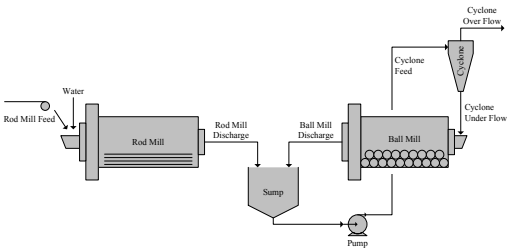

Figure 1. Esfordi comminution circuit

According to explained circuit, samples were collected from various points of circuit every 10 minute during 3 hours. The samples were analyzed to obtain size distributions, weight and percent solids. In next stage, the obtained data set was subjected to mass balance process by NORBAL software (Spring, 1992).

2.2 BMCS-based Modular Comminution Simulator (BMCS)

BMCS-based Modular Comminution Simulator (BMCS) is written in C language and can be run under MS DOS environment. Presently, it includes mathematical models to simulate the ball mills, hydrocyclones, air separators, efficiency curves, junctions, splits and convergence block.

The BMCS under MATLAB environment optimizer software has been developed recently. It receives the operating conditions of grinding circuit and can predict the variables so as plant operates in optimized conditions (Farzanegan and Vahidipour, 2009).

3 RESULTS AND DISCUSSION

The d_{80} of each stream is showed in Table 1. The circulating load was calculated 471.7% in steady state which it is much more than its predefined amount (150%). In Table 2 the reduction ratio of both mills is shown. The particle size distribution of streams around the hydrocyclone is shown in Figure 2. As it is seen, the performance of hydrocyclone is not in an appropriate condition and the particles go to underflow stream due to poor classification.

Table 1. Particle size (d_{80}) of various streams

Stream	d_{80} (μm)
RMF	9835.04
RMD	209.52
BMF	205.89
BMD	189.40
CYCF	195.10
COF	98.15
CUF	205.89

Table 2. Size reduction ratio for the both mills

	Current Size Reduction Ratio	Previous Size Reduction Ratio
Rod mill	46.98	64.65
Ball mill	1.08	1.15

In this figure, the particle size distribution of underflow is very similar to the feed.

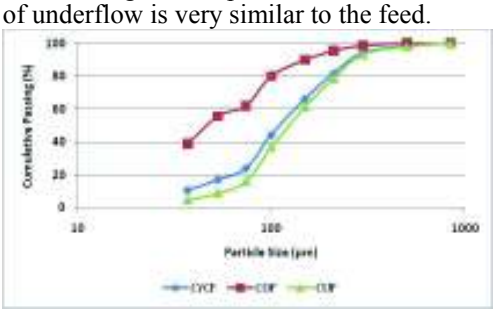

Figure **2**. Particle size distribution around the hydrocyclone

In Figure 3, it is seen that the plot has a deep slope in size of 60 μm. In addition, in size of 60 to 90 μm, the plot has an abnormal figure. According to mineralogical studies, Esfordi phosphate ore contains of a light component (fluorapatite) and a heavy component (hematite). So, the existence of two components in hydrocyclone feed is the reason for the abnormal figure of this plot and the calculation of d_{50c} is not possible exactly.

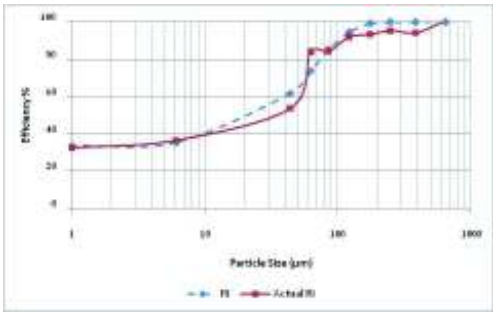

Figure 3. Actual (measured) and fitted efficiency curves of the hydrocyclone unit

Table 3. Fluid recovery, corrected cut size and separation sharpness obtained by fitting solids recovery model to measured data

Parameter	Value
Fluid recovery (R_f)	0.34
Corrected cut size (d_{50c})	51.74
Sharpness of classification (m)	1.50

3.1 Comparison of Present Performance of Plant With the Predicted Performance in Design Conditions

The purpose of this comparison is to obtain sufficient criteria for circuit optimization. As it was seen, the purpose of this project is not the optimization of rod mill but it seems to reach to an overall view of differences between present and predicted performance of circuit, it is better to comparison the current and past conditions of rod mill too.

Table 4. Comparison of present and predicted conditions of rod mill

Parameter	Design	Present
Fresh feed solids flow rate (t/h)	57.50	47.10
Feed size, d_{80} (mm)	14.00	9.84
Product size, d_{80} (mm)	0.60	0.20
Solids content (%)	30	66.50
Size reduction ratio	23.33	46.98

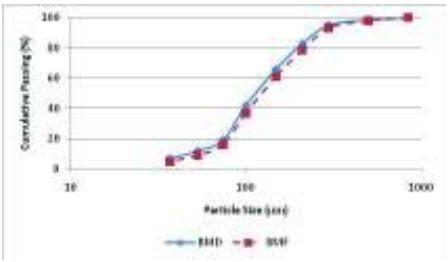

Figure 4. Particle size distributions of ball mill feed and product

Table 5. Comparison of present and predicted conditions of ball mill

Parameter	Design	Present
Pulp flow rate to closed circuit (t/h)	46	61.50
Feed size, d_{80} (mm)	75	205.89
Product size, d_{80} (μm)	100	189.40
Circulating load (%)	150	471.41
Size reduction ratio	7.5	1.08

Table 6. Comparison of present and predicted conditions of hydrocyclone

Parameter	Design	Present
Feed solids flow rate (t/h)	172.50	232.28
Feed pulp flow rate (m^3/h)	260.10	202.78
Cut size (μm)	100.00	51.47
Overflow particle size, d_{98} (μm)	150.00	175.72
Feed solids content (%)	45.00	63.00
Overflow solids content (%)	25.00	30.70
Underflow solids content (%)	75.00	81.10

Table 7. Comparison of present and past amount of Bond ball mill work index

Parameter	Design	Present
Bond Work Index	7.50	9.47

3.2 Circuit Performance Problems

According to operating conditions and investigations, it is observed that there are some problems:

- Inefficient comminution in ball mill
- Inefficient classification in hydrocyclone
- High percent solids in hydrocyclone feed
- Existence of fine particles in hydrocyclone underflow
- Increasing in fine particles containing iron in hydrocyclone overflow which causes the reduction in quality of flotation production.

The existence of two components in plant feed may be the basic reason for these problems. Containing feed of two components (heavy and light) in classification process, the heavy component (hematite) having fine particles, enters the underflow and increases the circulating load and percent solid of ball mill feed. The particles involving iron should be ground very much to reach a sufficient weight to exit from overflow. So, these particles subject to over grinding and consequently fine particles with high iron grade will be produced. In addition, increasing in feed percent solid and feed rate of ball mill simultaneously, leads to decrease of coarse particles comminution. So, inefficient performance of hydrocyclone is due to entrance of a two components stream with a high percent solid to the hydrocyclone. The limited capacity of hydrocyclone feed sump prevents of addition more water to this sump to increase the hydrocyclone dilution too.

3.3 Optimization of Ball Mill Circuit

Genetic algorithm starts to minimize the fitness function value by changing the

amount of predefined parameters. The lowest fitness function is the best. Every 12 optimization scenarios were done with default setting of Genetic Algorithm in MATLAB software. The stopping criterion was considered reach to 0.001 in function tolerance.

3.3.1 Optimization goals

The first purpose of optimization was set to adjust the of overflow at 100 µm that is 94.2 µm d_{80} presently. The second purpose was set to increase the d_{80} of underflow to 500 µm from the current value of 205 µm. Increasing the throughput is expected simultaneously. The single objective optimization was done for each goal.

3.3.2 Variable parameters in optimization

Based on circuit flowsheet shown in Figure 1, solids to the ball mill circuit, ball mill feed percent solid, water addition to the hydrocyclone feed and water addition to the ball mill feed were considered as variables to be optimized by GA search method. The practical adjustment ranges of these variables were determined by consulting with plant operators.

3.3.3 Optimization variables limits

The lower and upper limits of the variable parameters are shown in Table 8. Variable x_1 is the solids to the ball mill circuit in terms of tones per cubic meters. The current value of this variable is approximately 45 t/h. As it was mentioned earlier, one of the optimization goals is increase in throughput so; no upper limit was set for this parameter. Variable x_2 is solids content (%) of fresh feed to the ball mill which can be set between 45 to 65 percent. Through the optimization process it was seen that this parameter always is adjusted in lower limit. So, to ensure of appropriate performance of rod mill, its lower limit was set at 50 percent. Variable x_3 is the water addition to the hydrocyclone feed sump in cubic meters per hour. As the capacity of this sump is limited to prevent it overflowing, the upper limit of this parameter was set at present value. Variable x_4 is water addition to the hydrocyclone underflow or ball mill feed.

Table 8. Lower and upper limits for optimization variables

	x_1		x_2		x_3		x_4	
Variables Set	L. L.*	U. L.**	L. L.	U. L.	L. L.	U. L.	L. L.	U. L.
1	45	Inf	45	65	40	69	25	45
2	45	Inf	45	65	40	50	25	45
3	45	Inf	50	65	40	50	25	45

*Lower Limit
**Upper Limit

3.3.4 Optimization scenarios

The diameter of hydrocyclone apex can be adjusted in size of 3 and 4 in. and vortex finder is capable to be set in size of 8 and 9 in. too. Given two choices for each of apex and vortex finder diameter sizes and three optimization variable sets (Table 8), 12 scenarios were considered to achieve optimization goal for overflow and underflow separately. Circuit optimizations were done by BMCS under MATLAB software.

3.4 Single Objective Optimization in Overflow

The optimum values of various variables found by running BMCS under MATLAB for all scenarios are shown in Table 9. Addition to the fitness function value, cumulative percent passing from 100 µm in hydrocyclone overflow stream, ball mill feed percent solid, cumulative percent passing from 74 µm in hydrocyclone underflow stream and volumetric flow rate of hydrocyclone feed were considered as criteria for evaluation results.

Table 9. Optimum values for variables set found by simulation-based GA search

Scenario	x_1	x_2	x_3	x_4
1	45.47	47.19	64.00	34.02
2	45.00	45.00	49.62	25.00
3	45.00	50.01	49.96	25.18
4	45.30	51.78	69.64	27.98
5	45.00	45.07	49.31	25.00
6	45.03	50.34	46.57	25.04
7	45.03	45.00	68.96	37.89
8	45.11	45.01	49.87	25.12
9	45.80	50.00	49.87	25.00
10	47.05	46.13	67.60	28.05
11	25.25	49.98	45.20	45.00
12	45.09	50.00	49.88	28.10

The first criterion is the optimization goal and shows the ability of algorithm to define the optimum parameters. The second was considered to prevent of over grinding in ball mill.

Due to two-component composition of hydrocyclone feed which produces high content of fine particles in underflow stream, the third criterion can help to select the condition with lower fine particles in underflow stream. Finally, the last criterion prevents sump overflowing. The applied pump in this sump is capable to transfer 260 cubic meters per hour pulp.

The primary values of these criteria are shown in Table 10.

Table 10. Primary values of decision criteria

Parameter	Value
Cumulative passing from 100 μm in overflow (%)	82.84
Ball mill feed solids content (%)	78.00
Cumulative passing from 74 μm in underflow (%)	13.41
Hydrocyclone feed volumetric flow rate (m^3/h)	293.07

According to Table 11 it is observed that the size of 8 in. in vortex finder diameter combined with size of 4 in. in apex diameter is not acceptable for plant performance. But it is seen that in first and tenth optimization scenarios the value of fitness function equals to zero exactly.

Table 11. Optimization results of single objective optimization of overflow stream

Scenario	Vortex Finder Diameter (mm)	Apex Diameter (mm)	Variables Set	Fitness Function Value	Ball Mill Feed Solid Content (%)	Cumulative Passing from 100 μm in Overflow (%)	Cumulative Passing from 74 μm in Underflow (%)	Hydrocyclone Feed Volumetric Flow Rate (m^3/h)
1	20.32	7.62	1	0.000	59.65	80	1.93	180.15
2	20.32	7.62	2	0.672	60.53	79.18	2.8	159.06
3	20.32	7.62	3	6.708	58.43	77.41	3.07	149.33
4	20.32	10.16	1	118.592	45.69	69.11	15.71	362.78
5	20.32	10.16	2	123.209	45.55	68.90	16.24	330.22
6	20.32	10.16	3	133.40	45.07	68.45	16.90	322.78
7	22.86	7.62	1	1.439	57.22	78.80	0.87	211.31
8	22.86	7.62	2	10.176	57.91	76.81	1.82	156
9	22.86	7.62	3	36.936	55.96	74.81	2.09	146.34
10	22.86	10.16	1	0.000	61.50	80	5.81	200.75
11	22.86	10.16	2	2.496	59.07	78.42	6.89	176.47
12	22.86	10.16	3	10.824	56.73	76.71	7.08	168.92

In Tables 12 and 13 specifications of streams for 1st and 10th optimization scenarios are shown. It can be seen that in both optimization scenarios, ball mill feed percent solids are in the appropriate range. In tenth optimization scenario the possibility of disturbance in pump performance decreases. Hydrocyclone underflow percent solid in first optimization is very high whereas it is more suitable in tenth optimization. Particle sizes of various streams, particles size reduction ratios and circulating loads for 1st and 10th optimization scenarios are given in Tables 14.and 15.

Table 12. Specification of various streams for 1st optimization scenario

Stream	Pulp Flow Rate (t/h)	Solids Content (%)	Solid Flow Rate (t/h)	Water Flow Rate (t/h)	Pulp Density (t/m^3)	Pulp Flow Rate (m^3/h)
CFF	96.36	47.20	45.48	50.88	1.51	63.87
CYCW	64.00	0.00	0.00	64.00	1.00	64.00
BMD	91.09	59.65	54.33	36.76	1.74	52.28
CYCF	251.45	39.70	99.82	151.63	1.40	180.15
COF	194.38	23.40	45.48	148.90	1.20	161.90
CUF	57.06	95.22	54.33	2.73	3.13	18.25
BMW	34.03	0.00	0.00	34.03	1.00	34.03
BMF	91.09	59.65	54.33	36.76	1.74	52.28

Table 13. Specification of various streams for 10th optimization scenario

Stream	Pulp flow rate (t/h)	Solid content (%)	Solid flow rate (t/h)	Water flow rate (t/h)	Pulp density (t/m3)	Pulp flow rate (m3/h)
CFF	102.00	46.13	47.06	54.94	1.49	68.38
CYCW	67.60	0.00	0.00	67.60	1.00	67.60
BMD	115.50	61.50	71.03	44.47	1.78	64.76
CYCF	285.10	41.42	118.09	167.01	1.42	200.70
COF	197.64	23.81	47.05	150.59	1.20	134.0
CUF	87.45	81.22	71.03	16.42	2.38	36.71
BMW	28.05	0.00	0.00	28.05	1.00	28.05
BMF	115.50	61.50	71.03	44.47	1.78	64.76

Table **14.** Particle size (d_{80}) of various streams in 1st and 10th optimization scenarios

Stream	Scenario 1	Scenario 10
CFF	261.80	261.80
BMD	215.00	215.26
CYCF	237.42	234.80
COF	100.00	100.00
CUF	290.64	281.50
BMF	281.50	290.64

Table **15**. Size reduction ratio and circulating load in 1st and 10th optimization scenarios

Scenario	Size Reduction Ratio	Circulating Load (%)
1	1.35	119.46
10	1.30	150.93

In Figure 5 to Figure 8 particle size distributions of ball mill feed and discharge,

streams around the hydrocyclone for first and tenth optimization scenarios are shown.

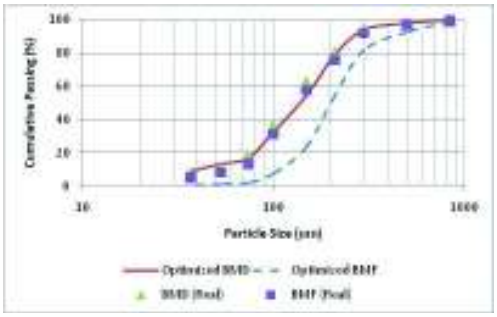

Figure 5. Particle size distributions of ball mill feed and discharge in 1st optimization scenario

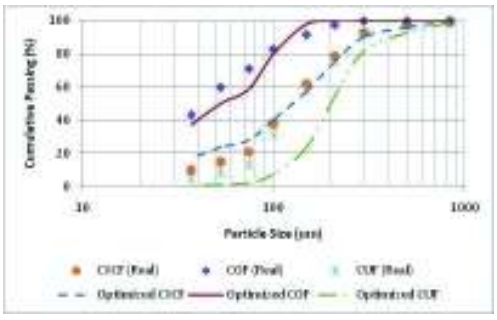

Figure 6. Particle size distributions of streams around the hydrocyclone in 1st optimization scenario

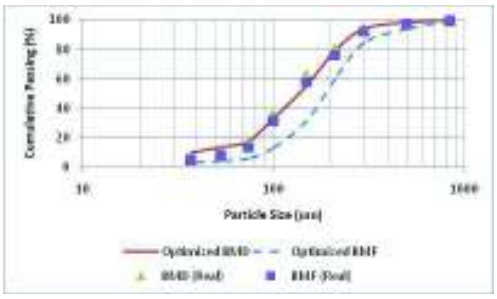

Figure **7**. Particle size distributions of ball mill feed and discharge in 10th optimization scenario

The size of 8 in. in vortex finder diameter combined with size of 3 in. in apex diameter or 9 in. in vortex finder diameter combined with 4 in. in apex diameter leads to produce a d_{80} equal to 100 μm in overflow.

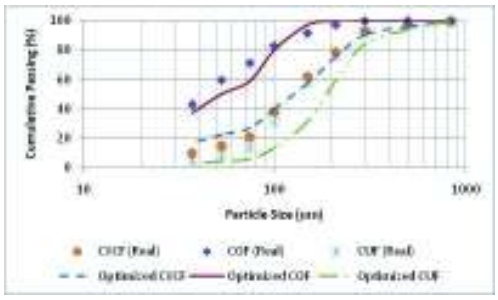

Figure 8. Particle size distributions of streams around the hydrocyclone in 10th optimization scenario

The second combination produces less fine particles content in hydrocyclone underflow and decreases the ball mill feed flow rate and consequently comminution will be more efficient. With this combination of overflow and underflow diameter sizes, the fresh feed to the ball mill circuit will be equal to 45 t/h and with solids content equal to 46.13 %. To obtain an overflow particle size (d_{80}) of 100 μm, it is necessary to adjust the water additions to the hydrocyclone and ball mill feeds equal to 67.6 t/h and 28 t/h, respectively.

These changes lead to decrease fine particles in underflow stream (considering cumulative percent passing of 74 μm) from 16 to 5.8 percent. Ball mill feed flow rate is adjusted in 115 t/h exactly. Solid content of hydrocyclone feed, overflow and underflow streams are equal to 41, 24 and 81 percent respectively. Simulation shows that the sharpness of classification is about 3 to 3.5 which represent a good classification in hydrocyclone. Moving down the particle size distribution of underflow shows that this stream becomes coarser.

These changes cause decrease in ball mill feed solid content from 78 to 61.5 percent and coarser particles with a lower feed flow rate, result in better comminution in ball mill. The most important change is observed in circulating load which decrease from 711 to 151 percent and consequently the

reduction ratio increase to 1.3. As it is seen, the reduction ratio is very low and there's opportunity to make its performance better. Making its feed coarser may be a good decision. To examine it, the whole of comminution circuit (containing rod mill) should be considered.

The d_{80} of underflow rather than before increases about 50 μm that represents a coarser feed to the ball mill. It seems that change in apex and vortex finder diameter can decrease the effect of existence of two components in the feed.

3.5 Single objective optimization in underflow

In Table 16 the optimum values of variable parameters for all scenarios are shown. Table 17 shows more details of optimization results including fitness function value for each scenario.

In this stage, the cumulative percent passing from size of 500 μm in hydrocyclone underflow, ball mill feed percent solid, cumulative percent passing from size of 74 μm in hydrocyclone underflow and feed were considered.

Table 16. Optimum values of variables set found by simulation-based GA search

Scenario	x_1	x_2	x_3	x_4
1	53.53	64.98	40.10	25.17
2	47.65	64.97	40.10	25.23
3	51.49	64.94	40.24	25.04
4	49.79	63.75	40.32	44.53
5	59.16	64.90	40.29	42.54
6	55.96	64.92	41.72	33.71
7	52.66	64.98	47.05	25.07
8	48.37	64.95	41.09	25.06
9	49.15	64.96	43.70	25.00
10	51.64	64.94	40.04	26.59
11	46.71	64.94	40.06	25.00
12	53.63	64.78	40.22	25.45

Table **17**. Optimization results of single objective optimization of underflow stream

Scenario	Vortex Finder Diameter (cm)	Apex diameter (cm)	Variables Set	Fitness Function Value	Ball Mill Feed Solids Content (%)	Cumulative Passing from 74 μm in Underflow (%)	Hydrocyclone feed Volumetric Flow Rate (m^3/h)
1	20.32	7.62	1	56.70	52.59	7.88	124.38
2	20.32	7.62	2	68.39	51.08	8.10	119.09
3	20.32	7.62	3	60.83	51.81	7.73	123.48
4	20.32	10.16	1	198.80	43.79	26.66	319.53
5	20.32	10.16	2	184.14	46.33	26.44	326.40
6	20.32	10.16	3	189.33	46.30	27.50	309.61
7	22.86	7.62	1	39.69	51.14	5.48	127.31
8	22.86	7.62	2	35.64	48.04	6.18	117.24
9	22.86	7.62	3	39.56	49.16	5.90	120.63
10	22.86	10.16	1	111.72	52.86	15.53	138.77
11	22.86	10.16	2	119.90	51.99	16.18	132.02
12	22.86	10.16	3	107.32	53.73	15.73	139.87

As it is clear from Table 17, the fitness function values in underflow optimization are much more than overflow optimization. Generally none of the obtained results are acceptable for the optimization performance of plant. Similar to the overflow optimization, the size of 8 in. in vortex finder diameter combined with size of 4 in. in apex diameter is not acceptable for plant performance. The lowest value of fitness function which corresponds to the best plant operating scenario is equal to 35.64. Therefore, in this case operating condition indicated in scenario number 8 can be recommended for performing real plant tests and further optimization studies.

4 CONCLUSIONS

The results indicate that an integrated environment of grinding simulation and GA search software can be used as a powerful tool to optimize comminution operations. The authors showed that operating condition of Esfordi ball mill grinding circuit can be modified and optimized based on a single-objective approach using the grinding simulation software BMCS coupled with GA search toolbox under MATLAB environment. In this approach, first, a number of feasible plant operating scenarios can be defined by consulting plant personnel and, then, try to find and designate the best scenario using simulation-based GA search method.

ACKNOWLEDGEMENT

The authors thank Mr. Tavakoli, the process manager of Esfordi phosphate plant. Also helps from Esfordi phosphate plant for providing access to their phosphate processing plant is greatly appreciated.

REFERENCES

Becker, J., Salazar, J. Magne, L., Cubillos, F., 2004. *Real-Time Optimization of SAG Mills Using Genetic Algorithms*. Facultad de Ingeniería, Universidad de Santiago de Chile

Farzanegan, A. and Vahidipour, S. M., 2009. Optimization of comminution circuits simulations based on genetic algorithms search method, *Minerals Engineering*, Vol. 22, Issues 7-8, pp. 719-726

Farzanegan, A., 1998, *Knowledge-Based optimization of mineral grinding circuits,* Ph.D Thesis, McGill University, Canada.

Mitra, K, Gopinath, R., 2004. *Multiobjective Optimization of an Industrial Grinding Operation Using Elisit Nondominated Sorting Genetic algorithm*, Chemical Engineering Science, Vol. 59, pp 385-396.

Spring, R, 1992. *NorBal3 Software for Material Balance Reconciliation,* NORANDA Technology Center.

While, L., Barone, L., Hingston, P., Huband, S., Tuppurainen, D. and Bearman, R. 2004. *A Multi-Objective Evolutionary Algorithm Approach for Crusher Optimisation and Flowsheet Design*, *Minerals Engineering*, Special Issue on Comminution.

A Decision Support System For Mine Project Selection Under Uncertainty Using Fuzzy Topsis Technique

Z. Gligoric
University of Belgrade, Faculty of Mining and Geology, Belgrade, Republic of Serbia

C. Beljic
University of Belgrade, Faculty of Mining and Geology, Belgrade, Republic of Serbia

B. Gluscevic
University of Belgrade, Faculty of Mining and Geology, Belgrade, Republic of Serbia

S. Jovanovic
Concern Farmakom M.B. Sabac, Mine Lece d.o.o. Medvedja, Medvedja, Republic of Serbia

ABSTRACT A mining ventures are often associated with diverse sources of uncertainties. Such uncertainties are usually related to ore grade, mill recovery, capital costs, operating costs, product prices, discount rate, etc. These items play a key roles in the process of the project profitability estimation. Having the ability to plan for these uncertainties, by incorporating flexibile alternatives into system design, is increasingly recognized as critical to long term mining company success. In this article, by using simulation and fuzzy TOPSIS technique we propose a method for underground mine project selection problem. After reviewing three common methods of comparing investment alternatives (Net Present Value, Profitability Index and Modified Internal Rate of Return) we use them as criteria in decision making process. Stochastic model has been built for the most influential input variables of the criterion calculation. Then by implementing fuzzy TOPSIS algorithm, assessment of projects has been done. A decision support system is developed for an underground lead-zinc mine as a example of application.

Keywords: mine project selection, uncertainties, multi criteria decision making, TOPSIS

1 INTRODUCTION

Underground mine project valuation has become truly interdisciplinary in nature. Therefore, most mining companies prefer to establish multidisciplinary groups which perform the evaluation function for new investment opportunities. This is the preferred approach to the problem, but many mining companies in our country cannot afford the luxury of so many specialistics and must rely on two or three individuals to perform all project evaluations. The main objective of this paper is to develop evaluation model in order to help small-scale underground mining companies in Serbia to manage its investments as good as possible. Underground mining businesses are burdened with more uncertainity then other freemarket endeavours at both strategic and tactical levels. At a strategic level these uncertainties might include ore grade, mill recovery, capital investment intensity, discount rate as well as current metal prices and cost revelations. The model incorporate process of decision making simulation with uncertainities mentioned above. The Net Present Value (NPV), Profitability Index (PI) and Modified Internal Rate of Return (MIRR) are used as a capital criteria to decision making process. To estimate uncertainties related to ore grade, mill recovery and investment intensity the

different probability density functions are used such as the normal, uniform and triangular distribution respectively. To estimate uncertainities related to discount rate the fuzzy triangular number is used. To estimate the future states of metal price and operating costs Monte Carlo Simulation of Mean Reversion Process and Monte Carlo Simulation of Geomteric Brownian Motion are used respectively. In order to select the most appropriate project of the proposed alternatives the multicriteria decision making process based on the application of the Technique for Order Preference by Similarity to Ideal Solution (TOPSIS method) is used.

There are times when mine company is faced with making investment decisions. Mining projects have always been risky ireversible investments. Selection of mining project can be treated as strategy selection problems often adhere to vague and imprecise data in the fierce competition environment. When a mine company is faced with several investment proposals, it becomes very important to evaluate the real value of each proposal. However, the final investment decision is not based solely on the outcome of the accept/reject decision resulting from estimation of the investment proposal. Rather, the investment decision must also be based on determination of which of the acceptable proposals is best in terms of meeting the objectives of the mine company. Suppose we have two mining projects, MP1 and MP2. The problem is not one of simply asking "Are MP1 and MP2 acceptable to the company", but also "Which project is better and how much is better"? Simply said, it is a problem of ranking investment alternatives. In such environment, TOPSIS method gives opportunity to create final rank of proposed mining projects and indicates the degree of priority of the each project.

2 LITERATURE REVIEW

Multi-attribute decision making (MADM) has been widely used in selecting one or more project alternatives from a finite number of alternatives with respect to multiple criteria or attributes. A review of the literature reveals that decision making techniques have been used for a variety of specific mining applications. Alpay and Yavuz [1] developed a model for underground mining method selection by using Analytic hierarchy process. Bimal et al. [2] applied a multi criteria decision making process to select opencast mining equipment. Elevli et al. [3] selected a new vertical shaft or ramp system by comparing the weighted alternative criteria for small-scale underground mine on the basis of total investment cost, ore transport unit cost and net present value of overall project for various depths. Trigergios presents Decision tree model for mining project in which the present value of the remaining cash flows is uncertain [4] . Gligoric et al. [5] developed a hybrid model of evaluation of underground lead-zinc mine capacity expansion based on only one criterion, i.e., Net present value.

3 METHODOLOGY

Investment activity plays an extremely important role in every mining company. Selection of a new project or a group of projects constitutes one of the main management functions required to ensure business survival. Maybe the most unique aspect of the mining is a fact that it deals with non-renewable resources. Previous fact shows that the management of the company must have a clear strategy of production development, i.e. that it must have a developed decision making procedure under the conditions of business characterized by very high level of uncertainty. We developed the following concept of the decision making (see Figure 1): *Step 1*: creation a finite set of alternatives or investment projects; *Step 2*: determination of decision making criteria; *Step 3*: determination of sources of uncertainty in mining project; *Step 4*: quantification of uncertainties by simulation and fuzzification; *Step 5*: simulation of decision making criteria; Step 6: decision making by ranking of alternatives or investment projects by using TOPSIS method.

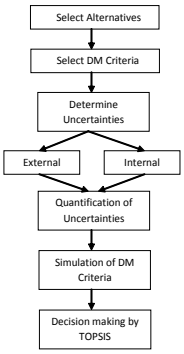

Figure 1. Flow chart of Decision Support System

3.1 Creation a set of alternatives

Alternatives represent the different choices of action available to the decision maker. Creation a finite set of alternatives or investment projects means a nomination of adequate number of realistically feasible proposals. A good set of alternatives cause good outcomes. A good set of alternatives will have: at least two alternatives, alternatives that are mutually exclusive and alternatives that differ substantially from one another. In the mining there are many problems which can be defined by set of alternatives. For example: mining method selection (room and pillar, cut and fill, room and pillar with fill, etc.), alternative access to orebody (ramp, shaft, shaft-ramp), etc.

3.2 Decision making criteria

Net Present Value is defined as the difference between the total of discounted cash flows expected from investment and the initial quantity of the invested capital. This relation is represented by the following equation:

$$\widetilde{NPV} = \sum_{t=0}^{T} \frac{CF_t}{\left(1+\widetilde{i}\right)^t} = CF_0 + \frac{CF_1}{\left(1+\widetilde{i}\right)^1} + \frac{CF_2}{\left(1+\widetilde{i}\right)^2} + \ldots + \frac{CF_T}{\left(1+\widetilde{i}\right)^T} \quad (1)$$

where: CF_T – cash flow in time t (year), $\widetilde{i}$ – fuzzy discount rate (%), T – overall project time (year).

This criterion should be maximized.

Profitability index (PI) is a measure calculated as a ratio between discounted cash flows and initial investment:

$$\widetilde{PI} = \frac{\sum_{t=1}^{T} \frac{CF_t}{\left(1+\widetilde{i}\right)^t}}{CF_0} \quad (2)$$

This criterion should be maximized.

Internal Rate of Return (IRR) is the discount rate which delivers a zero Net Present Value (NPV) on a given project. Technically, MIRR is the IRR for a project with an identical level of investment and NPV to that being considered but with a single terminal payment. While the IRR assumes that all cash flows are reinvested at the IRR, the MIRR assumes that all cash flows are reinvested at the firm`s cost of capital. This method is much more straightforward and employs a simple formula which is quick and easy to apply:

$$\widetilde{MIRR} = \sqrt[T]{\frac{\sum_{t=0}^{T} CIF_t (1+\widetilde{i})^{T-t}}{\sum_{t=0}^{T} \frac{COF_t}{(1+\widetilde{i})^t}}} - 1 \quad (3)$$

Here CIF_t refers to cash inflows and COF_t refers to cash outflows or the cost of the project.

$\sum_{t=0}^{T} CIF_t (1+\widetilde{i})^{T-t}$ - the compounded value of the inflows assuming that the cash inflows are reinvested at the cost of capital and it is also called the terminal value,

$\sum_{t=0}^{T} \frac{COF_t}{(1+\widetilde{i})^t}$ - the present value of the investment outlays when discounted at the cost of capital

MIRR is invariably lower than IRR and it makes a more realistic assumption about reinvestment rate. This criterion should be maximized.

3.3 Uncertainty in mining projects

Uncertainty in mining projects is generally evaluated with regard to internal

(endogenous) and external (exogenous) conditions. The internal conditions are in fact the product of characteristics of the deposit itself and the mining methods, as e.g., the ore grade, physical-mechanical characteristics of the working environment, management, planning, mining equipment and infrastructure. The external conditions are determined by external equivalents, such as, market price of the mineral raw material, demands for environment maintaining, political risks, government policy, demands of the share holders as well as social and industrial relations (Kazakidis and Scoble, 2003) [6].

3.3.1 Capital costs, mill recovery and ore grade

Models including variables not known and with satisfactory degree of accurateness are stochastic or probabilistic models. If we wish to describe the input parameters with continuous distribution of probability of their occurrence then there no more exists a final set of possible outcomes. For quantification of the uncertainty of the parameters belonging to capital costs, i.e. investments, the triangular distribution is used. When quantifying uncertainties of the size of capital costs, a less favorable situation is usually considered, i.e. that the costs are always greater than those desired, and the probability that lesser costs would occur is significantly decreased. When quantifying uncertainties that refer to mill recovery, it is usually taken into consideration that inside the range, the probability of occurrence of any value whatsoever is equal and the uniform distribution is used. For quantification of the uncertainty of parameter that refers to the ore grade the normal distribution is used. When quantifying uncertainty of the ore grade, it is usually supposed that probability of occurrence of ore with higher quality and of ore of a lesser quality decreases equally in relation to average ore quality.

3.3.2 Volatility of value of underlying asset (ore)

In most cases the companies own only the mine and ore processing plant, thus the final product they place on the market is the concentrate of lead and zinc. Transactions between a concentrate producer and a custom smelter are governed by the smelter contract. Annual incomes from the sale of the concentrate are defined by the following expression:

$$I_{year} = \sum_{i=1}^{n} K_i \cdot V_i \tag{4}$$

where: K_i – quantity of the i-th concentrate (t), V_i – market value of the i-th concentrate ($/t), i – kind of concentrate (lead concentrate and zinc concentrate)

Market value of the concentrate is determined on the basis of the concentrate sale contract (conditions). The value of lead concentrate is equal to:

$$V_{con}^{Pb} = S_{Pb} \cdot g_{con}^{Pb} \cdot i_{sm}^{Pb} - T_{sm}^{Pb} - T_{corr}^{Pb} - T_{pen}^{Pb} \tag{5}$$

where: S_{Pb} – market price of the Pb metal ($/t), g_{con}^{Pb} – lead content of concentrate (%), i_{sm}^{Pb} – smelter recovery of lead (%), T_{sm}^{Pb} – costs of smelting for the basic price of Pb, T_{corr}^{Pb} – correction of costs for lead smelting ($/t), T_{pen}^{Pb} – penalty costs for the content of bismuth, arsenic, antimony, mercury, etc ($/t).

The value of zinc concentrate is:

$$V_{con}^{Zn} = S_{Zn} \cdot (g_{con}^{Zn} - i_{sm}^{Zn}) - T_{sm}^{Zn} - T_{corr}^{Zn} - T_{pen}^{Zn} \tag{6}$$

where: S_{Zn} – market price of Zn metal ($/t), g_{con}^{Zn} – zinc content of concentrate (%), i_{sm}^{Zn} – smelter recovery of zinc (%), T_{sm}^{Zn} – costs of smelting for the basic price of Zn, T_{corr}^{Zn} – correction of costs for zinc smelting ($/t), T_{pen}^{Zn} – penalty costs for the content of ferrous ($/t).

Annual income expressed through quantity of produced ore is

$$I_{year}^{ore} = Q_{year}^{ore}\left(V_{con}^{Pb} \cdot \frac{g_{ore}^{Pb} \cdot i_{Pb}}{g_{con}^{Pb}} + V_{con}^{Zn} \cdot \frac{g_{ore}^{Zn} \cdot i_{Zn}}{g_{con}^{Zn}}\right) \tag{7}$$

where: g_{ore}^{Pb}, g_{ore}^{Zn}- ore grade (%), i_{Pb}, i_{Zn}- mill recovery (%), g_{con}^{Pb}, g_{con}^{Zn}- content of concentrate (%), Q_{year}^{ore} - annual production of ore (t/year)

Uncertainties related to mineral raw material market (metal prices) can be quantified (simulated) by way of special stochastic process, called Mean Reversion Process. Initially consider the following Arithmetic Ornstein-Uhlenbeck process for stochastic variable S(t).

$$\delta S = k(S^* - S)\delta t + \sigma\varepsilon\sqrt{\delta t} \tag{8}$$

where: S-the variable's previous value, S^*-the mean reversion level or long run equilibrium value, k-the mean reversion rate, σ-the annualized volatility, $\varepsilon\sqrt{\delta t}$ -Wiener process, ε is the standard Normal distribution N(0,1)

This means that there is a reversion force over the variable S pulling towards an equilibrium level. In order to estimate the parameters of the mean reversion process we run the following regression:

$$S_t - S_{t-1} = \beta_0 + \beta_1 \cdot S_{t-1} + \varepsilon \tag{9}$$

The solution of stochastic differential equation (8) is the form of

$$S(t) = e^{[(\ln S_0)\cdot e^{-kt}]+[(\ln S^*)\cdot(1-e^{-kt})]-[\frac{\sigma^2}{4k}(1-e^{-2k})]+[\sigma\cdot\sqrt{\frac{1-e^{-2kt}}{2k}}N(0,1)]} \tag{10}$$

Simulation process is carried out in the following way: by applying equation (10) we can calculate one possible way of variable motion consisting of a series of values (S_0, S_1, S_2, …, S_T) beginning with moment $t=1$, $t=2$, …, until the final moment $t=T$.

3.3.3 Operating cost simulation

If there are signs that cost changes will have a nonlinear character in the future, i.e. that their future value may have random values, then for simulation of costs motion should be used stochastic differential equation of The Geometric Brownian motion. The Geometric Brownian motion random walk process takes the form of:

$$\frac{\delta C}{C} = (\mu - \frac{\sigma^2}{2})\delta t + \sigma\varepsilon\sqrt{\delta t} \tag{11}$$

where: C-the variable's previous value, δC-the change in the variable's value from one step to the next, μ-the annualized growth or drift rate, σ-the annualized volatility, $\varepsilon\sqrt{\delta t}$ - Wiener process, ε is the standard Normal distribution N(0,1)

The solution of stochastic differential equation (11) is the form of

$$C(t) = C_{t-1}e^{(\mu-\frac{\sigma^2}{2})dt+\sigma N(0,1)\sqrt{dt}} \tag{12}$$

The solution (12) is the geometric Brownian motion model of the future value. It can be extended to any period of time t. In this case the future value of variables S_t can be derived from the initial value S_0 just by applying (12) on the period of time t when the time $dt=t$.

$$C(t) = C_0 e^{(\mu-\frac{\sigma^2}{2})t+\sigma N(0,1)\sqrt{t}} \tag{13}$$

Simulation process is performed in an identical way as when simulating Mean Reversion Process.

3.3.4 Selection of discount rate

Although the concept of discounting is widely accepted, the selection of the appropriate discount rate has been the source of considerable debate and much disagreement. To decrease uncertainty related to selection of the appropriate discount rate we have applied the concept of fuzzy sets theory. In order to deal with the vagueness of human thought, we applied the fuzzy set theory. Such a set is characterized by a membership (characteristic) function which assigns to each object a grade of membership ranging between zero and one. The role of fuzzy sets is significant when applied to complex phenomena not easily described by traditional mathematical methods, especially when the goal is to find a good approximate solution (Bojadziev 1998) [7]. A linguistic variable is a variable whose values are words or sentences in a natural or artificial language (Huang and

Huang, 2006) [8]. The concept of a linguistic variable provides a means of approximate characterization of phenomena which are too complex to be amenable to description in conventional quantitative terms (Huang and Huang, 2006) [8]. A fuzzy number $\tilde{M}$ is a convex normalized fuzzy set $\tilde{M}$ of the real line R such that it exists such that one $x_0 \in R$ with $\mu_{\tilde{M}}(x_0)=1$ (x_0 is called mean value of $\tilde{M}$); $\mu_{\tilde{M}}(x)$ is piecewise continuous.

Triangular fuzzy numbers (TFN) are very convenient to work with because of their computational simplicity and they are useful in promoting representation and information processing in fuzzy environment. In this paper, we use TFNs in the fuzzy TOPSIS method.

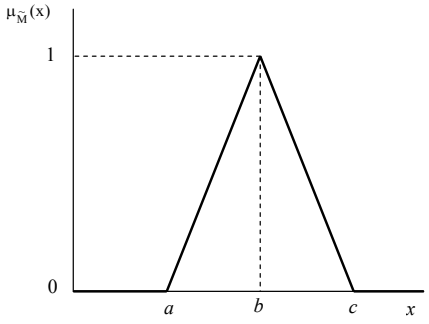

Figure 2. Triangular fuzzy number

Triangular fuzzy numbers can be defined as a triplet (*a*,*b*,*c*). The parameters *a*, *b* and *c* respectively, indicate the smallest possible value, the most promising value and the largest possible value that describe a fuzzy event. A fuzzy triangular number $\tilde{M}$ is shown in Figure 2.

The membership function is defined as (Huang and Huang, 2006) [8]:

$$\mu_{\tilde{M}}(x)=\begin{cases}0, & x<a\\ \dfrac{x-a}{b-a}, & a\le x\le b\\ \dfrac{c-x}{c-b}, & b\le x\le c\\ 0, & x>c\end{cases} \tag{14}$$

Triangular fuzzy numbers can be used to perform common mathematical operations. Let us assume that $\tilde{A}_i, i=1,2,...,n$ be sample of the random variable of fuzzy number. By the extension principle of fuzzy sets [9] and definition of the triangular fuzzy number the average operation for fuzzy number $\tilde{A}_i$ is as follows:

$$\bar{\tilde{A}}=\sum_{i=1}^{n}\tilde{A}_i/n \tag{15}$$

An important concept related to the applications of fuzzy numbers is defuzzification, which converts a fuzzy number into a crisp value. The most commonly used defuzzification method is the centroid defuzzification method, which is also known as center of gravity or center of area defuzzification. The centroid defuzzification method can be expressed as follows (Naaz et al. 2011) [10]:

$$\bar{x}_0(\tilde{A})=\int_a^c x\mu_{\tilde{A}}(x)dx \Big/ \int_a^c \mu_{\tilde{A}}(x)dx \tag{16}$$

where $\bar{x}_0(\tilde{A})$ is the defuzzified value. The defuzzification formula of triangular fuzzy numbers (*a*,*b*,*c*) is

$$\bar{x}_0(\tilde{A})=(a+b+c)/3 \tag{17}$$

and it will be used in this paper. Fuzzy linguistic variables used to describe discount rate are as follows: very low (VL), low (L), medium (M), high (H) and very high (VH). To estimate an adequate value of the discount rate, it is necessary to get opinions of experts dealing with it. Suppose we have *p* experts and each of them has given his opinion. The final value is expressed by aggregated fuzzy number obtained by averaging the fuzzy opinions of the experts. Table 1. presents the expert estimation process.

Table 1. Expert estimation of the discount rate

Expert				Aggregated value
E_1	E_2	…	E_p	
$\tilde{i}_1$	$\tilde{i}_2$	…	$\tilde{i}_p$	$1/p\otimes(\tilde{i}_1\oplus\tilde{i}_2\oplus...\oplus\tilde{i}_p)$

3.4 Simulation of decision making criteria

Without lost of generality the concept of simulation is explained by Net Present Value criterion. A stochastic model is created describing simultaneous behavior of risk factors that have the greatest effect on NPV. By simulating we arrive at the distribution of probability of these risk factors during the project. When these distributions get included into NPV calculations, we get distribution of probability for NPV. Since complete distribution of Net Present Value is at our disposal, we can choose a measure (indicator) of uncertainty, as is the reliability interval or the value at risk. The model calculates values of the project VPR_t for each year t during the period of the lasting of the project t=1,2,…T. Project value is a complex function of a great number of risk factors that have effect on incomes I_t and costs C_t at the annual level. Project value in year t is defined by the following expression:

$$VPR_t = I_t(RI_{1t},\ldots,RI_{Nt}) - C_t(RC_{1t},\ldots,RC_{Mt}) \quad (18)$$

where: $RI_{1t},\ldots,RI_{Nt}$ – risk factors that have effect on incomes, $RC_{1t},\ldots,RC_{Mt}$ – risk factors that have effect on costs

Applying annual fuzzy discount rates $\tilde{i}_1,\tilde{i}_2,\ldots,\tilde{i}_T$, and then NPV is defined by the following expression:

$$\tilde{NPV} = NPV(VPR_1,\ldots,VPR_T) = \sum_{t=1}^{T} \frac{VPR_t}{\prod_{k=1}^{t}(1+\tilde{i}_t)} \quad (19)$$

Frequently during the period while the project lasts, constant discount rate is applied, and in that case, $\tilde{i}_t$ in the above given equation is replaced with $\tilde{i}$. Investment costs (CAPEX) are included in the way that their value is subtracted from the net present value. In the model we start from an assumption that risk factors $RI_{1t},\ldots,RI_{Nt}$, $RC_{1t},\ldots,RC_{Mt}$ having effect on incomes and costs, are identified as critical for NPV calculations. The model produces simulations $SIM^j_{1t},\ldots,SIM^j_{Nt},SIM^j_{1t},\ldots,SIM^j_{Mt}$; $j=1,..,J$; $t=1,...,T$, where J represents the number of simulations. These simulations represent probability distribution of chosen (identified) risk factors and from there comes information on uncertainty. Simulated values for NPV are obtained by making NPV calculation, using simulated and fuzzified risk factors values, so that:

$$\tilde{NPV}^j = NPV(VPR_1^j,\ldots,VPR_T^j) \qquad j=1,\ldots,J \quad (20)$$

where we have:

$$VPR_t^j = I_t(RI_{1t}^j,\ldots,RI_{Nt}^j) - C_t(RC_{1t}^j,\ldots,RC_{Mt}^j) \quad (21)$$

Having obtained simulations NPV^j, $j=1,\ldots,J$, they can be used for the calculation of the fuzzy mean value (or expected value) of Net Present Value (see equation 15). The same procedure is applied to PI and MIRR criteria.

3.5 Decision making

The problem of underground mine project selection can be represented as Alternatives, Criteria, Evaluations model. We consider:

1. A finite set of alternatives or investment projects: $A=\{A_1,A_2,\ldots,A_m\}$;
2. A finite set of criteria: $\tilde{C}=\{\tilde{C}_1,\tilde{C}_2,\tilde{C}_3\}$;
3. A set of evaluations of investment projects with respect to criteria:

$$\tilde{D} = \left| E[\tilde{NPV}]_{m1} \quad E[\tilde{PI}]_{m2} \quad E[\tilde{MIRR}]_{m3} \right|$$

where: $E[\tilde{NPV}]$- fuzzy expected value of Net Present Value, $E[\tilde{PI}]$- fuzzy expected value of Profitability Index, $E[\tilde{MIRR}]$- fuzzy expected value of Modified Internal Rate of Return.

To obtain the most economic justified project it is necessary to execute the fuzzy TOPSIS procedure. TOPSIS method is a technique for order preference by similarity to ideal solution proposed by Hwang and Yoon (1981) [11]. The basic concept of this method is that the chosen alternative should have the shortest distance from the positive ideal solution and the farthest distance from the negative ideal solution. Positive ideal solution is a solution that maximizes the benefit criteria and minimizes cost criteria, whereas the negative ideal solution

maximizes the cost criteria and minimizes the benefit criteria (Wang 2006) [12]. In general, a multiple criteria decision making problem can be concisely expressed in matrix format as:

$$\widetilde{D} = \left| \widetilde{x}_{ij} \right| \tag{22}$$

where $\widetilde{x}_{ij}$ is the rating of alternative A_i with respect to criteria C_j. In this paper, the rating of alternative A_i with respect to criteria are represented as triangular fuzzy numbers. The fuzzy TOPSIS method is based on the following steps.

Step 1. Construct the normalized decision matrix $\widetilde{R}$

The first step concerns the normalization of the judgment matrix $\widetilde{D} = \left| \widetilde{x}_{ij} \right|$. Each element $\widetilde{x}_{ij}$ is transformed using the following equation

$$\widetilde{r}_{ij} = \frac{\widetilde{x}_{ij}}{\sqrt{\sum_{i=1}^{m} \widetilde{x}_{ij}^2}} = \frac{(a_{ij}, b_{ij}, c_{ij})}{\sqrt{\sum_{i=1}^{m} (a_{ij}, b_{ij}, c_{ij})^2}} \qquad j = 1,2,...,n \tag{23}$$

Step 2. Construct the weighted normalized decision matrix $\widetilde{V}$

In order to determine criteria importance, we applied concept of the entropy method. Shannon and Weaver proposed the entropy concept and this concept has been highlighted by Zeleny (1982) [13] for deciding the objective weights of criteria. The amount of decision information contained in equation (23) and associated with each criterion can be measured by the entropy value e_j as:

$$e_j = -k \sum_{i=1}^{m} r_{ij} \cdot \ln r_{ij} \tag{24}$$

where $k = 1/\ln m$ is a constant that guarantees $0 \le e_j \le 1$. The degree of divergence (d_{ij}) of the average information contained by each criterion C_j (j=1,2,…,n) can be calculated as:

$$d_j = 1 - e_j \tag{25}$$

The objective weight for each criterion C_j (j=1,2,…,n) is thus given by:

$$w_j = d_j / \sum_{j=1}^{n} d_j \tag{26}$$

Finally the weighted normalized decision matrix is as follows:

$$\widetilde{V} = \left| \widetilde{r}_{ij} \widetilde{w}_j \right| \tag{27}$$

Step 3. Define the ideal and the negative-ideal solutions

Let us suppose that $\widetilde{A}^+$ identifies the ideal solution and $\widetilde{A}^-$ the negative one. They are defined as follows:

$$\widetilde{A}^+ = \left\{ \left(\max_{i=1,2,...m} \widetilde{v}_{ij} \mid j \in J \right), \left(\min_{i=1,2,...m} \widetilde{v}_{ij} \mid j \in J' \right) \right\} = \left\{ \widetilde{v}_1^+, \widetilde{v}_2^+, ..., \widetilde{v}_n^+ \right\} \tag{28}$$

$$\widetilde{A}^- = \left\{ \left(\min_{i=1,2,...m} \widetilde{v}_{ij} \mid j \in J \right), \left(\max_{i=1,2,...m} \widetilde{v}_{ij} \mid j \in J' \right) \right\} = \left\{ \widetilde{v}_1^-, \widetilde{v}_2^-, ..., \widetilde{v}_n^- \right\} \tag{29}$$

where: $J = \{j = 1,2,...,n \mid j$ associated with the benefit criteria$\}$, $J' = \{j = 1,2,...,n \mid j$ associated with the cost criteria$\}$

With benefit and cost attributes, we discriminate between criteria that the decision maker desires to maximize or minimize, respectively.

Step 4. Measure the distance between alternatives and ideal solutions

To calculate the n-Euclidean distance from each alternative to $\widetilde{A}^+$ and $\widetilde{A}^-$ the following equations can be easily adopted:

$$\widetilde{S}_i^+ = \sqrt{\sum_{j=1}^{n} \left(\widetilde{v}_{ij} - \widetilde{v}_j^+ \right)^2} \qquad \mathrm{i} = 1,2,...,\mathrm{m} \tag{30}$$

$$\widetilde{S}_i^- = \sqrt{\sum_{j=1}^{n} \left(\widetilde{v}_{ij} - \widetilde{v}_j^- \right)^2} \qquad \mathrm{i} = 1,2,...,\mathrm{m} \tag{31}$$

Step 5. Measure of the relative closeness to the ideal solution and final ranking

The final ranking of alternatives is obtained by referring to the value of the relative closeness to the ideal solution, defined as follows:

$$\widetilde{C}_i = \frac{\widetilde{S}_i^-}{\widetilde{S}_i^+ + \widetilde{S}_i^-} \qquad \mathrm{i} = 1,2,...,\mathrm{m} \tag{32}$$

The best alternative is the one which has the shortest distance to the ideal solution.

Ranking the defuzzification values is carried out in descending order.

4 APPLICATION OF PROCEDURE

4.1. A numerical example statement

To illustrate the proposed procedure, we applied it to a case considering the increase of the production capacity in an operating underground mine. The new part of lead-zinc deposit is to be developed, the situation is hypothetical and the numbers used are in to permit calculation. Management of a lead and zinc mine is taking into consideration the option to expand the actual production range by opening three new levels. Activities need to be performed in order to realize the increase of the production capacity: to sink the shaft; to modernize the hauling system; to build a new bunker for skip filling; to prepare exploitation levels by carrying out the necessary range of development; to make a new orepasses; to purchase adequate mining equipment; to install a new crushing plant at the haulage level and to expand the capacity of the ore processing plant. Three scenarious have been considered with respect to different capacity options.

4.2 Input parameters

ORE CHARACTERISTICS	
Ore grade or Content of Pb metal in ore	Normal distribution: min 1,615%; medium 1,9%; max 2,185%;volatility 0,095%
Ore grade or Content of Zn metal in ore	Normal distribution: min 2,84%; medium 3,35%%; max 3,85%; volatility. 0,1675%
CONTRACT CONDITIONS FOR LEAD CONCENTRATE	
Lead content of concentrate	70%
Mill recovery	Uniform distribution: min 90%; medium 92%; max 94%; volatility 1,154%
Smelter recovery	95%
Smelting process costs per 1 t concentrate for basic price Pb metal of 475 USD/t	144 USD/t
Content of Bi metal in concentrate	0,2%
CONTRACT CONDITIONS FOR ZINC CONCENTRATE	
Zinc content of concentrate	50%
Mill recovery	Uniform distribution: min 78%; medium 80%; max 82%; volatility 1,1547%
Smelter recovery	42%
Smelting process costs per 1 t concentrate for basic price Zn metal of 1000 USD/t	185 USD/t
Content of Fe metal in concentrate	12%
METAL PRICES ON THE MARKET	
Pb metal price	3000 USD/t; equilibrium 2253 USD/t; reversion rate 0,245637; volatility 0,035752; time interval 1 year
Zn metal price	2470 USD/t; equilibrium 1875 USD/t; reversion rate 0,203958; volatility 0,029147; time interval 1 year
VALUE OF INVESTMENT	
Investment of Project 1	Triangular distribution; min 3,30 mil USD; medium 3,50 mil USD; max 3,90 mil USD; volatility 0,1247 mil USD
Investment of Project 2	Triangular distribution; min 2,90 mil USD; medium 3,00 mil USD; max 3,20 mil USD; volatility 0,06236 mil

Investment of Project 3	USD Triangular distribution; min 2,40 mil USD; medium 2,50 mil USD; max 2,80 mil USD; volatility 0,08498 mil USD
DISCOUNT RATE	
Discount rate	
Expert 1; Expert 2; Expert 3	VL (6 7 8)%; L (7 8 9)%; M (8 9 10)%
Aggregated value	(7 8 9)%
PRODUCTION COSTS	
Production and processing costs of 1 t ore	
Project 1	37 USD/t; drift rate 2%; volatility 10%
Project 2	32 USD/t; drift rate 2%; volatility 10%
Project 3	30 USD/t; drift rate 2%; volatility 10%
PERIOD OF INVESTMENT	
Time needed for the development	
Project 1; Project 2; Project 3	2 years; 3 years; 3 years
PRODUCTION RATE	
Capacity	
Project 1; Project 2; Project 3	120 000 t/year; 90 000 t/year; 100 000 t/year
PERIOD OF PRODUCTION	
Period of mining	
Project 1; Project 2; Project 3	8 years; 7 years; 7 years
NUMBER OF SIMULATION	
Number of simulation	500

4.3 Numerical example solution

Since the simulation has been done values of criteria are defined by following triangular fuzzy numbers (see Table 2). To simplify calculation we expressed criterion C_1 (NPV) by million.

Table 2. Values of criteria and fuzzy decision matrix

PROJECT	NPV	PI	MIRR
Project 1	(4.50 5.05 5.62)	(2.16 2.31 2.45)	(15.12 15.82 16.51)
Project 2	(3.91 4.38 4.88)	(2.18 2.32 2.47)	(16.29 16.89 17.48)
Project 3	(3.68 4.12 4.58)	(2.33 2.48 2.65)	(16.88 17.49 18.12)

According to procedure of TOPSIS method we obtained the closeness coefficient of each alternative (see Table 3).

Table 3. Closeness coefficient

	Closeness coefficient	Defuzzification
Project 1	0,5433 0,6298 0,4035	0,5256
Project 2	0,4862 0,3393 0,4753	0,4336
Project 3	0,4861 0,3701 0,4753	0,4438

According to Table 3, it can be seen that the closeness coefficients of the first alternative, namely the Project 1 is of the highest value followed by Project 3 and the Project 2. Closeness coefficients for the Project 1 is of 0.5256, while the Project 3 and Project 2, has value 0.4438 and 0.4336 respectively. Based on the closeness coefficients, an alternative to selecting the projects listed on the Project 1 should be the first choice, followed by selecting the projects listed on the Project 3 and the last one is to select a project on the Project 2. The greater the value of the closeness coefficient indicates the priorities of the decision to be made. TOPSIS method not only allows the decision maker to provide the rank of each alternative, but also shows the degree of likelihood of alternative selection as illustrated in Table 3. This table shows that difference between the first and last ranking project (Project 1 and Project 2 is 0.092, i.e., 9,2%. For someone who is not familiar with project selection problem it looks like small difference (almost negligible) but for the decision makers it is very significant result in determining the

order of the ranking. Therefore, the implementation of fuzzy TOPSIS method is really effective in real mining world applications. The proposed method is very appropriate when dealing with subjective assessment of the real environment of the mining industry that is full of uncertainties.

5. CONCLUSION

Every mine corporation is faced with different types of uncertainties which can be caused by characteristics of the deposit and changes in market. Identification and quantification of uncertainties, incorporation flexibile alternatives into system design and suitable method of decision making are crucial elements for estimation of underground mine projects. In this model, we defined six sources of uncertainties having the most influence on the value of the project. Every uncertainty is quantified by adequate form of measure. Next, we run the simulations to discover how they could potentially impact value of the proposed investment projcts. A model is created describing simultaneous behavior of risk factors that have the greatest effect on NPV, MIRR and PI. Upon completion of simulation process we obtained values of criteria as fuzzy values. Fuzzy TOPSIS method is used to rank the proposed projects. The model is universal and can be applied in solving other problems in underground mining with respect to specific environments and requirements.

FUNDING: This paper is part of research conducted on scientific projects TR 33003, TR 33025 that are funded by Ministry of Science and Technological Development, Republic of Serbia.

REFERENCES

[1] Alpay, S., Yavuz, M., (2007). A Decision Support System for Underground Mining Method Selection, H.G. Okuno and M. Ali (Eds.): IEA/AIE 2007, LNAI 4570, Springer-Verlag Berlin Heidelberg, pp/334-343.

[2] Bimal, S., Sarkar, B., Mukherjee, S.K., (2002). Selection of opencast mining equipment by a multi-criteria decision-making process, Mining Technology, Transactions of the Institute of Mining and Metallurgy, Section A, volume 111, pp.136-142.

[3] Elevli, B., Demirci, A., Dayi, O., (2002). Underground haulage selection: shaft or ramp for a small-scale underground mine, J.S. Afr. Inst. Min. Metall. 102, pp.255-260.

[4] Trigeorgis L. (1990). A real-options application in natural-resource investments, Adv Future Options Res; 4: pp.153-164.

[5] Gligoric Z, Beljic C, Gluscevic B, Jovanovic S.(2011), Hybrid model of evaluation of underground lead-zinc mine capacity expansion project using Monte Carlo simulation and Fuzzy numbers, Simulation; Transaction of the Society for Modeling and Simulation International 87(8), pp.726-742.

[6] Kazakidis VN. Scoble M. (2003). Planing for flexibility in underground mine production system, SME Mining Engineering Journal, pp.33-38.

[7] Bojadziev G., Bojadziev M (1998). Fuzzy sets and fuzzy logic applications, World Scientific, Singapore

[8] T.T.Huang, W.T.Huang (2006). Using signed distance and order statistics method for fuzzy evaluation of service quality, Journal of Information & Optimization Sciences, Vol.27.No.1, pp.211-223.

[9] L.A.R. Rivera., N.F. Hubele., F.P. Lawrence, (1995): C_{pk} index estimation using data transformation, Computers Industrial Engineering 29 (1-4), pp.55-58

[10] S.Naaz, A.Alam, R.Biswas (2011)., Effect of different deffuzification methods in a fuzzy based load balancing application, International Journal of Computer Sciences Issues, Vol.8, Issue 5, no.1, pp.261-267.

[11] Hwang C.L, Yoon K. (1981). Multiple attribute decision making: Methods and applications, Berlin; Springer

[12] Wang YM, Elhag TMS (2006) Fuzzy TOPSIS method based on alpha level sets with an application to bridge risk assessment. Expert Syst Appl 31, pp. 309-319

[13] Zeleney M. (1982). Multiple criteria decision making. New York: McGraw Hill.

Simulation Study on Fill Factor of a Drum Mill by Two Grinding Medium

L. Kuzev, E. Kostadinov, T. Damyanov
University of Mining and Geology "St. Ivan Rilski", Sofia, Bulgaria

K. Dedelyanova
Scientific and Technical Union of Mining, Geology and Metallurgy, Sofia, Bulgaria

N. Hristov
Chelopech Mining EAD, Chelopech, Bulgaria

ABSTRACT A simulation study on fill factor of a drum mill, expressed in bulk density of the grinding medium on the condition that each is composed of equal number of grinding bodies of equal weight but different shape was performed .

The studied media were: balls and tetraballpebs. The study was conducted in a 1200 mm drum module mill and with length exceeding the double diameter of the studied grinding body. Incisions were made perpendicular to the grinding medium along the axis of the drum, which show the spatial location of each element of the grinding medium in the volume.

Defects in the arrangement of the grinding elements and the contacts between them and with the inner surface of the drum were observed. In tetraballpebs application, contacts between both spherical surfaces of the grinding elements and also with the edges and vertices of the elements of the grinding medium were observed.

KEYWORDS: drum mill, grinding medium, fill factor, balls, tetraballpebs

1 INTRODUCTION

The functional body of the drum mill is grinding medium. Traditionally it is made up of spherical grinding bodies (balls) up to maximum diameter of 120 mm. The long production practice that is recognized as a grinding medium undeniable, despite some shortcomings touted in numerous publications.

Parameter characterizing the grinding medium is the bulk density, which is the mass of the grinding medium per unit volume. It is variable and depends on the size of constituent balls and ranges between 4500 and 4800 kg/m^3.

Operating parameters of the grinding process are:

- Degree of filling (fill factor) of the drum mill with grinding media;
- Particle size, shape, density and hardness of the elements constituting the grinding media (balls).

Possible ways to improve the productivity and efficiency of grinding are formulated by (Кармазин, 1968):

- Icreasing the bulk density of the grinding media;
- Creating conditions of grinding in which the share of attrition into the end product of grinding

These recommendations can be implemented in application of grinding medium composed of grinding bodies in a different shape other than balls. Such shape of grinding bodies can be a spheroidal tetrahedron. It is known as Franz Reuleaux tetrahedron (Gebrüder Hofmann & Co, 1935). The surface area of this body is about 9% larger than a ball of the same weight. A

family of spheroidal tetrahedrons with different sphericity of the surrounding walls called by the general name tetraballpebs were examined by Kuzev (2011).

2 BACKGROUND

The determination of volume and weight of the grinding media in industrial conditions is a demanding task. The bulk density of the grinding medium depends on the density of the material of which the body is made of and the degree of filling (fill factor) of the drum volume occupied by the body, depending on the way of the arrangement. The amount of grinding medium in the mill is expressed through the fill factor. It is known that, both overcharge and insufficient filling of the drum with grinding medium reduces the kinetics of grinding, which ultimately reduce the productivity and efficiency of grinding and also decrease the energy efficiency of the process by increasing the energy consumption of grinding unit material. Therefore, measuring and controlling the fill factor of the mill drum during grinding are essential issues (Kolacz, 1997), (Montini, 1988), (Moys, 1996).

There is a simple dependency which expresses the volume occupied by the grinding medium as a percentage of the volume of drum mill. Percentage of the volume V_B occupied by the grinding medium is given by (Gupta, 2006):

$$V_B = \frac{M_B / \rho_B}{V_M} \times 100 \qquad (1)$$

where:

V_B - Volume of the grinding bodies m^3
M_B - Mass of the grinding bodies t/m^3
ρ_B - Density of the grinding bodies t/m^3

The volume occupied by the grinding medium can vary in the interval depending on the type of the mill. As a rule, the ball mill with central unloading, the fill factor should not exceed 45% of the drum volume. In mills with grate discharge, the fill factor

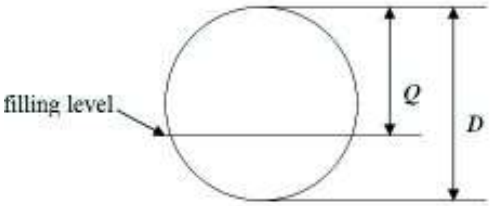

can hold up to 48% of the drum volume.

Figure 1. Diagram showing the height of the filling with grinding medium

A convenient statistical way to determine the percentage of the volume of grinding medium, depending on the diameter of the mill and filling height for various mills with different dimensions is (Kolacz, 1997):

$$V = \left[1{,}13 - 1{,}26\left(\frac{Q}{D}\right)\right] \times 100 \qquad (2)$$

where :

D - Inner diameter of the mill, m
Q - Vertical distance from the level of grinding media to the highest point of the drum, m.

Equation (2) is useful for practical purposes, but since it represents a weighted average, its use to determine the amount of grinding medium leads to relatively accurate results.

In certain geometric dimensions of the drum and the diameter of grinding balls graphical methods to determine the fill factor are successfully applied.

3 EXPERIMENTAL

The spheroidal tetrahedron is stereometry 3D body (tetraballpebs). Figure 2 shows the ball and tetraballpebs by their characteristic dimensions (Damyanov, 2012).

A simulation study was performed on the bulk density of the grinding media which consists of equal weight of balls and tetraballpebs that differ only in shape.

The condition observed in the creation of standard lines for tetraballpebs are all for bodies of a given type which have weight equal to the weight of the corresponding basic spherical body (ball) i.e keeping constant weight independently from radius variation of the sphericity wall of the tetraballpebs body.

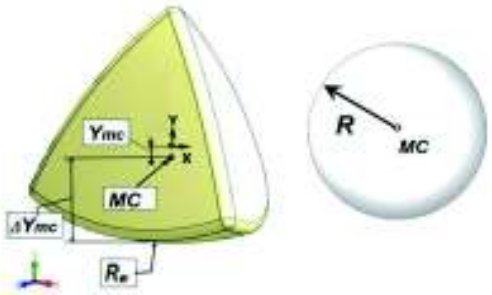

Figure 2. Main geometric dimensions of both grinding bodies

ΔYmc - the distance between the mass center and spherical surface of the tetrahedron;

Ymc - the distance between the mass center and geometrical centers of the body;

R - ball radius;

MC - mass center of the bodies;

Rw- walls sphericity radius on tetraballpebs;

In order to create a fully defined parametrical 3D CAD models of the grinding bodies, mechanical design software SolidWorks was used. The method, used to build the model is based on four intersecting spheres located at the top of the tetrahedron. The evolved total volume of the spheres formed the body of spheroidal tetrahedron (Damyanov, 2012).

There are standard lines of basic spherical grinding bodies with diameters of 40 mm, 50 mm, 60 mm, 80 mm, 100 mm and 120 mm for industrial sized mills. This work considered a standard line for tetraballpebs created on the basis of a spherical grinding body.

Balls with a diameter of 60 mm were marked as **B60**.

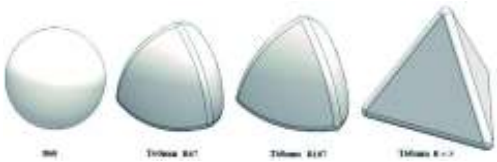

Tetraballpebs were marked as **T60**. Both grinding bodies are equivalent by weight.

Ball B60 and some tetraballpebs T60 are shown in Figure 3.

Figure 3. General view of CAD models of tetraballpebs T60 with a weight equal to that of the ball B60 with radius of sphericity walls R67, R107 and R ≈ ∞ mm

4 METHODOLOGY

In order to determine the bulk density of the grinding media a module representing a part of the drum with a diameter of 1200 mm and a length of the cylindrical part which allows the free positioning of two grinding bodies across each other in a horizontal plane (Kostadinov, 2011) was selected.

a) b)

Figure 4. The location of the grinding bodies at the end of the simulation of bulk density of the grinding medium

a) balls with a diameter of 60 mm

b) tetraballpebs by the same weight with that of balls and sphericity of the walls with a radius of 117 mm

The module with two grinding medium is presented in Figure 4. Simulations were

performed with SolidWorks software and SolidWorks Motion. In this software, parameters were dimensions of the grinding bodies, physical and mechanical properties of the material and gravity.

The filling of the module with the grinding medium is consistent with the practice of grinding in a ball mill, namely, filling the drum with balls in quantities between 30 and 40 percent. The filling of the module with tetraballpebs has the same number of equivalent weight of balls.

5 EXPERIMENTAL RESULTS

During the simulation under gravity, 3D contacts between the grinding bodies which were changed dynamically, occupy the most sustainable location. The parameters of the model are given in Table 1:

Table 1. Parameters of the model

Model parameters	
Internal diameter D, mm	1200
Length L, mm	150
Mass of grinding body M, g	882
Number of grinding bodies	275
Mass of grinding medium M_{av}, kg	242.55

Figure 5a present a position of the balls with a diameter of 60 mm at the end of the simulation. Figure 5b present a position of the tetraballpebs with equivalent weight and sphericity wall radius of 117 mm. In order to minimize the error in the calculation of volume of both grinding medium, maximum and minimum areas were calculated as shown in Figure 5a and 5b. Into a plane perpendicular to the axis of the model, the maximum area of the projection grinding medium, was accounted. It is composed of two parts – light and dark as given in Figure 5a and 5b. The minimum area is the tightly occupied area of the grinding medium in the observation plan of the module visible as a lighter part as given in Figure 5. The volume of the grinding medium was determined by multiplying the average of the minimum and the maximum areas of the grinding medium in planes perpendicular to the axis of the module multiplied by its length.

Marked increase was observed in the bulk density of tetraballpebs T60, weight of which is equivalent to that of ball B60 when the sphericity of the walls of tetraballpebs ranging from 47 mm to 117 mm were changed. For comparison, bulk density of the balls B60 was fixed.

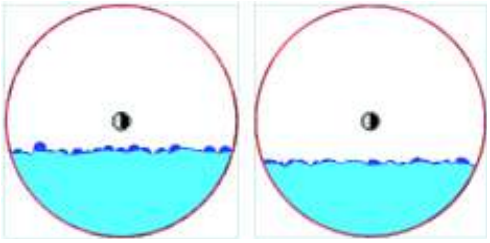

Figure 5. Areas occupied by the grinding medium for simulation study of the module drum mill:
a) balls with a diameter of 60 mm
b) tetraballpebs with equivalent weight of balls by radius of spherical surfaces 117 mm;

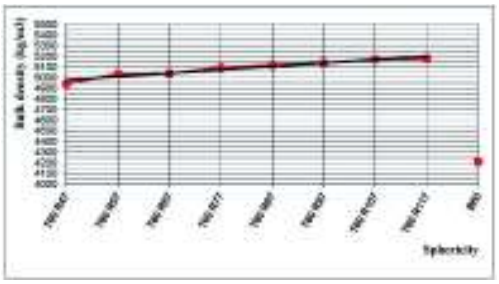

Figure 6. Graphical expression of the changes in bulk density of tetraballpebs depending on the change of sphericity of the surrounding walls

The conducted simulation studies to determine the bulk density of the two grinding media cross sections were made to identify the exact location of each body in the volume of the module. Cross sections were made on the three axes.

Data from the simulation study of tetraballpebs T60 with different sphericity of the surrounding walls with radii ranging from

47 mm to 117 mm with equal weight to the weight of a ball with a diameter of 60 mm are presented in Table 2.

Table 2. Data of the simulation study

Grinding medium size (mm)	Cross-sectional area of the grinding medium, S_{av} (mm^2)			Filling rate, (%)	Volume of the grinding medium, V_{av} (m^3)	Density of the grinding medium, P_{av} (kg/m^3)
	max	min	mean			
T60 R47	334728	319648	327188.0	29.0	0.0490782	4943
T60 R57	325867	316604	321235.5	28.5	0.048185325	5034
T60 R67	327134	314794	320964.0	28.4	0.0481446	5038
T60 R77	323316	311782	317549.0	28.1	0.04763235	5093
T60 R87	320864	311087	315975.5	28.0	0.047396325	5118
T60 R97	320725	308813	314769.0	27.9	0.04721535	5138
T60 R107	317143	308177	312660.0	27.7	0.046899	5172
T60 R117	318417	306243	312330.0	27.7	0.0468495	5178
B60	393725	374239	383982.0	34.0	0.0575973	4212

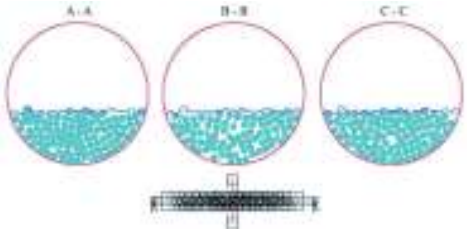

Figure 7. Topography of B60 balls

Figure 7 represent the position of the grinding balls B60 at the end of the simulation through the axis of the module $A-A$, $B-B$ and $C-C$. The length of the module is divided to equal distances from the planes perpendicular to the module axis as shown in Figure 7.

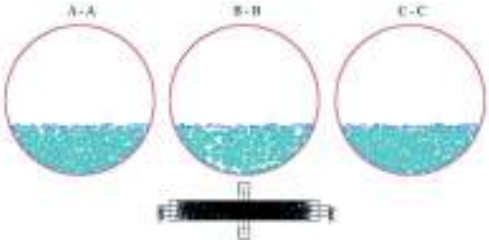

Figure 8. Topography of T60 tetraballpebs with sphericity of the walls having a radius of 107 mm

Figure 8 represent the position of the grinding bodies tetraballpebs T60 by sphericity of the walls with radius 107 mm by analogy through the cross-sections of $A-A$, $B-B$ and $C-C$ at the end of the bulk density simulation.

6 DISCUSSION

The use of Equation (1) to determine the fill factor of the grinding medium represented by the tetraballpebs is impossible since they differ only in outher shape of the spheres. Calculation leads to the same result, which is contradicted by the attached figures representing the same number of balls and tetraballpebs in the experimental module (Fig. 4, Fig. 5).

Equation 2 was empirically derived to calculate the fill factor. Fill factor for balls was determined as 38% and for tetraballpebs 30% i.e the difference between fill factor of drum with two grinding media is about 8%.

Experimental results show that, bulk density of the grinding medium consisting of balls B60 is 4212 kg/m^3 and tetraballpebs T60 for different radius of sphericity of the wall was found to be higher than and equal to the range of 4943 kg/m^3 to 5178 kg/m^3. This fact affects fill factor of the mill drum. According to the above methodology, fill

factor for balls is 34.0% and for tetraballpebs which have the radii of spherical surfaces is in the range of 27.7% to 29.0%. Upward line constructed which is given in. It was shown in Figure 6 that, increase in radius of the sphericity of the walls of tetraballpebs, increase the grinding medium density. Designated instantaneous values of the density of the tetraballpebs showed small deviations from the linear relationship built (Fig. 6). These variations are explained by the topography of the grinding elements in the grinding medium as shown in Figure 8. Figure 8 demonstrated the defects in the arrangement of the tetraballpebs in the module. Similar defects in the arrangement of the grinding medium balls were observed as shown in Figure 7.

These variations could be due to the inaccuracies in the calculation of the density of the grinding medium and the relatively short length of the module. Probably counts for the relatively small number of grinding bodies involved in the simulation, which is imposed by the hardware and software limitations.

7 CONCLUSIONS

Simulation modelling with tetraballpebs and balls were made and the following conclusions were drawn:

- Grinding media consisting of tetraballpebs have greater bulk density than that of balls.
- In the same equivalent amount of tetraballpebs T60, grinding medium bulk density increases as the radius of the sphericity of the walls increases.

The higher bulk density of the grinding media consisting of tetraballpebs gives reason to assume that, the contact area between grinding media and also with the lining of the drum is much larger than those of balls.

Bulk density was increased, by reducing the fill factor of the mill drum and increasing the contact area of the tetraballpebs, the condition of which is consistent with the recommendations in the literature (Кармазин, 1968).

The method used to determine the fill factor of the mill drum is promising because its implementation is to know the number of grinding bodies with their radius and the diameter of the drum mill.

Topography of the grinding media clearly demonstrated the contact between both grinding medium: balls and tetraballpebs.

8 ACKNOWLEDGEMENTS

The authors would like to thank to Ministry of Education and Science (Bulgaria) National Science Fund, contract ID 09 0048 for their supporting this research.

9 REFERENCES

Кармазин В.И., Денисенко А.И и др., 1968. Бесшаровое измельчение руд., Изд. Недра, Москва.

Gebrüder Hofmann & Co, 1935. Mehrflachiger Mahlkorper fur Rohr und Trommelmuhlen. Patent 440198, Koln, Deutschland.

Kolacz, J., 1997. Measurement system of the mill charge in grinding ball mill circuits, Minerals Engineering, Vol. 10, No. 12, pp. 1329-1338.

Montini, A., Moys M.H, 1988. The measurement of rheo1ogical properties inside a grinding mill, J. S. Afr. Inst. Min. Metall., Vol. 88, No. 6, pp. 199-206.

Moys, M.H., M.A. Van Nierop, I. Smit, 1996. Progress in measuring and modelling load behaviour in pilot and industrial mills, Minerals Engineering, Vol. 9, No. 12, pp. 1201-1214.

Gupta, A., D. Yan, 2006. Mineral Processing Design and Operations: An Introduction, Elsevier, pp.718.

Damyanov T, Kuzev L, Kostadinov E, Lazov L, 2011. 3D-CAD modelling and analysis of the geometric parameters of tetraballpebs for ball mills with different radius of spherical surfaces, Proceedings of the XIV Balkan Mineral Processing Congress, Vol.2, pp.566-572, Tuzla, Bosnia and Herzegovina.

Kostadinov E, Damyanov T, Kuzev L, 2011. Simulation study of volume and mass characteristics of the working medium of the drum ball mills using grinding bodies with tetraballpebs. Proceedings of the XIV Balkan

Mineral Processing Congress, Vol.2, pp. 573-576, Tuzla, Bosnia and Herzegovina.

Kuzev L, Hristov N and Dedelyanova K, 2011. Grinding media for drum mills. Proceedings of the XIV Balkan Mineral Processing Congress, Vol.1, pp.79-82, Tuzla, Bosnia and Herzegovina.

Damyanov T, Kostadinov E, Kuzev L and Hristov N, 2012. Behavior simulation study of two grinding media into drum mill, Proceedings of the XXVI International Mineral Processing Congress (IMPC 2012), September 24-28, pp. 2661-2672, New Delhi, India.

Practical Implications of the Effect of End Discharge Grate on Simulation of Ball Milling Performance

Z. S. Mirzaei
Faculty of Mining Engineering, University of Kashan.

A. Farzanegan
School of Mining, University College of Engineering, University of Tehran, Tehran, Iran.

ABSTRACT Discharge grate depending on its specification can significantly affect the product particle size distribution of ball mills, semi-autogenous grinding (SAG) and fully autogenous grinding (FAG) mills equipped with this type of discharge mechanism. The grate design, open area and grate aperture size affect grinding throughput. In SAG and FAG mills, the inadequate design of discharge grate can lead to inefficiency of comminution device and creation of a slurry pool which practically stops particles' breakage. In optimization studies, investigation on discharge grate and its effect on grinding process is critical due to the probable particle size classification at mill exit. This necessitates the effect of grate to be considered in process modeling and simulation. In this project, the effect of discharge grate on performance of two ball mills in Esfordi and Gol-e-Gohar plants was investigated in details to make sure that the modeling and simulation and subsequent optimization studies are accurate as much as possible. To study and determine the effect of the discharge grate, samples were collected from mill feed and discharge streams when the circuits were under steady-state operation. After mass balancing, the discharge streams were simulated by BMCS® (BMCS-based Modular Comminution Simulator). Then the observed and simulated particle size distribution of mill product was compared. The obtained results showed that the grate inside Esfordi ball mill does not affect the particle size distribution of mil output. However, in Gol-e-Gohar pilot plant ball mill the grate behaves like a fine screen which should be considered in mill mathematical modeling and simulation.

1 INTRODUCTION

Ball mills are classified according to their slurry discharge type. These types of mills are usually equipped with overflow or grate discharge and they are operated in open or closed circuits. In grate discharge type of ball mills, there is a grate installed between cylindrical section of mill shell and discharge trunnion. Slurry with fine particles can easily pass through the grate apertures and enter discharge trunnion (Figure 1) (Wills and Napier-Munn, 2006).

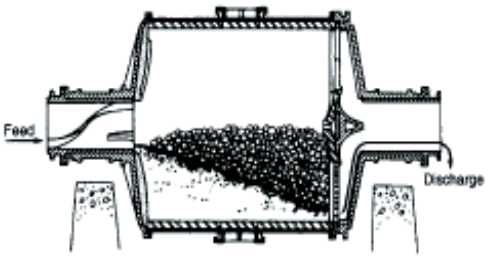

Figure 1. A mill with end discharge grate (Wills and Napier-Munn, 2006)

Discharge grates have a significant impact on performance of autogenous, semi-

autogenous and grate-discharge ball mills. Grinding capacity in these types of mills is highly depended on grate design, i. e., open area, location of grate openings or apertures and also pulp lifters. Nowadays, due to increased application of larger tumbling mills and closed grinding circuit, the importance of grate design and pulp lifer has been increased (Latchireddi and Morrell, 2003a; Latchireddi and Morrell, 2003b).

In ball mills with grate discharge, the slurry level is lower than that of overflow mills, therefore the residence time of particles inside these mills is reduced. In these mills overgrinding can happen less frequently and mill product contains coarse particles which are returned to the mill by classification system. It is noted that in compare with an open grinding circuit, grinding in a closed circuit with a high circulating load ratio produces more uniform smaller particles with a higher production rate per unit volume of the mill. The feed size in grate-discharge mills is relatively coarser that that of overflow mills and normally these mills are not used for fine feeds, e. g., ultrafine grinding. The main reason for this is that small grinding balls can easily block grate apertures. Ball mills with overflow discharge are practically the most convenient ball mills which are normally used for fine grinding and regrinding applications. While energy consumption in an overflow ball mills can be 15 percent less than the energy consumption of a grate ball mill with the same size, grinding efficiency of both types of mills is nearly equal. In overflow ball mills, charge volume is usually kept about 40 % of mill volume. However, in grate-discharge ball mills charge volume can be considered to be higher. In grate-discharge ball mills the mill rotational speed must be increased with increased charge volume (Wills and Napier-Munn, 2006).

In overflow ball mills operated in wet circuits, ground product is removed by discharge trunnion. The driving force for slurry to flow from feed end towards discharge end is due to larger discharge trunnion diameter in compare with the feed trunnion diameter. Nevertheless, grate-discharge ball mills have a more complicated material transport mechanism (Latchireddi and Morrell, 2003a; Latchireddi and Morrell, 2003b).

In addition to ball mills, discharge grates are also used in semi-autogenous and fully autogenous grinding mills. The function of the grate shown in Figure 2 is prevention of grinding balls to exit mill and at the same time providing a passage for fine particles and slurry to leave the mill. The shape of grate apertures can be square, circular or rectangular (slot) with a size between 10 to 40 mm. The total open area of grate is about 2 to 12 % of mill cross section area (Wills and Napier-Munn, 2006). Important grate variables are given in Table 1.

Table 1. Design variables of discharge grates (Latchireddi and Morrell; 2003b)

Property	Value
Open area	2 to 12 % of mill vertical cross section in mills with pan lifter and maximum 25% in mills with end discharge
Aperture size (mm)	10-40
Aperture shape	Square, circle, slot
Aperture arrangment	In various radial distances in diaphragm structure which are approximately parallel with vertical cross section of mill or in rows parallel to mill shell and near to each other

A simplified structure of a ball mill with discharge grate has been shown in Figure 2. Description of various components is as follows:

Feed trunnion: the cylindrical section at the beginning of the mill through which solids and water enter the mill

Mill shell: the main chamber of the mill in which ore particles are ground

Discharge Grate: the surface with a pattern of holes which only permits ground product and water pass through.

Discharge trunnion: the cylindrical section at the end of the mill through which ground product and water exit the mill.

In some mills, there is also a pulp lifter installed after grate to transfer pulp coming out of the grate to discharge trunnion.

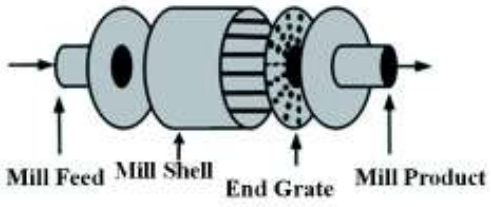

Figure 2. A schematic view of different parts of a grinding mill with grate discharge

In a number of previous research projects Latchireddi and Morrell (2003a, 2003b) investigated the effect of grate design on mill performance and concluded that grate design, solids content and feed flow rate have critical impact on the holdup of slurry in a mill. Also, it has been found that slurry holdup significantly depends on grate open area and apertures location and linear relationship between grate open area and flow rate. Also, they observed that when mill speed is increased, slurry holdup will be increased. These researchers studied the effect of grate open area on slurry holdup and observed that in flow through apertures, discharge flow rate is linearly proportional to grate open area. Discharge flow rate will be increased by increasing grate open area which can lead to a reduced slurry holdup inside the mill.

Modeling of exit classification and its effect on simulation predictions have been discussed by Austin et al. 1986, Cho and Austin, 2004 and Austin et al., 2007. In several case studies, these researchers attributed disagreement between predicted and measured particle size distribution of product in semi-autogenous grinding and ball mills in open circuit to exit classification applied by the grate. Cho and Austin (2004) presented results of a wet closed-circuit ball milling simulation at industrial scale and noted that ignoring the effect of exit classification in mathematical simulation model of grinding mill leads to incorrect prediction of discharge particle size distribution and therefore incorrect prediction of circulating load.

Also, Napier-Mann et al., 1999, studied exit classification process due to the existence of discharge grate at semi-autogenous and autogenous grinding mills and proposed a model for the effect of exit classification. This model considers a linear function for passing of particles smaller than grate aperture size or particles behaving like water.

In Iran, there has been no attempt to study modeling of exit classification due to end discharge grate so far. Dehghani Ahmadabadi, 2007, simulated ball milling circuit of Esfordi phosphate plant without considering end discharge effect on grinding simulation results. Azimi et al., 2008, reported the results of their investigation on end discharge grate of Sarcheshmeh semi-autogenous grinding mill. These researchers studied the variation of parameters such as grate slots size and open area during a given mill operating time in order to determine the useful life of installed discharge grate. The results of this study can help plant operators to plan repair and maintenance work to replace grate segments.

In this paper, authors have discussed the results of two case studies in which they have studied the effect of end discharge grate on modeling and simulation of two ball mills in Esfordi phosphate and Gol-e-Gohar iron ore processing plants.

2 THEORY

Cho and Austin, 2004, proposed a method for exit classification modeling based on considering a classifier at the end of the mill. The exit classification function of end discharge classifier is given in Equation (1):

$$c_i = \frac{1}{1+\left(x_i / d_{50}\right)^{-\gamma}} \tag{1}$$

In which c_i is classification function value for ith interval size, x_i representative size for ith size class interval, d_{50} is the specified size at which c_i is equal to 0.5 and

γ is a constant. The fractional mass which returns to the mill due to exit classification, s_i, is calculated using Equation (2):

$$s_i = \mathrm{a} + (1-a)c_i \tag{2}$$

Where a is the mass fraction returning to the mill due to bypass or short circuiting phenomenon occurring in actual classifiers. If $\mathrm{a} = 0$, which is normally a correct assumption for exit classification, then $s_i = c_i$ and we obtain Equation (3):

$$s_i = \frac{1}{1+(x_i/d_{50})^{-\gamma}} \tag{3}$$

The constant value γ in this special case is represented by γ_1 which is related to separation sharpness SI according to Equation (4):

$$\gamma_1 = \frac{0.9553}{-\log(SI)} \tag{4}$$

The modeling method explained above is an empirical method which can be implemented easily (Cho and Austin, 2004).

Napier-Munn et al., 1999, used a simple linear function to model discharge grate. In this method, the slurry leaving the mill is divided in two parts. One of these parts behaves similar to water and its discharge rate vs. particle size can be shown with nearly horizontal section in Figure (3). Second part goes under classification process due to grate and therefore behaves similar to solids. Figure 3 shows that for an aperture size equal to particles with a size less than x_m they behave like water and pass grate without any resistance and no classification. The value of classification function for these particles is equal to 1. However, for particles with a size larger than x_m, the value of classification function decreases and when particle sizes becomes x_g (aperture size), the value of classification function becomes equal to zero. This means that with increasing particle size more than x_m, resistance against passing particles grate becomes higher up to the point that value of classification function becomes zero there is impossible particles pass the grate.

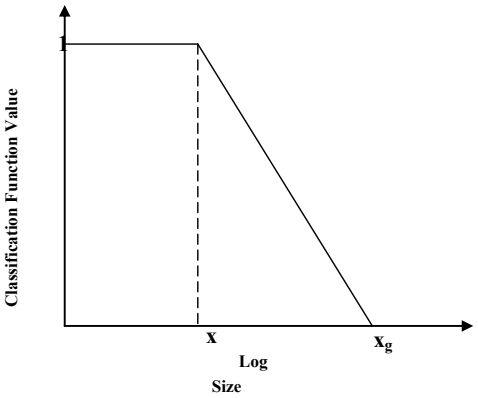

Figure 3. Classification function of discharge grate

3 MATERIALS AND METHODS

In this research two ball mills equipped with end discharge grates, one in Esfordi phosphate processing plant and the other in Gol-e-Gohar iron ore processing plant were considered in order to investigate the effect of discharge grate on grinding modeling and simulation. In both plants, necessary data were collected by sampling at two different times. Sampling campaigns were done when grinding circuits were at steady-state operation. Operating condition such as circuit fresh feed rate and water addition rates was also recorded during sampling. Then, laboratory tests were performed. First all samples were weighed and their solids content was determined. Next, particle size distribution of all samples and breakage function of mill feeds were determined by screen analysis and batch grinding tests. All raw data including streams flow rates, particle size distributions and percent solids were adjusted by mass reconciliation software.

Based on collected data, selection function of each mill was back-calculated using NGOTC® software (Farzanegan, 1998). Finally, circuit simulations were performed based on estimated grinding model parameters using BMCS® software (Farzanegan, 1998).

4 RESULTS AND DISCUSSION

4.1 Case Study 1: Esfordi Phosphate Processing Plant

4.1.1 Grinding circuit flowsheet

Comminution of run of mine ore (ROM) starts with crushing stage to produce smaller particles between 0 to 22 mm. Then, crushed product is sent to the rod mill in processing plant using three vibrating feeders and a conveyor belt (Figure 4).

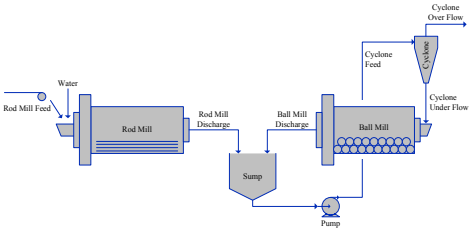

Figure 4. Grinding circuit of Esfordi phosphate processing plant

The first stage of grinding operation is performed continuously in a rod mill so that the feed particles with a size between 0 to 22 mm are ground to a product with d_{80} equal to 0.6 mm. The discharge of rod mill with a particle size between 0 to 5 mm enters a sump and becomes diluted according to a predefined set point before it is pumped to the primary hydrocyclone for particle size classification. The hydrocyclone overflow d_{98} is 150 µm. Hydrocyclone underflow is fed to the ball mill after being mixed with water addition. Ball mill discharge with particle size between 0 and 10 mm will be mixed with rod mill discharge in a collection sump and then the combined stream is fed to the primary hydrocyclone unit. Primary hydrocyclone overflow which is final product of grinding circuit is collected in a sump in which its solids content can be reduced to 18 % before entering de-sliming hydrocyclone package.

4.1.2 Esfordi ball mill

The ball mill unit installed in Esfordi phosphate plant is a grate-discharge type mill. Ball mill specification and steady-state operating conditions are given in Table 2.

Table 2. Design specification and operating condition of ball mill at Esfordi phosphate plant

Property Mill type	Value End grate discharge
Feed flow rate (t/h)	46
Circulating load (%)	150
Feed size d80 (mm)	0.75
Product size d80 (%)	0.1
Size reduction ratio	7.5
Installed power (kW)	315
Mill length (m)	3
Mill diameter (m)	2.4

Comparison of plant test results and ball mill design specification indicates that there is a big difference between current mill performance and designed performance. The most noticeable difference is between current and design size reduction ratios and circulating loads. Particle size distribution test results confirm that practically almost no comminution takes place in ball mill unit.

4.1.3 Grate specification

In Figures 5 and 6, two images of discharge grate of ball mill are shown. This grate is formed of 12 segments. In each grate segment there are 153 rectangular apertures with 27 by 12 mm dimensions. It is also noted that unlike many semi-autogenous discharge grate, there are no pebble ports in these grate segments and all apertures are the same in terms of shape and dimensions. The grate open area is equal to 0.59 m^2 which is equal to 4.73 % of vertical cross section of mill. Arithmetic mean of grate apertures dimensions roughly suggests that a spherical particle with a diameter size around 19.5 mm can be considered as a particle with a size equal to size of grate apertures.

Figure 5. Discharge grate segments of Esfordi ball mill unit

Figure 6. Inside view of Esfordi ball mill showing discharge grate

4.1.4 Circuit performance data

In Figure 7 particle size distributions of ball mill feed and product have been shown. The particle size of mill feed and product are based on 80 percent passing corresponding size which was obtained by fitting Rosin-Rammler model to adjusted particle size distribution data.

Operating condition including flow rates, solids contents and d_{80} of streams around the ball mill have been given in Table 3. Based on the reported data in Table 3, size reduction ratio and circulating load will be equal to 1.065 and 653 %, respectively.

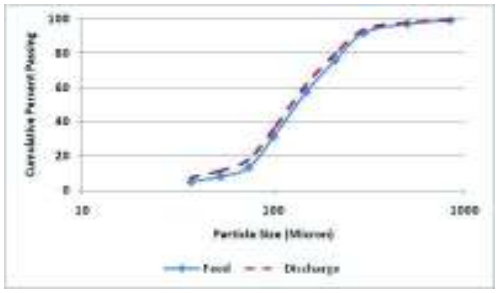

Figure 7. Particle size distributions of ball mill feed and product of Esfordi phosphate processing plant

Table 3. Specification of streams around ball mill of Esfordi phosphate processing plant

Stream	Slurry flow rate (t/h)	Solids content (%)	Water (t/h)	D80 (μm)
Feed	434.3	71.9	122.03	206.9
Product	434.3	71.9	122.03	194.3
Water addition to mill sump	32.1	0	32.1	-

As it can be seen in Figure 7, the maximum feed particle size is 841 μm. Therefore, considering the equivalent size of apertures (19500 μm), it can be concluded that the coarsest ball mill feed particles are smaller than 1/23 of grate apertures size which means that they can easily pass the discharge grate. Particle size distributions of simulated and measured product of ball mill have been plotted in Figure 8.

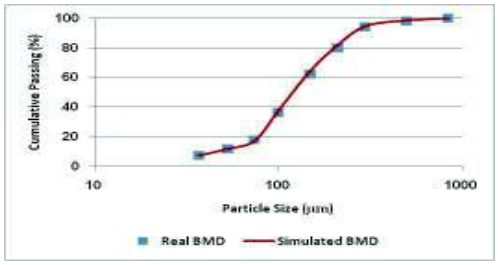

Figure 8. Comparison of simulated and measured (actual) ball mill output

As it can be seen in Figure 8, simulated and measured particle size distribution curves are almost the same. Hence, it can be concluded that selection function of the ball mill was estimated correctly. This is because in this case there is no exit classification at discharge and the samples taken from stream that passes the grate is representative of ball mill discharge (before passing the grate).

Cho and Austin 2004 reported that even particles with a size equal to 1/20 of grate apertures size are selectively kept inside the mill and discharge grate prevents them to leave the mill.

On the other hand, Benzer et al. 2001 and Özer et al. 2006 have reported their research results which indicate when the grate aperture size is less than 10 times of the coarsest particles in mill feed, then grate acts like a fine screen and its classification effect must be modeled. In fact, the probability of particles pass through grate open areas is decreased due to rotational motion speed of mill even though the size of grate apertures are much larger than the coarsest particles entering the mill. Hence, exit classification is applied on output product.

As mentioned above, based on measurements results in Esfordi phosphate processing plant particles entering ball mill are approximately 23 times smaller than grate apertures size. Therefore, considering previous findings by Cho and Austin (2004) it can be confidently concluded that under the current operating condition existence of discharge grate at the end of the ball mill has no effect on particle size distribution of ground product leaving the mill. This means that the ball mill acts exactly like an overflow discharge ball mill without any exit classification. Actually, the grate in this case prevents only grinding media from exiting the mill while solid particles freely pass through it. This conclusion is very important in circuit simulation studies and can help validation of models used for simulation and optimization studies.

4.2 Case study 2: Gol-e-gohar iron ore processing plant

4.2.1 Grinding circuit flowsheet

Gol-e-Gohar iron ore processing plant is located in Sirjan, Kerman province at South East of Iran. The ball mill unit which was studied in this project is primary mill of the Gol-e-Gohar pilot plant mill. The specification of this mill is given in Table 4. The ball mill is equipped with an end grate discharge and is operated in an open circuit. The grinding circuit is shown in Figure 9.

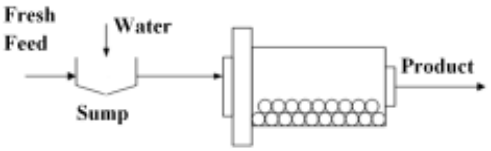

Figure 9. Ball mill circuit of Gol-e-Gohar pilot plant

Table 4. Technical specification and operating condition of ball mill at pilot plant of Gol-e-Gohar iron ore complex

Property	Value
Mill type	End grate discharge
Feed flow rate (t/h)	0.5 to 4
Feed size d80 (mm)	7.5
Product size d80 (%)	0.35
Size reduction ratio	21
Installed power (kW)	38
Mill length (m)	1.7
Mill diameter (m)	1.5

4.2.2 Ball mill grate specification

The discharge grate of Gol-e-Gohar pilot ball mill is shown in Figure 10.

This grate consists of 8 segments; each one with 132 square shape apertures. The size of each aperture is 9 by 9 mm. The equivalent diameter of an spherical particle which can pass through these apertures is considered to be equal to 9 mm (Rostami, 2010).

4.2.3 Circuit performance data

Particle size distributions of feed and product of the mill are plotted in Figure 11. Based on particle size distribution curve of mill feed, it is obvious that the equivalent size of grate apertures is nearly equal to the size of coarsest particles in feed.

Figure 10. End discharge grate of ball mill of pilot plant of Gol-e-Gohar iron ore processing complex

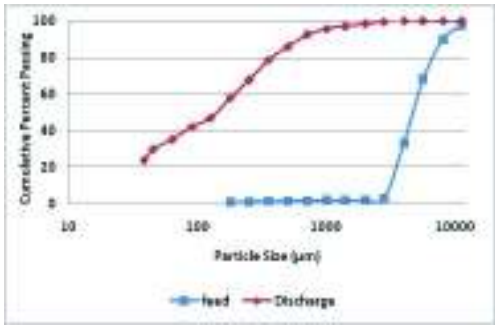

Figure 11. Particle size distributions of ball mill feed and product of Gol-e-Gohar

In Figure 12, there is a comparison of simulated and measured particle size distributions of mill product. It is clear that predications made by BMCS® software for coarser sizes are not as accurate as that of fine sizes.

Since samples of mill product are collected from the stream which comes out of mill trunnion, therefore they may not be representative of the ground product (i. e., ground powder charge just before passing the end discharge grate). In fact, if there is an exit classification, then they are representative of grate underflow or fines. When particles go under exit classification, the selection function estimated for the affected particle size classes will be higher than true value. In Figure 12, as small particles pass easily through discharge grate therefore selection function estimated for the fine size classes is close to true values and predicted remained mass for these size classes is close to measured values. However, for coarse particle size classes, as estimated selection function is higher that true value, the predicted mass is less than what has really been measured.

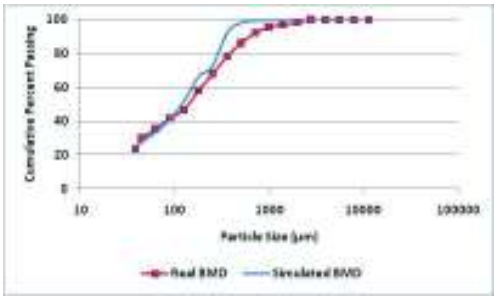

Figure 12. Comparison of simulated and measured (actual) ball mill product particle size distribution at Gol-e-Gohar

5 CONCLUSIONS

Discharge type at the end of tumbling mills can significantly impact their modeling and simulation. Because there is no exit classification in overflow mill types, simple population balance model of grinding can be used for simulation of these mills. In ball mills with end discharge grate population balance model may predict ground product particle size distribution inaccurately, if the effect of exit classification is not considered. In fact, in these types of mills, a single-stage particle size classification is applied on ground powder charge which prevents particles coarser than grate apertures leave

the mill and therefore are kept behind the grate. Hence, estimation of selection function which is one the main grinding model parameters is prone to error in compare with the case in overflow mills. In mills with overflow discharge, there is no resistance against slurry motion to exit the mill and sample collected from discharge stream is representative of grinding product. However, for mills with end discharge grate, in order to have representative samples of ground powder charge, the mill should be crash stopped and samples collected close to or just behind the discharge grate. This can help more accurate simulation of grinding process.

ACKNOWLEDGEMENT

The authors would like to acknowledge the financial support of University of Tehran for this research under grant no. 27943/1/01. Also, authors appreciate Esfordi phosphate and Gol-e-Gohar iron ore processing plants for their helps during this research.

REFERENCES

Austin, L.G., Barahona, C.A., Weymont, N. P., Suryanarayanan, K., 1986. An improved simulation model for semi-autogenous grinding, *Powder Technology*, Vol. 47, No.3 , pp. 265-283.

Austin,G. L., Julianelli., K., De Souza, A. S., Schneider, C., 2007. Simulation of wet ball milling of iron ore at Carajas, Brazil, *Int. J. Miner. Process*, 84, pp. 157–171.

Azimi, E., Banisi, S., Langarizadeh, Gh., Dehghani, M., 2008. A study on performance of discharge grates of Sarcheshmeh Copper Complex SAG mill, *Journal of Faculty of Engineering, University of Tehran*, Vol. 42, No. 5, pp. 565-575.

Benzer, A.H., Ergün, L., Lynch, A. J., Öner, M., Günlü, A., Çelik, I.B., Aydoğan, N., 2001. Modelling cement grinding circuits, *Minerals Engineering*, Vol. 14, No. 11, pp. 1469-1482.

Cho, H., Austin, L. G., 2004. A study of the exit classification effect in wet ball milling, *Powder Technology*, 143– 144, pp. 204– 214.

Dehghani Ahmadabadi, A., 2007. *An investigation on possiblility of removing ball mill from comminution circuit of Esfordi phosphate plant*, M. Sc. Thesis, University of Tehran.

Farzanegan, A., 1998, *Knowledge based optimization of mineral grinding circuits*, Ph. D. Thesis, Department of Mining and Metallurgical Engineering, McGill University, Montreal, Canada.

Latchireddi, S., Morrell, S., 2003a. Slurry flow in mills: grate-only discharge mechanism (Part-1), *Minerals Engineering*, pp. 625-633.

Latchireddi, S., Morrell, S., 2003b. Slurry flow in mills: grate-pulp lifter discharge systems (Part-2), *Minerals Engineering*, pp. 635-642.

Napier-Munn, T.J., Morrell, S., Morrison, R. D., Kojovic, T. 1999. *Mineral Comminution Circuits Their Operation and Optimisation*, JKMRC.

Özer, C.E., Ergün, S. L., Benzer, A.H., 2006. Modeling of the classification behavior of the diaphragms used in multi-chamber cement mills, *International Journal of Mineral Processing*, pp. 58-70.

Wills, B. A., Napier-Munn, T. J., 2006. *Mineral Processing Technology*, Elsevier Science & Technology Books.

Geomechanical Risk Analysis for the Historical Salt Cavern Saurau in "Wieliczka" Mine

W. Pytel, J. Parchanowicz, P. Mertuszka
KGHM CUPRUM CBR, Wroclaw, Poland

ABSTRACT Based on the finite element method formulated in three dimensions, a selected area of the salt mine has been modeled, embracing totally 2 separated, historically valuable mine rooms. The results of the computer simulations permitted elastic-viscous rock mass stability analyses identifying the areas being more susceptible to damage, presently and in a far future. The geomechanical risk assessment procedure utilized so called safety margins which were defined as a distance between the point characterized by the actual local strain/stress conditions and the instability (limit) surface(s) which location in the 3D stress/strain space could be determined using the well-known strength theories.

1 INTRODUCTION

1.1 General information

Due to 700-year ore exploitation, within mine field of the royal salt mine "Wieliczka", there has been developed the extremely complex and locally unrecognized structure of chambers and roadways. So far on nine levels of which the lowest is set about 327 m below ground level, there are 2177 chambers localized and marked on maps. The most important central part of a historically developed excavation system, localized on levels I-III between the Kościuszko and the Wilson shafts, includes about 350 historical objects, among them about 40 invaluable monuments of "0" class in different technical conditions.

In the end of 70-ties, when deterioration process caused by significant strata movement within some of the historical objects was observed, an action had been undertaken to preserve them for the next generations. This time, the experts agreed that a backfilling of the most of rooms located below the level V is necessary in order to create stable support for the valuable higher levels of the mine. The backfilling operations involving a huge volume of tailings has been successfully conducted during the years concluding with the rock mass higher stability clearly visible in the regional scale. However, in a smaller scale, most of the individual caverns located at the higher levels of mine, still suffer from time-dependent deformations concluding with spatially confined instabilities. These effects dealt also with the largest caverns, among them the Saurau chamber, are usually due to viscous behavior of surrounding shells of salt rock which are presently controlled using different ground support measures, mostly rock bolts and wooden complex support sets (see Fig. 1). However, for possible future instability potential, appropriate numerical modeling was recommended.

1.2 The Saurau cavern's location

1.3 General site description

The Saurau cavern is located within relatively complex mine workings system (Fig. 2), on the IIn (+141 m above sea level), III (+115 m) mine levels with inter-level Lichtenfels (+87 m above sea level). It had

been excavated within a one very large ZBt solid salt boulder.

Figure 1 Support sets' view in Saurau cavern

Figure 2 Saurau cavern at levels II and III

The total cavern's capacity is about 18,000 cubic meters with representative height of about 30 m, length of 50 and width of 20 m. Due to a complex shape, the cavern size depends on the location.

1.3.1 Site's hydro geological conditions

The Saurau cavern has been excavated in very large green salt rock ZBt lens (Fig. 3-4) associated with large number of smaller salt rock lenses spatially scattered within clayey waste rocks.

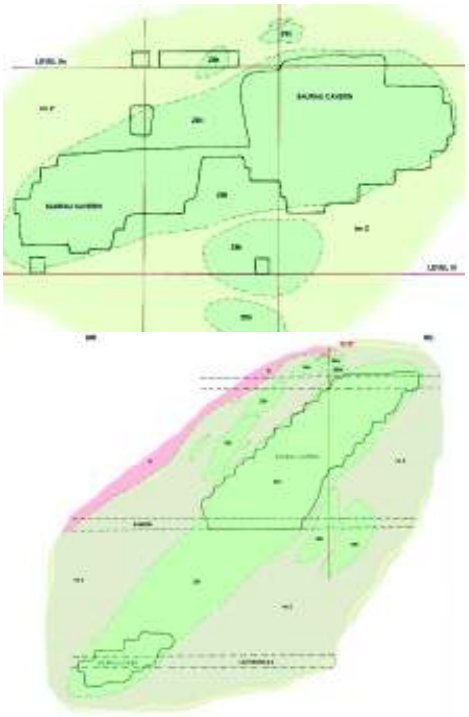

Figure 3 Vertical cross-sections of Saurau cavern (Przybyło, 2010)

The analyzed rock mass zone is located under the northern branch of solid salt seam with a dip of about 40 ÷ 45° in NW – SE direction. In this area, at the level IIn, insignificant water inflow is observed, however at the level III and below at Lichtenfels level, no water flow related phenomena has been noticed.

2 CURRENT TECHNICAL STATE OF THE SAURAU CAVERN

Taking into account that the analyzed cavern had been excavated in XVII century, its technical state may is considered to be relatively good. Renovation works made during last years were confined to thin shotkrete spraying and epoxy rock bolts installation supplemented by coated steel

mesh. Also, wooden and concrete support has

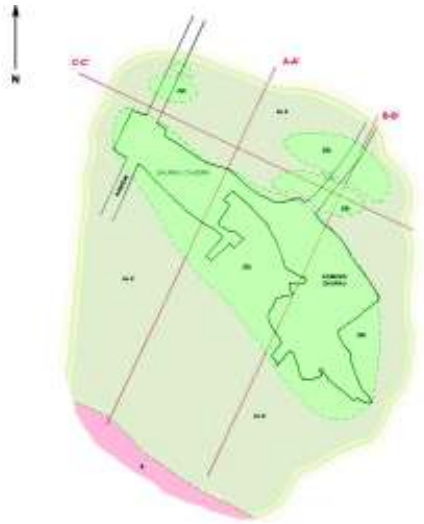

Figure 4 Saurau cavern horizontal cross-section (Level III) – Przybyło, 2010

been provided in the location where surrounding rock mass has deformed or/and fractured. Today however, due to the cavern's large size and the visitors' safety reasons, additional reinforcement and support has been recommended.

As a part of this activity, numerical modeling of the Saurau cavern and its vicinity has been therefore undertaken with the basic objective to identify the area prone to instability manifested by cracks and visible deformations.

3 GEOMECHANICAL ANALYSIS

3.1 3D numerical model of the cavern

Geomechanical problem solution and results visualization were based on the NEi/NASTRAN (2009) computer program code utilizing FEM in three dimensions with the option of creep behavior of selected materials.

In the frame of the presented approach, the different two models have been analyzed:

A. The Saurau cavern with including in the close vicinity the presence of the following chambers: Kraj, Przanowski and Długosz.
B. The Saurau cavern without including the presence of the Kraj, Przanowski and Długosz chambers, replacing them by large lenses of solid salt rock.

The model (Fig. 5), composed of 285345 finite elements linked by 304900 nodes, was built using available, however rather scarce, historical data confined to several technical and geological drawings.

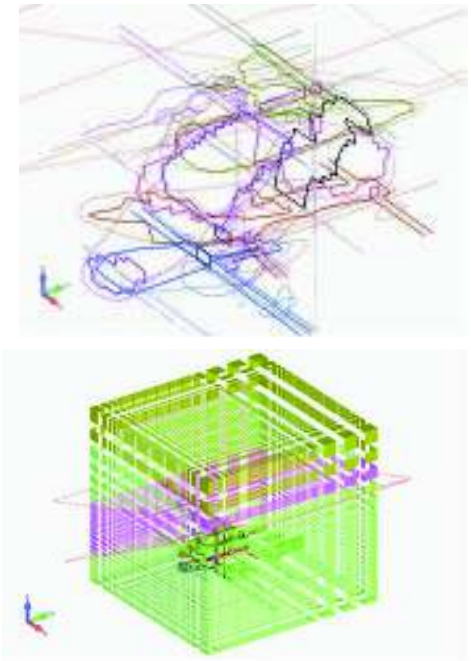

Figure 5 Drawing skeleton (top) and the numerical FEM model (bottom)

The model boundary conditions have been formulated as the displacement type limits, while the external load confined to rock mass self-weight was represented by density parameter (gravitation).
Having strength-deformation parameters of the local rock mass (Table 1) as well as results of numerical modeling (stress and deformation fields), one could determine values of so called margins of safety for surrounding rocks based on the Coulomb-Mohr strength theory:

$$F_{cm} = R_c - A \cdot \sigma_1 + \sigma_3 \quad (1)$$

where: R_c – rock mass unconfined compression strength, σ_1 and σ_3 – minor and major principal stress, and A – parameter given in Table 1. The negative value of F_{cm} indicates high potential for instability event.

Furthermore, the authors focused on the effective strain and the major principal stress spatial distribution considering them as good instability indicators involving shear and tensile type of mechanisms of failure. The appropriate limit criteria are as follows:

$$\varepsilon_{ef} = \frac{\sqrt{2}}{3}[(\varepsilon_{11} - \varepsilon_{22})^2 + (\varepsilon_{22} - \varepsilon_{33})^2 + (\varepsilon_{33} - \varepsilon_{11})^2 + 6 \cdot (\varepsilon_{12}^2 + \varepsilon_{23}^2 + \varepsilon_{31}^2)]^{0.5} \geq 0{,}03$$
$$\sigma_1 - R_r \geq 0 \quad (2)$$

where: R_r – tensile strength.

3.2 Rock mass geotechnical parameters

From the available database (e,g, Wojnar, 1996) one may conclude that the Saurau cavern is located within relatively soft and weak rock mass composed mostly of marlaceous claystone. In the numerical analysis, three-dimensional geological structure is modeled therefore by introducing three basic material types of different strain-strength and viscous parameters:

- stratiform deposit of outstanding viscous-elastic behavior, composed of stratiform and shaft salt with inclusions of barren rock
- boulder deposit representing a mixture of marlaceous clays, boulder and granular salt, generally revealing moderate viscous-elastic behavior,

Table 1 Average values of geotechnical parameters of rocks

Kind of Rock	R_c (MPa)	R_r (MPa)	Modulus of deformation E (MPa)	Poisson's ratio ν	Angle of internal friction φ	A	Coefficient of viscosity η (Pa sec)
Tertiary and Quaternary deposits			70				
Stratiform and shaft salt	40	3.5	180	0.4	40	4.6	4.2E17
Boulder salt deposits	37	2.4	150	0.4	37	4.02	4.2E17
Marlaceous claystone + 10% shaft salt	5	0.3	60	0.3	30	3.0	4.2E18

- marlaceous claystone representing all remaining, by assumption purely elastic rocks (claystone, marlaceous claystone, clayey marl, mudstone etc.).

The average strength-deformation parameters of rock mass located nearby of considered cavern and afterwards used in the numerical analyses, have been presented in Table 1.

Creep properties of salt rock, particularly of stratiform and shaft salt, are considered to be the most important factor inducing the presently observed rocks' movement within the Saurau cavern. This uniformly increasing with time movement reminds typical behavior of the Maxwell liquid model. The creep parameter η of a such simple model has been determined based on field and laboratory measurements and tests.

3.3 Geomechanical analyses of the Saurau cavern and its vicinity

3.3.1 Model Calibration

The model calibration has been done assuming that roof-floor convergence developed for the last year within the cavern is equal to actually measured of 2 mm distance. In this case, the value of creep parameter of marlaceous claystone has been established as the decision parameter. This implied that the marlaceous claystone contained the of salt additive of a given amount. The successive phases of modeling and computation process with gradually increasing salt ratio, assumed the Newton liquid creep parameter decrement according to the function:

$$\eta = \frac{4{,}5 \cdot 10^{17}}{Z_z} \qquad (3)$$

(where: Z_z – volumetric amount of salt within the claystone, 4.5E17 – creep parameter of salt deposits accepted as an average value from the appropriate literature (Slizowski, 2006; Wojnar et al., 1996). Since the assessed value of roof-floor convergence reached 2 mm/year for Z_z = 0,10 (10%), in basic geomechanical computations, creep coefficient for marlaceous claystone η = 4.5 E18 Pa sec has been set up.

3.3.2 Results of numerical computations

The numerical model of the Saurau and Kraj caverns shown in Figure 6 consisted of 37 layers along which the obtained results have been presented in the following categories of variables: yearly x-y-z translations increment, stresses in x-y-z coordinate system, values of the effective strain, and safety margin F_{cm} in 3D space.

3.3.3 Yearly translation increment

Calculation results have confirmed that the yearly increment of vertical displacement w_z (see Fig. 7) will not be greater than 0.003 m and are in agreement with values observed in the nature, accepted as the base for the model calibration process. Calculated values of horizontal deformation increment w_x i w_y may reach no more than ± 0.0005 m.

One may notice that rock mass located at southern part of the cavern tends moving in northern direction while increment of displacements in E-W direction is negligible.

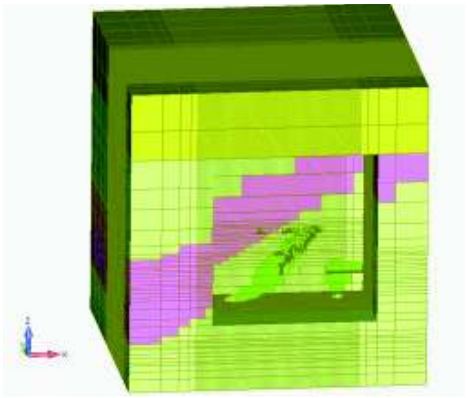

Figure 6 General view of the numerical model

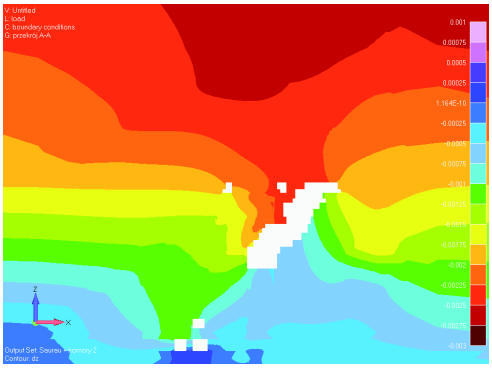

Figure 7 Yearly increment (m) of vertical displacement contour (cross-section A-A)

Although the calculated value of vertical translation at the model's surface reaches value of 0.00275 m, one may assume that his number is underestimated due to the limited volume of the analyzed model.

3.3.4 Stresses in x-y-z coordinate system

The obtained calculation results have revealed that horizontal normal stresses σ_x i σ_y (Fig. 8) reach relatively low, negative

values however, one may identify very limited areas of positive stresses located at the opened cavern's surface. This may suggest tendencies for scaling development at limited range.

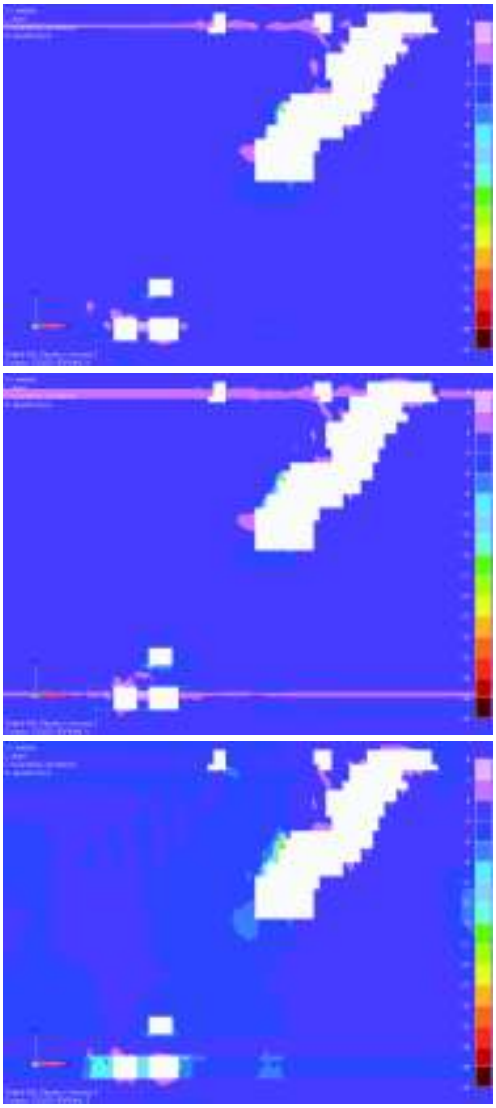

Figure 8 Normal stresses (MPa) contours at A-A cross-section (σ_x – top, σ_y – middle, σ_z – bottom)

Also vertical stress σ_z (see Fig. 8 bottom) reaches moderate values of about 2 – 4 MPa however the areas of positive stress may be noticed at the cavern's surface (scaling). Also, southern wall of the cavern located at the depth of 123 m is locally compressed due to the close presence of isolated salt lenses. This part of the cavern is reinforced already by rock bolts.

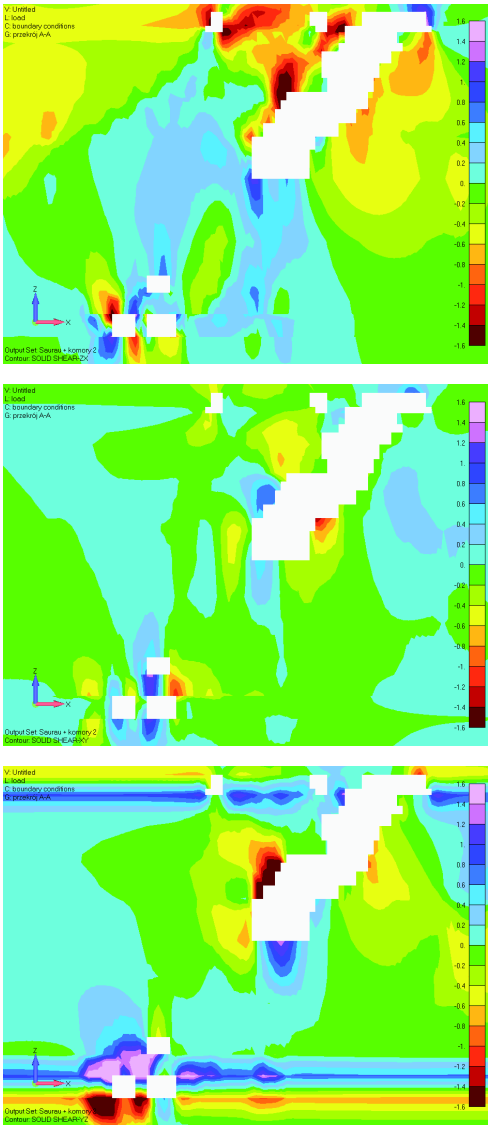

Figure 9 Shear stresses (MPa) at cross-section A-A (σ_{xz} – top, σ_{xy} – middle, σ_{yz} – bottom)

Calculated shear stresses contours (Fig. 9) indicate that σ_{xy} stress reaches generally values of very low magnitude and therefore they may be considered in geomechanical analyses to be a parameter of second order importance. Contours of remaining categories of shear stresses indicate however that the cavern's southern corner, at a depth of 123 m, is subjected to significant shearing and therefore in this area (also in the lower part of the cavern) one may expect fractures development.

3.3.5 Principal stress σ_1

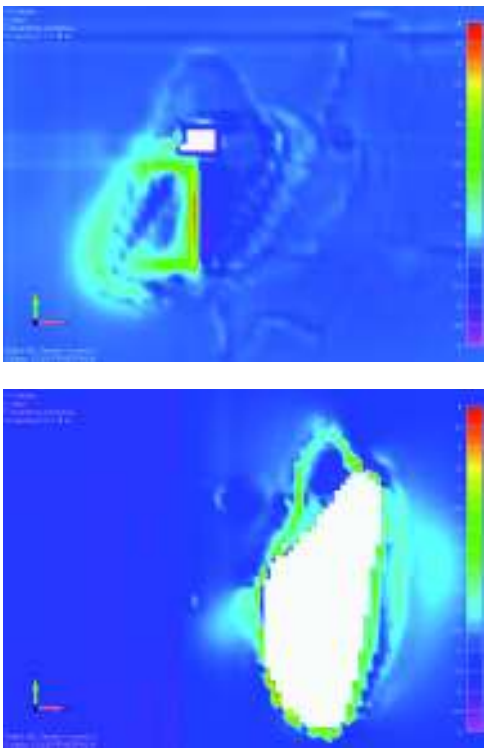

Figure 10 Principal stress σ_1 contours (MPa) at 148 m (top) and 115 m below surface (bottom)

The calculated minor principal stress $\sigma 1$ when reveals positive value may be considered as a good indicator of tendency to rock mass instability occurrence realized mostly by a tensile type mechanism of failure – open fractures.

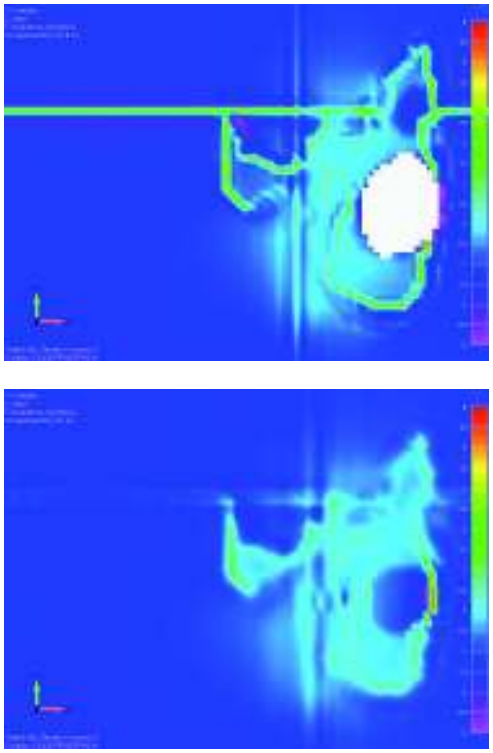

Figure 11 Principal stress σ_1 contours (MPa) at 101.5 m (top) and 101.0 m below surface (bottom)

Analyzing Figures 10-11 from this point of view, one may find that the areas of a positive σ_1 value are confined to the cavern walls of selected location (potential for scaling) or to a kind of the lower caverns projection formed in a characteristic pattern following these caverns' shape (see lower Saurau). Therefore open fractures development may be expected there.

3.3.6 Effective strain ε_{ef}

The effective strain (see Eq. 2), when is of higher value, may serve as a kind of indicator of the areas where a high potential for rock mass separation and its fracturing exists. When analyzing Figures 12-13 from

this point of view, one may conclude that rock mass in the Saurau cavern area is relatively intensively loaded, particularly along surfaces of the contact between marlaceous claystone and boulder salt deposits. Therefore one may expect that in those locations, the boulder salt elements shall work partially independently of surrounding rocks, forming a kind of blocked, distinct salt elements structure of lower potential for stability than that characteristic for the intact rock mass.

The calculated yearly increment of effective strain (see Fig. 14) confirms insignificant changes comparing with the initial state.

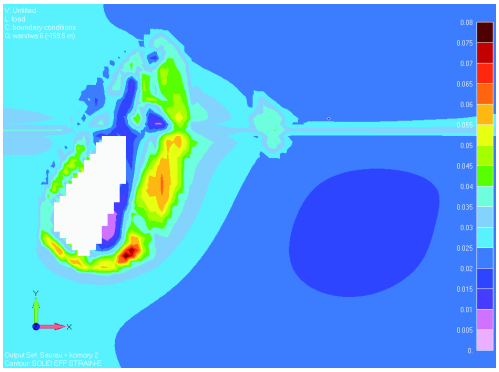

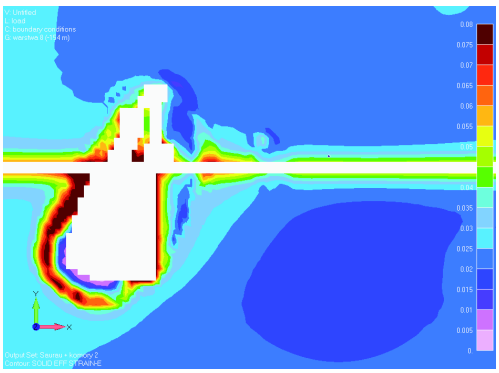

Figure 12 Effective strain contours at 159.5 m (top) and 154 m (bottom) below the ground surface

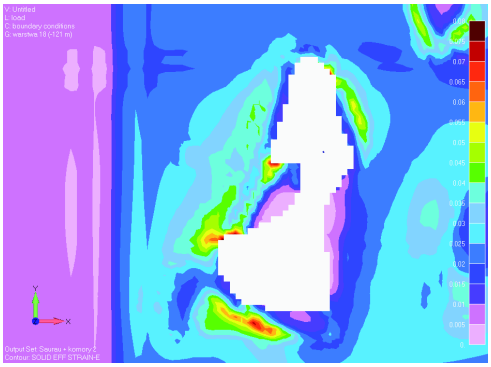

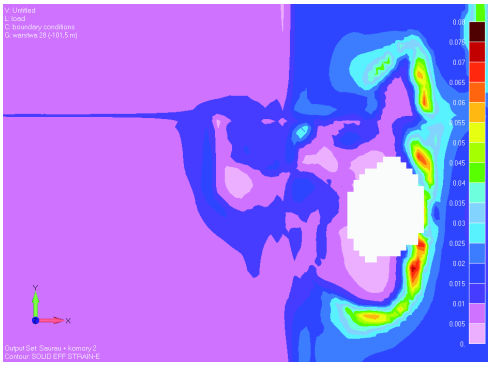

Figure 13 Effective strain ε_{ef} contours at 121.0 m (top) and 101.5 m (bottom) below surface

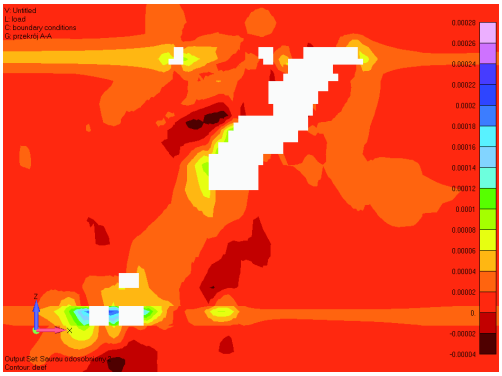

Figure 14 Effective strain increment contour (cross-section A-A)

3.3.7 Safety margin F_{cm}

Negative values of calculated safety margin F_{cm} (Fig. 15) indicate higher hazard from instabilities caused by shear stress overloading (Coulomb-Mohr strength hypothesis). The areas of transition between marlaceous claystone and salt deposits seem to be the most sensitive from this point of view however, since safety margin values are generally greater than zero, this kind of risk may be presently treated rather as an irrelevant hazard.

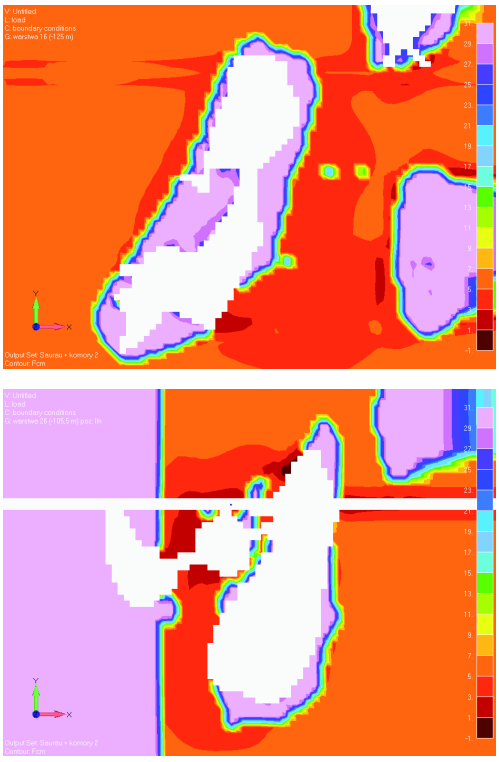

Figure 15 Safety margin F_{cm} (MPa) contours at 125.0 m (top) and 105.5 m (bottom) below surface

4 CONCLUSIONS

The comparative analytical material obtained using numerical modeling of the Saurau cavern and its vicinity for the present moment and for the future (365 days ahead), clearly indicate that the first importance causes of observed rock mass deformations are:
(1) viscous behavior of the most rocks composing the geological environment of the „Wieliczka" mine, and
(2) rock mass structure within the immediate vicinity of the caverns, where one may observe the area of transition between weak marlaceous claystone and stronger boulder salt structures weakened however by excavated caverns' presence.

Therefore in an extreme case one may encounter a shell-type structure which may break in bended parts and corners and afterwards works as a structure composed of distinct elements. Due to the high shear stress values, these distinct elements may develop mostly at the contacts of materials revealing strain properties of significant differences.

Presented above geomechanical analyses hale proved that instability hazards decrease very rapidly with the distance from the cavern's wall. This permits effective applying of rock bolts type, shotcrete and other means of ground support systems. The sensitive points of Saurau cavern which were identified above using numerical approach, may be then treated with a such stability tools (see Fig. 16).

One has to emphasize that the locally expected rock separation or fracturing phenomena do not create a serious hazard for the structure total stability. The presented calculation results do not reveal hazard of a large scale however some parts of the cavern will require rock mass reinforcement measures.

All results have proved insignificant effect of neighboring caverns on Saurau cavern's safety. This is probably due to the lateral distribution of the adjacent caverns resulting the lack of multilevel structures with inter-level rock benches usually weakening the caverns within the area of influence. From this point of view the favorable spatial configuration of Saurau cavern is also important from point of view of the hazard created by surface subsidence which is expected to be very low.

Figure 16 Supported salt roof strata in Saurau cavern

REFERENCES

Przybyło J., Personal communication, Wieliczka, 2010

NEi/NASTRAN, v. 10.1, (2009). Noran Engineering, Inc.

Ślizowski J. (2006). Geomechaniczne podstawy projektowania komór magazynowych gazu ziemnego w złożach soli kamiennej. Studia rozprawy Monografie nr 137, IGSMiE PAN, Kraków 2006

Wojnar W., Bieniasz J., Gołda J. and A. Biel, (1996). *Studium sposobów i warunków kotwienia mioceńskiego górotworu solnego,* Praca OBR Górnictwa Surowców Chemicznych CHEMKOP, Kraków

Pouya A., (1991) Correlation between mechanical behavior and petrological properties of rock salt, Rock Mechanics as a Multidisciplinary Science, Roegiers (ed.), Balkema, Rotterdam

Advancing in Grade Control Problem through a Possibilistic Approach

M. Kumral
McGill University, Department of Mining and Materials Engineering, 3450 University Street Montreal, Quebec, Canada H3A 2A7

ABSTRACT Grade control aims to minimize the misclassification of ore and waste in mining operations in a manner that head grade and satisfy processor capacities are controlled. The problem of grade control is an optimization problem on the contrary to traditional approaches used in mining industry at present. Furthermore, the problem has a stochastic nature because there are some uncertain/imprecise variables such as grade, price and costs in grade control problem. At the time mining extraction is planned, sparse data are used to estimate/simulate planning blocks. Unknown future event contribute to these uncertainties further. All global decisions on mine planning and assessment are made on uncertain images. This motivates stochastic techniques to solve the problem. In this paper, possibilistic fuzzy programming models are introduced to solve grade control problem in such a way as to regard the uncertainty of selective mining units (SMU) economic values. A case study is conducted to demonstrate the models and discussed pros and cons of the approaches. The proposed techniques are applied to a gold data. The stochastic model is able to consider uncertainties associated with grade, price and costs.
Keywords: Grade control, possibilistic programming, uncertainty management

1 INTRODUCTION

The goal of ore selection is to maximize profit, minimize possible losses from mis-classification, keep the mean grade of the ore sent to the processing plant within desired limits, meet capacity requirements or reduce grade fluctuations in the processing plant feed. Current ore selection approaches include grade estimations, simulation approaches, minimizing losses or maximizing profits from ore/waste classification, enhanced metal recovery, weighting minimum loss and utility function (Srivastava *et. al*.; 1994; Glacken, 1997; Richmond, 2001). An excellent review of some of these approaches can be found in Verly (2005). A weakness of most of these techniques is that they do not consider ore quality and quantity requirements. Richmond and Beasley (2003) and Richmond (2004) recognized the potential of mathematical programming approaches and expressed ore selection as an optimization problem. The approaches proposed herein take a further step in advancing understanding through new techniques. In next this paper, ore selection is expressed as a stochastic optimization problem, namely possibilistic fuzzy programming.

2 POSSIBILISTIC PROGRAMMING

In probabilistic programming, the uncertainty is modeled through discrete or continuous probability distributions. Possibilistic programming regards random parameters as fuzzy numbers and constraints

are treated as fuzzy sets (Sahinidis, 2004). This technique provides an opportunity to use imprecise probabilities. Zadeh (1978) introduced possibility theory as an extension of his theory of fuzzy sets and fuzzy logic. The possibility distributions can be defined as the degree of occurrence of an event. Possibility can be seen as an upper probability. Any possibility distribution defines a unique set of admissible probability distributions. In this paper, triangular possibility distributions are derived for all imprecise coefficients. The distribution defines the occurrence degree of SMU profit with imprecise data for $\tilde{r}_{nd} = (r_{nd}^p, r_{nd}^m, r_{nd}^o)$. $\tilde{r}_{nd}$ can be defined as below:

1. The most pessimistic value (r_{nd}^p) with a low likelihood of belonging to the set of available values (possibility degree is 0 if normalized).
2. The most likely value (r_{nd}^m) with belonging to the set of available values definitely (possibility degree is 1 if normalized).
3. The most optimistic value (r_{nd}^o) with a low likelihood of belonging to the set of available values (possibility degree is 0 if normalized).

In order to use the model developed, in addition to SMU profits, grade and tonnage are expressed by triangular possibility distribution as follows:

$$\tilde{o}_{nd} = (o_n^p, o_n^m, o_n^o) \quad \forall_n$$
$$\tilde{g}_{nd} = (g_n^p, g_n^m, g_n^o) \quad \forall_n$$

Various approaches have been proposed to obtain auxiliary crisp model from possibilistic programming model. Chanas's (1983) approach applied a parameter to solve the fuzzy linear programming in the simplest form. Tanaka and Asai (1984) used a membership function, which was based on central and spread of fuzzy numbers. Julien (1994) proposed an approach that incorporates the α-cut concept in a version of possibilistic programming. Rommelfanger (1996) recommended non-linear membership function in modeling fuzzy data.

In this approach, the problem is formulated in such a way as to maximize three objectives, zz^p, zz^m, zz^o, simultaneously. Triangular shape is kept by changing the objective in such a way as to maximize zz^m, minimize $zz^m - zz^p$ and maximize $zz^o - zz^m$ (Lai and Hwang, 1992).

This leads to three new crisp objective functions:

$$Min \; zz_1 = zz^m - zz^p \tag{1}$$
$$Min \quad \sum_{t=1}^{T}\sum_{n=1}^{N}\sum_{d=1}^{D}\left(r_{nd}^m - r_{nd}^p\right) x_{tnd} \tag{2}$$

$$Max \; zz_2 = zz^m \tag{3}$$
$$Max \quad \sum_{t=1}^{T}\sum_{n=1}^{N}\sum_{d=1}^{D} r_{nd}^m \, x_{tnd} \tag{4}$$

$$Max \; zz_3 = zz^o - zz^m \tag{5}$$
$$Max \quad \sum_{t=1}^{T}\sum_{n=1}^{N}\sum_{d=1}^{D}\left(r_{nd}^o - r_{nd}^m\right)x_{tnd} \tag{6}$$

In order to solve the problem, various multi-objective or goal programming approaches can be used. The problem is also a multi-objective optimization problem. Positive Ideal Solutions (PIS) and Negative Ideal Solutions (NIS) of three objective functions are generated using Hwang and Yoon (1981) proposal.

For each objective function, linear membership functions are defined. Three objective functions are put together by initiation of a new variable, λ. The objective is now to maximize λ such that any linear membership function will be greater than λ for given ore selection schedules.

3 CASE STUDY

A case study is conducted to demonstrate the approaches proposed using a hypothetical gold data set. There are four processing destinations: Dump leaching, heap leaching,

percolation leaching and carbon-in-pulp. The problem is to determine SMU destinations in such a way as to maximize profit under the capacity and process control constraints. There are 125 SMUs within each planning block.

Fuzzy possibilistic programming is implemented to solve the problem. The solution approach can be summarized as below:

Step 1. SMU grades and tonnages by conditional simulation and ore price by historical data are generated.

Step 2. For each imprecise datum in each SMU used in the objective function and/or the constraints, triangular possibility distributions are derived. The most pessimistic, the most likely and the most optimistic values are recorded to use in the optimization model.

Step 3. The objectives are the maximization of the most possible profit, the minimization of the risk of obtaining lower profit and the maximization of obtaining higher profit.

Step 4. The crisp objective functions of the auxiliary multi-objective mixed integer programming problem are solved. Positive and negative ideal solutions are determined.

Step 5. The objective function is expressed as maximin model. Using the selected minimum acceptable possibility, β, the imprecise constraints are converted into crisp equivalents.

Step 6. The maximin model is solved. If the decision maker is satisfied with the results, the algorithm stops. Otherwise, new values of some parameters are initiated or the model is modified using new membership function. The procedure is then repeated as from Step 2.

In order to convert the imprecise constraints into crisp equivalents for the minimum acceptable possibility, β, the weighted average is accepted as $w_1 = 4/6$ and $w_2 = w_3 = 1/6$. Linear membership functions of three objective functions are specified and converted to equivalent model in terms of maximin expression. Finally, the problem is solved until the decision maker is satisfied. Optimal output and some computational results are summarized in Table 2. Possibilistic programming is observed to generate a better financial output from higher reliability models but not deterministic model. It is difficult to compare probabilistic and possibilistic models. If one does not have reliable information about grade distribution, possibilistic programming model may be preferred. Otherwise, probabilistic model will be better.

The parameter file used for possibilistic programming is given in Table 1.

Table 1. Data file used in optimization models

Number of SMU	125
Number of destinations	5 (one waste dump and four processing destinations)
Number of periods	2
SMU sizes	4*4*4
Capacities	15 15 15 15 (SMUs for destination 2, 3, 4 and 5 respectively)
Minimum acceptable possibility	0.5
Weights used possibilistic programming	w1=4/6, w2=1/6, w3=1/6

Table 2. Results obtained by possibilistic programming model

	Number of SMUs		Average grades		Profit ($) (per SMU)	
	Period 1	Period 2	Period 1	Period 2	Period 1	Period 2
Waste	65	65	0.33	0.36	-20800	-20800
D1	15	15	0.63	0.6	3120	2400
D2	15	15	1.55	1.41	41100	35220
D3	15	15	2.73	2.56	100830	92160
D 4	15	15	5.97	4.93	285090	225810
Total (with constant recovery and processing cost)					409340	334790
Total (with varying recovery and processing cost)					410557	334367

4. CONCLUSIONS

In this paper, a fuzzy-based approach known as possibilistic programming was used to solve grade control problem. In this approach, fuzzy coefficients are treated with possibility distributions on the coefficient values. The approach has a two-stage solution methodology. First, the original possibilistic programming problem is converted into an equivalent auxiliary crisp multiple objective mixed integer linear model. Second, the model based on maximin is proposed for finding a preferred compromise solution in an interactive way.

REFERENCES

Chanas, S., 1983, The use of parametric programming in fuzzy linear programming, Fuzzy Sets and Systems, vol. 11, p. 243-251.

Hwang C.L. and Yoon K., 1981, Multiple Objective Decision Making, Springer, Verlag.

Glacken, I.M., 1997, Change of support and use of economic parameters for block selection, Geostatistics Wollongong'96, Ed(s): Baafi and Schofield, vol. 2, p. 811-821.

Julien, B., 1994, An extension to possibilistic linear programming, Fuzzy Sets and Systems, vol. 64, p. 195-206.

Lai, Y.J. & Hwang, C.L., 1992, A new approach to some possibilistic linear programming problems, Fuzzy Sets and Systems, vol. 49, p. 121-133.

Richmond, A., and Beasley, J.E., 2003, An iterative heuristic for the ore selection problem, Journal of Heuristics, vol. 10, p. 153-167.

Richmond, A., 2004, Financially efficient ore selections incorporating grade uncertainty, Mathematical Geology, vol. 35, no. 2, p. 195-215.

Rommelfanger, H., 1996, Fuzzy linear optimization and applicayions, European Journal of Operational Research, vol. 92, p. 512-527.

Sahinidis, N.V., 2004, Optimization under uncertainty: state-of-the-art and opportunities, Computers and Chemical Engineering, vol. 28, p. 971-83.

Srivastava, R. M., 1987, Minimum variance or maximum profitability? CIM Bulletin, vol. 30, no. 901, p. 63-68.

Tanaka, H. and Asai, K., 1984, Fuzzy linear programming with fuzzy parameters, Fuzzy Sets and Systems, vol. 13, p. 1-10.

Verly, G., 2005, Grade control classification of ore and waste: A critical review of estimation and simulation based procedures, Mathematical Geology, vol. 37, no. 5, p. 451-476.

Zadeh, L., 1978, Fuzzy sets as a basis for a theory of possibility, Fuzzy Sets and Systems, vol. 1, p. 3-28.

Some Experiences to Re-use Abandoned Mine Drifts in Korea

J.K. Kim, H. Moon, C. Choi, Y. Noh, H.S. Yang
Chonnam National University, Gwangju, Korea

ABSTRACT Some Korean limestone mines are developed by underground excavation of room and pillar method. Because environmental and geological requirements, some of these mines need to be remodeled. Authors conducted various researches for these mines. Some experiences are introduced and discussed in this paper, especially about the re-use of abandoned mine drifts or mined out caverns. They are re-used as underground crusher plants, explosive welding site and tour course for experience. Rock classification and numerical analysis with field investigations were main tools.

1 INTRODUCTION

In this study, rock mechanical research works on several underground mines are introduced which were conducted by the rock mechanics and blasting laboratory of Chonnam National University.

Crushers are main source of dust pollution around the mine. To avoid environmental issues, it is suggested to move the crushers to underground. Usually the limestone mine in thick layers is developed by room and pillar method. Some pillars need to be removed for the space and it can cause instability.

One mine made a plan to use the mined out cavern as blast welding site. Instant pressure from blast can be used for welding but the pressure can cause instability of the surrounding structures.

Another mine planned to re-use an abandoned drift as tour course for experience. Since it was abandoned for a long type, safety investigation and enforcement was inevitable.

Stability assessments on the pillar of large rock cavern, distribution of load to the single pillar in the cavern, and safety evaluation of cavern walls under the pressure by blast welding were carried out for those mines. These research works include RMR(Rock Mass Rating) classification, site investigations and numerical analysis.

2 CRUSHER ROOM

2.1 Removing Pillars and Supporting the Room

Sambo Mine planned to construct crusher room at underground cavern to avoid noise and dust pollution. The space would be provided by removing 4 pillars.

Because there was some rice field above the site, water flows was expected at rainy season through discontinuities developed in overburden from the surface to the roof. And stress change by removing the pillars was supposed to affect overall stability of the rock structure.

Safety of the rock structure was evaluated based on the results of site investigation, field and laboratory experiments, to construct the crusher facilities in the mined out cavern. Distribution of discontinuity showed probability of wedge failures for all the pillars.

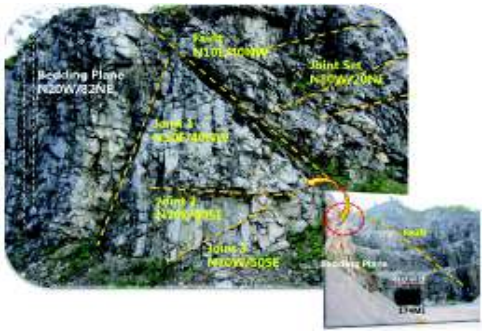

Figure 1. Geological structure of the surface above the portal

Mechanical properties and characteristics of discontinuities at the site was investigated and classified.

Crusher room array is shown in Fig. 2.

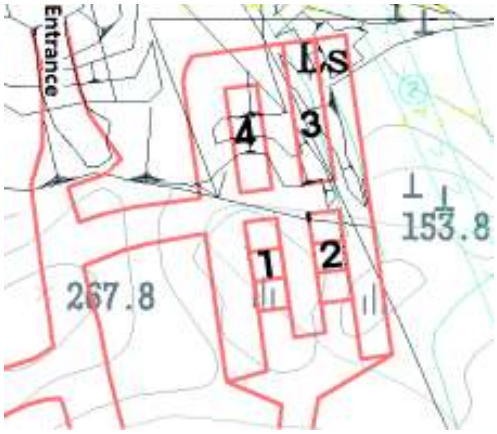

Figure 2. Crusher room array at the site

Model configuration and one of the FLAC^{3D} numerical results is shown in Fig. 3

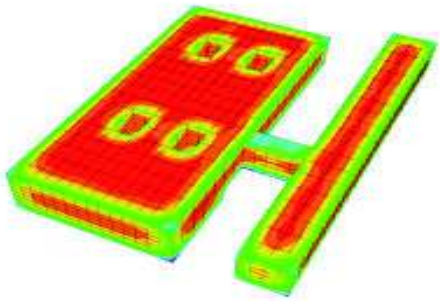

Figure 3. Model configuration and shear stress distribution

Fig. 4 shows the change of principle stresses with the excavation and support stage.

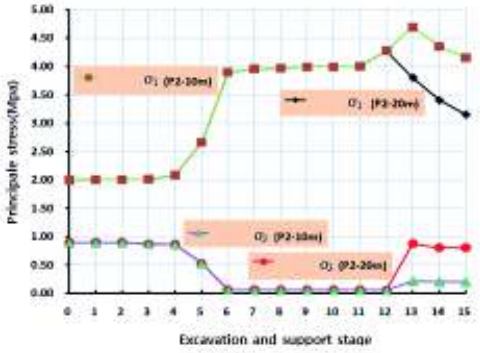

Figure 4. Principle stress at pillar 2 with different pillar size

Numerical analysis showed that to keep the safety factor larger than 2 for long period maintenance, enlarging the pillar size was inevitable and additional support was required.

To prevent the weakening of the rock support which was expected by inflow of surface water, it was suggested that the clay seams be replaced by urethane and water inflow should be controlled systematically.

2.2 Single pillar stability at large cavern

Crusher and loading rooms are assembled at underground caverns which was located at mined out area of Sindong Mine. The span of crusher room is as large as 100 meters. One pillar supports the roof. The area of pillar section is about 3% of the cavern area. Fig. 5 shows the plan of cavern and pillar

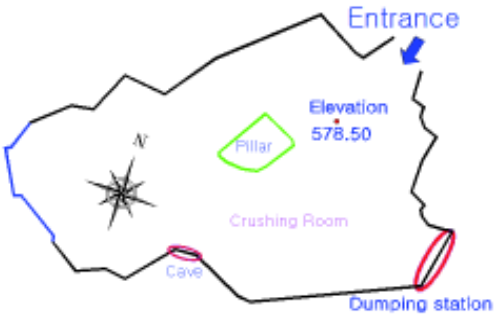

Figure 5. Crusher room array at the site

Fig. 6 is the pillar in the crusher room.

Figure 6 The pillar in the crusher room

Vibrations from blasting and crushing machine work as repetitious dynamic loading. Planned shotcrete thinner than standards and rock bolts shorter than 1 m exposed the safety problem of the crusher room.

Rock quality of the pillar was evaluated as a medium strength in terms of strength and velocity index. Walls at the entrance of the cavern showed possibility of wedge failure.

Fig. 7 shows the numerical model for the FLAC^{2D} analysis.

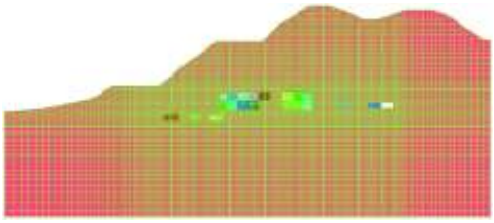

Figure 7. Model configuration for the FLAC^{2D} analysis

Fig. 8 shows the safety factor distribution to shear failure. It concluded that the safety factor of the pillar was less than the required value.

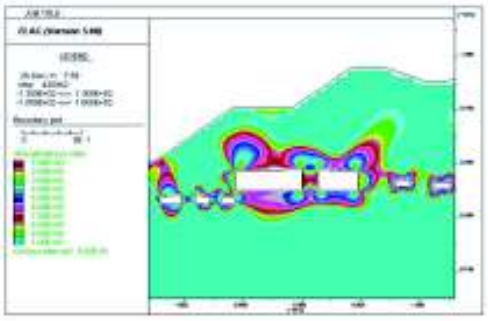

Figure 8. Distribution of safety factor to shear failure

Steel support or artificial concrete pillar was suggested to disperse the overburden load. Cable or rock bolts were suggested as an alternative to reinforce the roof.

3 BLAST WELDING SITE

JS mine studied to re-use its abandoned drift for blast welding. In blast welding, the impact pressure is used to weld a clad metal to a different, base metal (Fig. 9). Since enormous overpressure and noise occur in this process, it is necessary to make the place to be confined.

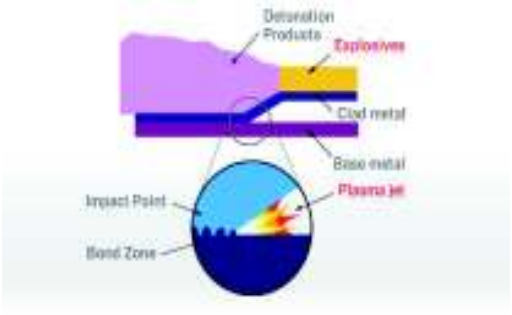

Figure 9. Concept of blast welding

Most concerned question was whether the ceiling and surrounding pillars of the mined out cavern are safe from the pressure induced from the blast. This study was carried out to evaluate the influence. USBM, CONWEP and DDESB equations were applied to determine the effect of air blast to the pillar in terms of distance and volume. Determined results were compared with mechanical properties of rock mass and simple safety factors were calculated

Fig. 10 shows one example of pressure decay along the distance. Pressure at a certain distance was compared to UCS and tensile strengths and safety factors were calculated. Since the UCS is the least strength of material under confined state, it was simply assumed that the safety factor is the ratio of the strength over the stress.

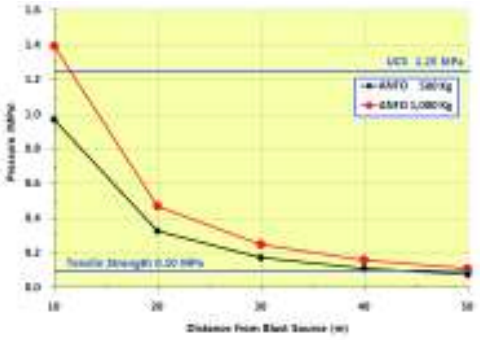

Figure 10. Pressure decay along the distance

Analysis shows that the nearest 9 meter high pillar at the distance of 20 meter was required to be protected. 15m×7m drift for discharge of blast gas is planned to excavate. For the blast welding, as much as 1 ton of ANFO is planned to be used for one blast.

Incident pressure by the blasting in the cavern decrease gently compared to the surface blasting with the same size. Air blast in the cavern has tendency to decrease in proportion to the distance from the source. Various calculation results show that stability of mined out cavern can be influenced when more than 0.5 ton of ANFO is exploded. The DDESB equation evaluated that the roof be most unstable.

4 TOUR COURSE FOR MINE EXPERIECE

G Co. planned to re-use the abandoned drift of old Dongwon Mine to tour course for mine experience. Since the place will be used by innocent tourists, it must be investigated and strictly maintained with high safety.

Deformation of supports, leakage, rock falls, over break cavity were investigated. Unrevealed cavity beneath the supports was determined by the CMS, or the cavity monitoring system. Key block analysis as

well as 3D numerical analysis were applied on this site.

Fig. 11 and 12 show an example of deformation on steel supports and cavity by rock fall.

Fig. 11 Deformation on steel supports

Fig. 12 Cavity by rock fall

Fig. 13 shows scanned profile of cavity and CAD transformed data.

It was concluded that there were lots of defects in the drift like cavities, rock fall areas and over breaks. Discontinuities developed in and vicinity of the drift shows there is lots of opportunity of small scale rock falls.

Existing supports must be replaced or reinforced before the drift is re-used as tour course for mine experience.

Other methods for water and air control suggested.

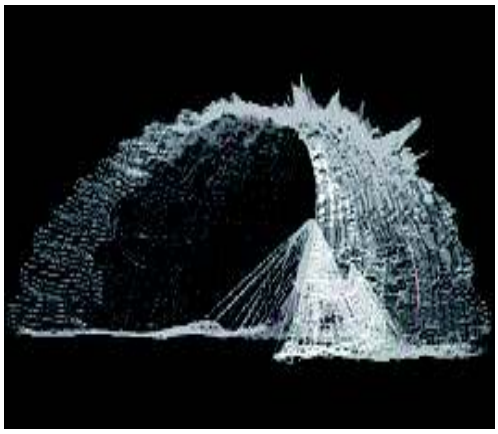

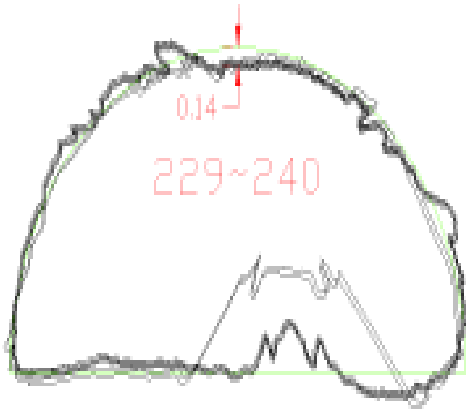

Fig. 13 CMS analysis

5 CONCLUSION

This paper represented some recent research works on the re-use of underground mine drift or caverns. These mining problems of pillar and/or cavern stability of various conditions and blasting caused stability and blast design problems also were solved by numerical, experimental and empirical techniques of rock mechanics. Rock classification, numerical analysis of wedge

and block analysis, differential approach with FLAC 2D and 3D was successfully applied to mining problems.

REFERENCES

Jang, MH et al., 2011. *Stability Evaluation and Support Design for Large Crusher Cavern*, Sindong Mine Co., JungSun, Korea, 151 p. (in Korean)

Jang, MH et al., 2012. *Stability Evaluation and Reinforcement for 650 drift of old Dongwon Mine*, Gangwon Land Co., Taeback, Korea, 333 p. (in Korean)

Park, JH et al., 2010, *Stability Evaluation and Supportis for rock structures to construct underground crusher facilities*, Sambo Mine Co., Danyang, Korea, 131 p. (in Korean)

Yoon, CH et al., 2009. *Effect of pressure caused by blast welding operation on the stability of mine drift*, Chungmoo Chemical Co., JungSun, Korea, 32 p. (in Korean)

Selecting an Optimum Technique for Evaluating the Mining Projects Using Fuzzy-AHP and Fuzzy-Topsis Methods

M. H. Basiri,
Mining Dept., Tarbiat Modares Univ., Tehran, Iran

N. Mesripoor,
Mining Dept.,Tarbiat Modares Univ., Tehran, Iran

ABSTRACT Selecting a suitable method for evaluation of mining projects involves complicated process. There are different techniques for decision making such as multi criteria decision making, delphi and expert system. In this paper by hybrating the Fuzzy-AHP and Fuzzy-Topsis, an optimum technique was chosen among the four methods; Real Option (RO), Monte Carlo Simulation (MCS), Decision Tree (DT) and Net Present Value (NPV).The result presents that the RO has more advantages than the other methods. The MCS, DT and NPV stand in the next priorities respectively.

Keywords: Fuzzy-AHP, Fuzzy-Topsis, Real Option, Monte Carlo Simulation, Decision Tree, Net Present Value

1 INTRODUCTION

Nowadays there are several methods for evaluating the mining projects. Each of these techniques has its own strength and weakness. There are varieties of reasons lead to select a particular evaluating method in which some criteria are conflicted with each other. Since the mining projects involve substantial amount of investment and long term payback period, therefore the economic valuation of such projects are central and need exclusive considerations. Furthermore, the methods such as discount cash flow, DT, MCS and RO are the most common evaluation techniques in the mining industries.

The major challenges in this issue are risks, uncertainties, the role of time in the projects and management flexibility. Uncertainty is a main part of real world systems. It is created through two factors (a) uncertainty due to physical variability, and (b) uncertainty due to lack of knowledge (Markowski and Mannan ,2009). Fuzzy logic is a powerful tool to handle the uncertainty and solve problems where there are no sharp boundaries and precise values. According to capability and efficiency of fuzzy logic in modeling uncertainty, this technique is employed in different aspects of risk management (Alidoosti et al., 2012). It is clear that fuzzy logic has demonstrated its capabilities and efficiencies as a practical engineering and problem-solving tool. In this paper a new methodology based on hybrating the Fuzzy-AHP and Fuzzy-Topsis to select an optimum technique for evaluating the mining project among the four methods; RO, MCS, DT and NPV. The result demonstrates the RO techniques.

2 VALUATION METHODS IN THE MINING INDUSTRIES

2.1Net Present Value

One of the most common methods to evaluate the mining projects is the NPV. This technique constitutes the basis of investment decisions for the most mining companies. Also the discounted cash flow (DCF) and Rate of Return (ROR) may categorize under this method (Bhappu and Guzman, 1995).

2.2 Decision Tree

DT analysis is a method that comes from operation research and game theory. It is simply a flowchart or diagram representing a classification of a system or a probabilistic model (Clemen, 1995).

The tree is structured as a series of simple questions. The answers to these questions generate a path down the tree. The values are determined for each of the possible outcomes in the analysis. In order to construct the decision tree, all the appropriate decision nodes and probabilities of occurrence must be determined (Moore et al., 2001).

A decision tree consists of nodes and branches. There are two types of nodes: decision nodes, represented by squares, i.e., whether to make the investment or not, and undertrained event nodes, represented by circles, i.e., ore grade, commodity price, project investment and ore recovery. Branches are straight lines that emanate from the nodes. At the end of each branch the generated NPV is denoted (Moore et al., 2001).

2.3 Monte Carlo Simulation

Due to the development of computer technologies, the MCS technique has been used increasingly as an important tool for analyzing the projects with uncertainties. In order to perform a MCS, the first step is to develop an analytical model. The second step is to generate a probability distribution from subjective or historical data for each variable (not defined) in the model. MCS calculates the outcome of the project by using the marginal distribution of all the parameters appearing in the NPV equation (Degarmo, et al., 1997).

2.4 Real *Option*

A financial model for valuing options was described by Black and Scholes (1973).Since then, puts and calls contracts began to be developed. These contracts give their owners the right, but not the obligation, to sell or buy a specified number of shares or a quantity of a commodity such as gold, copper, oil at or before a specified date. If the option is exercised only on the expiration date specified in the option contract, this option is called a European. If it takes place any time, it is called an American option (Black and Scholes, 1973).

It is easier to evaluate a European option than an American one because while the European option can only be exercised on a specific date, the American option can be exercised at any time up to the maturity date (Topal, 2008).

An option valuation technique is mainly based on the flexibility of the project. The more flexible the project is, the more valuable it is, because it allows the owner to respond to future events in ways that will increase the value of the firm. Option valuation gives extra value to the project because of flexibility (Figure 1) (Topal, 2008).

Keswani and Shackleton (2006) presented that the value of the projects can increase dramatically with increasing degrees of future managerial flexibility. In the example case, the expected NPV of the project increase from $1000 to $5079 with increased managerial flexibility using real option analysis (Topal, 2008).

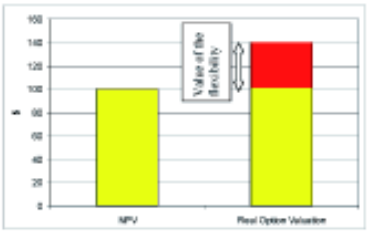

Figure1- The additional value of flexibility

3 DECISION MAKING METHODS

3.1Analytic Hierarchy Process (AHP)

The AHP pioneered in 1971 by Saaty is a widespread decision-making analysis tool for modeling unstructured problems in areas such as political, economic, social, and management sciences (Saaty, 2008, Mahmoodzadeh et al., 2007).

The AHP method is based on three principles: first, structure of the model; second, comparative judgment of the alternatives and the criteria; third, synthesis of the priorities (Mahmoodzadeh et al., 2007).

3.2Fuzzy Set Theory

To deal with vagueness of human thought, Zadeh first introduced the fuzzy set theory, which was oriented to the rationality of uncertainty due to imprecision or vagueness (Zadeh, 1965). A major contribution of fuzzy set theory is its capability of representing indistinct data. The theory also allows mathematical operators and programming to apply into the fuzzy domain. A fuzzy set is a class of objects with a continuum of grades of membership. Such a set is characterized by a membership (characteristic) function, which assigns to each object a grade of membership ranging between zero and one. A tilde "~" will be placed above a symbol if the symbol represents a fuzzy set (Mahmoodzadeh et al., 2007).

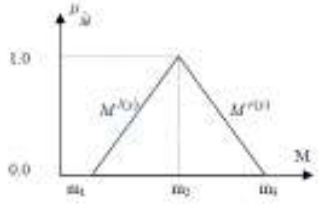

Figure 2- A triangular fuzzy number

3.3 Fuzzy AHP

Though the purpose of AHP is to capture the expert's knowledge, the conventional AHP still cannot reflect the human thinking style. Therefore, Fuzzy AHP, a fuzzy extension of AHP, was developed to solve the hierarchical fuzzy problems (Kahraman et al., 2003).

In the Fuzzy-AHP procedure, the pair wise comparisons in the judgment matrix are fuzzy numbers that are modified by the designer's emphasis (Kahraman et al., 2003).

According to the method of Chang's, extent analysis, each object is taken and extent analysis for each goal is performed respectively Chang, 1992). Therefore, m extent analysis values for each object can be obtained, with the following signs (Mahmoodzadeh et al., 2007):

$$M^{1}gi, M^{1}gi, \ldots, M^{m}gi \qquad i=1,2,\ldots,n \qquad (1)$$

Step 1:

The value of fuzzy synthetic extent with respect to the i^{th} object is defined as:

$$S_k = \sum_{j=1}^{n} M_{kl} \times \left[\sum_{i=1}^{m}\sum_{j=1}^{n} M_{ij}\right]^{-1} \qquad (2)$$

Step2:

As $M_1= (l_1, m_1, u_1)$ and $M_2= (l_2, m_2, u_2)$ are two triangular fuzzy numbers, the degree of possibility of $M_2= (l_2,m_2,u_2) \geq M_1= (l_1,m_1, u_1)$ is defined as:

$$\begin{aligned} &V(M_1 \geq M_2)=1, && M_1 \geq M_2 \\ &V(M_1 \geq M_2)=0, && M_1 \leq M_2 \\ &V(M_1 \geq M_2)=\text{hgt}\,(M_1 \geq M_2), && \text{else} \end{aligned} \qquad (3)$$

That:

$$\text{hgt}(M_1 \geq M_2) = \frac{u_1 - l_2}{(u_1 - l_2) + (m_2 - m_1)} \qquad (4)$$

Step3:

The degree possibility for a convex fuzzy number to be greater than k convex fuzzy M_i (i=1, 2, k) numbers can be defined by:

$$\begin{aligned} &V(M \geq M_1, M_2, \ldots, M_k) \\ &= [(M \geq M_1) \text{ and } (M \geq M_2) \ldots \text{ and } (M \geq M_k)] \\ &= \min V(M \geq Mi) \qquad i=1,2,\ldots,k \end{aligned} \qquad (5)$$

Then the weight vector is given by:

$$w'(xi) = \min\{V(S_i \geq S_k\}, k = 1,2,\dots n \quad k \neq i \qquad (6)$$

$$w' = [w'(c_1), w'(c_2), \dots, w'(c_n)]^T \qquad (7)$$

Where A_i= (i =1,2,...,n) are n elements.

Step4:

Via normalization, the normalized weight vectors are:

$$w_i = \frac{w'(c_i)}{\sum_{i=1}^{K} w'(c_i)} \qquad (8)$$

$$W = [w_1, w_2, w_3 \dots . w_n] \qquad (9)$$

Where W is a non-fuzzy number.

3.4 Topsis

The general Topsis processes with six activities are listed below (Olson, 2004):
-Establishing a decision matrix for ranking.
-Calculating the normalized decision matrix.
-Measuring the weighted normalized decision matrix.
- Determination of the positive-ideal solution (PIS) and negative-ideal solution (NIS) (ChiSun, 2010).
- Calculating the separation measures.
- Calculate the relative closeness to the idea solution and ranking the alternatives in descending order.

Stage 1:

Establishing a decision matrix for ranking: The structure of the matrix can be expressed as follows:

$$D = \begin{array}{c} \\ A1 \\ A2 \\ \vdots \\ An \end{array} \begin{array}{c} \begin{array}{cccc} F1 & F2 & \dots & Fn \end{array} \\ \begin{bmatrix} f11 & f12 \dots . & & f1n \\ f21 & f22 \dots . & & f2n \\ \vdots & \vdots & & \vdots \\ fm1 & fm2 & \dots & fmn \end{bmatrix} \end{array} \qquad (10)$$

Where A_i denotes the alternatives i,
i = 1, . . . ,m.

F_j represents j^{th} attribute or criterion,
j = 1,…, n,
The formula calculates the separation measures, using the m dimensional related to i^{th} alternative.

Stage 2:

The normalized value r_{ij} is calculated as:

$$r_{ij} = \frac{f_{ij}}{\sum_{j=1}^{n} f_{ij}^2} \qquad (11)$$

Where j = 1. . . n; i = 1, . . . ,m.

Stage 3:

Measuring the weighted normalized decision matrix:

By multiplying the normalized decisions with its associated weights, the weighted normalized value V_{ij} is calculated as:

$$\tilde{v}_{ij} = \tilde{r}_{ij}(\cdot)\tilde{w}_{ij} \qquad (12)$$

Where w_j represents the weight of the j^{th} criterion.

Stage 4:

Determination of the PIS and NIS respectively:

$$V^- = \{V_1^-, \dots, V_n^-\} = \{(Min\, V_{ij} | j \in J), (Max\, V_{ij} | j \in J')\}$$

$$V^+ = \{V_1^+, \dots, V_n^+\} = \{(Max\, V_{ij} | j \in J), (Min\, V_{ij} | j \in J')\}$$

Where J is associated with the positive criteria and J` is associated with the Negative criteria.

Stage 5:

Calculating the separation measures by using the m dimensional Euclidean distance:

The separation measure d_i of each alternative from the PIS is given as:

$$d_i^+ = \sqrt{\sum_{j=1}^{n} (V_{ij} - V_j^+)^2}$$

Similarly, the separation measure of each alternative from the NIS is as follows:

$$d_i^- = \sqrt{\sum_{j=1}^{n} (V_{ij} - V_j^-)^2}$$

Stage 6:

Calculate the relative closeness to the idea solution and ranking the alternatives in descending order:

The relative closeness of the alternative A_i with respect to PIS, V^+, can be expressed as:

$$CL_i^* = \frac{d_i^-}{d_i^- + d_i^+}$$

Where the index value of CL_i^* lies between 0 and 1.

3.5 Fuzzy Topsis

The method is based on the concept that the chosen alternative should have the shortest distance from the positive-ideal solution. The longest distance from the negative-ideal solution TOPSIS defines an index called similarity to the positive-ideal solution and the remoteness from the negative-ideal solution. Then, the method chooses an alternative with the maximum similarity to the positive-ideal solution (Hwang and Yoon 1981).

The mathematics concept of the Fuzzy TOPSIS is reviewed briefly as follows:

Step 1: Forming decision-makers committee:
In this committee there are K decision-makers. Decision makers can be represented by a linguistic term.

Step2: Evaluation of the criteria:

The criteria are evaluated as in table 2:

Table2- Linguistic scales

Very Poor(VP)	(0,0, 2)
Poor(P)	(1, 2, 3)
Medium Poor(M)	(2, 3.5, 5)
Fair(F)	(4, 5, 6)
Medium Good(MG)	(5, 6.5, 8)
Good(G)	(7, 8, 9)
Very Good(VG)	(8,10,10)

Step 3: Normalizing the fuzzy-decision matrix:
The normalized fuzzy-decision matrix is measured as the following formula:

$$\widetilde{\mathbf{R}} = [\widetilde{r}_{ij}]_{m\times n} \qquad i=1,2,\ldots,m \quad j=1,2,\ldots,n$$

The normalization process can be performed by the following formula:

$$\widetilde{r}_{ij} = \left(\frac{a_j^-}{c_{ij}}, \frac{a_j^-}{b_{ij}}, \frac{a_j^-}{a_{ij}}\right), \quad j \in C$$

$$\widetilde{r}_{ij} = \left(\frac{a_{ij}}{c_j^*}, \frac{b_{ij}}{c_j^*}, \frac{c_{ij}}{c_j^*}\right), \quad j \in B$$

B: Profit criteria set; C: Loss criteria set

Step 4: Determining the fuzzy positive-ideal solution (FPIS) and fuzzy negative-ideal solution (FNIS):

According to the weighted normalized fuzzy-decision matrix, the elements $\sim v_{ij}$ are normalized positive and their ranges belong to the closed interval [0, 1]. Then, the FPIS A^+ (the aspiration levels) and FNIS A^- (the worst levels) are defined as the following formula: (Hwang and Yoon 1981).

$$A^+ = (\widetilde{v}_1^*, \widetilde{v}_2^*, \ldots, \widetilde{v}_n^*),$$
$$A^- = (\widetilde{v}_1^-, \widetilde{v}_2^-, \ldots, \widetilde{v}_n^-),$$

Step 5: Calculating the distance of each alternative from FPIS and FNIS:

The distances of each alternative from A^+ and A^- can be calculated by the area compensation method, as follows:

$$d_i^* = \sum_{j=1}^{n} d(\widetilde{v}_{ij}, \widetilde{v}_j^*), \quad i = 1, \ldots, m,$$

$$d_i^- = \sum_{j=1}^{n} d(\widetilde{v}_{ij}, \widetilde{v}_j^-), \quad i = 1, \ldots, m,$$

Step6: Obtaining the closeness coefficients (relative gaps-degree) and improving the alternatives for achieving aspiration levels in each criterion.

$$CC_i = \frac{d_i^-}{d_i^* + d_i^-}, \qquad A_i (i = 1, \ldots, m)$$

3 Selection of an optimum evaluation technique

The general stages of selecting an optimum evaluation technique are as follow:

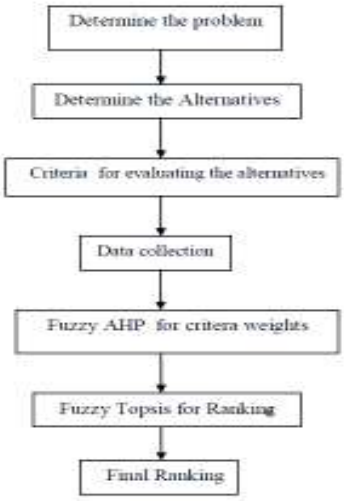

Figure3-The General Stage of Method

Step 1: Fuzzy AHP

1) Evaluating criteria matrix formed by decision-makers committee:

	C_1	C_2	C_3	C_4
C_1	1	0.14	0.5	2
C_2	7	3	1	9
C_3	2	0.33	1	3
C_4	0.5	0.11	0.33	1

C_1: Complexity of the mehod,C_2: Handling the time value of money, C_3: flexibility, C_4 :Knowledge about the input variables In the projects.

2) Determining the Fuzzy matrix

	C_1	C_2	C_3	C_4
A_1	(1,1,1)	(0.14,0.17,0.2)	(0.11,0.23,3)	(0.11,1.32,3)
A_2	(5,6,7)	(1,1,1)	(0.17,2.4,9)	(0.25,5.17,9)
A_3	(2,6,9)	(0.17,0.94,3)	(1,1,1)	(0.33,3.08,8)
A_4	(0.33,2.72,9)	(0.11,1.40,8)	(0.13,0.7375,3)	(1,1,1)

A1: NPV, A2: DT, A3: RO, A4: MCS

3) Calculating the value of fuzzy synthetic extent

S1	0.020	0.080	0.366
S2	0.092	0.426	1.790
S3	0.050	0.323	1.634
S4	0.023	0.171	1.634

S: value of *fuzzy synthetic* exten

4) Measuring the degree of possibility

$V(S_1 \geq S_2) = 0.44, V(S_1 \geq S_3) = 0.57, V(S_1 \geq S_4) = 0.79$

$V(S_2 \geq S_1) = 1, V(S_2 \geq S_3) = 1, V(S_2 \geq S_4) = 1$

$V(S_3 \geq S_1) = 1, V(S_3 \geq S_2) = 0.937, V(S_3 \geq S_4) = 1,$

$V(S_4 \geq S_1) = 1, V(S_4 \geq S_2) = 0.86, V(S_4 \geq S_3) = 0.91$

5) Calculating the possibility degree for a convex fuzzy number

$V(S_1 \geq S_2, S_3, S_4) = Min(0.44,0.57,0.79) = 0.44$, $V(S_2 \geq S_1, S_3, S_4) = Min(1,1,1) = 1$
$V(S_3 \geq S_1, S_2, S_4) = Min(1,0.937,1) = 0.937$, $V(S_4 \geq S_1, S_2, S_3) = Min(1,0.86,0.91) = 0.86$

$W' = (0.44,1,0.937,0.86)^T$
$W = (0.136, 0.309, 0.289, 0.266)$

Step2: The alternatives ranking with Fuzzy Topsis method

1) Fuzzy matrix

	C_1	C_2	C_3	C_4
A_1	(0.4,0.8,2.4)	(1,1.85,3.3)	(0.4,0.8,2.4)	(7.4,8.8,9.4)
A_2	(2.1,3.35,4.6)	(0.7,1.35,2.89)	(3,4.25,5.5)	(3.4,4.7,6)
A_3	(5.9,7.1,8.3)	(5.6,6.8,8)	(3.3,4.55,5.8)	(4.5,5.75,7)
A_4	(7.3,8.6,9.3)	(2.2,3.35,4.5)	(7.6,9.2,9.6)	(0.4,0.8,2.4)

2) Normal matrix

	C_1	C_2	C_3	C_4
A_1	(0.167,0.5,1)	(0.125,0.231,0.412)	(0.042,0.083,0.25)	(0.787,0.936,1)
A_2	(0.087,0.119,0.19)	(0.087,0.169,0.361)	(0.312,0.443,0.573)	(0.362, 0.5,0.638)
A_3	(0.048,0.056,0.068)	(0.7,0.85,1)	(0.344,0.474,0.604)	(0.479,0.611,0.745)
A_4	(0.043,0.046,0.055)	(0.275,0.419,0.562)	(0.792,0.958,1)	(0.042,0.085,0.255)

3) Weighting the normal matrix

	C_1	C_2	C_3	C_4
A_1	(0.023,0.068,0.136)	(0.039,0.071,0.127)	(0.012,0.024,0.072)	(0.209,0.249,0.266)
A_2	(0.012,0.016,0.026)	(0.027,0.052,0.112)	(0.09,0.128,0.166)	(0.096, 0.133,0170)
A_3	(0.007,0.008,0.009)	(0.216,0.263,0.309)	(0.099,0.137,0.175)	(0.127,0. 163,0.198)
A_4	(0.006,0.006,0.007)	(0.085,0.129,0.174)	(0.229,0.277,0.289)	(0.011,0.023,0.068)

4) Determining the FPIS and FNIS

V_j^+=[(0.006,0.006,0.007),(0.216,0.263,0.309),(0.229,0.277,0.289),(0.209,0.249,0.266)]

V_j-= [(0.023,0.068,0.136),(0.027,0.052,0.112),(0.012,0.024,0.072),(0.011,0.023,0.068)]

5) Calculating the distance of each alternative from FPIS and FNIS

d_1^+= 0.49587, d_2^+= 0.45803 , d_3^+= 0.2089, d_4^+=0.34121
d_1^-= 0.223856 , d_2^- =0.26254 , d_3^- = 0.511377, d_4^-= 0.378637

The closeness coefficients are:

Cc_i (NPV) = 0.31103 , Cc_i (DT) = 0.364348
CC_I (RO) = 0.710002 , CC_I (MCS) = 0.525995

4 CONCLUSIONS

Selecting the appropriate method for valuating and evaluating the projects is important in mining and industries. There are different criteria which affect the selection of valuation methods. Therefore selecting an optimum technique is a complicated multi-criteria process. In this study with the multiple-criteria techniques, fuzzy-AHP and Fuzzy Topsis, an appropriated method was selected among the four projects valuation methods. i.e. Net present value, Decision tree, Monte Carlo simulation and Real option. The result of this study shows that the RO is the superior method and the MCS, DT and NPV stand in the next priorities respectively.

REFERENCES

Markowski, A.S. and Mannan, M.S. (2009) Fuzzy logic for piping risk assessment (pfLOPA). *Journal* of Loss Prevention in the Process Industries 22(6): 921–927.

Alidoosti A., Yazdani M., Fouladgar M. and Basiri M. H. (2012), Risk assessment of critical asset using fuzzy inference system, Risk Management 14, 77–91. doi:10.1057/rm.2011.19

Bhappu, R.R. and Guzman, J. (1995) 'Mineral investment decision making', Engineering and Mining Journal, pp.36–38.

Clemen, R.T. (1995) *Making Hard Decisions*, Fugue School of Business Duke University, Duxbury Press, CA, USA.

Moore, T., Jesse, C. and Kittler, R. (2001) 'An overview and evaluation of decision tree methodology', *ASA Quality and Productivity Conference*, Austin, Texas, USA, http://www.

Amstatonline.org/sections/qp/qpr/QPRC2001/contri buted/Moore.pdf.

Degarmo, P.E., Sullivan, G.W., Bontadelli, J.A. and Wicks, E.M. (1997) *Engineering Economy*, 10th ed., Prentice–Hall, New Jersey, pp.546–563.

Black, F. and Scholes, M. (1973) 'The pricing of options and corporate liabilities', *Journal of Political Economy*, pp.637–654.

Topal, E. (2008), Evaluation of a mining project using Discounted Cash Flow analysis, Decision Tree analysis, Monte Carlo Simulation and Real Options using an example. Int. J. Mining and Mineral Engineering, Vol. 1, No. 1.

Saaty,TL. (2008), The analytic hierarchy process . McGrraw-Hill, Mineral Engineering, Vol. 1, No. 1.

Mahmoodzadeh, S., Shahrabi J., Pariazar M., and Zaeri M. S. (2007), Project Selection by Using Fuzzy AHP and TOPSIS Technique. World Academy of Science, Engineering and Technology 30.

Zadeh LA.(1965), Fuzzy sets. Inf Control 8:338-353,.

Kahraman C., Cebeci U., Ulukan Z.(2003), "Multi-criteria supplier selection using fuzzy AHP", Logistic Information Management. Volume 16. Number 6. pp. 382-394.

D. Y. Chang,d, 1992, "Extent analysis and synthetic decision", Optimization Techniques and Application, vol (1) . p. 352.

D. L. Olson, 2004 "Comparison of weights in TOPSIS models", Mathematical and Computer Modeling, 40, (7) 21-727.

ChiSun Ch. A performance evaluation model by integrating fuzzy AHP and fuzzy TOPSIS methods.Expert Systems with Applications 37 ,2010; 7745–7754

Hwang, C.-L., & Yoon, K. (1981). Multiple attribute decision making: methods and applications. In Lecture notes in economics and mathematical systems. Now York: Springer.

Simulation and Optimization of Heap Leaching for Low Grade Copper Oxide Ore

D. Moradkhani, R. Safari
University of Zanjan, Zanjan, Iran

M. Rajaie Najafabadi
Amirkabir University of Technology, Tehran, Iran

B. Sedaghat
R&D Center, Research & Engineering Co. for Non-ferrous Metals (RECo), Zanjan, Iran

ABSTRACT Because of the high value and application of copper, the extraction of this metal from primary sources has always been emphasized. In this study, the simulation and optimization of heap leaching process of low grade copper oxide ore using Design Expert 7 and Minitab statistical software was investigated.

In order to simulate the heap leaching, the columns were used and also for optimizing the number of samples for column leaching test, Taguchi method was applied. The orthogonal array L9 (3^4) comprising four parameters at three levels was chosen. Under optimum conditions of acid concentration: 100 g/l, particle size: +10-15 mm, flow rate: 2.5 cc/min, time: 3 days; the recovery and concentration of copper was obtained 97.03% and 5.92 g/l, respectively. Using analysis of variance showed acid concentration as the effective parameter for copper recovery.

Keywords: Copper, Heap leaching, Optimization, Taguchi method, Design of experiment.

1 INTRODUCTION

Generally copper ores are classified into sulfide and oxide ores, whereas oxide ores are a naturally oxidation product of sulfide ores. Therefore usually oxide and sulfide copper ores are in adjoining sites (Bartlett, 1998). Whereas sulfide copper ores are mainly treated by pyrometallurgical processes; oxide ores are treated by hydrometallurgical processes. Leaching of copper from ores has focused mainly on oxide ore types (Woods, 2010). Oxide ore cannot be treated by pyrometallurgical processes because they would be very noncommercial (Sheffer & Evans, 1968).

Heap leaching and in-situ leaching have been employed in the mineral industry for many years. In the mid-sixteenth century, mines in Hungary recycled copper-bearing solutions through waste heaps to recover copper (Hiskey, 1985). In Spain, miners circulated acid solutions through large heaps of oxide copper ore on the banks of Rio Tinto around 1752 (Dorey et al., 1988).

As the price of copper climbed to a peak of US $1.40 per pound on the London Metals Exchange in 1995, the mining industry continued to embrace heap leaching as a method to both develop lower grade resources and thereby expand production capacity, and as a way to bring projects on line in a fraction of the historic time (Breitenbach & Smith, 2006). Approximately 20% of worlds copper productions are gained by hydrometallurgical leaching processes, mainly by heap leaching with sulfuric acid

and subsequent solvent extraction (SX) and electro winning (EW) treatment.

Typical ore heaps in heap leaching are 4-12 m high and have a base area of several thousand square meters and are made up of 100,000 - 500,000 tons of ore. Depending on the type of ore leaching of these heaps, it is require several months. During this time, approximately 70 - 75% of the leachable copper compounds are dissolved and extracted from the ore (Bartlett 1998, Thiel & Smith 2003). An improvement of the leaching conditions must aim on shorter leaching times as well as on a higher copper extraction rate, thus to an increase in copper productivity and lower costs per ton of copper.

Although a number of experimental studies have been carried out which have allowed better understanding of the phenomenon and the operation of heap leaching (Wu et al. 2007, Yorio et al. 2006, Petersen & Dixon 2007, Leahy et al. 2007), few studies have been carried out with the objective of optimizing the process. Most of the studies either experimentally or through the use of models, have done from the technical perspective, for example analyzing the effect of other operations, such as agglomeration, on the optimization of recovery (Bartlett, 1997).

The determination of the optimum condition of leaching parameters is one of the main concerns in the design of heap leaching process (Koleinin & Khodadadi, 2007). The optimum conditions for the dissolution of malachite leaching, using Taguchi experimental design, and the optimum leaching conditions were determined (Ata et al., 2010).

Copper oxide minerals containing copper in the divalent state, such as azurite [$Cu_3(OH)_2(CO_3)_2$], malachite [$Cu_2(OH)_2CO_3$], tenorite (CuO) and chrysocolla ($CuSiO_3.2H_2O$), are completely soluble either in acidic or alkaline medium at room temperature (Ata et al. 2010, Barlett 1992, Oudenne & Olson 1983).

Parameters such as temperature, grading size, permeability, acid concentration, and discharge of acid have great effect on the leaching process which should be optimized. The above mentioned parameters are dependent on the type of minerals; mineral impurities which can be optimized based on leaching experiment for the specific mine (Wadsworth & Miller 1979, Ekmekyapar & Oya 2003).

The aim of this study is to investigate the optimum conditions for heap leaching of low grade copper oxide ore with special attention to the effects of acid concentration, flow rate, time, and size of minerals on leach ability of copper by simulating the heaps through special columns.

2 EXPERIMENTAL WORK

2.1 Materials

Oxidized copper sample for the heap leaching study was obtained from Chodarchaie, Zanjan, Iran. After drying, the sample was ground and homogenized. The chemical analysis was carried out by a Perkin-Elmer AA300 model atomic absorption spectrophotometer. Table 1 shows the chemical analysis of the samples used in this experiment.

Table 1. Chemical composition of samples used in the experiment (Wt. %)

Component	Cu	Fe	Si	Al	K
Wt. (%) for particle size: +1-5	1.06	3.11	31.67	14.10	3.77
Wt. (%) for particle size: +5-10	1.13	2.91	30.51	12.80	3.47
Wt. (%) for particle size: +10-15	1.19	2.83	34.45	13.79	3.58

The X-ray diffraction analysis (Fig.1) of the ore revealed the presence of the mineralogical species. Mineralogy XRD analysis indicated the main phase as quartz, the minor phase as malachite and the trace phase as muscovite and calcite.

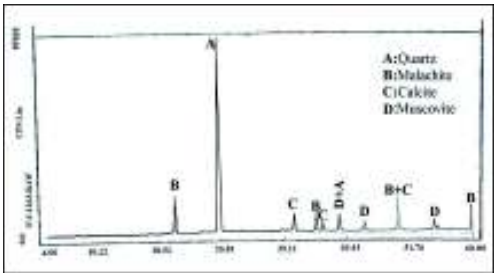

Figure 1. X-ray diffraction analysis of the ore

2.2 Procedure and Equipment

Column leaching was chosen for a simulation of natural situation. This test consisted of 9 cylindrical glasses with a diameter of 6 cm and height of 50 cm. The columns were filled of 1400 grams dry soil sample; and 2-4 cm layer of washed and dried sand with a Whatman paper was put on the top of the ore in order to steady distribution of input solution.

A supply system was employed for adding acid solution at the top of column and outflow system was made for the leach out solution. Process variables were particle size, acid concentration of input solution, rate of input solution and time. The value of the parameters was chosen by considering natural situation. All of tests were done for 9 days and sampling of the leachate was performed on every day. Filtration was made after each leaching experiment. The solutions were analyzed for Copper and Iron and the recovery of each test was calculated. The picture of columns employed in this study is shown in Figure 2.

Figure 2. Columns used for leaching tests

2.3 Taguchi Method

For experimental design and determining the important factors which affect the leach ability of minerals, the Taguchi method was used. Primitive studies indicated that four parameters including: acid concentration of input solution, flow rate, particle size, and time were effective.

Thus, to investigate the effects of the above mentioned parameters in heap leaching of copper and iron, three levels of them were selected. Recovery of copper and iron were selected as responses of this process. Orthogonal array L9, which clarifies 4 parameters at 3 levels, was chosen to carry out the tests. Table 2 shows the process variables for all the tests.

Table 2. Experimental parameters and their levels

Parameters	Level 1	Level 2	Level 3
Acid conc. (g/l)	40	70	100
Flow rate (cc/min)	2.5	5	7.5
Ore particle size (mm)	+1-5	+5-10	+10-15
Time (day)	3	6	9

The orthogonal array of experimental design method was chosen to determine experimental plan. Orthogonal array (OA), L9 (3^4), which denotes four parameters each with three levels, was chosen since it is the most suitable for the conditions being investigated. The performance statistics were chosen as the optimization criterion. The order of experiments was obtained by inserting parameters into columns of orthogonal array, L9(3^4), chosen as the experimental plan, but the order of experiments was made random in order to avoid noise sources which had not been considered initially and which could take place during an experiment and affect results in a negative way.

The interactive effect of parameters was not taken into consideration while some preliminary tests showed that they could be neglected. The validity of this assumption was checked by confirmation experiments conducted at the optimum conditions.

Table 3 is an L9 orthogonal array, a table of integers whose column elements represent the low, medium, and high levels of the column factors. Each row of orthogonal array represents a run, which is a specific set of factor levels to be tested (Copur, 2001).

One of the advantages of Taguchi method over the conventional experimental design methods, in addition to keeping the experimental cost at minimum level, is that it minimizes the variability around the target when bringing the performance to the target value. Another advantage is that optimum working conditions determined from the laboratory work can also be reproduced in the real production environment.

Table 3. Experimental procedure

RUN	Acid conc. (g/l)	Flow rate (cc/min)	Ore particle size (mm)	Time (day)
1	70	7.5	+1-5	6
2	70	2.5	+5-10	9
3	40	5	+5-10	6
4	100	2.5	+10-15	6
5	100	5	+1-5	9
6	40	2.5	+1-5	3
7	40	7.5	+10-15	9
8	70	5	+10-15	3
9	100	7.5	+5-10	3

Taguchi method recommends the use of the loss function to measure the performance characteristics deviating from the desired value (Roy, 1995). The value of the loss function is further transformed into a signal-to-noise (SN) ratio. Usually, there are three categories of performance characteristics in the analysis of the SN ratio: that is, the lower, the better; the higher, the better and the nominal, the better. The SN ratio for each level of the process parameters is computed based on the SN analysis.

Using of the SN ratio of the results, instead of the average values, introduces some minor changes in the analysis as follows:

• Degrees of freedom of the entire experiments are reduced: DOF with SN ratio = number of trial conditions−1 (i.e., number of repetitions is reduced to 1).

• SN ratio must be converted back into meaningful terms.

When the SN ratio is used, the results of the analysis such as estimated performance from the main effects or confidence intervals are expressed in terms of SN. To express the analysis in terms of experimental results, the ratio must be converted back into the original units of measurements.

3 RESULTS AND DISCUSSION

In this research to heap leaching of low grade copper ore, Taguchi technique was used. Orthogonal array L9, which clarifies 4 parameters at 3 levels were chosen to carry out the tests. Parameters studied included: acid concentration of input solution, particle size, flow rate, and time. Recovery was calculated for copper and iron and daily outflow was investigated with respect to volume of solution and copper content. The target was to maximize dissolution of copper, while the dissolution of iron is minimal. Design Expert 7 and Minitab statistical software for the analysis of the data were used.

3.1 Investigation of Effective Parameters on the Copper Recovery

The graphs in Figure 3 show the results of the copper recovery. The effect of acid concentration on copper recovery is shown in Figure 3a. The results indicated that acid concentration is an important parameter for copper recovery. With increasing acid concentration from 40 to 70 g/l, copper recovery increase too; whereas recovery of copper decreased from 70-100 g/l. This behavior was due to increasing H^+ concentration which is an important factor in extracting copper from the ore, but when sulfuric acid increased to more than a certain concentration (70 g/l), other materials also leached and the recovery decreased.

As shown in Figure 3b, three flow rates of 2.5, 5, and 7.5 cc/min examined. An inverse

relation exists between the copper recovery and the flow rate. As demonstrated in Figure 3b, with increasing flow rate from 2.5 to 7.5 cc/min, recovery of copper is reduced. Since increasing the flow rate cause to reduce the contact time between acid solution and ore particles, then copper extraction reduced and the recovery decreased.

The effect of particle size was examined in three levels of +1-5, +5-10, and +10-15 mm. According to Figure 3c, minimum recovery of copper was at +5-10 mm. This is due to fine particles.

Copper recoveries for, 3, 6 and 9 days of heap leaching by H2SO4 solution are given in Figure 3d. Results indicated that the copper recovery increase with increasing heap leaching times. Increasing of time resulted in more copper extraction by acid solution, due to more contact time between acid solution and ore particles.

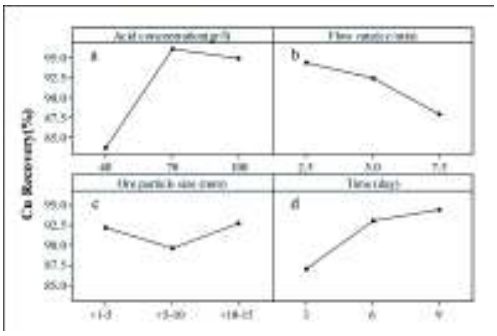

Figure 3. Effect of parameters on the recovery of copper

3.2 Investigation of Effective Parameters on the Iron Recovery

The graph giving the result for the iron recovery is shown in Figure 4. The results (Figure 4a) indicated that acid concentration is an important parameter for iron recovery. Overall, the recovery of iron increases with increasing acid concentration because of high H^+ concentration. Figure 4b shows the effect of flow rate on the recovery of iron. According to this graph, increasing the flow rate up to 7.5 cc/min did not make a significant change in iron recovery. The effect of particle size on iron recovery is demonstrated in figure 4c which was almost insensitive. This means that particle size had no effect on iron recovery. Iron recoveries for, 3, 6 and 9 days of leaching by H_2SO_4 solution are given in Figure 4d. Iron recovery increases sharply when time increases from 3 days to 9 days. The minimum recovery of the iron in 3 days was 33.84%.

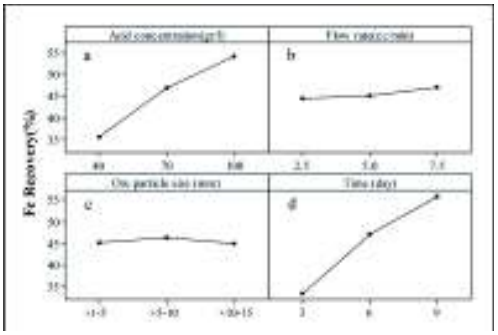

Figure 4. Effect of parameters on the recovery of iron

3.3 Contour Plot of Copper Recovery vs. Iron Recovery

Using Minitab 14, the influence of each parameter on the recovery of copper and iron was calculated which is shown in figure 5. Figure 5a shows the effect of acid concentration on the recovery of copper and iron. It can be seen that in the range 90 to 100 g/l, the maximum amount of copper is recovered. With increasing acid concentration from 90 to 100 g/l, the iron recovery increased from 50% to 60%. Since the pregnant leach solution (PLS) goes through solvent extraction process, the iron concentration is not important as copper concentration; so acid concentration of 100 g/l selected as the optimum level.

As you can see in figure 5b, the effect of flow rate parameter on the recovery of copper and iron is shown. The range of the color is dark green, with the highest recovery of the copper. By increasing the flow rate from 4 to 5cc/min, the iron recovery increased from 50% to 60%. It seems that 2.5 cc/min is suitable as optimum flow rate.

The particle size effect can be observed in figure 5c. Most copper is recovered in the coarse particles (+10-15 mm), which is equal to 97%. In this case, the recovery of iron will change between 55% and 65%.

Also figure 5d shows the effect of time on the recovery of copper and iron. It can be seen that in the range 6 to 9 days, the maximum amount of copper is recovered. With increasing time from 6 to 9 days, the iron recovery increased from 55% to 60%. It seems that 3 days is suitable as optimum time, because most of the copper (>85%) extracted with least iron recovery.

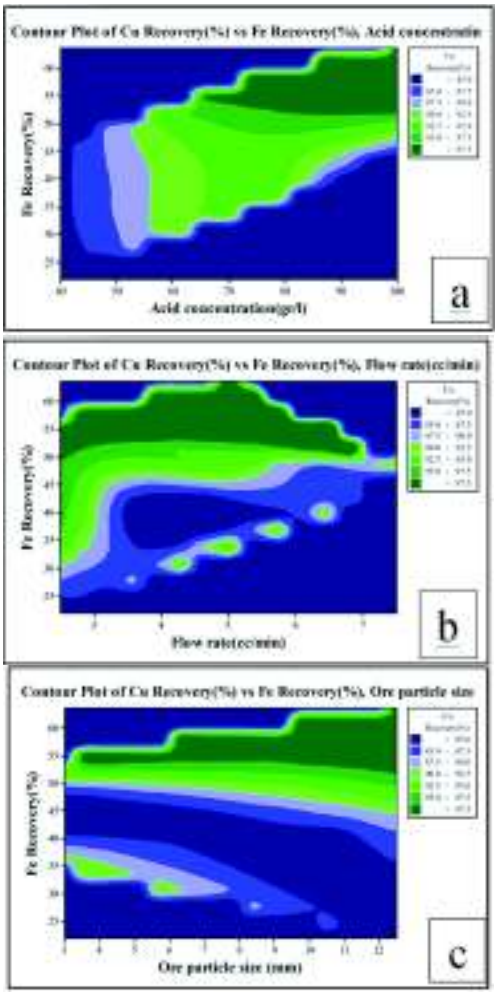

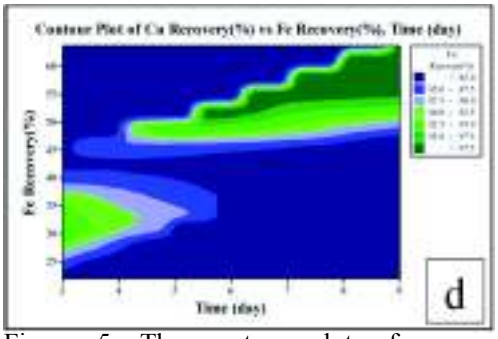

Figure 5. The contour plot of copper recovery predicted by statistical result

3.4 Analysis of Variance

Taguchi oriented practitioners often use analysis of variance (ANOVA) to determine the factors that influence the average response and signal-to-noise ratio. So the statistical analysis of variance (ANOVA) was performed to see whether the process parameters are statistically significant. The F-value for each parameter indicates which parameter has a significant effect on the leaching efficiency and is simply a ratio of the squared deviations to the mean of the squared error. Because of the change of the process parameter, usually the larger F-value has greater effect of the leaching efficiency. Optimal combination of the process parameters can be predicted using ANOVA analysis and performance characteristics.

3.4.1 Analysis of variance for copper recovery

The F-value for all factors is smaller than the extracted F-value from the table for 95% confidence level (F=23). This means that the variance of all factors is insignificant compared with the variance of error and none of them had meaningful effect on the responses. Since the F-value for acid concentration is more than other parameters and is near to the amount of extracted F-value from the table (F=23), it can be concluded that acid concentration had more effect than other parameters. Table 4 presents the statistical results for copper recovery.

Table 4. Statistical results for recovery of copper

Factors	Sum of Squares	df	Mean Square	F-Value	P-Value
Acid conc.	279.35	2	139.68	16.98	0.0556
Flow rate	68.02	2	32.01	3.89	0.2045
Particle size			Pooled		
Time	93.62	2	46.81	5.69	0.1495
Error	16.46	2	8.23	-	-
Total	453.45	8	-	-	-

Figure 6 shows the predicted values versus the actual values for recovery of copper. actual response values were measured for a particular run, and the predicted values were evaluated from the model and generated by using the approximating equations. As can be seen, the predicted value obtained was quite close to the actual values, indicating that the model developed was reasonable. The best way to visualize the influence of the independent variables on the response is to draw surface response plots of the model.

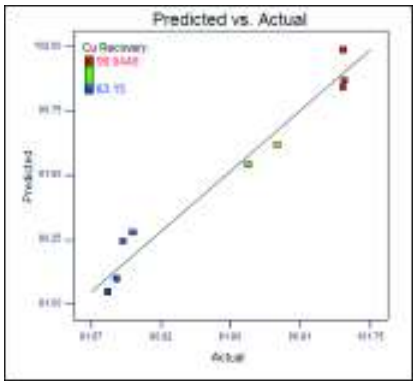

Figure 6. Predicted vs. actual recovery of copper

3.4.2 Analysis of variance for iron recovery

According to table 5, F-value for acid concentration and time parameters is greater than extracted F-value from the table for 95% confidence level (F=23). Therefore variation of these parameters has significant role on the performance of the process. Table 5 shows statistical results for iron recovery.

Table 5. Statistical results for recovery of iron

Factors	Sum of Squares	df	Mean Square	F-Value	P-Value
Acid conc.	538.71	2	269.36	165.76	0.006
Flow rate	10.62	2	5.31	3.27	0.234
Particle size			Pooled		
Time	774.67	2	387.33	238.37	0.004
Error	3.25	2	1.62	-	-
Total	1327.25	8	-	-	-

Figure 7 shows a satisfactory correlation between actual values and predicted ones. It could be seen that the predicted values obtained are quite close to the observed values, and the deviation between the actual and predicted ones is less. The fitted regression equation showed the fitting is good.

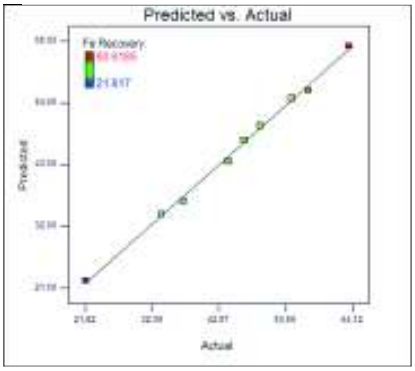

Figure 7. Linear correlation between actual and predicted values

3.5 Optimum Conditions

Finally, using these findings about influential parameters on the process, optimum working conditions could be predicted. The proposed optimum conditions are: Acid concentration on level three (100gr/l), flow rate on level one (2.5cc/min), Particle size on level three (+10-15mm), and time should be on level one (3 day). The recovery and concentration of copper predicted 96.62% and 5.72 gr/l respectively, using Design Expert 7 statistical software. Also, the optimal conditions proposed for iron were the recovery and concentration of 42.27% and 3.84 gr/l, respectively. To investigate the accessibility of this result, a

test on the optimum conditions was done. The experimental recovery and concentration of copper obtained 97.03% and 5.92gr/l, respectively.

3.6 Working Diagram

After optimizing the operational parameters in heap leaching, we proposed the working diagram. The process starts with the crushing of copper oxide ore. The ground material is collected in large heaps, which are sprayed with an acid solution to dissolve out the metal from the ore. The metal is transferred to the aqueous phase, called the pregnant leach solution (PLS). After the leaching stage, the solution contains impurities, which have to be removed. A simplified flow diagram of the process is shown in Figure 8.

The solvent extraction stage decreases the proportion of impurities and concentrates the solution. The metal ions are selectively removed from the aqueous PLS via the organic phase and pass back into the aqueous phase. The flow is divided between several parallel SX trains. Extraction and stripping, i.e. the transfer of metal ions into the organic phase and back into the aqueous phase are performed within the mixer-settlers. In the mixer, the organic and aqueous phases are brought into close contact with each other by dispersing the organic or aqueous phases into droplets, a few millimeters in size within another phase. After mixing, the two phases are separated in large settlers by gravity. To improve the overall efficiency of the transfer of metal from the aqueous solution, the solvent extraction process has internal recycling and some material is returned to the leaching stage.

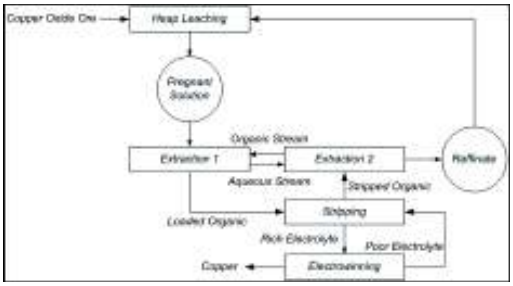

Figure 8. Flow diagram of an HLX–SX–EW process

4 CONCLUSION

In this study, the optimization of heap leaching for low grade copper oxide ore was investigated using Design Expert 7 and Minitab 14 statistical software. In this research to heap leaching of copper, Taguchi technique was used. Orthogonal array L9, which clarifies 4 parameters at 3 levels, was chosen to carry out the tests. Optimum leaching conditions from copper ore by acid solution was found as: acid concentration of 100 g/l, flow rate of 2.5 cc /min, particle size of +10-15 mm, and time of 3 days. Under these conditions, recovery of copper and iron obtained 97.03% and 42.27% respectively. In this study, statistical data analysis was performed and the most important parameter for dissolution of copper was acid concentration in range studied.

ACKNOWLEDGEMENTS

The authors are thankful to the Research and Engineering Co. for Non-Ferrous Metals for financial and technical support and the permission to publish this paper.

REFERENCES

Ata, S.; Çolak, Z.; Çopur M.; 2001. Determination of the optimum conditions for leaching of malachite ore in H_2SO_4 solutions, *Chemical Engineering & Technology*, 24, p 409– 413.

Bartlett, R. W., 1998. Solution mining - Leaching and Fluid recovery of materials, *2ed Gordon and Breach, Amsterdam*, ISBN 90-5699-633-9.

Bartlett, R. W., 1997. Metal extraction from ores by heap leaching, *Metallurgical and Materials Transactions B-Process Metallurgy and Materials Processing Science*, 28, 4, pp.529–545.

Barlett, R.W., 1992. Solution mining, leaching and fluid recovery of materials, *Gordon and Breach Science Publishers*, vol. 5, Philadelphia, p 76–107.

Breitenbach, A. J. and Smith, M. E., 2006. Overview of Geomembrane History in the Mining Industry, *Proceedings of the 8th Bi-annual meeting of the International Geosynthetics Society (8IGS)*, Japan.

Copur, M., 2001. Solubility of ZnS concentrates containing pyrite and chalcopyrite in HNO_3 solutions, *Chem. Biochem. Eng. Q.* 15 (4), p 181–184.

Dorey, R.; Van Zyl, D.; and Kiel, J.; 1988. Overview of heap leaching technology, in *Introduction to Evaluation, Design and Operation of Precious Metal Heap Leaching Projects*, edited by D. J. A. van Zyl, I. P. G. Hutchison and J. E. Kiel, Society of Mining Engineers Inc., pp3-22.

Ekmekyapar, A.; Oya, R., 2003. Dissolution kinetics of an oxidized copper ore in ammonium chloride solution, *Chemical and Biochemical Engineering Quarterly*, 17, p. 261–266.

Hiskey, J. B., 1985. Gold and silver extraction: The application of heap leaching cyanidation, Field Notes, *Arizona Bureau of Geology and Mineral Technology, Tucson*, vol. 15, no.(4), pp 1-5.

Koleini, S. M. J.; Khodadadi, A., 2007. A Study on Leaching Behaviour of Copper Oxide Ore of Sarcheshmeh Mine, *Mineral Processing Technology*, p 250.

Leahy, M. J.; Davidson, M. R.; Schwarz, M. P., 2007. A model for heap bioleaching of chalcocite with heat balance: mesophiles and moderate thermophiles. *Hydrometallurgy*, 85, 1, pp.24–41.

Oudenne, P.D.; Olson, F.A., 1983. Leaching kinetics of malachite in ammonium carbonate solutions, *Metallurgical Transactions*, 14, p 33–40.

Petersen, J.; Dixon, D. G., 2007. Modeling zinc heap bioleaching. *Hydrometallurgy*, 85, 2–4, pp.127–143.

Roy, R. K., 1995. A Primer on the Taguchi Method, Van Nostrand Reinhold, NewYork.

Sheffer, Herman W.; Evans, LaMar G.; 1968. Copper leaching practices in the Western United States, U.S. Dept. of the Interior, Bureau of Mines.

Thiel, R. and Smith, M.E., 2003. State of the practice review of heap leach pad design issues, *Proceedings of the 17th Annual GRI Conference Hot Topics in Geosynthetics – IV*, Las Vegas, NV, Geosynthetics Institute, Folsom, PA.

Wadsworth, M.E.; Miller, J.D., 1979. Rate processes of extractive metallurgy In: Hydrometallurgical processes (section 3), Sohn, H.E, and Wadsworth, M.E., Editors, Plenum Press, New York, pp.133–153.

Woods, R., 2010. Extracting metals from sulfide ores, School of Science, Griffith University, Nathan, Queensland 4111, Australia.

Wu, A. X.; Yin, S. H.; Yang, B. H.; Wang, J.; Qiu, G. Z.; 2007. Study on preferential flow in dump leaching of low-grade ores. *Hydrometallurgy*, 87, 3–4, pp.124–132.

Yorio, C.; Betancourt, E.; Vivas, R.; Rus, J., 2006. Ni, Co recovery study and Fe by acid leaching in columns. *Revista de Metalurgia*, 42, 1, pp.41–48.

Depth Factors of Limit Loads on Strip Footing in Clay

H. Yahia-Cherif, A. Mabrouki, D. Benmeddour, M. Mellas
Department of Civil and Hydraulic Engineering, University of Biskra, Algeria

ABSTRACT Current studies of bearing capacity for shallow foundations tend to rely on the hypothesis of an isolated footing located on the ground surface. In practice a footing is never placed at the ground surface; it is mostly embedded at depth *D* below the ground surface. This study focuses on a numerical analysis using the finite-difference code FLAC (Fast Lagrangian Analysis of Continua), to evaluate the bearing capacity of embedded, rough strip footings, subjected to centered vertical loads. The soil is modeled by an elasto-plastic model with a Mohr–Coulomb yield criterion. The results have been compared with those available in the literature.
Keywords: limit loads, strip footing, depth factors, vertical loads, elasto-plastic model.

1 INTRODUCTION

The bearing capacity of a vertically loaded shallow, rough, rigid, foundation in plane strain conditions is generally evaluated using the superposition equation proposed by Terzaghi (1943). Terzaghi defined a shallow foundation as a foundation where the width *B* is equal to or less than its depth *D*. Since Terzaghi's founding work, numerous experimental and numerical studies to estimate the ultimate bearing capacity of shallow foundations have been conducted.

Based on the solution methods, analytical solutions to the bearing capacity problem can be classified into the following categories:

- limit equilibrium method (e.g., Terzaghi, 1943; Meyerhof, 1951; Kumbhojkar, 1993);
- slip line method (e.g., Sokolovskii, 1960; Hansen, 1970; Bolton and Lau, 1993);
- limit analysis method (e.g., Chen, 1975; Michalowski, 1997; Lyamin et al., 2007);
- finite element or finite difference analyses (e.g., Frydman and Burd, 1997 ; Mabrouki et al., 2009; Loukidis and Salgado, 2009).

When the frictional soils is loaded with a uniform surcharge pressure (q), according to Terzaghi's equation, the bearing capacity of a shallow, strip footing can be obtained from the following equation:

$$q_u = \frac{1}{2}\gamma B N_\gamma + qN_q \quad (1)$$

Where γ = unit weight ; B is the width of the strip footing ; N_q and N_γ are the bearing capacity factors, represent the effects of surcharge q, and soil unit weight γ, respectively, these bearing capacity factors depending only on the internal friction angle φ of the soil under the footing. The simple bearing capacity factors in Equation (1) do not take into account the resistance of the soil above the foundation level which increases the bearing capacity. For clays, the bearing capacity equation has the following form:

$$q_u = c_u N_c d_c + q \quad (2)$$

where N_c is a bearing capacity factor; c_u is a representative undrained shear strength; $q = \gamma D$ is the surcharge at the footing base

level; γ is the wet unit weight of soil; D is the distance from the ground surface to the base of the foundation element; d_c is a depth factor. The depth factor, d_c, is defined as the ratio of the net bearing capacity, $(q_u - q)$, for a strip footing at depth D to that for an identical strip footing at the soil surface (for which $q = 0$).

Undrained vertical bearing capacity of shallowly embedded foundations has been addressed extensively, through empirical, analytical and numerical studies for a range of foundation soil interface conditions (Skempton, 1951; Meyerhof, 1951; Hansen, 1970; Salgado et al., 2004; Edwards et al., 2005). The depth factors available in the literature are given in Table 1.

Table 1. Depth factors commonly used for clays

Reference	depth factor
Meyerhof (1951)	d_c=1+0.2D/B
Skempton (1951)	d_c=1+0.2$D/B \leq$ 1.5 d_c=1.5 for $D/B >$ 2.5
Hansen (1970)	d_c=1+0.4D/B for $D/B <$ 1 d_c=1+0.4tan$^{-1}D/B$ B for $D/B \geq$ 1
Salgado et al. (2004)	d_c=1+0.27$\sqrt{D/B}$

The purpose of this paper is to report some recent numerical analysis to evaluate the ultimate bearing capacity of embedded strip footing in clay, a series of numerical computations using the finite-difference code FLAC (2005) are carried out to evaluate the bearing capacity factor, for embedded strip rough footing subjected to centered vertical loads and placed on clay.

2 PROBLEM PRESENTATION

In practice, the possible embedment of the footing is taken into account through the surcharge q, i.e. the footing is placed at the ground surface with surcharge $q = \gamma.D$ where D is the embedment. The present study is concerned with the undrained bearing capacity of strip rough footing of width B embedded at depth D in clay, as shown in Figure 1.

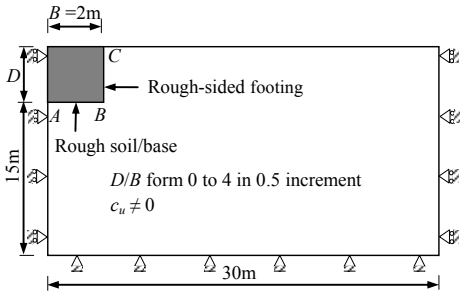

Figure 1. Problem geometry and boundary conditions

The bearing capacity is calculated according to the Equation (2). The D/B ratio was varied from 0 (footing at the ground surface) to 4.

The depth factors are defined as the ratio of the net bearing capacity for a strip footing at depth D to that of a strip footing at ground surface, which is calculated according to the following expression:

$$d_c = \frac{q_{net,strip\left(\frac{D}{B}\right)}}{q_{net,strip\left(\frac{D}{B}=0\right)}} \quad (3)$$

Where $q_{net}, strip(D/B)$ is the net bearing capacity for a strip footing at depth D; $q_{net}, strip(D/B = 0)$ is the net bearing capacity for a strip footing at ground surface.

3 NUMERICAL MODELLING PROCEDURE

In this study, the finite difference code FLAC (2005) was used to reach the limit loads (bearing capacity) for embedded strip rough footing in clay. FLAC is a two-dimensional explicit finite difference program for engineering mechanics computation. This program simulates the behavior of structures built of soil, rock or other materials that may undergo plastic flow when their yield limits are reached. Though FLAC was originally developed for geotechnical and mining engineers, the program offers a wide range of capabilities to solve complex problems in mechanics.

The embedded strip footing was rigid, rough and of width B = 2 m, subjected to a

centered vertical load and located on clay. Because of the symmetrical nature of the problem, only half of the model is considered in the computations. The displacement of the left and right vertical sides is constrained in the horizontal direction only. The base of the model is constrained in all directions (Fig.1).

The soil was considered to be a linearly elastic-perfectly plastic material, obeying Mohr–Coulomb criterion with $\varphi = 0$ (Tresca criterion). A constant undrained strength, cu with depth equal to 20 kPa, a Young's modulus, E = 14 MPa and a Poisson's ratio υ=0.49 were assigned to the soil.

The evaluation of the bearing capacity for the strip footing is based on subdividing the soil into a number of elements, to simulate the rigid footing, the vertical and horizontal displacements of nodes which discretize the strip footing are constrained in the vertical and horizontal directions. The loading of the rigid strip footing is simulated by imposing equal vertical velocities at the all nodes representing the footing. It is worthwhile noting that different mesh sizes with several vertical velocity values have been tested. In all cases, the mesh in the footing neighbourhood is refined to capture significant displacement gradients.

The rigid footing is connected to the soil via interface elements defined by Coulomb shear strength criterion following Equation (3).

$$F \le c.L + F_n \tan\delta \tag{3}$$

where F = maximum shear force, c = cohesion along the interface, L = effective contact length (Fig. 2), F_n = normal force, and δ = friction angle of interface surfaces. From the FLAC manual (2005), a good rule is that K_n and K_s be set to ten times the equivalent stiffness of the stiffest neighbouring element. The apparent stiffness (expressed in stress-per-distance units) of a zone in the normal direction used by the code is:

$$\max\left[\frac{\left(K+\frac{4}{3}G\right)}{\Delta z_{\min}}\right] \tag{4}$$

where K and G are the bulk and shear modulus, respectively; Δ_{zmin} is the smallest width of an adjoining element in the normal direction (FLAC, 2005).

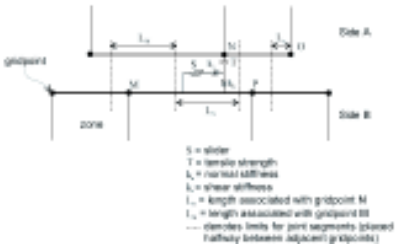

Figure 2. An interface represented by sides A and B, connected by shear (K_s) and normal (K_n) stiffness springs (FLAC, 2005)

The interface elements along the boundary ABC of foundation always represented a rough interface. They were assigned a cohesion c_u = 20 kPa, a normal stiffness K_n= 10^9 Pa/m, and a shear stiffness K_s =10^9 Pa/m.

The loading of the rigid rough footing is simulated by imposing equal vertical velocities at the nodes represented the footing. The progressive movement of the rigid footing induced by the horizontal velocity applied at the wall nodes is accompanied by the increase of the load in the soil. Finally, this load stabilizes for a value that indicates a limit load or bearing capacity.

4 NUMERICAL RESULTS

The bearing capacity factors d_cN_c obtained from the finite difference analysis in this study were compared with those obtained by theoretical results of (Salgado et al., 2004; Edwards et al., 2005). Figure 3 shows bearing capacity factors d_cN_c obtained by aforementioned authors as a function of the ratio D/B.

From the results of Figure 3, it is seen that the bearing capacity factors d_cN_c increases

substantially with increasing D/B. The values of d_cN_c for $D/B \leq 3$, obtained from the present study are in good agreement with the solutions reported by Edwards et al. (2005) (using the finite elements analysis). For $D/B>3$ the results predicted by the finite-difference solutions are greater than the finite elements results of Edwards et al. (2005). The lower-bound and upper bound results predicted by Salgado et al. (2004) deviate significantly from both the finite element and finite-difference solutions.

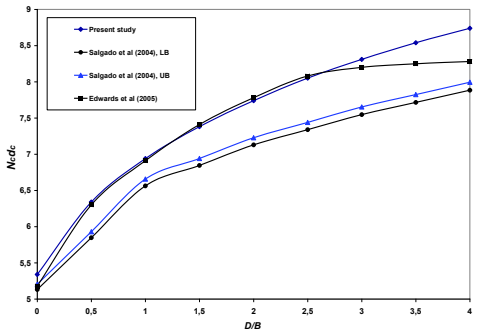

Figure 3. Comparison of present N_cd_c values with theoretical and numerical results

The finite difference results are also used to derive depth factors d_c. This is achieved by dividing the bearing capacities obtained for the footings at depth by that obtained for the surface footing. The results are presented in Figure 4. The values of d_c proposed by Skempton (1951), Meyerhof (1951), Hansen (1970) and Salgado et al. (2004) and found by finite element analysis of Edwards (2004) are also presented in this figure. The values of d_c obtained from the present study for $D/B \leq 2.5$ are in good agreement with Hansen (1970) results, $D/B > 2.5$, the depth factor obtained with FLAC are greater than those obtained by Hansen (1970).

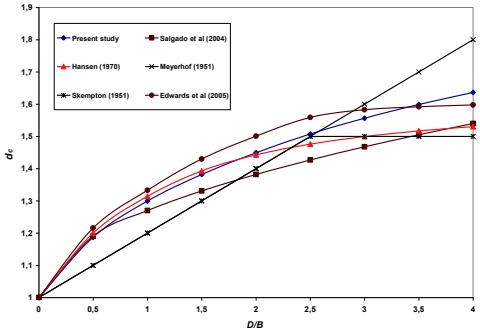

Figure 4. Comparison of present d_c values with those obtained from the expressions available in the literature

5 CONCLUSIONS

Two-dimensional finite difference analyses of embedded rough strip footings in clay were performed to study the depth factor. The footings have been considered under centered vertical load. The results of depth factor were compared with the existing solutions published in the literature, using the finite elements analysis method and approximations that are commonly used in practice. The d_c values depend on the ratio D/B, for $D/B \leq 2.5$, the dc results from the present study are in excellent agreement with the solutions obtained by with the expression of Hansen (1970).

REFERENCES

Bolton, M.D. and Lau, C.K. 1993. Vertical bearing capacity factors for circular and strip footings on Mohr–Coulomb soil. *Canadian Geotechnical Journal*. Vol. 30, pp. 1024 -1033.

Chen, W.F. 1975. *Limit analysis and soil plasticity*. Elsevier, Amsterdam.

Edwards, D. H., Zdravkovic L., and Potts D. M. 2005. Depth factors for undrained bearing capacity. Géotechnique, Vol. 55, pp. 755-758.

FLAC (2005)-Fast Lagrangian Analysis of Continua. ITASCA Consulting Group, Inc., Minneapolis.

Frydman, S. and Burd, H.J. 1997. Numerical studies of bearing capacity factor N_γ. *Journal of Geotechnical and Geoenvironmental Engineering*. Vol. 123, pp. 20-29.

Hansen, B.J., 1970. A revised and extended formula for bearing capacity. *Bulletin of the Danish Geotechnical Institute*. Vol. 28, 5-11.

Kumbhojkar, A.S. 1993. Numerical evaluation of Terzaghi's N_γ. *Journal of Geotechnical Engineering*. Vol. 119, 598-607.

Loukidis, D., and Salgado, R., 2009. Bearing capacity of strip and circular footings in sand using finite elements. *Computers and Geotechnics*. Vol. 36, pp. 871-879.

Lyamin, A., Salgado R., Sloan S.W. and Prezzi M. 2007. Two- and three-dimensional bearing capacity of footings in sand. *Géotechnique*. Vol. 57, pp. 647-62.

Mabrouki, A. Benmeddour, D. and Mellas, M. 2009. Numerical study of bearing capacity for a circular footing. *Australian Geomechanics*. Vol. 44, pp. 91-100.

Meyerhof, G.G. 1951. The ultimate bearing capacity of foundations. *Géotechnique*. Vol. 2, pp. 301–332.

Michalowski, R.L. 1997. An estimate of the influence of soil weight on bearing capacity using limit analysis. *Soils and Foundations*. Vol. 37, pp. 57-64.

Salgado, R., Lyamin, A. V., Sloan, S. W., Yu, H. S. 2004. Two and three-dimensional bearing capacity of foundations in clay. Géotechnique Vol. 54 , pp 297–306.

Skempton, A. W. 1951. The bearing capacity of clays. Proc. Building Research Cong. London, 1, pp.180–189.

Sokolovskii, V.V. 1960. *Statics of soil media* (translated from the 1942 Russian edition). London: Butterworths.

Terzaghi, K. 1943. *Theoretical soil mechanics*, Wiley, New York.

Introducing an Empirical New Model to Predict SAG Mill Power Consumption

M. Jahani, M. Noaparast, A. Farzanegan, M. Yaghobi Moghaddam
School of Mining Engineering, University college of Engineering, University of Tehran, P.O. Box 14395-515, Tehran, Iran.

G. Langarizadeh
Senior Expert, National Iranian Copper Industries Company, Kerman, Iran.

ABSTRACT Because of high power draw in SAG mills, optimizing their power consumption as well as finding a new model to compute and predict their power consumption is of specific importance. In this research, using results obtained from eight sampling campaigns from SAG mill circuit as well as using SPI test, an empirical model to predict power consumption of SAG mill of Sarcheshmeh Copper Complex was introduced. To validate the model, three sampling campaigns from the entire comminution circuit, under different operational conditions and times, were conducted. Results showed that the introduced model is best able to predict SAG mill power consumption with a small error, $\overline{X}$ = 1.90% and S = 9.40%. Also, obtained results showed that SAG mill with consuming 48.37% of total power, generates 55.38% of suitable product for flotation while ball mill with consuming 51.63% of total power, generates 44.62% of final product.

Keywords: Modeling, Power consumption, SAG mill, SPI, Sarcheshmeh Copper Complex.

1 INTRODUCTION

At mineral processing plants, comminution circuits are of the most proportion in power consumption. However, in most cases, because of intrinsic complexity of operation, comminution circuit efficiency is less than expected value. On the other hand, optimum performance of these circuits causes decreasing consumed power and costs. Thus, determining the proportion of each of the circuit parts at consumed power, to produce suitable product, helps optimization trend of circuit performance (Napier-Munn et al. 1996; Lynch, 1997). Also, considering that most of the power in mineral processing plants is consumed in grinding part, it is always tried to reduce consumed power with offering new methods and equipment such as using AG and SAG mills. SAG mills are usually used as a comminution stage especially for copper minerals, causing an increase in mill capacity and a decrease in operational and investment costs (Wills and Napier-Munn, 2006; Mular et al., 2002).

To examine performance of a system, there are two methods. The first method is examining performance of individual system parts and finally concluding towards system performance. The second method is to

consider the whole system as a part with distinct inputs and outputs, and examining performance of this system and comparing it with system design targets. It is noteworthy that the second method is also well-known as black box method (Jahani, 2009). In this research, black box method was used to determine comminution circuit efficiency of Concentrator Plant 2 of Sarcheshmeh Copper Complex, the largest producing copper plant in Iran, located in the Kerman province. In comminution circuit of this plant, two disparate systems with distinct inputs and outputs are definable. SAG mill and vibrating screens could be considered as a system its input is SAG mill feed and its output is passing materials from vibrating screens, underscreen, (system 1). On the other hand, initial ball mill and initial cyclones would be considered as a system its input is underscreen flow and its output is cyclone overflow, rougher feed, (system 2), Fig. 1. An existing problem is that sampling of underscreen flow is impossible at the plant. But, considering previous studies (Azimi, 2006; Paimard, 2007; Jahani, 2009), because of high efficiency of vibrating screens, 99.89%, with sampling of SAG mill out flow, screen feed, and separating particles coarser than 5 mm (reject or over screen) of it, underscreen sample can be obtained with around 0.1% error.

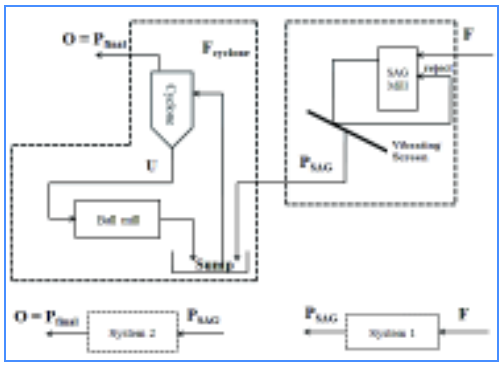

Figure 1. Systems 1 and 2 of comminution circuit of Concentrator Plant 2 of Sarcheshmeh Copper Complex

In recent years, some projects were introduced to study on existing problems at 'Concentrator Plant 2 of Sarcheshmeh Copper Complex' and improving its performance (Azimi, 2006; Paimard, 2007; Jahani, 2009; Hadizadeh, 2006). At these projects, design and construction of a SAG mill sampler and preparing sampling sites, design and construction of a laboratory mill to determine SAG mill power index (SPI), and introducing a formula to predict consumed power of the SAG mill was performed (Azimi, 2006). The formula is as Eq. 1 (Azimi, 2006):

$$P = 0.55(SPI)^{0.01} - 7.36(K_{80})^{0.01} + 0.69\left(\frac{H}{1000}\right) + 2.81\left(\frac{p}{1000}\right) \quad (1)$$

where, P is specific consumed power of SAG mill (kWh/t), SPI is SAG mill Power Index (min.), K_{80} is size of the final product of SAG mill, underscreen, (microns), H is time period of shell liner function (hours), and P is trunnion pressure of the free head of SAG mill

(kPa). Eq. 1 suffers from this fault which with changing the SPI number from 100 to 200 min., amount of predicted power changes 0.004 kWh/t, too little amount. Namely, the SPI role in comparison with other three parameters available in the formula is very few: when SPI = 100, 0.55 $(SPI)^{0.01}$ = 0.5759 kWh/t and when SPI = 200, 0.55 $(SPI)^{0.01}$ = 0.5799 kWh/t. Also, the relation between trunnion pressure and consumed power in SAG mill was obtained and explained, Eq. 2 (Paimard, 2007).

$$p = 0.2525\,P + 3213.2;\ R^2 = 0.865 \quad (2)$$

where, p is SAG mill free trunnion pressure (kPa) and P is consumed power at SAG mill (kW). Also, at another project, modeling of liner surface during their life, and their surface changes due to abrasion was examined as well as their consumption pattern was obtained (Hadizadeh, 2006; Yahyaei et al. 2009; Banisi and Hadizadeh, 2007). Also, with three-dimensional modeling of liners during time, calculation of their weight and volume at each stage was allowed. Finally, considering this modeling, abrasion rates were calculated with high accuracy and as a result estimation of liner life, prediction of their replacement time, became possible at this stage (Hadizadeh, 2006; Yahyaei et al. 2009; Banisi and Hadizadeh, 2007).

As Starkey SPI mill was not accurate enough and the formula introduced (Eq. 3) was only valid at specific cases, in recent years, Starkey et al. have sought to find a relation to predict SAG mills' consumed power to be applicable for all SAG mills, like Bond's work index valid to all ball mills. For this reason, they have tried to solve this problem using a laboratory mill, SAGDesign laboratory mill (Starkey, 2006, 2009; Starkey et al., 2006, 2009). Feed of this mill is provided from core samples of almost 10 kg which their K_{80} is 152 mm and is then crushed to reach sizes of passing 80% of 19 mm screen. Product of this mill is particles with sizes of passing 80% of 1.7 mm screen.

In previous studies, some modeling was performed by Starkey and Dobby (Starkey and Dobby, 1996). In 1996, they obtained a relation to calculate consumed power of industrial SAG mills, using Starkey SPI test as well as using information from four plants in Canada (Starkey and Dobby, 1996). This relation well-known as a MinnovEX relation for a cycle under standard condition is as following, Eq. 3. Standard cycle is a cycle which F_{80} of input feed to its SAG mill is between 120–180 mm and pebble mill was not used in its circuit (Starkey and Dobby, 1996).

$$P = (K_{80})^{-0.33}\left(2.2 + 0.1\,SPI\right);\ R^2 = 0.94 \quad (3)$$

where, P is power of industrial SAG mill (kWh/t), K_{80} is size of final product of SAG mill (mm), and SPI is time of the test (min.).

Finally, SAG mill's product is used to the work index test of the standard Bond ball mill (Starkey et al. 2006, 2009). Calibrated equation to SAGDesign test is as following (Eq. 4) (Starkey et al. 2006):

$$\left(\frac{kWh}{t}\right) = Revs \times \frac{(g + 16000)}{447.3 \times g} \quad (4)$$

where, Revs is the number of mill revolution to grind ore to sizes of 80% finer than 1.7 mm, g is weight of tested ore (g), 16000 is weight of steel balls (g), and 447.3 is calculated coefficient of empirical tests.

Considering high power draw in SAG mills (5 – 10 MW), optimizing their power consumption as well as finding a new model to compute and predict their power consumption is of specific importance. On the one hand, considering differences between comminution mechanisms at ball and SAG mills, the Bond's standard work index test method for ball mills cannot be used to compute amount of power consumption at SAG mills. On the other hand, Starkey formula (Eq. 3) is only valid in specific cases. Thus, nowadays finding a new model to compute SAG mill power consumption is in the limelight. Therefore, the aim of this research is to find an empirical model, using operating parameters related to selection and breakage functions, to predict power consumption of SAG mills. Also, the proportion of each of the systems in power consumption and generating suitable product for flotation process, particles finer than 74 microns, is calculated.

2 METHODOLOGY

To examine comminution circuit efficiency, it was essential to prepare the required samples. To determine apparatus performance condition as well as circuit balance, samples from SAG mill feed, SAG mill discharge, overscreen materials, SAG mill final product (underscreen), initial cyclone feed, initial cyclone underflow, and initial cyclone overflow are necessary to be taken. In addition, using standard Bond ball mill, laboratory work index of ball mill feed was calculated. To estimate or predict SAG mill power consumption and to calculate its feed hardness, Starkey SPI mill was used to measure SAG mill power index.

Considering that a model to be introduced to predict SAG mill power consumption should be comprehensive so that it can be usable for any circuit, thus samplings should be conducted in difference operational conditions. To determine efficiency of mills and size classification equipment, three different sampling campaigns from comminution circuit were implemented in different dates. The sampling campaigns carried out over out flows of SAG mill, overscreen, cyclone feed, cyclone underflow, and cyclone overflow. After the end of sampling of these streams, feeding conveyor belt to SAG mill stopped and contents of 6 meters of the conveyor belt was completely discharged into barrels. Then, recorded operational information within the first, second, and third samplings was provided through plant control room, presented in Table 1.

Table 1. Control room information within the 1st, 2nd, and 3rd sampling campaigns

	1st Sampling			2nd Sampling			3rd Sampling		
	Min	Max	Ave	Min	Max	Ave	Min	Max	Ave
SAG mill power consumption (kW)	6675	7246	6917	6254	6964	6754	7941	8528	8142
Ball mill power consumption (kW)	7568	7794	7668	7837	8090	7904	7574	7850	7710
Humid input feed tonnage to SAG mill (t/h)	726.3	791.4	754.6	750.0	850.0	793.8	586.5	1101	1022
Humid reject tonnage (t/h)	98.3	128.9	117.9	40.0	114.0	93.0	59.53	124.90	72.84
Pressure of initial cyclone cluster (kPa)	62.88	90.80	83.43	54.0	80.0	69.11	88.11	104.7	96.8
Pressure of SAG mill free trunnion (kPa)	4962	5169	5036	4482	4598	4560	5193	5467	5300

Each 15 minutes, one sample was taken from overscreen, cyclone feed, and cyclone underflow flows. Thus, during sampling time, 7 samples were gathered of these flows, which mixed together. The sample of cyclone overflow was provided using an automatic sampler of a X-ray analysis instrument installed at Concentrator Plant 2, in this manner that each 10 minutes, 5 cuts was transferred into sampling vessel using predicted facilities over the instrument. One sample was provided from out flow of SAG mill, and then this sample was discharged into a barrel. After the end of sampling and material settling inside the barrel, its extra water was discharged. After drying the sample, the entire sample was size analyzed to sizes coarser than 6730 microns, and materials finer than 6730 microns divided using a splitter (rifle type), and about 1.5 kg of them was used to continue size analysis down to sizes finer than 37 microns. Over the taken samples of overscreen, cyclone feed, cyclone underflow, and cyclone overflow flows, a size analysis test was done down to 37 microns. Also, solid weight percentage of cyclone feed, cyclone underflow, and cyclone overflow flows was determined.

3 RESULTS AND DISCUSSION

3.1 Results of the Three Sampling Campaigns

In the first sampling campaign, prepared sample from feeding conveyor belt to SAG mill with total weight 965 kg was size analyzed. First, the whole sample was analyzed to sizes coarser than 6730 microns, then the rest of the sample, finer than 6730 microns, which had a weight of 238 kg divided by a splitter and 1.5 kg of the new sample was used in size analysis down to 37 microns. The second sampling campaign was carried out about 4 months after the first one. Sampling stages, preparation, and performed operation over the samples was similar to the first sampling. At the second sampling, total weight of the provided sample over the feeding conveyor belt to the SAG mill was 792 kg. Also, weight of materials finer than 6730 microns was 78 kg. The third sampling campaign was implemented about three months after the second one. Sampling stages, preparation, and performed operation over the samples was similar to the first and second

samplings. The weight of third sample prepared from the feeding conveyor belt to the SAG mill was 1010 kg. In addition, weight of materials finer than 6730 microns was 244 kg.

Based on recorded information at control room, average tonnage of dry input ore to SAG mill within the first sampling was 721 t/h, equivalent to 67% of nominal capacity of the plant, 1080 t/h. At time of the first sampling, shell liners had worked 3162 hours. Average tonnage of dry input ore to SAG mill during the second sampling was 751.4 t/h, equivalent to 69.6% of nominal capacity of the plant. At time of the second sampling, shell liners had worked 1376 hours and were in a good condition. Average tonnage of dry input ore to the SAG mill during the third sampling was 968.2 t/h, equivalent to 89.6% of nominal capacity of the plant. At time of the third sampling, shell liners had worked 3440 hours. Characteristics of the first, second, and third samples and their comparison with plant design numbers, targets, could be observed in Table 2.

Table 2. Characteristics of the 1st, 2nd, and 3rd samples and their comparison with plant design numbers (targets)

	1st sampling	2nd sampling	3rd sampling	Circuit design numbers (Metso, 1998)
Size of the largest particles (mm)	200	200	250	250
K_{80} of SAG mill feed (mm)	48	101	42	38
K_{80} of underscreen (mm)	0.415	0.604	0.854	0.505
Amount of particles finer than 25 mm (%)	62.0	30.7	62.9	No data
Comminution ratio	115.7	167.2	49.3	75.2

Size analysis of screen feed, underscreen, and overscreen during the first, second, and third samplings are available in Table 3. Using existing numbers in Table 3, vibrating screen efficiency within the first, second, and third samplings was obtained, 99.91%, 99.81%, and 99.96%, respectively.

Table 3. Parameters related to working condition of vibrating screens at the 1st, 2nd, and 3rd samplings

	K_{80} (μm)			Particles finer than 5 mm (%)			Particles coarser than 25 mm (%)		
	1st sampling	2nd sampling	3rd sampling	1st sampling	2nd sampling	3rd sampling	1st sampling	2nd sampling	3rd sampling
Screen feed	827	807	1150	91.8	93.5	92.5	2.1	4.9	2.4
Underscreen	415	604	854	98.8	100.0	98.7	0.0	0.0	0.0
Overscreen	25558	28232	20241	0.9	2.66	0.43	79.5	26.7	9.3

During the first sampling average pressure of cyclones was 83.4 kPa. It is noteworthy to mention that cyclone design pressure is 93.0 kPa. Solid weight percentage of cyclones' feed, underflow, and overflow within the first sampling was obtained, 46.4%, 65.6%, and 29.0%, respectively. During the second sampling average pressure of cyclones was 69.1 kPa. Solid weight percentage of cyclones' feed, underflow, and overflow at the

second sampling was obtained, 54.0%, 58.9%, and 31.4%, respectively. At time of the third sampling average pressure of cyclones was 96.8 kPa. Solid weight percentage of cyclones' feed, underflow, and overflow at the third sampling was obtained, 48.1%, 70.3%, and 28.2%, respectively.

To calculate ball mill efficiency, the Bond work index method was used. For the first, second, and third samples, ball mill efficiency was 78.31%, 59.35%, and 81.23%, respectively. Considering that final product of comminution circuit, rougher cell feed, should be finer than 74 microns, determining tonnage of particles finer than 74 microns at input and output of black box systems 1 and 2 is of specific importance (Table 4). Using recorded information at plant control room, within the first sampling average consumed power of SAG mill was 6917 kW and average consumed power of ball mill was 7668 kW (Table 1). Therefore, considering available amounts in Tables 1 and 4, average amount of consumed power of SAG and ball mills to produce one ton of product finer than 74 microns was calculated, 28.91 kWh/t. Using recorded information from plant control room, within the second sampling average consumed power of SAG mill was 6754 kW and average consumed power of ball mill was 7904 kW (Table 1). Consequently, considering available amounts in Tables 1 and 4, average amount of consumed power of SAG and ball mills to produce one ton of product finer than 74 microns was 29.82 kWh/t. Using recorded information from plant control room, within the third sampling average consumed power of SAG mill was 8142 kW and average consumed power of ball mill was 7710 kW (Table 1). Thus, considering available amounts in Tables 1 and 4, average amount of consumed power of SAG and ball mills to produce one ton of product finer than 74 microns was calculated, 33.10 kWh/t.

Table 4. Amount of particles at input and output of black box systems 1 and 2 within the 1st, 2nd, and 3rd sampling

	Rate of flow (t/h)			Particles finer than 74 microns (%)			Particles finer than 74 microns (t/h)		
	1st sampling	2nd sampling	3rd sampling	1st sampling	2nd sampling	3rd sampling	1st sampling	2nd sampling	3rd sampling
SAG mill feed	720.64	751.4	968.2	5.66	2.79	6.05	40.79	20.96	58.58
Underscreen	720.64	751.4	968.2	48.73	41.12	28.29	351.17	308.98	279.00
Initial cyclone overflow	720.64	751.4	968.2	75.67	68.21	55.52	545.31	512.53	537.54

With six, five, and eight times of repetition of SPI test for the first, second, and third samples, respectively, the following results were obtained (Table 5). Average SPI value for the second sample was 155.4 (min.), lower than the first sample, 186.5 (min.). Therefore, the second sample was softer than the first one. On the other hand, average amount of obtained SPI from the third sample, 184.7 (min.), is approximately equal to the resulted SPI from the first sample, 186.5 (min.), but it is so higher than resulted SPI from the second sample. So, the third sample has hardness approximately equal to the first one while it is harder than the second one.

Table 5. Results of SPI tests for the 1st, 2nd, and 3rd samples

SPI_1 (min)	SPI_2 (min)	SPI_3 (min)	SPI_4 (min)	SPI_5 (min)	SPI_6 (min)	SPI_7 (min)	SPI_8 (min)	**SPI_{ave} (min)**
199	197	152	182	204	185	No data	No data	**186.5**
146	164	149	143	175	No data	No data	No data	**155.4**
203	204	170.6	182	165	185.5	183.4	184.3	**184.7**

3.2 Modeling Consumed Power of Sarcheshmeh Copper Complex's SAG Mill

Considering previous examinations (Azimi, 2006; Jahani 2009; Jahani et al., 2011), it became known that use of Starkey equation (Eq. 3) to predict consumed power of SAG mill of Concentrator Plant 2 of Sarcheshmeh Copper Complex is not possible. Thus, it is tried to find an empirical model, using results obtained from eight sampling campaigns from SAG mill circuit (system 1) as well as using SPI test, to predict power consumption of SAG mill of the plant.

3.2.1 Parameters related to breakage and selection functions

Effective factors at power consumption of SAG mill, regarding existing operational conditions in the plant, include ore hardness, size of SAG mill's output product, mill filling, percentage of charged ball to the SAG mill, and condition of installed liners inside the mill. In current conditions, SAG mills' filling cannot be exactly calculated. However, ratio between SAG mill's overall filling and amount of charged ball to it can be attributed to average density of load inside the mill. In fact, in a constant filling with increase of ball amount, average density of load increases and vice versa. Considering these issues, the only factor which can indicate changes of filling and percentage of balls of SAG mill, in any moment is pressure of mill trunnions. Hence, to introduce a relation to predict SAG mill's consumed power, pressure of free trunnion of SAG mill was used as agent of ball amount and also SAG mill filling. Therefore, it can be said that SAG mill power consumption, P (kWh/t), is a function of its free trunnion pressure, p (kPa). In other words, P = f(p). Also, change of lifters' height in turn influences SAG mill's consumed power so that with decrease of lifters' height usually load does not rise up to desirable height and as a result during fall does not enjoy enough energy to be crushed, due to collision of rock to mill shell or collision of ball to rock, or to crush other particles, due to collision of rock to finer particles. Additionally, materials' retention time inside SAG mill increases as well. It is remarkable that increase of retention time and decrease of particles' energy during collision cause more power consumption at SAG mill to crush materials. Therefore, time period of shell liner function is an effective factor in SAG mill's consumed power. On the other hand, it can be said that SAG mill power consumption, P (kWh/t), is a function of time period of its shell liner function, H (hours). In other words, P = f(H). In addition to pressure of SAG mill's free trunnion and time period of its shell liner function related to SAG mill's operational conditions, parameters related to selection function, characteristics of feed and final product of SAG mill, parameters related to breakage function, are also effective in SAG mill's specific consumed power. Characteristics of SAG mill's feed can be expressed as SPI number and characteristics of SAG mill's final product can be expressed as underscreen K_{80}. Therefore, feed SPI number

and underscreen K_{80} are other effective factors in SAG mill's consumed power. On the other hand, it can be said that SAG mill power consumption, P (kWh/t), is a function of its feed SPI number, SPI (min.) as well as is a function of its underscreen K_{80} (mm). In other words, P = f(SPI) and P = f(K_{80}). Given that these four parameters are independent, it can be said that there are four different methods to predict SAG mill power consumption.

3.2.2 Introduced model to predict Sarcheshmeh SAG mill power consumption

To find a relation between SAG mill power consumption (kWh/t) and its feed SPI number (min.), its underscreen K_{80} (mm), and its shell liner function, H (hours), eight sampling campaigns from SAG mill circuit (system 1) was conducted. Also, in order to find a relation between SAG mill power consumption (kWh/t) and its free trunnion pressure, p (kPa), control room information of Sarcheshmeh Copper Complex plant was used.

Having conducted eight sampling campaigns and using SPI mill, relations between SAG mill's specific consumed power and SPI, underscreen K_{80}, and time period of shell liner function were obtained (Fig 2. and Eqs. 5 – 7) as well as considering control room information of the plant, relation between SAG mill's free trunnion pressure (kPa) and SAG mill's consumed power (kW) was obtained (Fig 2.). Reason of using control room information instead of data from eight sampling campaigns is that they are more accurate as they are obtained from 2500 operational data. However, relation between P (kWh/t) and p (kPa) is our favorite. Given rate of flow (t/h), relation between P (kWh/t) and p (kPa) is in the form of Eq. 8.

$$P = a_1 (SPI)^{b_1};\ a_1 = 0.2026; b_1 = 0.7338; R^2 = 0.8601 \quad (5)$$

$$P = a_2 (K_{80})^{b_2};\ a_2 = 8.3041; b_2 = -0.1753; R^2 = 0.8931 \quad (6)$$

$$P = a_3 H + b_3; a_3 = 0.0004; b_3 = 7.7770; R^2 = 0.9238 \quad (7)$$

$$\mathrm{P}\left(\frac{\mathrm{kWh}}{\mathrm{t}}\right) = a_4 \mathrm{p} + b_4;\ a_4 = 5.5 \times 10^{-3};\ b_4 = -17.66;\ \mathrm{R}^2 = 0.865 \quad (8)$$

So far, Given that these four parameters are independent, relation between specific consumed power and each of these parameters was individually calculated. Consequently, SAG mill's specific consumed power can be represented in the form of an average of predicted specific powers by each of these four parameters. Considering Equations 5 to 8, the overall relation is in the form of Eq. 9.It is noteworthy that, Eq. 9 is applicable in any plant and circuit while Starkey model (Eq. 3) is only applicable in standard circuits. In each plant and circuit, coefficients a, b, c, d, e, f, g, and h should be calculated and calibrated so that the introduced model can be applicable. For Sarcheshmeh Copper complex, using data from equations 5, 6, 7, 8, and 9, the overall relation is in the form of Eq. 10.

$$\mathrm{P} = \left[a(\mathrm{SPI})^b\right] + \left[c(\mathrm{K}_{80})^d\right] + \left[eH + f\right] + \left[gp + h\right]; a = \frac{a_1}{4}; b = b_1;$$
$$c = \frac{a_2}{4}; d = b_2; e = \frac{a_3}{4}; f = \frac{b_3}{4}; g = \frac{a_4}{4}; h = \frac{b_4}{4} \quad (9)$$

$$P = \left[5.065 \times 10^{-2} (SPI)^{0.7338}\right] + \left[2.076 (K_{80})^{-0.1753}\right] + \left[10^{-4} H + 1.944\right]$$
$$+ \left[1.375 \times 10^{-3} p - 4.415\right] \quad (10)$$

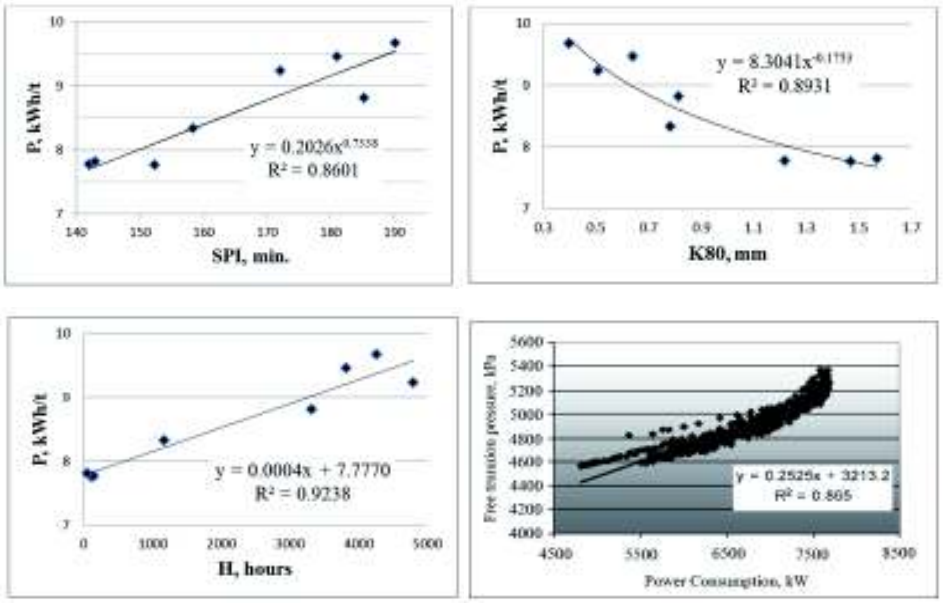

Figure 2. Relation between SAG mill's specific consumed power and SPI, underscreen K_{80}, and time period of shell liner function as well as Relation between SAG mill's free trunnion pressure and SAG mill's consumed power

3.2.3 Model validation

To validate the introduced model for Sarcheshmeh Copper Complex (Eq. 10), it is necessary to examine capability of the model to predict SAG mill power consumption for new data. To this end, data from three sampling campaigns from the entire comminution circuit was used. Data related to the first, second, and third samplings are available in Table 6.

Table 6. Data from the 1st, 2nd, and 3rd sampling campaigns to validate the model

	1st sampling	2nd sampling	3rd sampling
SPI (min)	186.5	155.4	184.7
K_{80} (mm)	0.415	0.604	0.854
H (h)	3162	1376	3440
p (kPa)	5036	4560	5300
P_{actual} (kWh/t)	9.60	8.99	8.41
$P_{predicted}$ (kWh/t)	9.54	8.26	9.63
$P_{starkey\ model}$ (kWh/t)	27.87	20.95	21.78
Starkey model Error (%)	190.31	133.04	158.98
New model Error (%)	-0.63	-8.12	14.51

As it is observed through comparison of amounts of actual and predicted specific consumed power in all three samplings (Table 6), the introduced model (Eq. 10) also for the new data enjoys relatively high accuracy and is best able to predict SAG mill power consumption with a small error, $\overline{X}$ = 1.90% and S = 9.40%, supposing T-student distribution, while Starkey SPI model (Eq. 3) cannot be used to predict SAG mill power consumption of Sarcheshmeh copper plant because of its huge error, $\overline{X}$ =160.78% and S = 23.42% (Fig. 3).

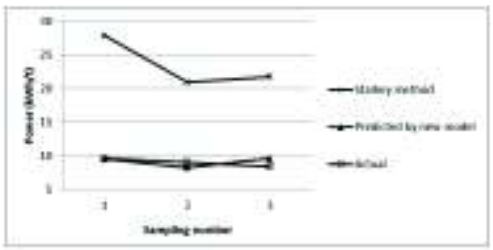

Figure 3. Comparison between predicted data by Starkey model and new introduced model

4 CONCLUSION

In this research, using parameters related to breakage function (SPI and K_{80}) and selection function (p and H) an overall relation applicable in any plant and circuit to predict power consumption of all SAG mills was introduced (Eq. 9). Also, using results obtained from eight sampling campaigns from SAG mill circuit (system 1) as well as using SPI test, an empirical model to predict power consumption of SAG mill of Sarcheshmeh Copper Complex was introduced (Eq. 10). To validate the model, three sampling campaigns from the whole comminution circuit, in different operational conditions and times, were conducted. Meanwhile, efficiency of vibrating screens, ball mill (system 2), and hydrocyclones was computed during these three sampling campaigns. To compute efficiency of ball mill, Bond work index method was used. Also, the proportion of each of the systems in power consumption and generating suitable product for flotation process, particles finer than 74 microns, was calculated. Results showed that the introduced model is best able to predict SAG mill power consumption with a small error, $\overline{X}$ = 1.90% and S = 9.40%, while Starkey SPI model cannot be used to do this because of its huge error, $\overline{X}$ = 160.78% and S = 23.42%. The following conclusions were obtained through averaging results from three sampling campaigns:

- Average of the proportion of SAG and ball mills consumed power from total consumed power at mills, was 48.37% and 51.63%, respectively. Generally, ball mill power consumption is about 3.26% more than SAG mill.
- Average of the proportion of SAG and ball mills to produce final product, particles finer than 74 microns, was 55.38% and 44.62%, respectively. That is, SAG mill about 10.76% more than

ball mill plays the role in producing final product.

- Average of consumed power at SAG and ball mills to produce one ton of final product was 27.56 kWh/t (43.33%) and 36.05 kWh/t (56.67%), respectively. That is to say, ball mill about 8.49 kWh/t (13.34%) more than SAG mill consumes power to produce final product.
- Average of consumed power to produce one ton of final product was 30.61 kWh/t.

REFERENCES

Anonymous, Metso Report of performed tests over Sarcheshmeh copper ore to select equipment for development scheme of Concentrator Plant, 1998. Kerman, Iran.

Azimi, E., 2006. Examination of grinding circuit efficiency of new concentrator plant of Sarcheshmeh Copper Complex, M.S. thesis in mineral processing, technical and engineering faculty, university of Shahid-Bahonar of Kerman, Kerman, Iran.

Banisi, S., Hadizadeh, M., 2007. 3-D liner wear profile measurement and analysis in industrial SAG mills. Minerals Engineering 20, 132–139.

Hadizadeh, M., 2006. Examination of the amount and mode of liner abrasion in the SAG mill of new concentrator plant of Sarcheshmeh Copper Complex, M.S. thesis in mineral processing, technical and engineering faculty, university of Shahid-Bahonar of Kerman, Kerman, Iran.

Jahani, M., 2009. Examination of energy consumption in the SAG and Ball Mills at Concentrator Plant 2 of Sarcheshmeh Copper Complex, M.S. thesis in mineral processing, School of Mining Engineering, University college of Engineering, University of Tehran, Tehran, Iran.

Jahani, M., Noaparast, M., Farzanegan, A., Langarizageh, G., 2011. Application of SPI for modeling energy consumption in Sarcheshmeh SAG and ball mills. Journal of Mining & Environment (JME), Vol.2, No.1, 27 – 40.

Lynch, A.J., 1997. Mineral Crushing and Grinding Circuits – Their Operation and Optimization, Design and Control, Elsevier, New York, 1997.

Mular, A.L., Halbe, D.N., Barratt, D.J., 2002. Mineral Processing Plant Design Practice and Control, vol. 1. Soc. for Mining, Metallurgy and Exploration, Inc., Litleton, Colorado.

Napier-Munn, T.J., Morrell, S., Morrison, R.D., Kojovic, T., 1996. Mineral Comminution Circuits – Their Operation and Optimisation. Julius Kruttschnitt Mineral Research Centre, Monograph, vol. 2. The University of Queensland, Brisbane, Australia.

Paimard, M. 2007. Determining the optimum amount of balls into the SAG mill of Sarcheshmeh Copper Complex, M.S. thesis in mineral processing, mining engineering faculty, Yazd university, Yazd, Iran.

Rowland, C.A., 1998. Using the Bond Work Index to measure operating comminution efficiency. Minerals & Metallurgical Processing, Vol. 15 No.4, pp. 32–36.

Starkey, J., 2006. Accurate, economical grinding circuit design using SPI and Bond. Starkey & Associates 336-268 Lakeshore Road East, Oakville, Ontario L6J 7S4.

Starkey, J., 2009. New discoveries in the relationship between macro and micro grindability. Starkey & Associates Inc. and Mike Samuels, Fortune Minerals Limited, Paper for the CIM AGM, Toronto, ON May 13.

Starkey, J., Dobby, G., 1996. Application of the MinnovEX SAG power index at five Canadian SAG plants. Int. Autogenous and Semi-autogenous Grinding Technology, Vancouver, Oct. 6 – 9, Vol. 1, pp. 345–360.

Starkey, J., Hindstrom, S. and Nadasdy, G., 2006. SAGDesign Testing – What it is and why it works. department of mining engineering, university of British Colombia, Vancouver, B. C., Canada.

Starkey, J.H., Meadows, D., Thompson, P. and Senchenko, A., 2009. SAGDesign testing review – case studies. Starkey & Associates 212-151 Randall St. Oakville, ON L6J 1P5, Canada.

Wills, B.A., Napier-Munn, T.J., 2006. Mineral Processing Technology, seventh ed. Butterowrth-Heinemann, Oxford.

Yahyaei, M., Banisi, S., Hadizadeh, M., 2009. Modification of SAG mill liner shape based on 3-D liner wear profile measurements. International Journal of Mineral Processing 91, 111–115.

Modeling and Simulation of Banana Screens Using Discrete Element Method

A. Farzanegan

School of Mining, University College of Engineering, University of Tehran, Tehran, Iran.

Z. Faraji

Faculty of Mining Engineering, University of Kashan.

Z. S. Mirzaei

Faculty of Mining Engineering, University of Kashan.

ABSTRACT With progress in various mineral processing technologies, particle size classification equipment has also been changed to satisfy the needs of modern plants. Accordingly, design, manufacturing and utilization of banana screens in mineral processing plants have led to increased screening process efficiency at industrial scale. Banana screen is an important invention occurred in the past decade which increases screening capacity. This type of screens has screening segments with different slopes. While this invention has been used increasingly in the industry, its control and optimization has been limited due to the lack of fundamental knowledge about the screening process. Using numerical simulation is an effective method to overcome such limitations in design and optimization studies. Discrete element method is a numerical approach which computes particle interactions and their motion. In this paper, the results of modeling and simulation of particles' motion and classification in banana screens using DEM method in PFC3D software environment is presented. Hence, DEM simulation of a three-segment banana screen was done to study the effect of design and operating variables on classification performance. To validate our DEM simulations, the results obtained in this study were compared with the previous results reported in the literature. The comparisons show the correctness of authors DEM simulations.

Keywords: Banana screens, Screening, Discrete element method, DEM

1 INTRODUCTION

Screening is one of oldest particulate material classification methods based on particle size which plays an important role in mineral processing plants (Wills and Napier-Munn, 2006). Banana screen is one of the newest types of vibrating screens which consist of several plates connected together with different slopes (Figure 1). The slope is high at the feed end and it decreases at the end of the screen to produce a layer with a fixed thickness along the screen which leads to increase in screen capacity. Control and optimization of these types of screens is an important goal in mineral processing plants which requires basic information about screening process (Dong et al., 2009).

There are many mathematical models of screening process which are basically empirical and phenomenological models (Karra, 1979, Ferrara, 1988). These models have not been derived from first (physical) principles, hence due to the lack of complete understanding of screening operation; some of the involved parameters in these models must be determined experimentally. The lack of complete understanding of screening operation stems from the fact that the

distribution of particles, which have different sizes, between screen underflow and overflow streams is very complicated. Also, the effect of particles motion in various operational conditions contributes to their final classification. Some proposed models are based on reaction kinetics and statistical theories. For example, first order kinetics is a well-known theory which states that the rate of change in remaining mass on the screen is proportional to the remaining mass on the screen as a function of screening time. Equation (1) represents this relationship mathematically.

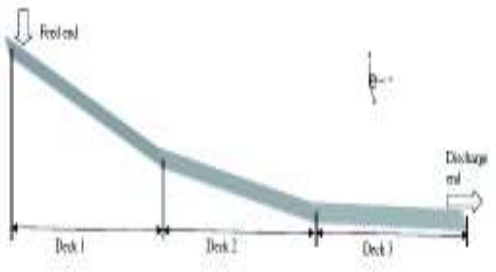

Figure 1. Banana screen with three plates with different slopes

$$\frac{\partial W}{\partial t} = -kW \tag{1}$$

where W is remaining mass on screen and k is the screening rate constant.

In practice, overall behavior of particles in a system depends on particle-particle and particle-wall interactions. So screening process should be understood at particle scale (Dong et al., 2009). As tracking and understanding of particles' motion at microscopic scale by the laboratory methods is very complicated, a numerical simulation method such as discrete element method can be used. Li et al. (2003) studied the motion of discrete particles on the screen by discrete element method that confirmed the negative effect of particles with a size near to that of the nominal screen aperture size and the positive effect of large particles in the feed stream on screen efficiency which was derived by Standish (Li et al., 2003).

Song et al. (2005) explained an algorithm about the impact contact of discoid particles. Finally, this method was expanded for screen simulation and Yan-hua and Xin (2009) made a three-dimensional simulation of screening process. Cleary et al. (2009a, 2009b) used DEM simulation to study the nature of particle flow in an industrial double-deck banana screen and linked it to separation performance. In a more recent article, Fernandez et al. (2011) introduced combining DEM and Smoothed Particle Hydrodynamics (SPH) to model the flow of slurry composed of water and fine material through a double deck banana screen.

In this paper, industrial banana screens have been simulated and the effect of various parameters on the screen efficiency has been investigated according to the available information from previous studies.

2 THEORY

The discrete element method was developed by Cundall to solve the geomechanic problems in 1970 (Cundall and Strack, 1979). In this method, the contacts among the particles and between particles and the wall which is the screen surface are modeled by the rule of contact forces. In this model a simple numerical plane is used to monitor the motion and response of particles. Translation and swirl for particle i is calculated as:

$$m_i \frac{dv_i}{dt} = \sum_j \left(F_{ij}^n + F_{ij}^s \right) + m_i g \tag{2}$$

$$I_i \frac{d\omega_i}{dt} = \sum_j \left(R_{ij} \times F_{ij}^s - \mu_r R_i \mid F_{ij}^n \mid \hat{\omega}_i \right) \tag{3}$$

where v_i, is translational velocity, ω_i, angular velocity, I_i, moment of inertia of particle i, g, acceleration of gravity, R_{ij}, a vector from center of particle i to contact point with particle j, F_{ij}^n , normal force of contact, F_{ij}^s , tangential force of contact. Normal and tangential components of contact are calculated as:

$$F_{ij}^{\mathrm{n}} = \left[\frac{2}{3} E\sqrt{\overline{R}}\xi_{\mathrm{n}}^{\frac{3}{2}} - \gamma_{\mathrm{n}} E\sqrt{\overline{R}}\sqrt{\xi_{\mathrm{n}}}\left(v_{ij}\cdot\hat{n}_{ij}\right)\right]\hat{n}_{ij} \quad (4)$$

$$F_{\mathrm{s}} = \mu_{\mathrm{s}}\left|F_{\mathrm{n}}\right|\left[1-\left(1-\min\left(\xi_{\mathrm{s}},\xi_{\mathrm{s,max}}\right)/\xi_{\mathrm{s,max}}\right)^{\frac{3}{2}}\right]\hat{n}_{ij} \quad (5)$$

$$\overline{R} = R_i R_j /\left(R_i + R_j\right) \quad (6)$$

$$\xi_{\mathrm{s,max}} = \mu_{\mathrm{s}}\left[\left(2-\tilde{\sigma}\right)/2\left(1-\tilde{\sigma}\right)\right]\xi_{\mathrm{n}} \quad (7)$$

$$\hat{n}_{ij} = \left(R_i - R_j\right)\Big/\left|R_i - R_j\right| \quad (8)$$

$$E = Y/\left(1-\tilde{\sigma}^2\right) \quad (9)$$

where R_i and R_j, are radius of particles i and j, Y, Young's modulus, $\tilde{\sigma}$, Poisson's ratio, Y_n, simple damping coefficient, μ_s, coefficient of friction, ξ_s, overall tangential displacement, μ_r, coefficient of rolling friction. The action between the particles and wall is calculated according to above equations and the process is dry (Dong et al., 2009).

DEM simulation is highly sensitive to model parameters which are basically related to material properties including particles' shape, size, and distribution; Poisson's ratio; shear modulus and density. Also, interaction properties of materials consisting of coefficients of restitution, static friction, and rolling friction must be accurately defined for reliable DEM predictions.

3 MATERIALS AND METHODS

In this project, authors used PFC3D (Particle Flow Code in Three Dimension) developed by Itasca Consulting Group, Inc., 1998 to simulate the screening process. At first step of simulation, it is necessary to design and generate the screen surface. In this project, the virtual screen was produced in the software environment according to the details of screen design and geometry explained in Dong et al., 2009 which can be seen in Figure 2 by considering X, Y and Z axis in 3D.

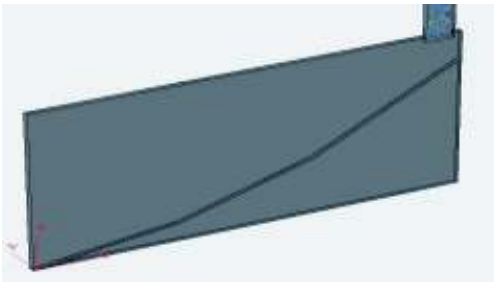

Figure 2. Generated virtual screen in PFC3D software

The feeding part of the screen containing various balls as the feed particles is shown in the top right of the Figure 2. In this part of research, it was also considered that the shape of the feed particles to be spherical which is clearly a simplifying assumption. This assumption causes inaccurate predictions. However, more realistic DEM simulations of screening process can be performed by defining non-spherical particles. It is noted that in these DEM simulations the size of computations and simulation time will be increased significantly (Cleary, 2009a).

The number of the screen surfaces is calculated from the point where the feed enters into screen to the point where particles leave the screen and will be discharged. This screen has 3 plates (Dong et al., 2009). Figure 3 shows the defined balls that act as the feed particles in simulation, with different colors from red (the largest particle) to dark blue (the finest particle). The particle size distribution of the feed (coal) is about 0.45 to 2 mm (Table 1). Figure 4 shows the screen surface in a close-up view.

The details of the screen geometry and the operating condition are observed in Table 2 (Dong et al., 2009).

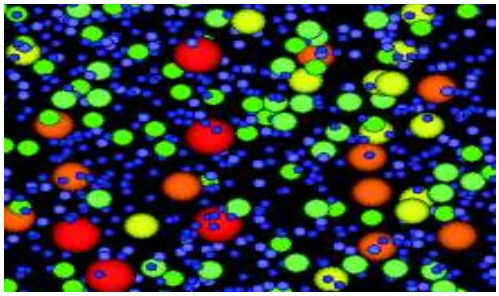

Figure 3. Feed particles with color of red, orange, yellow, light green, dark green and light blue to dark blue showing various range of particle sizes

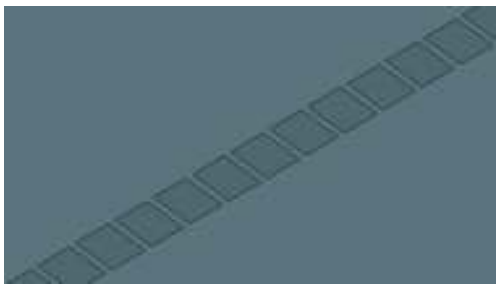

Figure 4. A close-up view of simulated screening surface

Table 1. Particle size distribution of coal particles in feed stream

Size class	Size class interval (mm)	Remaining mass (%)
1	-200 to +140	5
2	-140 to +100	5
3	-100 to +70	10
4	-70 to +60	10
5	-60 to +49	10
6	-49 to +42	10
7	-42 to +35	10
8	-35 to +28	10
9	-28 to +22	10
10	-22 to +18	10
11	-18 to +15	10

Table 2. The details of the screen geometry and operating condition

Property	Value
Screen width (mm)	9
Aperture size (mm)	1
Length of wire (mm)	5
Open area (%)	17
Height of feed downfall (mm)	30
Vibration frequency (Hz)	15 (5 to 25)
Vibration amplitude (mm)	2 (1 to 3)
Particles motion	Linear in slope of 45 degree
Particles density (kg/m^3)	1400
Wall density (kg/m^3)	1050
Damping coefficient among particles	5×10^{-5}
Damping coefficient between particle and wall	5×10^{-4}

With starting the simulation, a composite stream of particles with different sizes conflux with each other and drop down on the vibrating screen which some of them pass through the screen and some of particles discharge from the discharge end. As can be seen in Figure 5, large particles remained on the screen surface and fine particles passed through the screen apertures can be observed.

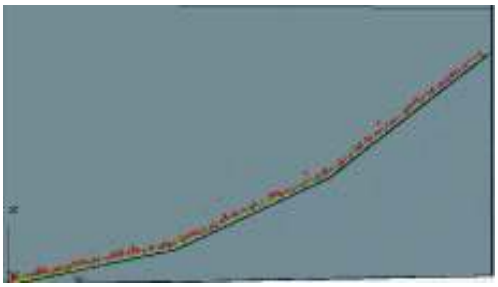

Figure 5. A view of three-plate screen at the end of DEM simulation

It is clear that the separation of fine particles occurs from the beginning of the screen. The partition curve concept is applied to define the screen performance and the effect of various parameters on it. In this paper, the partition curve is calculated as the

percent of recovered mass of feed particles in specific size to the screen overflow which is the screen coarse product.

4 RESULTS AND DISCUSSION

4.1 Vibration Amplitude

To investigate the screen efficiency, as mentioned earlier, the partition curve was calculated and plotted in which the horizontal axis shows the average diameter of size fraction and the vertical axis shows the ratio of the number of remaining particles in screen overflow (stream with large particles) to the total number of particles in the feed for each specified particles size class. According to Figure 6, it is observed that the decrease in amplitude of frequency leads to increase in separation efficiency.

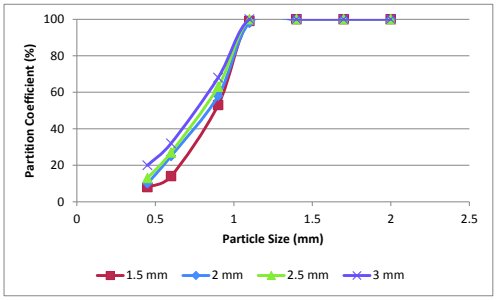

Figure 6. Simulated partition curves for particles recovered to overflow stream at various vibration amplitudes

Here, it can be noted that the reduction in amplitude causes reduction of force applied on the particles. So, the particles in a specific time snag more with the screen and have greater chance to pass through the apertures. It is important that for very small vibration amplitude (less than 1 mm), the particles gather on the screen surface and because of insufficient force to move the particles, a good separation will not occur.

4.2 Vibration Frequency

The effect of changes in screen vibration frequency was investigated and the partition curves for these changes were plotted. According to Figure 7, it can be seen that the reduction of vibration frequency from 25 Hz to 10 Hz causes an increase in screen efficiency.

The effect of reducing vibration frequency is similar to what was observed in reducing vibration amplitude. The low vibration frequency causes the increase in simulation time. A lower screen vibration frequency leads to remaining of particles on the screening surface for a longer time; therefore transmission probability of particles through screen apertures will be increased. It is noted that very low vibration frequencies will decrease the separation efficiency.

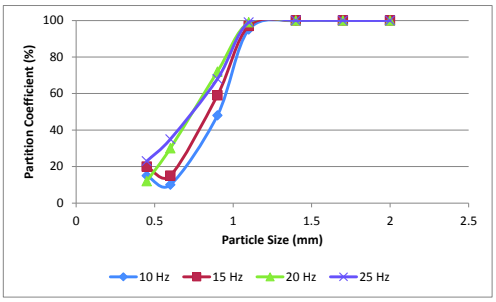

Figure 7. Simulated partition curves for particles recovered to overflow stream at various vibration frequencies

4.3 Slope of Screening Plates

The slope of the screen surface is one of the important parameters which affects the screening process. In this project, the slopes of other plates were considered to be constant while studying the effects of the slope of any plate.

Firstly, according to the conditions defined in Dong, et al., 2009, the slope of first plate was equal to 34 degrees, the slope of the second plate was equal to 22 degrees and the slope of the last plate were considered to be equal to 10 degrees. The results of simulations related to the first, second and third plates in different slopes are shown in Figure 8 to 10. For each screening plate four different slopes were considered.

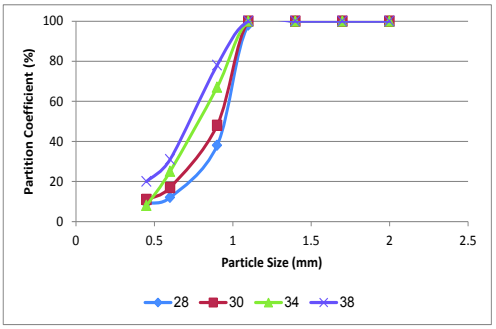

Figure 8. Simulated partition curves plotted for particles recovered to overflow stream for first screening plate with various slopes

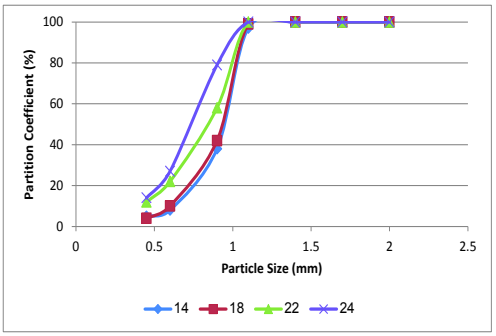

Figure 9. Partition curve of screen overflow with change in the slope of the second plate

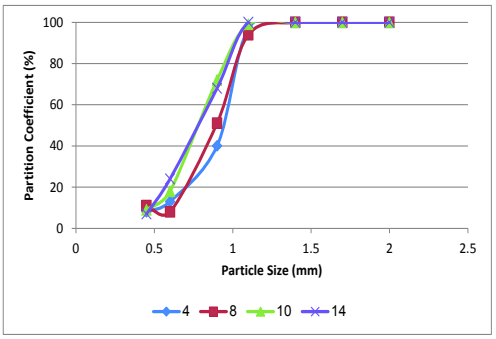

Figure 10. Simulated partition curves for particles recovered to overflow stream for third screening plate at various slopes

Considering the screen overflow partition curves, it can be seen that reduction in the slope of each plate improves the separation process. Reduction in the slope of a single-deck screen leads to increase in effective size of apertures, decrease in particles velocity and increase in probability of particle passing through the screen which results in increased percent passing. However, how a change in a plate slope angle affects overall screen efficiency is very complicated.

It is notable that the reduction of a plate slope has no effect on the percent passing of particles in previous plates. Change in slope angle of various plates is an effective method to control the particle velocity and percent passing of particles.

4.4 Validation of simulation predictions

To evaluate the simulation results of this study, the results obtained from Dong, et al., 2009, were considered.

Figure 11 shows the results of present simulation and previous studies for vibration amplitude equal to 1.5 mm. it is obvious that all particles larger than the screen aperture (> 1.1 mm) have remained on the screen and both curves are coinciding.

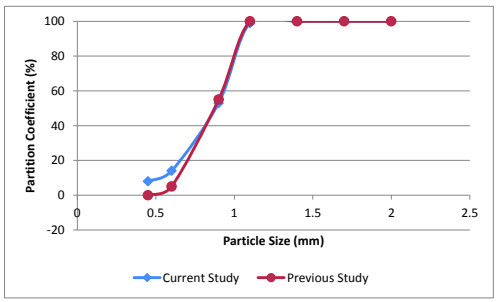

Figure 11. Comparison of simulated partition curve plotted for particles recovered to overflow stream with that of previous studies with vibration amplitude equal to 1.5 mm

For smaller particle sizes, the curves show a good similarity and the slight difference is due to the diversity in software and the simulation conditions which could not be

easily specified due to inaccessible original data and models and algorithms implemented in the proprietary software.

Figure 12 shows the comparison of vibration frequencies. The partition curves associated with current simulation and previous study have been plotted in vibration frequency of 10 Hz. In overall, the partition curves are in good agreement while a notable difference can be seen in particles around 0.45 to 0.80 mm particle size. The disagreement for fine particle sizes can be attributed to the low vibration frequency which is insufficient to detach fine particles attached to coarse particles and causing them to pass through the screen aperture.

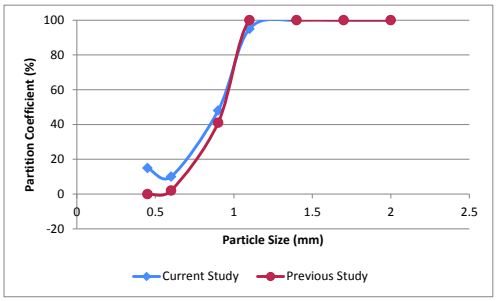

Figure 12. Comparison of simulated partition curve plotted for particles recovered to overflow stream with that of previous study in vibration frequency of 10 Hz

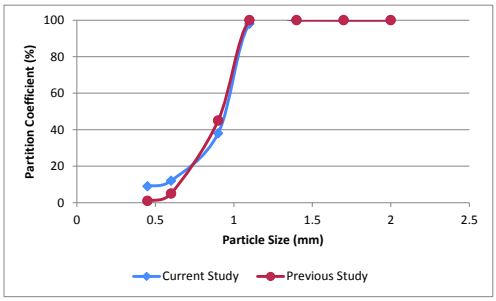

Figure 13. Comparison of simulated partition curve plotted for overflow stream with that of obtained in previous studies for the first plate with a slope of 28 degree

In Figure 13 the partition curves obtained in both current and previous studies related to first plate of screen in slope angle of 28 degree have been shown. Comparing the plotted curves confirms that the obtained results of both simulations match each other and the differences are negligible.

5 CONCLUSIONS

Modeling by discrete element method is able to predict the performance curve of new screens in details. In this paper, the particle flow on the screen was numerically simulated and the effect of various operating conditions and geometry of banana screen on the screen performance (partition curve) were investigated.

The results showed that reduction in vibration amplitude and frequency improves the screen efficiency because the increase in vibration frequency leads to an increase in infiltration rate, contact rate and return rate.

The reduction of slope angle of the plates increases the screen efficiency, because of increasing the effective aperture size, reduced particles velocity and increased time to pass through screen.

Percent passing of particles relates to their velocity in various conditions. An appropriate decrease in particles velocity causes increase in percent passing of particles but very low particles velocity can lead to particles aggregation.

The obtained results clearly show that discrete element method can be used for process analysis and optimization in mineral processing.

REFERENCES

Cleary, P.W., Sinnott, M. D., Morrison, R. D., 2009a. Separation performance of double deck banana screens – Part 1: Flow and separation for different accelerations. Minerals Engineering.Vol. 22, pp. 1218–1229

Cleary, P.W., Sinnott, M. D., Morrison, R. D., 2009b. Separation performance of double deck banana screens – Part 2: Quantitative predictions. Minerals Engineering. Vol. 22 , pp. 1230–1244

Cundall, P. A., Strack, O. D. L. 1979. *A discrete numerical model for granular assemblies*, Geotechnique 29, pp. 47-65.

Dong, K. J., Yu, A. B., Brake, I., 2009. DEM simulation of particle flow on a multi-deck banana screen, *Minerals Engineering*, Volume 22, Issue 11, pp. 910-920.

Itasca Consulting Group, Inc., 1998. Distinct Element Particle Flow Codes PFC2D and PFC3D, Minneapolis MN, USA

Fernandez, J. W., Cleary, P. W., Sinnott, M. D., Morrison, R. D., 2011. Using SPH one-way coupled to DEM to model wet industrial banana screens, Minerals Engineering. Vol. 24, pp. 741-753.

Ferrara, G., Preti, U., Schena, G.D., 1988. Modelling of screening operations. International Journal of Mineral Processing, Vol. 22, pp. 193–222.

Karra, V. K., 1979. Development of a model for predicting the screening performance of a vibrating screen, CIM Bulletin,72, pp. 168-171.

Li, J., Webb, C., Pandiella, S. S., Campbell, G. M, 2003. Discrete particle motion on sieves-a numerical study using the DEM simulation, *Powder Technology,* pp. 190-202.

Song, Y., Turton, R., Kayihan, F., 2005. Contact detection algorithms for DEM simulations of tablet-shaped particles, *Powder Technology,* pp. 32-40.

Wills, B.A., Napier-Munn, T. J., 2006. *Mineral Processing Technology, An Introduction to the Practical Aspects of Ore Treatment and Mineral Recovery,*7th Edition, Elsevier.

Yan-hua, C., Xin, T., 2009. *Application of the DEM to screening process: a 3D simulation*, Mining Science & Technology 19, pp. 493-497.

Simulation of Combined HPGR and Ball Milling Circuits in Cement Production Plants

A. Farzanegan
School of Mining, University College of Engineering, University of Tehran, Tehran, Iran

V. Hasanzadeh
School of Mining, College of Engineering, University of Tehran, Tehran, Iran

A. Valian
Department of Mining, Faculty of Engineering, University of Kashan, Kashan, Iran

ABSTRACT In this paper, developing a novel approach based on integration of evolutionary-based modeling and sequential simulation for optimization of grinding circuits which include HPGR (High Pressure Grinding Rolls) devices in closed circuit particularly in cement plants was investigated. A previously published HPGR model was implemented in ANSI C language and was added to BMCS-based Modular Comminution Simulator (BMCS®) as a separate module. The HPGR module was successfully integrated with other modules such as those for ball mill, hydrocyclone, and general reduced efficiency curve in BMCS environment and was tested by simulation a closed cement grinding circuit. The simulator and also applied procedure for calibration of devices were successfully verified and validated in various development stages by experimental data sets.

The HPGR model parameters, i. e., breakage distribution function and selection function and air separator efficiency curve parameters were back-calculated using GA evolutionary search method. The ball mill selection function was back-calculated using an interval-by-interval binary search method implemented in Numerical Grinding Optimization Tools in C (NGOTC®). In NGOTC, a population balance model of an overflow ball mill based on three parameters including ore breakage function, selection function and residence time distribution of particles is used to search and find the best selection function value for every size class interval so that predicted mill product size distribution is sufficiently close to the measured mill product particle size distribution. The closed circuit simulation results demonstrate that the integration of a GA-based modeling algorithm with a sequential simulation algorithm can provide a powerful environment to accurately predict particle size distribution and flow rate of all streams in grinding circuits which include HPGR units.

1 INTRODUCTION

Comminution operations with high capacity throughput and low specific energy consumption such as those observed in HPGR applications is of interest in mineral processing plants particularly cement grinding circuits. Morrell et al. (1997) believed that availability of an appropriate HPGR model for prediction of product size distribution and scale up is an important reason for expanding of using of HPGR in future grinding circuit designs.

Today, simulation and its related software are widely used for plants pre-feasibility, feasibility and final studies. Optimization and design of a new processing circuit require a simulator which must be sufficiently capable to simulate a wide range of inter-connected units. With increasing HPGR usage in many mineral processing plants, particularly cement grinding circuits,

an appropriate model is needed to predict its product size distributions in distinct operational conditions. In this context, the most important works were done by Morrell and several co-assistants. Their developed model is based on ore characteristics obtained from drop-weight device and HPGR dimensions (Morrell et al., 1997; Daniel and Morrell, 2004). Recently, a new model based on population balance modeling approach was developed for simulation of HPGR units (Torres and Casali, 2009). The new model proposed by Torres and Casali has the advantage that it just needs sampling of HPGR feed and discharge streams and their particle size distribution determination for model calibration.

After introduction of HPGR, its application was rapidly increased in cement grinding circuits due to its high throughput capacity and low specific energy consumption against traditional semi-finishing grinding circuits including tube mills (Patzelt, 1992). Also, due to the micro cracks caused by applying high pressures in compression zone, the Bond work index of the material which is fed to subsequent grinding operations is reduced (Benzer et al., 2003).

The evaluation of HPGR performance in closed grinding circuits especially in cement applications requires a suitable model for prediction of HPGR product size distribution and also an appropriate simulation algorithm. The BMCS-based Modular Comminution Simulator (BMCS®) provides a sequential simulation structure for incorporating the HPGR module for HPGR simulation in closed circuits connecting to other comminution devices such as ball mill and air separators. Simulation of HPGR unit in open circuit based on Torres and Casali new approach was investigated by researchers (Torres and Casali, 2009, Hasanzadeh and Farzanegan, 2011). In this article, procedure of using of the model to simulate HPGR in closed grinding circuits with applying of Genetic Algorithm (GA) optimization search method for calibration of the model, were discussed. The details of GA applications for comminution simulation optimization and HPGR model calibration have been discussed elsewhere (Farzanegan and Vahidipour, 2009, Hasanzadeh and Farzanegan, 2011). The main objective of this work is to explore the benefits of GA-based modeling if it is integrated with a sequential simulation algorithm. Also, modeling and simulation of an industrial cement grinding circuit utilizing an HPGR unit which is used in a closed grinding circuit connected to an air separator is investigated.

2 SIMULATION OF HPGR IN OPEN CIRCUIT

In order to model and simulate HPGR units, authors used the new approach for modeling of HPGR units which has been presented by Torres and Casali, 2009. The model was implemented in both MATLABTM and ANSI C programming languages as separate stand-alone modules. For modeling and simulation of HPGR based on the new approach, a calibration step is needed to determine model parameters, i.e., the breakage and selection functions parameters. For this purpose, a new numerical script based on Genetic Algorithm (GA) was developed for calibration of model. GA tool of MATLABTM was used to minimize sum of the squared of differences (SSD) between measured and predicted particle size distributions of HPGR discharge stream. By minimizing of SSD using GA, the best model parameters are obtained. Validation of the HPGR simulator program was investigated using laboratory and industrial scales data sets. Obtained results confirmed high capability of GA for model calibration and also, correctness of programmed computational procedure of HPGR model in programming environment was supported (Hasanzadeh and Farzanegan, 2011).

3 SIMULATION OF HPGR IN CLOSED CIRCUIT

Process simulation tools are widely used to design new circuits and also optimize pre-existing circuits. Simulation of closed grinding circuits needs computer programs which can numerically handle a large number of processing units and streams. BMCS is a recursive initialization which refers to a modular and sequential simulation program which has been written in ANSI C language and can be run currently under DOSTM environment. The first version of BMCS, Ball Milling Circuit Simulator, had been developed for simulation of ball milling circuits (Farzanegan, 1998; Farzanegan et al., 1997). The current version of BMCS includes mathematical models for simulation of ball mill, rod mill, hydrocyclone, multi-deck vibrating screens, reduced efficiency curve based on Whiten model (for simulation of air separators and also intermediate and exit diaphragms in multi-compartment tube mills), junction, split and convergence units. In this work, authors tried to add HPGR module in BMCS. HPGR model was implemented in ANSI C programming language and added to BMCS. Incorporating HPGR module into BMCS made it possible to simulate HPGR units in closed circuit with air separators. The current BMCS is capable to simulate complex cement grinding circuits consisting of HPGR, air separators and multi-compartment tube mills in any configuration. Figure 1 shows structure of BMCS and interactions between main simulation module and various processing and auxiliary modules.

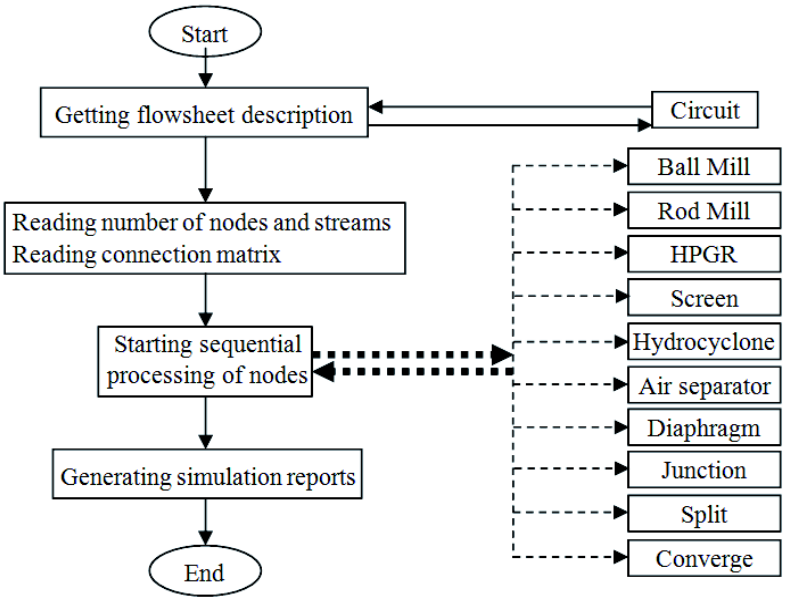

Figure 1. Simplified structure of BMCS program

4 SIMULATION OF AIR SEPARATORS

Researches done by JKMRC in Australia indicate that the Whiten relationship is valid for modeling of air separators (Napier-Munn et al., 1999). This approach is included in JKSimMet software. Conceptually, Whiten relationship is a mathematical description of a classifier's separation efficiency curve. This model is able to fit efficiency curves which exhibit fish hook phenomenon at fine sizes. Parameters of the air separator model are estimated by curve fitting process. They are found to be independent of operational variables and this makes the model suitable for simulation over various conditions. Whiten relationship is written as:

$$E_{\mathrm{OA}} = C\left[\frac{(1+\beta.\beta^{*}.x)(e^{(\alpha)}-1)}{e^{(\alpha.\beta^{*}.x)}+e^{(\alpha)}-2}\right] \quad (1)$$

Where is E_{OA} the fraction of feed entering the overflow, C is fraction of material which is subjected to real classification (by-pass fraction is 1-C), β is fish hook parameter of the normalized efficiency curve, β^{*} is a parameter used to define d_{50c}, α is parameter of separation sharpness of normalized efficiency curve ($d=d_{50c}$ when $E_{OA}=C/2$), x is d/d_{50c} ratio, d is mean size of size class, and d_{50c} is corrected cut size.

5 MODELING OF CEMENT CIRCUIT

The simulated flowsheet in this study includes a two-stage clinker and gypsum grinding circuit as shown in Figure 2.

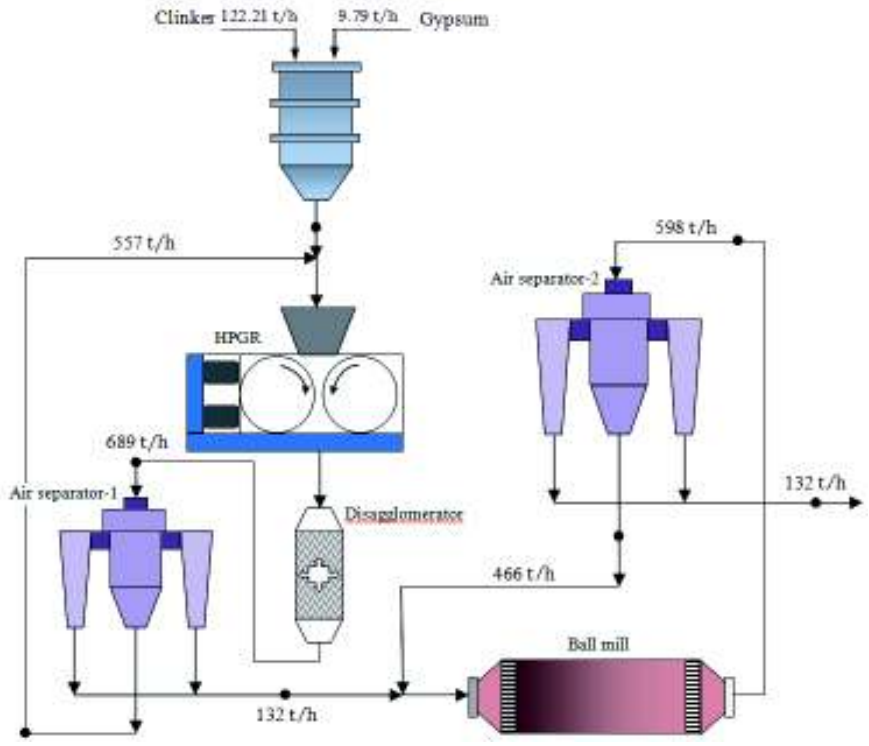

Figure 2. Flowsheet, sampling points and flow rate of circuit streams

The required information for circuit modeling was based on data published by Aydoğan et al., 2006. At first stage, HPGR operates with air separator in closed circuit. As HPGR product is agglomerated due to high pressures, so a simple impact unit was used after HPGR as disagglomerator. Product of first stage, air separator fines, is fed to the second stage. The second stage includes a ball mill and an air separator in closed circuit. The air separator fines stream in this stage is considered as final product. Sampling locations are depicted by black solid circles in Figure 2. Also, flow rates of streams are shown. Modeling and simulation steps of the cement circuit were done based on the algorithm depicted in Figure 3.

5.1 Calibration of HPGR model

Simulation of HPGR based on the model used in this work, needs input data such as roll diameter, roll length, rolls gap, roll peripheral speed, roll pressure, feed bulk density, flak density, particle size distribution of feed and also breakage and selection functions parameters. All input data except breakage and selection function parameters can be measured, but the breakage and selection function parameters (or model parameters: α_1, α_2, α_3, ζ_1, ζ_2, S_1^E) which are presented by following functional expression (Eqs. 2 and 3) should be calculated by calibration of model (Austin and Luckie, 1972; Herbst and Fuerstenau, 1980):

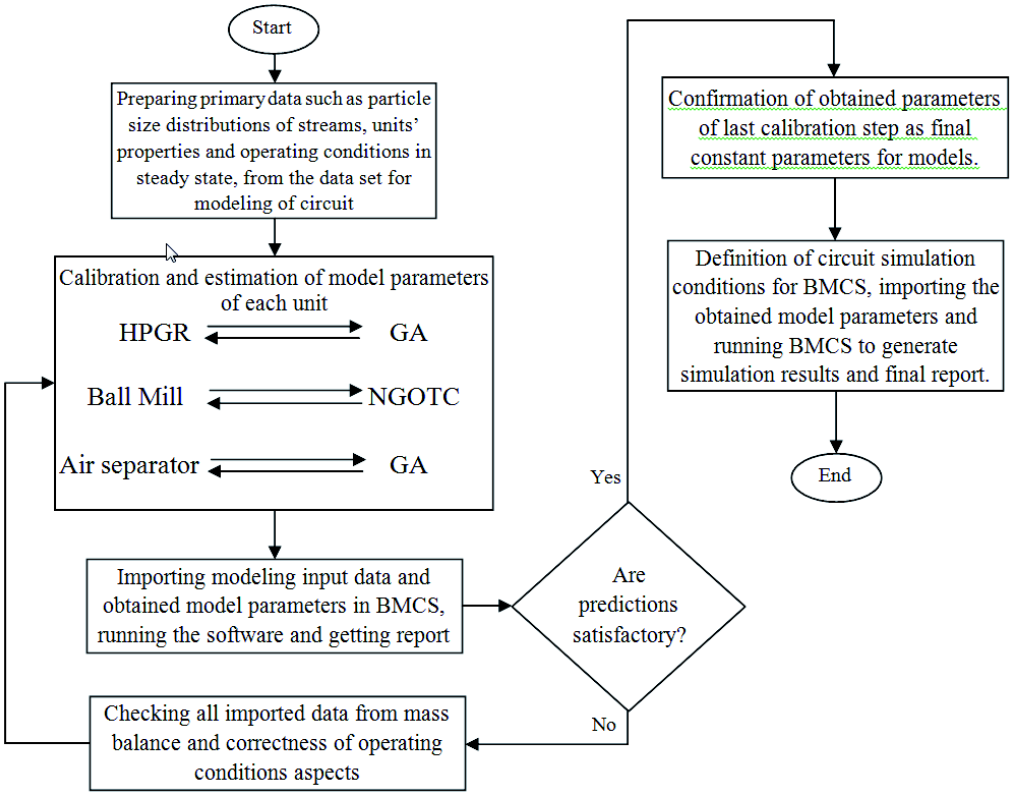

Figure 3. Modeling and simulation procedure

$$B_i(x_i) = \alpha_1\left(\frac{x_i}{x_1}\right)^{\alpha_2} + (1-\alpha_1)\left(\frac{x_i}{x_1}\right)^{\alpha_3} \quad (2)$$

$$\ln\left(\frac{S_i^{\mathrm{E}}}{S_1^{\mathrm{E}}}\right) = \zeta_1 \ln\left(\frac{\overline{x_i}}{x_1}\right) + \zeta_2\left(\ln\left(\frac{\overline{x_i}}{x_1}\right)\right)^2 \quad (3)$$

Where B_i is cumulative breakage function of ith size, S_i^{E} is specific selection function and x_i is particle size. As it was mentioned earlier, in this step, GA tool of MATLAB™ is used to minimize the SSD of predicted and measured product size distribution of HPGR discharge. For this purpose, feed and discharge particle size distributions of HPGR and other operational conditions at steady state of circuit were used. Results of calibration step are presented in Table 1.

Table 1. Summary of results and stopping criteria for HPGR model fitting using GA: breakage function parameters constraints: $0 \le \alpha_1 \le 1$, $0 \le \alpha_2 \le 10$ and $0 \le \alpha_3 \le 10$

	Stopping Criteria		Breakage Function Parameters			Selection Function Parameters			Goodness of Fit
	Generations	Stall generations	α_1	α_2	α_3	ζ_{11}	ζ_{21}	S_{11}^{E}	SSE
Run 1	1000	1000	0.994	1.022	1.154	0.182	0.004	0.75	43.94
Run 2	3000	3000	0.935	1.159	1.16	0.142	0.002	0.732	42.46
Run 3	5000	5000	0.934	1.204	1.215	0.116	0	0.712	41.79

Calibration using GA was done in several runs with increasing of number of generations to confirm that the obtained parameters lead to global minimum for SSD and also are the best model parameters. Since increasing of the generations in third run of GA search did not change the value of SSD significantly (Table 1), it can be concluded that the search algorithm has been converged to the SSD global minimum value. The parameters which generate the minimum value of SSD (run 3) were kept as the best model parameters. Figs. 4 and 5 show the calculated breakage and selection functions curves using estimated parameters presented in Table 1 (run 3), respectively.

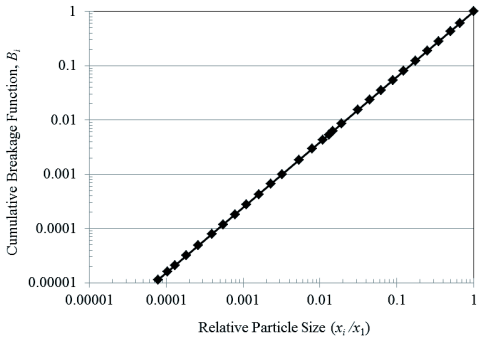

Figure 4. The plot of estimated breakage function

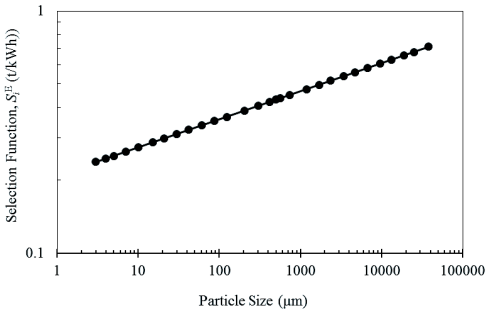

Figure 5. The plot of estimated selection function

5.2 Calibration of Air Separator Efficiency Curve Model

To estimate the parameters of Whiten relationship the actual recovery of material to overflow for each size fraction was calculated using Equation [4]. Then, the best values of Whiten model was computed by minimizing the sum of the squared of differences between actual and model predicted recoveries. Genetic algorithm of MATLABTM with required constraints for each parameter was again applied here to perform nonlinear model fitting process.

$$E_{\mathrm{OA},i} = \frac{Oo_i}{Ff_i} \tag{4}$$

in which $E_{\mathrm{OA},i}$ is the fraction of material in size class i of feed which is entered to overflow, O and F are respectively overflow and feed flow rate, and o_i and f_i are fraction of size class i in overflow and feed respectively.

5.3 Calibration of Ball Mill Model

Modeling of ball mills in BMCS is based on the solution of the linear system of rate mass balance equations, Equation [5], for batch grinding and using Weller's residence time model, Equation [6], for describing the mass transport through the mill in continuous operations (Austin and Luckie, 1972; Prasher, 1987, Weller, 1980):

$$\frac{dm_i}{dt} = -S_i m_i + \sum_{j=1}^{i-1} b_{ij} S_j m_j, \quad for\ i = 1,2,\ldots,n \tag{5}$$

Where m_i is mass remained on ith screen, S_i is selection function of ith size and b_{ij} is non-cumulative breakage function of ith size class when particles are broken from jth parent size class.

$$f(t) = \frac{\alpha}{\tau_l}\left[-\frac{t-\tau_{pf}}{\tau_s}\exp\left(-\frac{t-\tau_{pf}}{\tau_s}\right) - \alpha\exp\left(-\frac{t-\tau_{pf}}{\tau_s}\right) + \alpha\exp\left(-\frac{t-\tau_{pf}}{\tau_l}\right)\right]; \quad \alpha = \frac{\tau_l}{\tau_l - \tau_s} \tag{6}$$

τ_{pf}, τ_l and τ_s denote parameters of Weller's residence time distribution model. As breakage function is an inherent property of materials and is constant for any type of material, the breakage function obtained in HPGR calibration step was used for ball milling, too. NGOTC® (Numerical Grinding Optimization Tools in C) program was used for back calculation of ball mill selection function. In this step, feed and product size distribution of ball mill in steady state of circuit and also the obtained breakage function were used as input data to calculate selection function.

5.4 Results of Modeling

After calibration of units' models and preparing of required input data for each unit, it is possible to run whole of the circuit (Figure 1) in BMCS environment. For this purpose, at first step the circuit should be defined for BMCS and afterward input data file should be prepared based on the circuit. Particle size distribution of fresh feed and its flow rate are the only known information of the circuit streams. So, fresh feed information and parameters of units' models which were obtained from calibration step are imported in BMCS input data file. After running of BMCS, results of simulation including tonnages and particle size distribution of streams are obtained, which are presented in Table 2 and Figure 6, respectively.

Table 2. Measured and predicted flow rates of streams at modeling step

	Measured Stream Flow Rate (t/h)	Predicted Stream Flow Rate (t/h)	Error (%)
HPGR feed	689	704.83	2.3
Air separator-1 fines	132	132.11	0.09
Air separator-1 coarse	557	572.86	2.85
Ball mill feed	598	616.59	3.11
Air separator-2 fines	132	131.99	0.01
Air separator-2 coarse	466	484.48	3.97

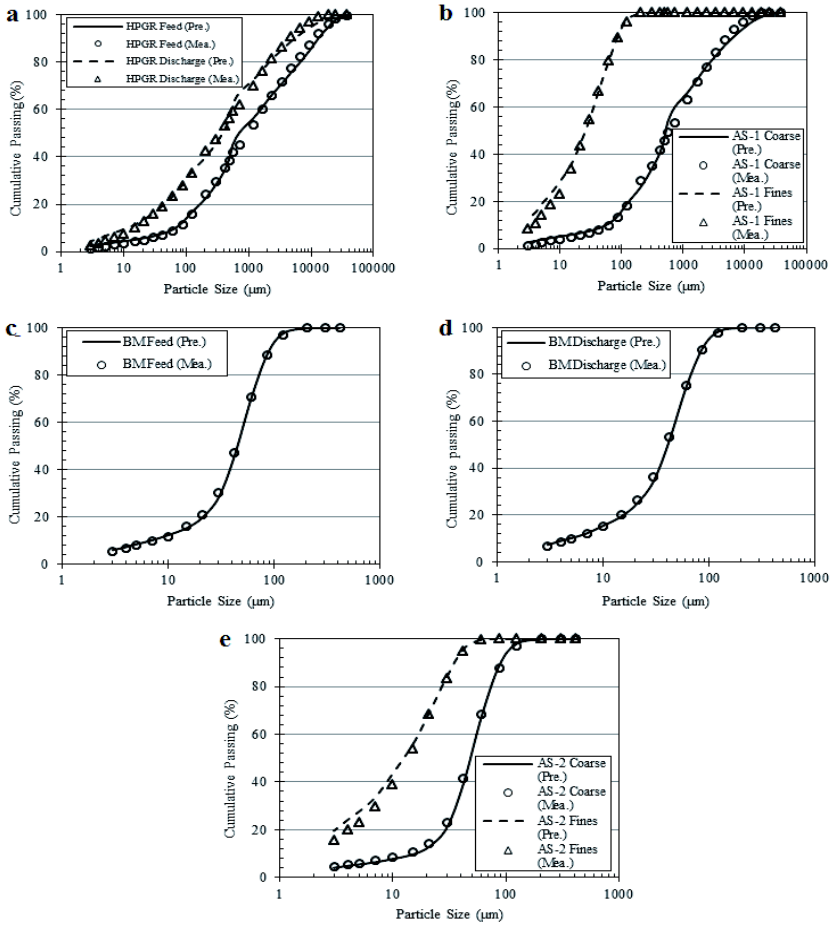

Figure 6. Measured and predicted particle size distribution of streams at modeling step: a. HPGR feed and discharge; b. first air separator fines and coarse; c. ball mill feed d. ball mill discharge; e. second air separator fines and coarse

As it is clear in above table and graphs, using the approach of independent model calibration (separate calibration of each unit's model based on steady state information of circuit) which is more based on back-calculation of breakage and selection functions using robust GA and numerical search method, resulted to high accuracy prediction of particle size distributions and tonnages of various streams in the circuit. Results of this stage showed that independent calibration of the models with powerful search methods such as GA leads to highly accurate models.

6 SIMULATION OF CEMENT CIRCUIT

Simulation studies were done on the same circuit (Figure 2). This stage, simulation, was used to confirm correctness of the calibration procedure and to validate the obtained models' parameters. The required input information for this stage was based on the data reported in a recently published article for the circuit operating under new conditions (Aydoğan and Benzer, 2011). For simulation purpose, new conditions of circuit fresh feed size distribution and increased fresh feed flow rate were used. The flow rate was increased from 132 t/h in modeling step to 150 t/h in simulation step. Figure 7 shows particle size distribution of fresh feed which were sampled for modeling and simulation steps.

Circuit simulation under new conditions was carried out considering the fact that models' parameters obtained from modeling step do not change and can be assumed as constants. Fresh feed new conditions were applied on simulation data file and then BMCS was run. Results of simulation step including streams' flow rates and particle size distribution of all streams are presented in Table 3 and Figure 8, respectively.

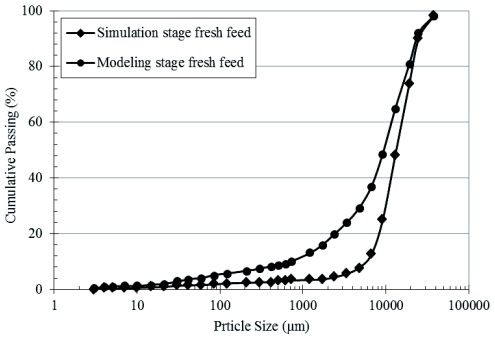

Figure 7. Circuit feed size distribution used in modeling and simulation steps

Table 3. Measured and predicted tonnages of streams at simulation step

	Measured Stream Flow Rate (t/h)	Predicted Stream Flow Rate (t/h)	Error (%)
HPGR feed	720	859.75	16.25
Air separator-1 fines	150	149.93	19.7
Air separator-1 coarse	570	709.82	0.05
Ball mill feed	447	662.99	32.58
Air separator-2 fines	150	149.92	0.06
Air separator-2 coarse	297	513.08	42.11

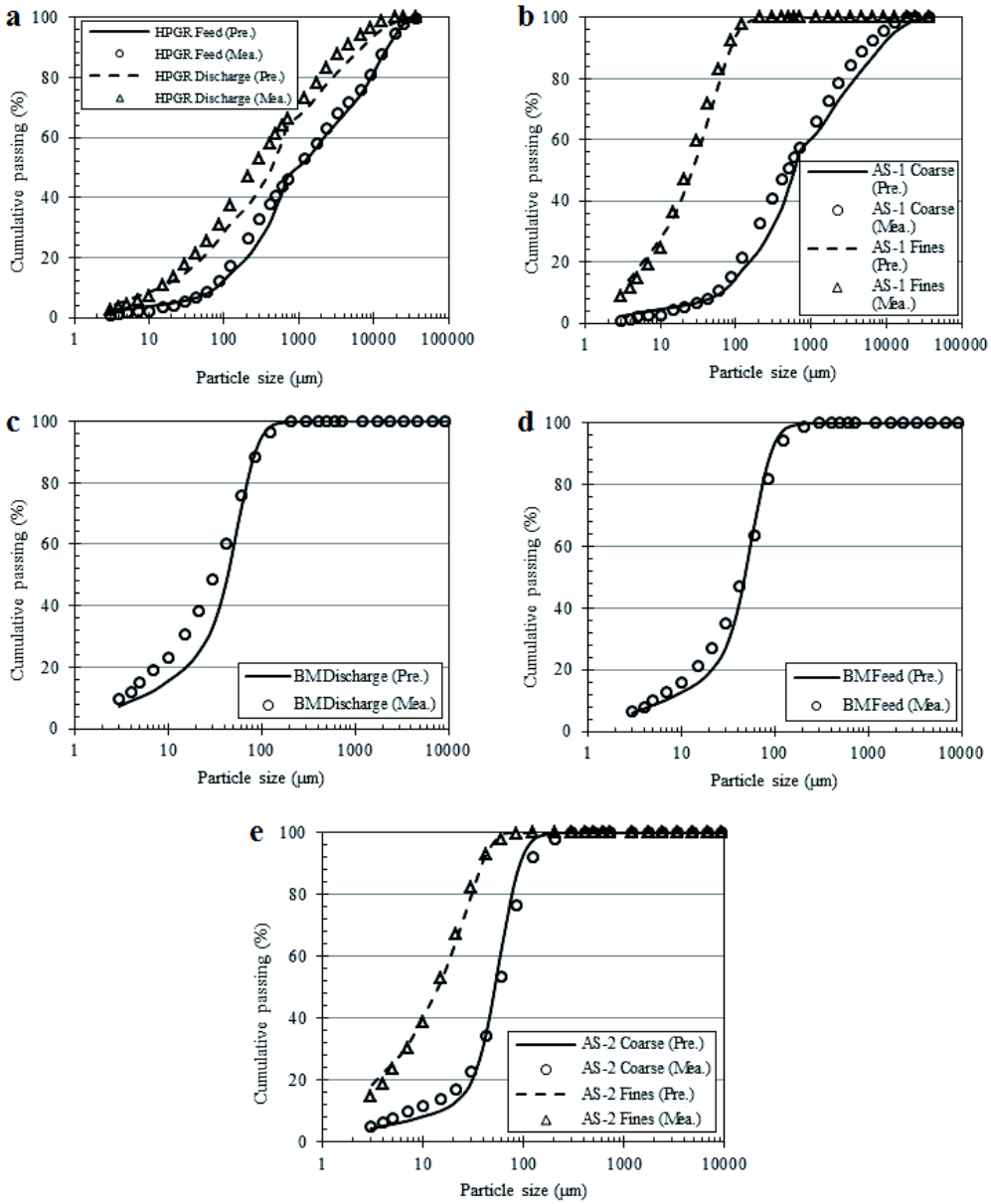

Figure 8. Measured and predicted particle size distribution of streams at simulation step: a. HPGR feed and discharge; b. first air separator fines and coarse; c. ball mill feed d. ball mill discharge; e. second air separator fines and coarse

The simulation results for the first stage of the grinding circuit, HPGR in closed circuit with the first air separator, are quite acceptable. The low differences between measured and predicted values for this stage are due to the imprecise values of rolls' gap and pressure used to perform simulations. The values of the rolls' gap and pressure parameters which were used in simulation step were the same as ones used in modeling step. It must be noted that when the fresh feed flow rate of the circuit is increased, the rolls' gap and pressure will be changed, accordingly.

For the second stage of grinding circuit, i. e., ball mill in closed circuit with the second air separator, simulation results particularly flow rate of streams do not agree with the measured ones. Considering to measured flow rates of the streams (Tables 2 and 3), despite to increasing of fresh feed of circuit from 132 t/h in modeling step to 150 t/h in simulation step, the circulating load of second part of circuit decreased. Whereas the measured particle size distribution of the both air separators' fines in modeling step are closed to the same streams in simulation step, so with increasing of flow rate, the circulating load of the second part of the circuit should be increased similar to what happened for the first part of circuit, but as it can be seen in Tables 2 and 3, the circulating load decreased from 466 t/h in modeling step to 297 t/h in simulation step. The differences between measured and predicted flow rate in second part of the circuit in simulation step are attributed to reported changes applied on the ball mill unit after sampling had done for calibrating the ball mill model. Replacing liner and lifters and also charging new balls are the changes which can be applied to the ball mill for optimization of comminution. These changes cause improvement in mill selection function and therefore materials are comminuted faster and finally the circulating load decreases. Considering aforementioned reasons, the discrepancy between measured and predicted streams' flow rate and also low differences between particle size distributions of the streams are plausible.

7 CONCLUSIONS

The integration of GA-based model fitting and sequential grinding simulation approaches for prediction of closed circuits performances with recycle streams was investigated. It was shown that calibration of HPGR and air separator models can be done with a high degree of reliability in MATLAB™ environment using GA search method. HPGR and air separator models were coded in ANSI C language as new modules and were added to BMCS program to simulate cement grinding plants. The preliminary results from this research show that incorporating powerful new search methods such as genetic algorithms into mineral processing simulators can be very helpful for more successful and better process modeling. The goodness of fit shows that the applied calibration procedure can be used successfully for simulation of HPGR in closed grinding circuits. This procedure can be very helpful for optimization of an existing plant when drop weight or other ore hardness characterization tests are unavailable.

REFERENCES

Aydoğan, N. A., Ergün, L., Benzer, H., 2006. High pressure grinding rolls (HPGR) applications in the cement industry. *Miner. Eng.*, 19, pp. 130–139.

Aydoğan, N. A., Benzer, H., 2011. Comparison of the overall circuit performance in the cement industry: High compression milling vs. ball milling technology. *Miner. Eng.*, Vol. 24, pp. 211-215.

Benzer, H., Ergün, L., Aydoğan, N.A., Dikmen, S., Erdem, S., Genc, O., Ozer, C.E., 2003. Performance evaluation of the cement and raw meal grinding circuits of Bati Anadolu Cimento Sanayii AS, unpublished report.

Daniel, M.J., Morrell, S., 2004. HPGR model verification and scale-up. *Miner. Eng.*, 17 (11–12), pp. 1149–1161.

Farzanegan, A., 1998. *Knowledge-based Optimization of Mineral Grinding Circuits*. Ph.D. Thesis, University of McGill, Montreal, Canada.

Farzanegan, A., Laplante, A.R., Lowther, D.A., 1997. A knowledge-based system for an off-line optimization of ball milling circuits. In: *Proceedings of 29th CMP Conference*, Ottawa, pp. 165–185.

Farzanegan, A., Vahidipour, S. M., 2009. Optimization of comminution circuit simulations based on genetic algorithms search method. *Miner. Eng.*, 22, pp. 1137–1146.

Hasanzadeh, V., Farzanegan, A., 2011. Robust HPGR model calibration using genetic algorithms. *Miner. Eng.*, 24, pp. 424-432.

Herbst, J. A., Fuerstenau, D. W., 1980. Scale-up procedure for continuous grinding mill design using population balance models. *International Journal of Mineral Processing*, 7, pp. 1–31.

Luckie, P.T., Austin, L.G., 1972. A review introduction to the solution of the grinding equations by digital computation. *Miner. Sci. Eng.* 4 (2), pp. 24–51.

Morrell, S., Shi, F., Tondo, L.A., 1997. Modeling and scale-up of high pressure grinding rolls. In: *Proceedings of the XX International Mineral Processing Congress (IMPC)*, Aachen, Germany.

Napier-Munn, T.J., Morrell, S., Morrison, R. D. and Kojovic, T., 1996. *Mineral Comminution Circuits; Their Operation and Optimisation*, JKMRC Monograph Series in Mining and Mineral Processing, No. 2, Jullius Kruttschnitt Mineral Research Center, Australia.

Patzelt, N., 1992. High pressure grinding rolls, a survey of experience. *IEEE Cement Industry Technical Conference*, Dallas/Texas 0 (14), 180.

Prasher, C.L., 1987. *Crushing and grinding process handbook*. John Wiley & Sons Ltd.

Torres, M., Casali, A, 2009. A novel approach for the modeling of high pressure grinding rolls. *Miner. Eng.*, 22, pp. 1137–1146.

Weller, K. R., 1980. Hold-up and residence time characteristics of full scale grinding circuits. In Automation in mining, mineral and metal processing: *Proceedings of the 3rd IFAC symposium*, Montreal, pp. 303-309.

Stochastic Mine Planning in the Las Cuevas Coal Mine

G. Franco, J. Branch and P. Alvarez

Mines Faculty, National University of Colombia, Medellin

ABSTRACT In the mine planning processes for open pit coal mines in Colombia, there is no evidence of the use of tools for decision making under scenarios of uncertainty that make it possible to conduct such processes using meta-heuristic techniques.

Key variables were identified as well as the uncertainties associated with them in the process of stochastic mine planning. Likewise, a model for optimization under uncertainty is presented that reduces associated risks and maximizes the profits and goals of the mine planning process. Some of the stochastic variables defined in this model are: coal price, percentage of recovery, capital costs, operating costs, availability of equipment in mines, and plant and port availability. These variables have probability distribution functions ranging from *lognormal* and *triangular* to *normal*. Finally, the Colombian mining sector requires the development of a solution algorithm for the stochastic optimization model combining optimization and simulation techniques.

1 THE MODEL

During the past three decades research has led to the development of the basis of uncertainty. This has in turn led to the implementation of new methodologies for modeling and addressing geological and market risks during mine planning. These methods have been incredibly helpful for PNV optimization and decision making whenever there is uncertainty in mining projects.

In the current projects for mining mineral resources, mine planning and design are carried out using deterministic techniques that disregard the risk and uncertainty involved in mining.

Current economic analyses are carried out on the assumption that the values of all the variables are known with certainty. Nevertheless, there is never absolute certainty in mining projects, as there are a number of factors with considerable uncertainty. Applying probabilistic models to the analysis of investment projects provides a more rigorous procedure and, consequently, a more secure basis for decision making. (Bustillo & Lopez Jimeno, 1997).

Mine planning is a process which depends on a system of complex, interdependent, and highly uncertain inputs (Tokin, 2009). These inputs include the geological model, the block model, and the ore's market price. One of the results of the planning process is the identification of the exploitation limit. Figure 1 shows the main inputs of the mine planning process with a high degree of uncertainty. The result of the mine planning process can be observed.

The classical estimates of reserves used in open pit mines are obtained through geostatistical methods (ordinary Kriging or other). This classical method provides information on the quality and quantity of

the ore in the block without directly taking into account uncertainty. (Marcotte & Caron, 2012)

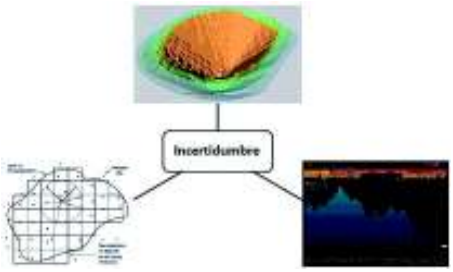

Figure 1: Uncertainty regarding the mine planning process(Whittle, 2009; Sinclair, 2004).

Deterministic methods generate unrealistic expectations of the Net Present Value (NPV), since there is no absolute certainty regarding the quality and tonnage of the ore contained in the blocks that are to be extracted. Therefore ore production performance, mine size, and the final pit design are flawed and inefficient, which leads to lower expected earnings for each period of the mine's life (Dimitrakopoulos, 2010).Furthermore, the future price of the ore cannot be known with certainty.

Figure 2 shows the possible planning options (deterministic and stochastic methods) for a small gold deposit. Figure 2 shows that if the profitability of the conventional open pit design that has been built is compared to the profitability of the site's equally probable simulated scenarios, its performance will possibly not meet expectations, and the PNV of the expected conventional scenario is 2% to 4% likely to occur, while the PNV is expected to be 25% less than expected. (Dimitrakopoulos, 2010).

This is why proper design and mine planning using stochastic optimization tools will increase the productivity and competitiveness of these mines in the short and long terms. This will lead to sustainable exploitation (in technical, economic, social, and environmental terms) (Franco, Branch, & Jaramillo, 2012).

There are results showing that the selection process for the design and flexibility of the operation can be improved by including uncertainty. In the near future, schedules could include more mechanisms to analyze risk and other types of flexibility management, such as the flexibility to redefine the cut off grade in order to further improve the design of the selection process. (Sabur and Dimitrakopoulos, 2010).

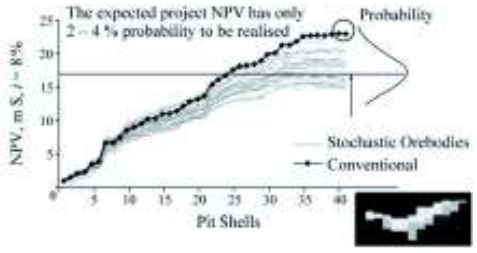

Figure 2: Comparison of the Deterministic vs. Stochastic methods. Dimitrakopoulos, 2010

The planning process in mining is basically an optimization problem that can be solved using linear programming, integer programming, or stochastic programming. (Franco, Branch, & Jaramillo, 2012).

2 UNCERTAINTY IN THE MINERAL EXTRACTION OPERATION

Methods were found such as simulated annealing, stochastic integer programming, genetic algorithms, etc. with regards the

uncertainty relating to mining activity (Dimitrakopoulos, 2010).

2.1 Simulated Annealing

Simulated annealing is a heuristic optimization method used for solving problems. When several production programs are being studied, there is always a set of blocks that is assigned to the same production period across all the production programs. These are known as certain probability blocks, meaning that there is a 100% probability of finding ore within them. In order to handle the uncertainty in the blocks that do not have a probability of 100%, the simulated annealing method redistributes these blocks among candidate production periods in order to minimize the mean deviation of the production objectives for N mining periods, and for an S series of models of simulated sites. The objective function representing this model is:

$$Min\emptyset = \sum_{n=1}^{N}\left(\sum_{s=1}^{S}\left|\theta^{*}{}_{n}(s)-\theta_{n}(s)\right|+\sum_{s=1}^{S}\left|\omega^{*}{}_{n}(s)-\omega_{n}(s)\right|\right) \quad (1)$$

Where $\theta^{*}_{n}(s)$ and $\omega^{*}_{n}(s)$ are the production objectives for ore and sterile waste respectively, and θns and ωns are the real production of ore and sterile of the disturbed mining sequence. Each block redistribution is termed a disturbance. The probability of accepting or rejecting a disturbance is given by:

$$Prob\{accept\}\begin{cases} 1, & si\ O_{new} \le O_{old} \\ e^{\frac{O_{new}-O_{old}}{T}}, & otherwise \end{cases} \quad (2)$$

This implies that all the positive disturbances ($O_{new} \le O_{old}$) are accepted with a probability of one and the negative disturbances are accepted on the basis of a distribution whose probability is exponential, where T represents the annealing temperature.

The steps used in this approach are illustrated in figure 3. These steps are: (a) defining the rates of mined ore and mining waste; (b) defining a set of nested pits using the Lerchs-Grossmann algorithm or any other pit parameterization procedure; (c) using a commercial scheduler to schedule a number of simulations for a given site (a) and (b); (d) using simulated annealing as shown in equation (2), using the results from (c) and a set of simulated sites; and (e) quantifying the risk in the resulting schedule and key indicators of the project through the related site simulations.

S_1 ... S_n are site simulations performed using a conditional simulation algorithm; S_{eq1}... S_{eqn} are the mining sequences for each S_1 ... S_n. Extraction rates are entered into the process

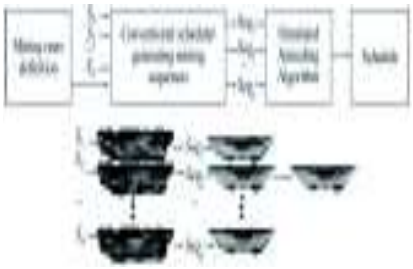

Figure 3: Graphic demonstration of the simulated annealing method (Dimitrakopoulos, 2010)

2.2 Stochastic Integer Programming

Stochastic Integer Programming (SIP) provides a framework for optimizing mine production schedules while taking uncertainty into account. The SIP method generates a sequencing of the optimal production using equally probable simulated block models from the site as input. The

related qualities are not averaged. The optimal production schedule is thus the sequencing which can produce the maximum PNV that can be attained in the project, given the level of uncertainty available in the site described through a set of stochastic simulation models.

The proposed SIP model makes it possible to manage geological risk in terms of meeting the objectives set for the current production. This is unlike traditional programming methods, which use a single site model in which the risk is randomly distributed between production periods while there is no control over the magnitude of the risks in the sequencing. The general form of the objective function is:

$$Max \sum_{t=1}^{p}\left[\sum_{i=1}^{n} E\left[(NPV)_i^t\right] b_i^t - \sum_{s=1}^{m}\left(c_u^{to} d_{ui}^{to} + c_l^{to} d_{li}^{to} + c_u^{tg} d_{ug}^{tg} + c_l^{to} d_{lg}^{to}\right)\right] \quad (3)$$

Where p is the production period, n is the number of blocks, and bit is the decision variable for the moment in which the block is extracted i (if extracted during period t, bit is one. For all other blocks, bit is zero). The c variables are the costs per unit of deviation (represented by the d variables) of the production objectives for the degrees and tons of ore. Subscript u corresponds to the deviations and costs of excess production (upper limit), whereas subscript l stands for production shortage (lower limit). Subscript s is the number of the simulated ore deposit, and subscripts g and o are ore quality and production.

Figure 4 shows a graphical representation of the SIP model. The sequencing was optimized by focusing on the second component of the objective function expressed in equation (3) and minimizing the deviation of the production objectives while optimizing the sequencing.

This leads to sequencings where the potential deviations in the production objectives are reduced to the minimum amount obtained in the production schedules, seeking to first extract not only the blocks with the highest quality, but also those with a high probability of containing ore.

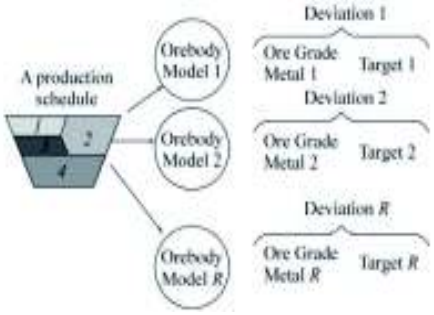

Figure 4: Graphical representation of the stochastic integer programming model (Dimitrakopoulos, 2010)

2.3 Genetic Algorithms

Genetic algorithms are a search process imitating the way in which genetics and natural selection work. The search starts with a population of random solutions. This population evolves over a series of generations by applying probabilistic techniques and reproduction operators for each member of the population. The reproduction operation consists of two main steps known as crossover and mutation. The crossover operator combines selected pairs of solutions to produce new and potentially better ones. The mutation operator provides the possible diversity within the population. The solutions' chance of survival for the next generation depends on their quality.

The major steps of the genetic algorithms approach are (Sattarvand & Niemann-Delius, 2008):

a. Representing the Pit as a Chromosome.

The shape of any possible pit in a particular block model could be represented by a simple integer matrix. Each element of this matrix describes the geometric depth of the pit in a column of the block model.

Therefore, for a large block model of $I_{num}\times J_{num}\times K_{num}$ size, the length of any pit will be $I_{num}\times J_{num}$, where the pit's depth is in a grid (i,j) and will be stored in the matrix at position $(I_{num}\times i)+j$. Similarly, a particular long-term planning schedule for an open pit mine can be represented using a matrix, considering the depth of the mine in each column of the block model for each of the production periods.

b. Initial Population

The process starts when a random population of feasible sequencings is generated. The population size is one of the controllable parameters in the system. This parameter's value is established as 50 based on experience.

c. Assessing Pit Performance

Calculating performance is crucial for the success of a genetic algorithm. The performance value is calculated for each of the schedules in the population that is the Net Present Value (NPV) of the sequencing.

d. Reproduction of the Population in the Pits.

During the reproductive stage that gives rise to a new generation, individual sequences either survive into the next generation or are completely discarded. In this process the schedules with higher profitability are more likely to survive than those with lower profitability. The reproduction phase is critical, therefore there must be sufficient genetic diversity, and it should be maintained from generation to generation. Convergence to an optimum result must also be sufficiently fast, thus making it possible to obtain good schedules to reproduce faster than bad schedules.

During the crossover phase approximately 70% of the schedules are combined randomly on a probabilistic basis. This will result in crossed pairs which have changed the characteristics of the sequencings. Some of these pairs have higher performance values which improve their chance of surviving into future generations; other pairs, however, have lower performance values, reducing their chances of survival.

The mutation is also performed on a probabilistic basis, its value being approximately 0.1% of the cells in the random sequencings in order to maintain genetic diversity and prevent the system from converging on a false optimal value.

e. Normalizing Pits

Both crossover and mutation can cause the resulting pits to violate operational constraints. After each operation of this kind, the resulting pits should be normalized. This involves modifying the sequencing as little as possible to ensure that the exploitation limits, i.e. the number of cells in each planning period, are not incorrect.

f. Termination Condition of the Algorithm.
The number of generations required to reach optimal sequencing varies depending on the complexity and the scale of the problem. However, the manner in which the genetic algorithm is formulated has a significant effect on system efficiency.

Figure 5 shows a graph of the previously described steps.

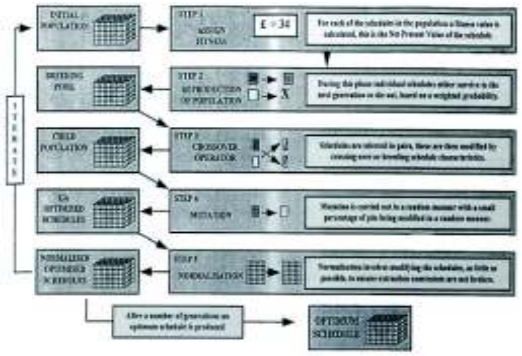

Figure 5 : Graphical representation of the genetic algorithm (Sattarvand and Delius, 2008)

3 CONCLUSIONS

A. The advantage that stochastic models have compared to traditional models is the quantification of the risk and uncertainty present in each of the proposed scenarios. This facilitates decision-making and provides knowledge regarding the risk associated with this decision.

B. The application of stochastic programming models goes beyond mine planning, since they can also be applied to any process in the mining sector where the uncertainty of the variables makes it difficult to find an optimal solution.

C. In Colombia these methods have considerable scope, as no mining operation has implemented them up to this point.

D. A single deterministic simulation with a fixed price is not enough for mining design and planning, since the uncertainty in the market or in other variables of the mining business renders this simulation unable to provide sufficient information concerning the behavior of the deposit. The various simulations and their assessments make it possible to choose an optimal pit design, make adequate deposit estimates, and evaluate the projects during their pre-feasibility stage. The application of stochastic ideologies in the Colombian mining sector becomes more necessary in order to increase company profits.

E. Due to the formation of the ore deposits, the pits generated have an elongated shape along the line of outcrop of the mantles. Likewise, since the mantles are located in a syncline, they have a 70º dip in the outcrop which decreases as the mantles become deeper. The dip reaches up to 30º. For those reasons, implementing an open pit exploitation method is not enough to extract the entirety of the optimistic reserves. A pit would extract 50% of the reserves in the area; hence the possibility of combining open pit and underground exploitation methods is proposed in order to exploit as

many reserves as possible, thus maximizing the project's profitability.

F. It is necessary to change the current mine planning methodologies in Colombia for methodologies that have more satisfactory scopes for the entire mining sector. This should be done while taking into account uncertainty, which is usually disregarded when the mine's lifespan is being planned.

REFERENCES

Bustillo, M., & Lopez Jimeno, C. (1997). *Evaluacion y Diseño de Explotaciones a Cielo Abierto.*Madrid: Entornos Graficos, S. L.

Dimitrakopoulos, R. (2010). Stochastic Mine Planning Optimisation: New Conceots, Applications and Financial Contribution. *MININ 2010*, p173 - 182.

Franco, G., Branch, J., & Jaramillo, P. (2012). Planeamiento de Minas a Cielo Abierto Mediante Programación Estocástica. *Revista Boletín Ciencias de la Tierra*, p107 - 113.

Hillier, F. S., & Lieberman, G. J. (2010). *Introducción a la Investigación de Operaciones*.

Marcotte, D., & Caron, J. (2012). Ultimate open pit stochastic optimization. *Computers & Geosciences*.

Sabur, A., & Dimitrakopoulos, R. (2010). Mine desing under geologic and market uncertainties. *MININ 2010*, p183 - 194.

Sattarvand, J., & Niemann-Delius, C. (2008). Perspective of metaheuristic optimization methods in open pit production planning. *21st World Mining Congress*, P 143 - 154.

Sinclair, A. J., & Blackwell, G. H. (2004). *Applied Mineral Inventory Estimation.*

Tokin, C. (2009). Advancing Strategic Mine Planning - A Software Perspective. *Advances in Orebody Modelling and Strategic Mine Planning I*, P 135 - 140.

Whittle, G., Stange, W., & Hanson, N. (2007). Optimising Project Value and Robustness. *Project Evaluation Conference*, P 147 - 155.

Defining the Coal Layer (Block 61) 3D Model in Brown Coal Mine Đurđevik, BiH

M.Omer, G.Kemal
University of Tuzla, Faculty Mining Geology and Civil engineering, Tuzla, BiH

O.Dean
University of Tuzla, Faculty Mining Geology and Civil engineering, Tuzla, BiH

ABSTRACT Defined coal layer, blocks 67a, 67b and 68 in coal mine "Đurđevik'" with a network of wells, active mining operations and the 3D model, can be used for the interpretation of the block 61, which is a larger area, and with considerably less research works. The aim was to define the continuation of coal seam that is block 61 with its basic elements and present in the 3D model.

1 GENERAL PART

1.1 Geographical Location of Coal Mine „Đurđevik"

Coal mine "Đurđevik" is located on northeastern part of Bosnia, south of the town of Tuzla, at a distance of about 15 km, on the left side of the road Sarajevo-Zupanja. Relief from the foothills of the mountains to the south Djedinske is hilly with a general inclination towards the north where the hills gradually disappear. The average elevation of exploitation field is 350 meters above sea level. The area of the basin "Đurđevik" is elongated in the NW-SE, 5.5 km in length and the width varies from 1 to 2.5 km. Torque "Đurđevik" surface coal basin is approximately 13 km^2 and is located approximately 4 km east of Banovići basin (DRP, 2008).

1.2 History of Research

Research of the "Đurđevik" basin originate from the end of last and the beginning of this century. The greatest value of the papers Kattzera 1921. They are more accurate and more analyzed coal series "Đurđevik" basin and provides information on the amount of coal. The first harvesting starts 1936th years and is still going to break the 1943-45.godine. Exploration drilling began after the 1945 trial a rare network of wells, and later a denser network in those localities that could dig up superficial manner. The main aspect of the research was exploratory drilling with a total of 45 exploration wells and the 100 x 100 m networks. In addition to exploration drilling at this site has been created and a large number of mining premises have also yielded useful information about the geological relations of the reservoir. Exploratory drilling of the entire area are continued in the later period where usually aggravated the research of pit "Đurđevik II" where until 1990. Were drilled 71 wells and the achieved drilling 50x100 m networks (DRP, 2008).

1.3 Geological Characteristics

Coal seam thickness ranges from 12 to 25 m by blocks. Coal layer is a special lithostratigraphic member in the total series young and according to some faunistic findings and analogy with other basins old coal layer and parts of the top of the lower Miocene. Coal layer in this section is to provide an east-west direction with drop south to 30 °. On the northern edge of the coal layer is shallow, and such areas are

affected by surface mining. Overlaying makes thick series marl and marly limestones with interbeds of other varieties similar in composition. The transition from coal seam in the immediate overlaying is sharp and clear that is not the case with the slope. Over the carbon layer is a solid package of calcareous marl in places up to 40 meters. Medium overlaid with the composition of the gray marl which rotate with dark marl. The higher the roof of the middle of the top of the continuation and quality and schedule classes (DRP, 2008).In "Đurđevičk" basin younger rocks are densely dotted. Larger fragmentation attributable orogen stages post Miocene period, however, there are many small faults that are difficult to orient and assign stage belong. On a small horizontal distance during pit mapping corridor in the pit "Đurđevik" I encountered five meter line disturbances coal seam, whose jump was 1-2 meters. It should be noted that there are long fault zone (100 meters) without the disorder. Fault tectonics is not equally represented in the basin, and it probably contributes to the density and intensity of the fault from the basic mounts.

Pit area is crisscrossed by faults of different directions and intensities. The biggest among them is the gravitational normal fault that separates this area from open pit. It stretches by the middle of the basin, east-west direction with the fall of the south, from digging up Brezje to Visce. Along with him, to the south at a distance of 50-200 meters there are two reverse faults fall between the faults which run north-south, which are quite complicated this middle area. The biggest faults are along the periphery of the basin in the middle of the"Đurđevičk" basin. Simultaneously along them drawn boundaries pits.

Other faults are low-intensity, but generally so large that interrupt coal layer, closing one block of coal to the amount of 100,000 tons to 2,500,000 tons. Among them we should mention whose fault direction of the largely coincides with the flow of the stream Stupnica. In the pits "Đurđevik-II" was also noted by several faults which are ranked papers present pit. Their lines penetrate deeper into this area and disrupt the continuity of the coal deposit, Figure 1 (DRP, 2008).

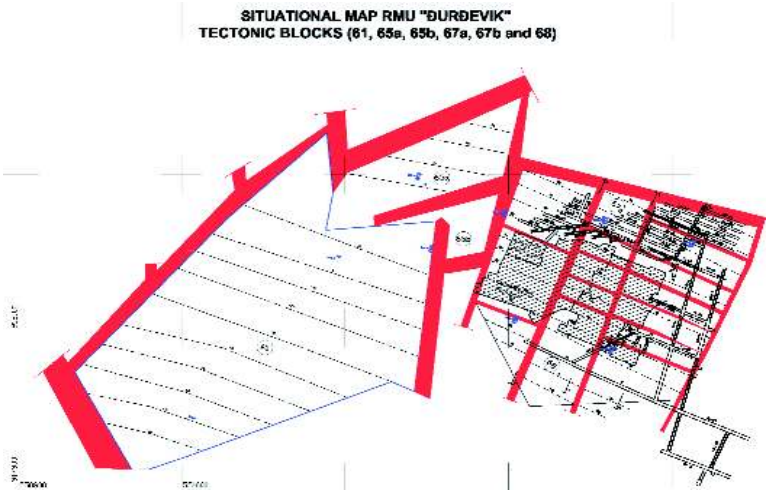

Figure 1. Situation map pits „Đurđevik II“ (bloks 61, 65a, 65b, 67a,

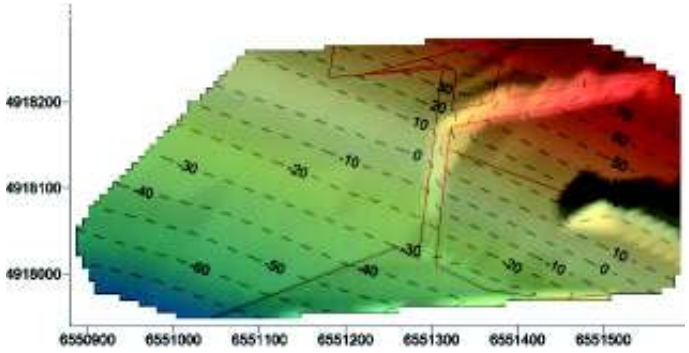

Figure 2. Situation map of the spatial relationship between tectonic blocks

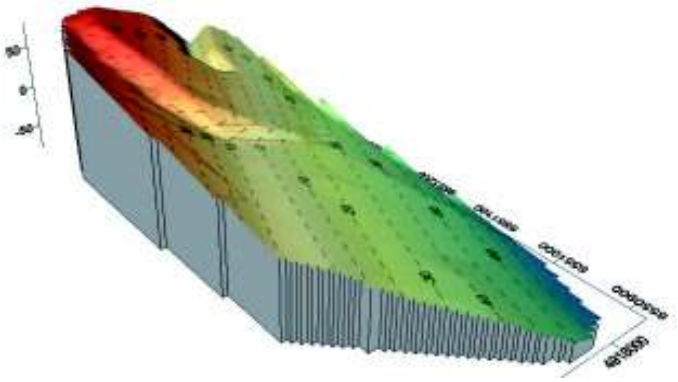

Figure 3. Situation map of the spatial relationship between tectonic blocks

On Figures 2 and 3 give a Situation map of the spatial relationship between tectonic blocks in the plan and profile. These models are made in the Surfer 11 software, where was chosen linear interpolation, the produces the best results.

2 CREATE 3D MODELS (BLOKS 67A, 67B, 68 AND 61)

2.1 Data exploration wells

In the area we have a total of 18 exploration wells. In Table 1 are important data for each well and the processing of table 1 we get Table 2 which contains the minimum and maximum values of y, x, z coordinates in the coordinate system of the state as well as data related to the coal layer (minimum thickness, maximum thickness and average thickness). Geological reserve blocks are given in Table 3.

Table 1. Data exploration wells

Name borehole	coordinates borehole			elevation of the top	elevation of the base	layer thickness
	Y	X	Z			
368	6551598	4918085	320.7	16.36	12.26	4.1
374	6551598	4918131	317	59.8	37.1	22.7
308	6551537	4918073	318.8	21.1	3.9	17.2
883	6551501.5	4918169	318.34	34.74	16.24	18.5
869	6551404.2	4918131	309.72	42.22	18.22	24
361	6551401.4	4918196.5	312.3	61.3	51.6	9.7
868a	6551480	4918248	315.7	41.7	38.7	3
868	6551412.8	4918298	313.43	24.43	15.43	9
307A	6551385	4918324	312.56	19.5	16.5	3
882	6551498	4918204	309.5	65.5	58.5	7
881b	6551534	4918238	300.05	69.05	59.05	10
67	6551620	4918289	312	92.5	69	23.5
373	6551691	4918200	311	113	110	3
960a	6551620	4918045.5	311.57	97.07	94.07	3
900	6551562	4918295.2	306	58	56	2
B-4	6552269	4917388	307	4.5	-10	14.5
859	6551287	4918301	290	1.4	-17	18.4
869	6551383	4918201	306.0	1	-16	17

Table 2. Minimum and maximum values of the coordinates of wells, min. max. value of the thickness of coal seam

Y min.=	6551287	Xmin.=	4917388	Zmin.=	290
Ymax.=	6552269	Xmax.=	4918334	Zmax.=	326.7
Min.layer thickness (m)=	2				
Max.layer thickness (m)=	34				
Average layer thickness (m)=	11,04444444				

Table 3. Geological reserves of tectonic blocks

Block	Area (m^2)	Average thickness (m)	Vuolume (m^3)	γ (t/m^3)	Q (t)
67a	12500	9,08	113500	1,38	156630
67b	38500	16,45	633325	1,38	873988,5
68	24640	17,2	423808	1,38	584855,04
61	101913	14	1426782	1,38	1968959,16
				Σ=	3.584.432,7

2.2 3D Model

To create a 3D model of coal deposits Đurđevik" II" (block 67a, 67b, 68 and 61) used the software Rockworks. The model was developed using data from a network of exploration wells. Necessary data to create 3D models are position of wells (yxz), elevation of the top of drilled and base. All necessary data are given in the preceding table (Table 1 and Table 2). To determine the limits of the 3D model using the data Ymin-max, Xmin-max, Zmin-max.

After determining the boundaries of "Borehole Manager" we are entering data on wells (coordinates, depth of wells, and the elevation of the top of base, etc.). In addition, these data can also import in software. After the data processing approach to making models. Rockworks software offers several types of models (lithological, stratigraphic, and other 2D contour).

In picture 4 shows the 3D model that shows the relationship of the terrain and the coal layer and the layer geometry with gentle pleats.

As the coal layer was very fault it's needed to develop a model in which it is clear that tectonic block 61 is lowered relative to the blocks (picture 6 and 7) which is located on the east side (blocks 67a, 67b and 68).

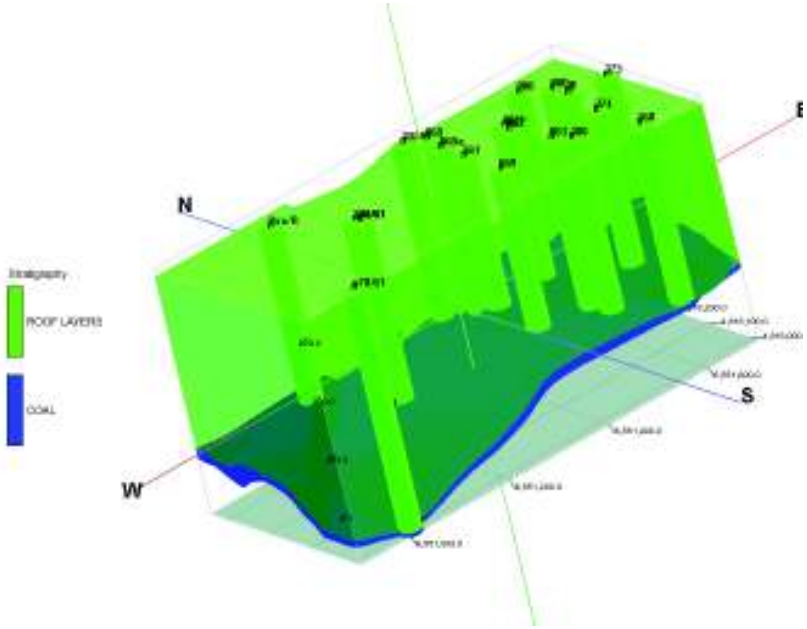

Figure 4. 3D model of the coal deposit with positions

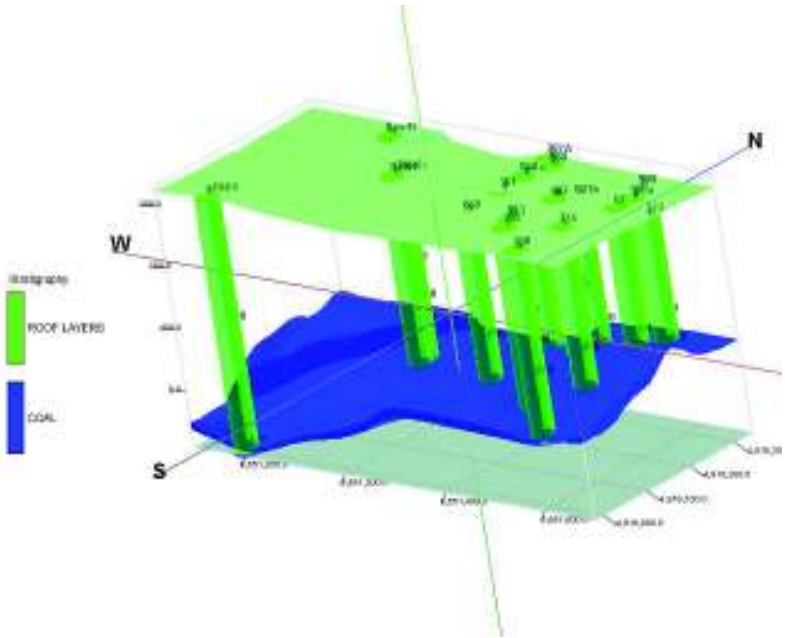

Figure 5. 3D model coal seam (blue-coal, green- surface rock)

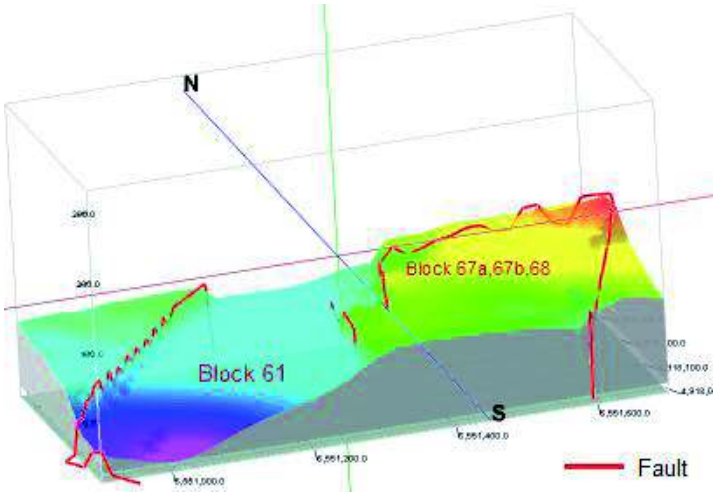

Figure 6. 3D model of tectonic blocks

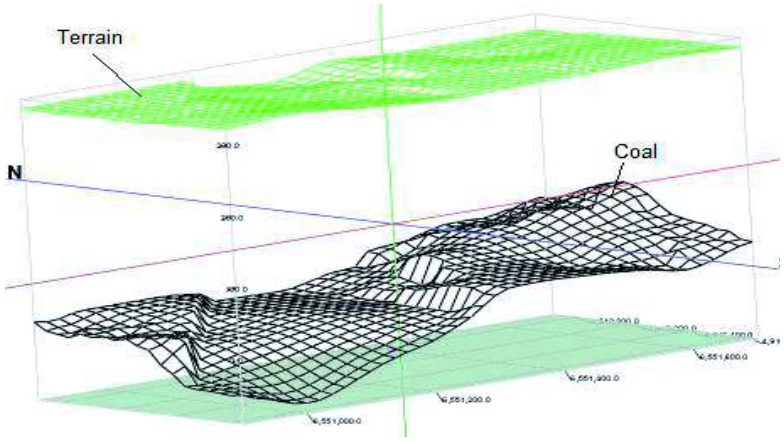

Picture 7. 3D Wireframe model tectonics block and terrain

3 CONCLUSION

RockWare offers a wide range of software for the purpose of mining, geology, geotechnical and other areas. The paper used Rockworks software to create 3D models of coal deposits, and gives a short overview of some of the possibilities of interpretation and reservoir modeling. On the basis of exploratory wells and legality of the elements carbon layers 67a, 67b and 68 in the paper a block 61 with its basic elements in the 3D model.

REFERENCES

DRP, Otvaranje i priprema tektonskih blokova 67a, 67b i 68 revira „Đurđevik II“,.2008.g

Dr.sc.I.Galić,dipl.ing.rud.,Modeliranje površinskih kopova i jamskih prostorija primjenom računalnih programa, Nastupno predavanje Zagreb, 07. listopada 2005

M.Miladinović, V.Čebašek, N.Gojković Računarski programi za projektovanje i modeliranje u rudarstvu 2011.god.

www.rockware.com

O. Musić: Uskočelne metode otkopavanja slojevitih ležišta, Tuzla 2010.

O. Musić, Š. Sarajlić, H. Čičkušić: Uticaj složenih rudarsko-geoloških faktora na izbor metode otkopavanja u RMU „ĐURĐEVIK“blok 75, Savremene tehnologije u rudarstvu i zaštiti životne sredine, Tara 2010.

D. Osmanović, J. Mehić,: 3D model mrkog uglja Đurđevik II“ (blok 67a, 67b i 68), VI regionalni kongres studenata geotehnoloških fakulteta, Niš jun. 2012.